

IMPERIAL COLLEGE LONDON

DOCTORAL THESIS

---

# Bulk Space-time Geometries in AdS/CFT

---

Author:

Andrew Mark HICKLING

Supervisor:

Toby WISEMAN

*A thesis submitted in fulfillment of the requirements  
for the degree of PhD*

*in the*

Theoretical Physics Group  
Department of Physics

December 29, 2016



## Declaration of Authorship

I, Andrew Mark HICKLING, declare that this thesis titled, “Bulk Space-time Geometries in AdS/CFT” and the work presented in it are my own. I confirm that:

- Where I have consulted the published work of others, this is always clearly attributed.
- I have acknowledged all main sources of help.
- Where the thesis is based on work done by myself jointly with others, I have made clear what was done by others and what I have contributed myself.

Signed:

---

Date:

---

The copyright of this thesis rests with the author and is made available under a Creative Commons Attribution Non-Commercial No Derivatives licence. Researchers are free to copy, distribute or transmit the thesis on the condition that they attribute it, that they do not use it for commercial purposes and that they do not alter, transform or build upon it. For any reuse or redistribution, researchers must make clear to others the licence terms of this work



IMPERIAL COLLEGE LONDON

# *Abstract*

Faculty of Natural Sciences  
Department of Physics

PhD

## **Bulk Space-time Geometries in AdS/CFT**

by Andrew Mark HICKLING

The AdS/CFT correspondence provides a geometric description of certain strongly coupled conformal field theories (CFTs). These CFTs are conjectured to have a dual description involving ‘bulk’ space-time geometries that solve Einstein’s equation. It is a holographic correspondence, so the CFTs in some sense lives on the boundary of the bulk. In the regime where this description is applicable, the holographic CFTs are at strong coupling, and can be placed on non-trivial curved space-times. In these contexts, other available tools, such as perturbation theory and lattice techniques, break down.

Under this correspondence, physical quantities in the CFT can be extracted from the bulk geometry. This means that properties of the CFT will be reflected in features of the dual bulks. Using a mix of basic geometry and numerical methods, we explore ways in which the bulk space-time geometries in the AdS/CFT correspondence reflect physical properties of the dual CFTs. We will, for instance, discuss the role of certain features of the bulk geometry in describing a large scale limit of the CFT state. This will motivate us to construct a class of bulk geometries numerically that describe this large scale limit.

We will also find that the geometric tools that come with the bulk description allow us to make powerful statements about the CFTs which would be non-trivial to derive using traditional quantum field theory methods. We will be able to derive bounds on the energy gap and vacuum energy density of these CFTs using basic geometric methods. Finally, we will end with a conjecture of a bound on a finite temperature phase transition in the CFT, which we will present analytical and numerical evidence for using similar bulk geometric arguments.



## *Acknowledgements*

I would like to thank Toby Wiseman for his supervision, guidance, and advice. I would also like to thank James Lucietti and Sebastien Fischetti for their collaborations, along with Paul McFadden for many useful conversations. Finally, I would like to thank all the PhD students in the Theoretical Physics group for helpful discussions and debates. This PhD was supported by an STFC Studentship.



# Contents

<b>Declaration of Authorship</b>	<b>iii</b>
<b>Abstract</b>	<b>v</b>
<b>Acknowledgements</b>	<b>vii</b>
<b>1 The AdS/CFT Correspondence</b>	<b>1</b>
1.1 Origin of the Correspondence . . . . .	3
1.1.1 Maldacena’s Conjecture . . . . .	3
1.2 Statement of the Correspondence . . . . .	4
1.3 More General Correspondence and The Universal Sector . . . . .	6
1.4 Gravity in Asymptotically Locally AdS Spacetimes . . . . .	7
1.4.1 The Conformal Boundary and AIAdS . . . . .	8
1.5 CFTs in General Dimensions . . . . .	10
1.5.1 Example: Free Scalar CFT . . . . .	11
1.5.2 Example: $\mathcal{N} = 4$ SYM . . . . .	11
1.6 The AdS/CFT Dictionary . . . . .	11
1.6.1 The Universal Sector and the Stress Tensor . . . . .	13
1.6.2 Primary Scalar Operators . . . . .	14
1.6.3 Global U(1) symmetry - a Chemical Potential . . . . .	15
1.7 Holography on Simple Spaces . . . . .	16
1.7.1 Flat Space: Poincaré AdS and the AdS Black Brane . . . . .	16
1.7.2 The Sphere: Global AdS and the Hawking Page Transition . . . . .	17
1.7.3 The Torus . . . . .	19
1.7.4 Chemical-Potential - Reissner-Nordstrum Black Branes . . . . .	19
1.8 Applications of the correspondence . . . . .	20
1.8.1 Condensed Matter - AdS/CMT . . . . .	20
1.8.2 Heavy Ion Collisions, QGP, and the Fluid/Gravity Correspondence . . . . .	21
1.9 Evidence for the Correspondence . . . . .	22
<b>2 Numerical Methods for Gravity</b>	<b>23</b>
2.1 Coming up with a well-posed Problem . . . . .	23
2.1.1 The Harmonic Einstein Method . . . . .	24
2.2 Asymptotics of the reference connection and a maximum principle for $\xi$ . . . . .	25
2.3 Choosing an Ansatz . . . . .	26
2.4 Discretize . . . . .	27

2.5	Solution of Discretized System	28
2.6	Implementation in C++	29
<b>3</b>	<b>Extremal Horizons and the Infrared in AdS/CFT</b>	<b>31</b>
3.1	Scale-invariant CFT states	32
3.1.1	Spacetimes consistent with static, scale-invariance	32
3.1.2	Fields that preserve the static, scale-invariance	34
3.2	Introduction to Extremal Horizons	35
3.3	Enhanced Symmetry of Static near-horizon Geometries	37
3.4	Near Horizon Geometries with Conformal Boundaries	38
3.4.1	AdS Example	39
3.4.2	4d Einstein Near Horizon Geometries	40
3.4.3	4d Einstein-Maxwell Near-Horizon Geometries	41
3.5	Extremal Horizons and Large Scale Limits in AdS/CFT	42
3.5.1	Large Scale Limit of a CFT state	42
3.5.2	Holographic CFT on 2+1 dimensional resolved cones	43
3.5.3	The General Statement	45
	FG Coordinates for Near Horizon Geometries	46
	Large Scale limits and Near Horizon limits related through the Fefferman Graham Expansion	46
	Obstructions to Null Infinity extending to an Extremal Horizon	48
3.5.4	Beyond the universal sector	49
3.6	Discussion	50
<b>4</b>	<b>Singular Scale Invariant Geometries</b>	<b>51</b>
4.1	Linearised Construction of Solutions	52
4.2	Setup for Numerical Construction of Solutions	54
4.2.1	The Harmonic Einstein's Equation and our Ansatz	54
4.2.2	A Generalization of the Maximum Principle	55
4.2.3	Boundary Conditions	56
4.2.4	Discretization	59
4.2.5	The Reference Metric	61
4.2.6	Computational Resources	62
4.2.7	Aside on Calculation of Boundary Charge	62
4.3	Numerical Solutions	64
4.3.1	Gauge Field Solutions	64
	Dependence of Charge on Boundary Parameters	64
	Dependence of Charge Density on Boundary Parameters	65
	Dependence of Energy Density on Boundary Parameters	67
4.3.2	Metric Deformation Solutions	67
4.3.3	Comparison with Linearised Solutions	70
4.3.4	Convergence and Smoothness	70
	Direct Convergence	73

Harmonic Gauge Condition . . . . .	73
Boundary Expansions . . . . .	75
Coordinate Axis Expansions . . . . .	77
4.4 Analysis of the Singularity . . . . .	79
4.5 Discussion and Generalizations . . . . .	82
<b>5 Holographic Description of Energy Gaps</b>	<b>85</b>
5.1 CFT on a Sphere - Radial Quantization . . . . .	86
5.2 Free Scalar CFT . . . . .	87
5.3 General Scalars - Conformal Perturbation Theory . . . . .	89
5.4 Holographic Energy Gap . . . . .	95
5.4.1 The bulk equations and the optical geometry . . . . .	95
5.4.2 Scalar Fluctuations . . . . .	97
5.4.3 Bulk Assumptions . . . . .	98
5.4.4 Lower Bound on the Scalar Fluctuation Spectrum . . . . .	99
5.4.5 An Upper Bound . . . . .	100
5.4.6 Range of Applicability of the Bounds . . . . .	101
5.5 Discussion . . . . .	102
<b>6 Vacuum Energy</b>	<b>103</b>
6.1 The Bound on the Free Energy . . . . .	103
6.1.1 An Alternative Derivation of this Bound . . . . .	106
6.1.2 A Vacuum Bound . . . . .	107
6.1.3 Addition of a Massless Scalar . . . . .	108
6.1.4 Saturation of the bound . . . . .	109
6.2 A local statement . . . . .	109
6.3 Spacelike Symmetries and Stress . . . . .	111
6.4 A positivity constraint . . . . .	113
6.4.1 Existence of Weak Solutions to IMCF flow . . . . .	115
6.4.2 Hawking Mass at Conformal Boundary . . . . .	115
IMCF on Global AdS . . . . .	117
6.4.3 What IMCF can tell us . . . . .	118
6.5 Discussion . . . . .	119
<b>7 Temperature Gaps</b>	<b>121</b>
7.1 Einstein Boundary Metric . . . . .	122
7.2 Small Black Holes . . . . .	123
7.2.1 Addition of a massless Scalar . . . . .	124
7.3 Large Black Holes . . . . .	125
7.4 The Product of Spheres . . . . .	127
7.4.1 Numerical Solution of the ODEs . . . . .	129
7.5 Linearised Perturbations of a Sphere . . . . .	129
7.6 Deformations of Spheres . . . . .	132

7.6.1	Numerical Solution of the PDEs on Deformed Spheres . . . . .	133
7.6.2	Convergence Tests for PDEs . . . . .	137
7.7	Discussion . . . . .	140
<b>8</b>	<b>Summary</b>	<b>145</b>
	<b>Bibliography</b>	<b>147</b>

# Chapter 1

## The AdS/CFT Correspondence

The AdS/CFT[1, 2, 3], or Gauge/Gravity, correspondence is an example of a duality. A duality relates two equivalent descriptions of the same underlying theory. This particular duality relates certain string theories (or M-Theories) to gauge theories (which are also conformal field theories (CFTs)). These theories look very different. They are written in terms of different degrees of freedom, one theory with strings, the other particles. What's more, string theory is a theory of quantum gravity, so its spacetime geometry is dynamical, whereas for the gauge theory the spacetime is a static background which the theory responds to but does not affect. Despite this, the AdS/CFT conjecture asserts that these are simply two different ways of describing the same underlying theory.

There is no proof of this correspondence, although it has been extensively tested and there are limits in which it is thought to be understood. However it provides a powerful tool to further our understanding of both string theory and gauge theory. In particular, this duality has the potential to help in the search for a theory of quantum gravity, by recasting the problem in terms of gauge theories. The focus in this thesis will be on the application of this correspondence in the other direction. We will focus on a limit where string theory can be described by classical supergravity. Under the duality, this gets mapped to a limit of the field theory where it is strongly coupled, and has a large number of degrees of freedom. Strongly coupled field theories turn up in the standard model (QCD), as well as in effective descriptions of condensed matter systems. While the duality in its current form only applies to a very particular class of gauge theories (to which QCD does not belong), one might hope to get a qualitative understanding of features of such strongly coupled field theories by studying those that can be described in this way.

In this limit, the physical properties of the gauge theories are encoded in features of classical supergravity solutions. In fact, there is always a particular sector of solutions within the supergravity where the only non-trivial field is the metric, and where this metric satisfies the vacuum Einstein's equation with negative cosmological constant. In this 'universal' sector, the physics of the field theory is described by the geometry of this gravitational metric. As we will see, this geometric description makes it quite natural to put the gauge theory on a curved spacetime.

As a stepping stone towards quantum gravity, curved space quantum field theory has received many decades of attention. This has yielded many important results, such as Hawking radiation[4]. However, basic physical quantities in curved space QFT can

be hard to calculate when the spacetime is generic. By this I mean that, given a specific theory defined on a curved spacetime, it's very difficult to work out how these physical properties depend on the choice of spacetime. For instance, consider the problem of trying to find the energy spectrum of modes in a scalar field theory defined by the action

$$S = \int \sqrt{-g} (\partial_\mu \phi \partial^\mu \phi + m^2 \phi^2). \quad (1.1)$$

On flat space, or on a given highly symmetric spacetime, this is simple. Once the spacetime is made general, however, the problem of finding this spectrum as a functional of the spacetime is prohibitively difficult.

As we will describe, under the duality, the gauge theory's spacetime becomes a boundary condition for the string theory partition function. In the 'universal' sector of the supergravity limit, this duality translates the problem of studying strongly coupled gauge theories on arbitrary spacetimes into the problem of solving Einstein's equation for some general boundary conditions. This is also not a solved problem, but recasting curved space quantum field theory in terms of this geometric problem means there is a new set of tools to use to derive results.

In this thesis we will explore how features of this dual gravitational spacetime known, as we will explain, as the 'bulk' spacetime, reflect properties of the CFT, and also how they can be used to constrain these features. We will use a mix of numerical and analytical methods. The numerical methods will be introduced in Chapter 2, and the analytical methods will be introduced in this chapter, with more details when we use them. We will start in Chapter 3 by exploring the role of a special class of bulk spacetimes, which are the near-horizon geometries of extremal horizons, in describing a large-scale limit of CFT states. In so doing we will find that we can write down CFT states with similar large scale limits to those captured by these bulks, but which can't themselves be described by the large scale limit of near-horizon geometries. This will motivate us to consider more general bulk spacetimes in Chapter 4 which fill this gap. In Chapters 5 and 6 we will then explore how the bulk geometry can allow us to derive bounds on the energy gap and vacuum energy of the CFT as a function of the CFT's spacetime geometry. Finally, in Chapter 7 we will present some evidence for a bound on a 'temperature gap' which is relevant for a confinement/deconfinement phase transition that the CFT undergoes when it is put on certain spacetimes.

In this chapter we will begin by giving a brief introduction to the AdS/CFT conjecture and why it works. We will start with a short description of the origin of the conjecture, and its precise statement. Then, moving to the supergravity limit, we will explain how the duality works in practice in this case. We briefly discuss aspects of the gravitational side in 1.4, and CFTs in 1.5, before moving into the dictionary that maps between the two in Section 1.6. We will give examples of how this works in the simplest cases in 1.7. Finally we will briefly describe some promising applications of this correspondence to condensed matter and high energy physics in 1.8, and conclude in 1.9 with a summary of some of the evidence we have that the correspondence holds. For more detailed reviews

of the AdS/CFT correspondence see [5, 6, 7], and for a review of the use of AdS/CFT to explore CFTs in curved spacetime see [8].

## 1.1 Origin of the Correspondence

### 1.1.1 Maldacena's Conjecture

This surprising conjecture was first arrived at by Maldacena through the following thought experiment [1] which is also described in, for instance, [6]. He considered a stack of  $N$  D3-Branes in  $9+1$  dimensional type IIB string theory in two different regimes, and asked what low energy physics decoupled in each of these cases.

1. The first case is  $g_s \rightarrow 0$  with  $N$  fixed. In this case we can ignore the gravitational back-reaction of the branes. The vacuum state is then a stack of D-branes sitting in Minkowski space. The low energy theory of excitations about this state has two decoupled sectors. One sector corresponds to open strings that start and end on the branes. Thought of as a theory on the  $3+1$  dimensional brane, this is a  $U(N)$   $\mathcal{N} = 4$  SYM gauge theory. The other sector is the massless spectrum of the closed strings propagating in the bulk. This is type IIB supergravity on a flat background. These two sectors are decoupled at low energy.
2. The second case is  $g_s \rightarrow 0, N \rightarrow \infty$  but with  $g_s N$  fixed. In this regime we can use supergravity, but we can no longer ignore the gravitational back-reaction of the branes. Type IIB supergravity admits black p-brane solutions that carry the charge to source a  $p+1$  form potential (R-R field). In this case, we are interested in the  $p=3$  solutions.

There are two free parameters for these solutions, the mass  $M$  and charge  $N$ . These are constrained by the requirement that the supergravity solution doesn't have a naked singularity[5]

$$M \geq \frac{N}{(2\pi)^p g_s l_s^{p+1}}. \quad (1.2)$$

The low energy limit corresponds to taking the extremal solution that saturates (1.2), so this is the vacuum solution we should consider. The low energy theory then consists of excitations about this vacuum, and this again has two decoupled sectors.

If you consider modes close to the horizon, then their energy as measured by an observer at infinity can be made arbitrary low because of the redshift. We can take an infinite red shift limit, and consider modes living in the  $AdS_5 \times S^5$  near horizon geometry of the extremal horizon. This is type IIB string theory on  $AdS_5 \times S^5$ . Since the low energy limit is provided by the redshift rather than a long-wavelength limit, this theory includes the full spectrum of the massive string states and not just the massless supergravity sector.

You can also consider long wavelength excitations that live in the asymptotically flat spacetime away from the horizon. In the infinite long wavelength limit, this is described by Type IIB supergravity on Minkowski space.

These two sectors are decoupled at low energy because the infrared excitations near the extremal horizon can't escape the gravitational well, and the supergravity modes away from the horizon have a long wavelength compared to the absorption cross-section of the black brane.

These two theories are both low energy effective descriptions of the same theory, which hold in different limits. We can take the large  $N$  limit of the first case, then both have  $g_s \rightarrow 0$  and  $N \rightarrow \infty$ . Maldacena's claim is that these two low energy effective theories are equivalent descriptions of the same theory, that have merely been written down in terms of degrees of freedom that are appropriate to different limits. Both theories consist of two decoupled sectors, and they share a common  $9 + 1$  dimensional type IIB flat space supergravity sector. The assertion is therefore that the other pair of sectors that apparently differ are dual. In other words, type IIB string theory on an  $AdS_5 \times S^5$  background is equivalent to  $U(N)$  SYM in  $3 + 1$  dimensions. It should be noted that although the above argument was made in a large  $N$  limit, he made the stronger conjecture that the two theories are in fact equivalent at any value of  $N$ .

## 1.2 Statement of the Correspondence and a 'Classical' Limit

The correspondence argued for above can be stated more precisely as a relation between two partition functions [3]

$$Z_{string}|_{\Phi} = Z_{SYM}[J]. \quad (1.3)$$

The left-hand side is the partition function for Type IIB string theory on  $AdS_5 \times S^5$ , and the right hand side is the partition function for  $U(N)$  SYM in  $4d$ . The string theory partition function is a functional of some asymptotic boundary conditions, represented schematically by  $\Phi$ . These include, for instance, fixing the spacetime to be asymptotically  $AdS_5 \times S^5$ . In the gauge theory we're actually considering the generating function, which is a functional of some applied source terms  $J$ . Under this correspondence, the gravitational boundary conditions get mapped to the gauge theory sources  $\Phi \rightarrow J$ . In fact, the  $AdS_5$  factor has a particular type of asymptotic structure at infinity called a conformal boundary, which we will explain in 1.4.1. On this  $3 + 1$  dimensional conformal boundary there is, as we will discuss, a conformal class of metrics. The boundary conditions fix a representative of this conformal class. This metric is the spacetime that the SYM lives on, and we think of it as one of the sources  $J$  in the generating function. A more precise map, along with a more detailed description of these boundary conditions will be discussed in 1.6.

For now, we just need the relationship between a few parameters in the two theories[9, 6]

$$\begin{aligned} g_s &= g_{YM}^2 \\ \ell^4 &= 4\pi g_s (\alpha')^2 N \end{aligned} \tag{1.4}$$

where  $g_s$  is the string coupling,  $g_{YM}$  the Yang-Mills coupling and  $\ell$  is the  $AdS_5$  and  $S_5$  radius.

We are going to consider a particular limit in which the gravitational theory simplifies. The first step is to take a weak coupling  $g_s \rightarrow 0$  limit of the string theory. The precise limit is to take  $g_s \rightarrow 0$  while keeping

$$\lambda = g_s N = g_{YM}^2 N \tag{1.5}$$

fixed[9]. From the point of view of the gauge theory this corresponds to the t'Hooft planar limit introduced in [10].

The next stage is to take the large  $\lambda$  limit. From the gauge theory perspective, this means taking the planar CFT to be strongly coupled. From (1.4) we see that from the gravitational perspective the AdS length scale becomes very large compared to the string length  $\ell_s = \sqrt{\alpha'}$ . In this limit, we can ignore corrections arising from quantum loops on the worldsheet[6], and excited states on the string have large masses. We are left with an effective theory with only a small number of massless fields, namely classical supergravity.

Under these conditions the action is approximated by that of the massless supergravity sector, and the partition function is approximated by a sum of classical saddle points[8]

$$Z_{\text{string}} \approx \sum_{\phi_i | \Phi} e^{-S[\phi_i]_{\text{sugra}}}. \tag{1.6}$$

Here the  $\phi_i$  stand for field configurations that solve the supergravity equations. The boundary conditions  $\Phi$  for the partition function become the boundary conditions for the field equations, so the sum above is restricted to those  $\phi_i$  which are consistent with  $\Phi$ . In this limit, it is these supergravity boundary conditions that get mapped to the sources in the SYM under this correspondence. One of the fields is a metric, and its boundary conditions are what determine the conformal boundary, and hence the spacetime the SYM lives on. Boundary conditions on the other fields in the supergravity are mapped to source terms for various local operators in the field theory. It should be stressed that this is not a classical limit for the field theory, so this limit of the correspondence allows us to study a strongly coupled quantum field theory outside of the classical limit, by solving the classical equations of motion of a dual theory.

In this limit the supergravity actions are very large, so in the case that there are multiple solutions with the same boundary condition, the minimum action solution dominates this sum. If as we vary the boundary conditions the values of  $S(\phi_i)$  for two different solutions cross, you will get a discontinuous jump from one solution dominating the partition

function to another. This leads to a discontinuous phase transition in the dual field theory in this large  $N$ , strong coupling, limit, as the corresponding sources are varied in the same way[3].

The relationship between the partition functions in (1.6) works as well at finite temperature[8]. In the supergravity, we can consider static thermal equilibrium states at temperature  $T$  by going to Euclidean signature and including a thermal circle of period  $\beta = \frac{1}{T}$  in the metric. This gets carried over to the conformal boundary, and so to the SYM's spacetime. The field theory is therefore also at finite temperature and, in this way, the temperature is one of the boundary conditions that you can fix.

The process for performing calculations in this limit of AdS/CFT can therefore be summarized as follows

1. Choose sources in the SYM generating function. These will get mapped to boundary conditions for the supergravity equations.
2. Solve the supergravity equations using these boundary conditions
3. If there is more than one solution, choose the one with minimum action
4. Evaluating its action yields a saddle point approximation for the SYM's generating function in a large  $N$ , strong coupling, limit.

How we go about these steps in practice, will be explained in more detail in the following sections.

### 1.3 More General Correspondence and The Universal Sector

In Maldacena's original argument, the bulk spacetime described by the string theory was asymptotically locally  $AdS_5 \times S_5$ . In fact we can consider more general cases where we start from Type IIB String theory in  $9 + 1$ , or M theory in  $10 + 1$ , dimensions and compactify in different ways so that we end up with bulk spacetimes which are asymptotically locally  $AdS_{n+1} \times X$ , where  $X$  is some internal space. The dual field theory is then some conformally invariant field theory (CFT) that lives on the  $n$  dimensional conformal boundary of the  $AdS_{n+1}$  factor. The details of the theory depend on the choice of internal space  $X$ [8].

There is then a corresponding limit like in Section 1.2, and we can solve supergravity equations for bulks that are asymptotically locally  $AdS_{d+1} \times X$  to describe a strongly coupled CFT in an analogous large 'N' limit. In fact, for various choices of  $X$ , there is always a class of solutions which factorize globally to the form  $\mathcal{M} \times X$ , where  $\mathcal{M}$  is a solution to the vacuum  $d + 1$  dimensional Einstein's equation with a negative cosmological constant[8]. This is called the universal sector because it's independent of the details of the particular CFT, which is encoded in the space  $X$ . As we'll explain in more detail in Section 1.6 this corresponds to a sector of dynamics in the CFT which describes how the one-point function of the stress tensor depends on the spacetime the CFT lives on. Since there is no non-trivial dependence on any other supergravity fields, the source terms for

local operators in the CFT corresponding to the boundary conditions of these fields have not been turned on.

The parameters of this gravity sector are related to the full  $D = 9 + 1$  or  $D = 10 + 1$  dimensional supergravity parameters via[8]

$$\begin{aligned} G_{d+1} &= \frac{1}{\text{vol } X} G_D \\ \Lambda &= -\frac{d(d-1)}{2\ell^2} \\ c_{\text{eff}} &= \frac{\ell^{d-1}}{16\pi G_{d+1}}. \end{aligned} \tag{1.7}$$

The parameter  $\ell$  is a length scale associated with the internal space  $X$  which sets the size of the cosmological constant  $\Lambda$ . The parameter  $c_{\text{eff}}$ , is proportional to  $N^2$  for gauge theories, and is related to the number of degrees of freedom in the CFT [8].

To look at other operators, we need to deform the field theory by sources, and as we'll see this corresponds to adding fields to the bulk gravitational theory. Strictly speaking, we should only add combinations of fields that are consistent from the supergravity perspective. By this we mean that we can only add bulk fields that are present in the full supergravity (either in the full  $D$  dimensional theory, or ones that arise from the dimensional reduction), and we need to check that it's consistent to set the rest to zero, so it constitutes a 'consistent truncation'. For an example of a 'top-down' consistent truncation see for instance [11, 12]. However, we will take a 'bottom-up' perspective in this work, as is often done in applications to condensed matter physics (called AdS/CMT) [13], and add the fields corresponding to the deformations we want to consider, without worrying about finding a consistent truncation of a full supergravity with this combination of fields.

## 1.4 Gravity in Asymptotically Locally AdS Spacetimes

We are left with  $d + 1$  dimensional gravity, satisfying Einstein's equation with negative cosmological constant

$$R_{\mu\nu} = -\frac{d}{\ell^2} g_{\mu\nu}. \tag{1.8}$$

The maximally symmetric vacuum solution to these equations is AdS space. A nice way to arrive at  $AdS_{d+1}$ , which makes its symmetry group manifest, is by considering the space  $R^{d+2}$  with a diagonal metric of signature  $(2, d)$  [14]. This metric is invariant under the group  $SO(2, d)$ . We then consider the orbit under the action of  $SO(2, d)$  of a point a distance  $\ell$  from the origin of this space, so we consider a slice of this space which is a constant distance from the origin

$$X_0^2 + X_{d+1}^2 - \sum_{i=1}^d X_i^2 = \ell^2. \tag{1.9}$$

This space is  $AdS_{d+1}$ , but with a compactified time direction, and is by construction invariant under  $SO(2, d)$ .

To obtain an intrinsic description of AdS we can solve the constraint (1.9) by setting

$$\begin{aligned} X_0^2 + X_{d+1}^2 &= \ell^2 + r^2 \\ \sum_{i=1}^d X_i^2 &= r^2. \end{aligned} \quad (1.10)$$

At fixed  $r$  these describe a circle and a  $d - 1$  sphere, so we use polar coordinates to write the induced metric as

$$g_{\text{AdS}} = -(\ell^2 + r^2)d\psi^2 + r^2 d\Omega_{d-1}^2 + \ell^2 \frac{dr^2}{\ell^2 + r^2}. \quad (1.11)$$

Here  $\psi$  is a timelike coordinate but it is periodic with period  $2\pi$ , which means we admit closed timelike curves. However, we can get around this simply by considering instead the universal covering of this space, obtained by decompactifying  $\psi$  to arrive at a non-periodic time coordinate  $t$ [15].

### 1.4.1 The Conformal Boundary and AIAdS

AdS (1.11) has a conformal boundary, which we can think of as the spacetime on which the dual CFT lives, in a sense which will become clearer when we discuss the map between the CFT and gravity in more detail. When we say that a spacetime  $(g_{\mu\nu}, \mathcal{M})$ , defined by a metric  $g_{\mu\nu}$  and a manifold  $\mathcal{M}$ , has a conformal boundary  $\partial\mathcal{M}$ , we mean that the following holds[16, 17]

- There is a smooth spacetime  $(\bar{g}, \bar{\mathcal{N}})$  with a boundary  $\partial\bar{\mathcal{N}}$ , such that  $\mathcal{M}$  is diffeomorphic to the interior of  $\bar{\mathcal{N}}$ ,  $\mathcal{N}$
- There is a smooth function  $Z(x)$  on  $\bar{\mathcal{N}}$ , called the defining function, such that in the interior  $\mathcal{N}$ ,  $\bar{g} = Z(x)^2 g$
- $Z(x) > 0$  throughout  $\mathcal{N}$  and on  $\partial\bar{\mathcal{N}}$   $Z(x) = 0$ , and  $dZ \neq 0$ .

The conformal boundary  $\partial\mathcal{M}$  of  $\mathcal{M}$  is defined as the regular boundary  $\partial\bar{\mathcal{N}}$  of  $\bar{\mathcal{N}}$ . Given a defining function  $Z(x)$  that satisfies the above properties, the function  $\omega(x)Z(x)$  satisfies them too for any everywhere positive  $\omega(x)$ . For any given choice of  $Z(x)$ ,  $\bar{g}$  induces a metric on the boundary  $\partial\mathcal{M}$ . The set of all possible boundary metrics on  $\partial\mathcal{M}$  defined in this way forms a conformal class  $\{\bar{g}\}$ , and  $(\partial\mathcal{M}, \{\bar{g}\})$  defines the conformal boundary on which the CFT is defined.

For AdS (1.11), if we set  $r = \frac{4-\ell^2 z^2}{4z}$  then we find

$$g_{\text{AdS}} = \frac{1}{z^2} \left( \ell^2 dz^2 - \left(1 + \frac{\ell^2 z^2}{4}\right)^2 dt^2 + \left(1 - \frac{\ell^2 z^2}{4}\right)^2 d\Omega_{d-1}^2 \right). \quad (1.12)$$

We see therefore that  $\bar{g} = z^2 g_{\text{AdS}}$  has a smooth boundary at  $z = 0$ , on which the metric is

$$g_{\partial\text{AdS}} = -dt^2 + d\Omega_{d-1}^2. \quad (1.13)$$

This is the conformal boundary, we've taken  $Z = z$  as the defining function, and  $g_{\partial\text{AdS}}$  is the corresponding representative of the induced conformal class.

More generally, if a manifold  $\mathcal{M}$  with a conformal boundary satisfies Einstein's equation, then it can be shown that you can choose coordinates near the conformal boundary such that the metric takes the form[18]

$$g = \frac{1}{z^2} \left( \ell^2 dz^2 + h_{ab}(x, z) dx^a dx^b \right). \quad (1.14)$$

We see that (1.12) is a special case of these coordinates. Here the indices  $a, b$  run over the  $d$  dimensional conformal boundary spacetime directions, and the  $x^a$  are coordinates over this boundary. This construction with the coordinates  $(z, x^a)$  is known as Fefferman-Graham coordinates. We can use the coordinate  $z$  as the defining function in the above construction, and the metric  $h = h_{ab}(x^a, 0) dx^a dx^b$  extracted in this way is a representative of the conformal class  $\{\bar{g}\}$ . In fact, the AdS isometry group in the bulk  $SO(d, 2)$ , is the  $(d - 1) + 1$  dimensional conformal group, and its action on the conformal boundary is to generate conformal transformations[14].

Given this, we can now define an asymptotically locally AdS (AlAdS) spacetime as a solution to (1.8) with a conformal boundary[17]. Given a choice of conformal boundary<sup>1</sup>, the gravitational theory is then described in this universal sector by AlAdS spacetimes with this conformal boundary, and the dual CFT lives on this conformal boundary. This is the sense in which the duality is holographic, we refer to the gravitational description as the 'bulk', and the CFT as the boundary. We will always use the parameter  $d$  to label the number of dimensions, where the bulk is  $d + 1$  dimensional, and the boundary is  $(d - 1) + 1$  dimensional.

We can start to see how this holographic duality will work by building a holographic CFT from a scalar field theory on AdS[6]. The scalar field theory can be defined in the usual way in terms of some action  $S = \int_{\text{AdS}_{d+1}} \mathcal{L}(\Phi)$ . However, if we want to have a theory that we can evolve in time, then we need to supply boundary conditions in addition to this action. This is because there are no Cauchy surfaces in AdS, we always have to apply extra boundary conditions at the conformal boundary[14], since light rays can get to the conformal boundary and back in finite time [6]. These boundary conditions will be written in terms of some function  $J$  on the conformal boundary. We can consider the semi-classical approximation of the scalar field theory partition function as a functional of these boundary conditions<sup>2</sup>

$$Z[J] = \exp \left( - \int_{\text{AdS}_{d+1}} \mathcal{L}(\Phi_J) \right), \quad (1.15)$$

<sup>1</sup>A choice of spacetime and a corresponding conformal class of metrics.

<sup>2</sup>As we will discuss below, this is divergent and needs to be renormalized.

where  $\Phi_J$  is the solution to the ‘bulk’ field equations. Now we can treat the function  $J$  as the source conjugate to a field  $\phi$  living on the conformal boundary, and think of the functional  $Z$  as a generating function for a theory on this boundary spacetime. Since the  $SO(2, d)$  isometry generates conformal transformations on the boundary, this ‘boundary’ theory will be conformally invariant so long as the ‘bulk’ action  $\mathcal{L}(\Phi)$  respects this isometry.

## 1.5 CFTs in General Dimensions

A regular relativistic quantum field theory, such as the standard model, has Lorentz symmetry. The fields in the theory organise themselves into representations of the Lorentz group, labelled by the Casimirs of the group, their mass and spin (scalars, spinors, vectors etc.). If we consider theories with increased symmetry, then these might not be the appropriate way to label degrees of freedom. In a supersymmetric theory, for instance, we add transformations to the symmetry group that change the spin of particles, so it makes more sense to consider multiplets of fields of different spin that get mixed together under the transformations.

Another extension of the Lorentz group we can consider, and one that plays a central role here, is the conformal group. The Lorentz group can be thought of as the set of coordinate transformations in  $(d-1)+1$  dimensions that leaves the Minkowski metric  $\eta_{\mu\nu}$  invariant. The conformal group generalizes this, and consists of these transformations, together with any that leave  $\eta_{\mu\nu}$  invariant up to a Weyl scaling. So, it is all transformations of the form

$$x^\mu \rightarrow \zeta^\mu(x) \text{ s.t. } \eta_{\mu\nu} \rightarrow \phi(x)\eta_{\mu\nu}. \quad (1.16)$$

For a nice introduction to Conformal Field Theories see [19], or [20]. This symmetry has important consequences for what local physical observables look like. As a consequence, it’s more natural not to think of this theory as living on a pseudo-Riemannian manifold with a given metric, but rather on a space with a given conformal class of metrics. Crucially, everything has to be scale invariant, so in particular, you have no scale with respect to which to measure distance in a such a theory.

Another consequence is that you can no longer have massive particles. One class of transformations in the conformal group is the simple dilations, where

$$x \rightarrow \lambda x. \quad (1.17)$$

The mass of a field would be scaled under this transformation, so all fields must be massless. The types of fields you can consider are instead labelled by their spin and their scaling dimension  $\Delta$ , which describes how the field transforms under these dilations. There is not always even a particle interpretation of CFTs, so they don’t necessarily have an S-matrix[19]. The natural way to study such theories is by looking at the expectation values and  $n$  point correlators of operators in the theory, which can be derived from a generating functional  $Z[J]$ . These will be our focus when we consider holographic CFTs.

### 1.5.1 Example: Free Scalar CFT

A free scalar field theory is a theory with one scalar degree of freedom, and a quadratic action. On flat space, if you want this to be Lorentz invariant, you are restricted to<sup>3</sup>

$$S = \int d^n x \partial_\mu \phi \partial^\mu \phi - m^2 \phi^2. \quad (1.18)$$

On curved spacetime, demanding instead that the Lagrangian is a scalar, we can have as well a coupling to the curvature. Restricting ourselves to a canonical kinetic term we can consider

$$S = \int d^n x \partial^\mu \phi \partial_\mu \phi - m^2 \phi^2 - f(R) \phi^2. \quad (1.19)$$

The particular choice  $m = 0$  and  $f(R) = \frac{d-2}{4(d-1)} R$  is conformally invariant, where the scalar has scaling dimension  $\Delta = \frac{d-2}{2}$  [21].

### 1.5.2 Example: $\mathcal{N} = 4$ SYM

The original AdS/CFT correspondence has as its CFT side 3 + 1 dimensional  $\mathcal{N} = 4$  Super-Yang-Mills with gauge group  $SU(N)$ . This can be constructed by taking  $SU(N)$   $\mathcal{N} = 1$  SYM in 9 + 1 dimensions

$$S = \frac{1}{g_{YM}^2} \int d^{10} x \text{Tr} \left( -\frac{1}{2} F^2 + i \bar{\chi} \gamma^M D_M \chi \right) \quad (1.20)$$

and reducing it to 3 + 1 dimensions by classical Kaluza-Klein compactification, and then truncating the theory by throwing away all the resulting massive modes [7]. Under this reduction the gauge field becomes a gauge field and 6 scalar fields, and the spinor becomes 4 Weyl spinors.

## 1.6 The AdS/CFT Dictionary: Sources and Boundary Conditions

The physical state for the classical gravitational bulk is characterized by field configurations. We will be limiting ourselves to the universal sector we discussed in 1.3, plus a few additional fields that don't effect the internal space  $X$ . Our fields are therefore geometric objects defined on a  $d + 1$  dimensional manifold. In contrast, the dual CFT is a Quantum Field theory, and the physical observables can be reduced to expectation values and correlation functions of operators defined on a  $d$  dimensional manifold. We need to specify how to relate such physical observables across the duality. These rules constitute the AdS/CFT 'dictionary'.

Recall the statement of the duality

$$S_{\text{gravity}}|_{\Phi|_{\partial\mathcal{M}}} = -W_{\text{CFT}}[J], \quad (1.21)$$

<sup>3</sup>A potential constant in front of the kinetic term can be absorbed by scaling  $\phi$

so that the classical gravitational action, when boundary conditions are imposed, corresponds to the generating function of the CFT with corresponding sources. The boundary conditions are applied at the conformal boundary, and the corresponding sources are functions on this boundary, which is why this is the spacetime in which the CFT is defined. There is a map, which pairs of the boundary conditions  $\Phi$ , with sources  $J$  in the CFT, which we will give some examples of below. From the sources  $J$ , we can define conjugate fields  $\phi$  in the CFT through

$$\langle \phi \dots \rangle = \frac{\delta}{\delta J} \langle \dots \rangle_J \Big|_{J=0}, \quad (1.22)$$

where  $\dots$  refers to some combination of local operators, and  $\langle \dots \rangle_J$  is the expectation value of these operators when the source  $J$  is turned on. In particular, the one-point functions are given by

$$\langle \phi(x) \rangle = \frac{\delta}{\delta J(x)} W_{\text{CFT}} = -\frac{\delta}{\delta J(x)} S_{\text{gravity}}. \quad (1.23)$$

Naïvely, it would seem that this means that in order to find  $\langle \phi(x) \rangle$  for any given  $J(x)$ , we would have to know the gravitational solutions for general  $J(x)$ , and so the on-shell action  $S_{\text{gravity}}$  as a functional of  $J(x)$ . Luckily, it turns out that by finding the classical gravity solution for a given  $J(x)$ , we can immediately extract  $\langle \phi(x) \rangle_J$ . This only applies to the one point functions of the particular operators  $\phi(x)$  conjugate to the sources  $J(x)$  which are dual to the gravitational boundary conditions  $\Phi(x)$ . To find two point functions for instance, you would need to look at linear perturbations to these solutions, since

$$\langle \phi_1(x_1) \phi_2(x_2) \rangle_{J_1 J_2} = \frac{\delta}{\delta J_2(x_2)} \langle \phi_1(x_1) \rangle_{J_1 J_2}. \quad (1.24)$$

One subtlety is that both sides of (1.21) are divergent. The right hand side is divergent for the usual Quantum Field Theory reasons, while the left hand side diverges because of the infinite volume of the gravitational bulk. Both sides need to be renormalized, and the method of renormalization on the gravitational side is known as ‘Holographic Renormalization’ [22, 23, 24]. A nice introduction to the program is provided by [17].

The process involves cutting off the bulk integral that gives  $S_{\text{gravity}}$  at some surface before the conformal boundary. Near the conformal boundary we can choose the coordinates (1.14), and then we can choose  $z = \epsilon$  as the cut-off surface. The action will have a finite number of terms that diverge with inverse powers of  $\epsilon$ , which can be cancelled by adding counter terms which are integrals over the  $z = \epsilon$  surface. These counter terms can be written as functionals of the fields on these surfaces, with no explicit dependence on the particular solution.

We will now discuss three different types of operators in the CFTs, which are the three we will study in this thesis. We will explain how the source terms conjugate to these operators get mapped to boundary conditions of dual fields in the gravitational bulk, and how to extract the one point functions of these CFT operators from the bulk solutions involving these dual fields. While we will only focus on local operators here,

other observables such as entanglement entropy [25] and Wilson loops [26, 27] can also be studied in this limit of the correspondence.

### 1.6.1 The Universal Sector and the Stress Tensor

In the universal sector we have pure gravity in the bulk, so the only field we have to set boundary conditions for at the conformal boundary is the metric. Taking the Fefferman-Graham coordinates from (1.14), we can expand  $h_{ab}(x, z)$  in  $z$  for solutions to (1.8). The form of the expansion depends on whether the  $d + 1$  dimensional bulk is even or odd dimensional.

If  $d$  is odd it takes the form[23]

$$h_{ab}(x, z) = h_{ab}^{(0)}(x) + h_{ab}^{(2)}(x)z^2 + \dots + h_{ab}^{(d-1)}(x)z^{d-1} + t_{ab}z^d + \dots \quad (1.25)$$

$h_{ab}^{(0)}(x)$  is the boundary metric (or rather a representative of the conformal class of boundary metrics) from 1.4.1, and solving Einstein's equation order by order in  $z$  determines the  $h^{(n)}$  in terms of the curvatures of this metric. However, Einstein's equation are second order PDEs, so at some point there is a second piece of data that is not determined by the expansion<sup>4</sup>. This happens at order  $z^d$ . The only constraints on this free tensor  $t_{ab}$  implied by the equations are that it must be traceless and conserved.

If  $d$  is even, then this is complicated slightly. Now the expansion takes the form[23]

$$h_{ab}(x, z) = h_{ab}^{(0)}(x) + h_{ab}^{(2)}(x)z^2 + \dots + h_{ab}^{(d-2)}(x)z^{d-2} + \left( t_{ab} + h_{ab}^{(l)}(x) \log z \right) z^d + \dots \quad (1.26)$$

The tensor  $t_{ab}$  is still conserved, but it is no longer traceless. Its trace, however, is determined in terms of some local function of the boundary geometry. This trace and the term  $h_{ab}^{(l)}(x)$  are connected to the conformal anomaly.

The boundary condition to be applied at the conformal boundary is to fix  $h_{ab}^{(0)}(x)$ . This fixes geometry that the CFT lives on. Thinking of this geometry as an applied source in the CFT generating function, the conjugate operator is the stress tensor. The expectation value of the stress tensor for a holographic CFT on a given spacetime  $h^{(0)}$  is given by

$$\langle T_{ab} \rangle = \frac{2}{\sqrt{h^{(0)}}} \frac{\delta W_{cft}}{\delta h_{ab}^{(0)}} = \frac{2}{\sqrt{h^{(0)}}} \frac{\delta S_{\text{gravity}}}{\delta h_{ab}^{(0)}}. \quad (1.27)$$

In this sense the CFT operator dual to the bulk metric is the stress tensor.

As discussed above,  $S_{\text{gravity}}$  is divergent and needs to be renormalized. This can be done by cutting of the space-time on some surface  $z = \epsilon$  and adding counter terms to the action involving geometric quantities on this surface. The result is a stress tensor that was found in [28]<sup>5</sup>, with the result being the Brown-York stress tensor[29] defined

<sup>4</sup>When you consider the full solution to the equations, with sufficient boundary conditions elsewhere in the bulk, this second piece of data should be determined.

<sup>5</sup>Although they did not use the action, instead adding counter terms directly to the Brown-York stress tensor.

in terms of the extrinsic curvature of the surface  $z = \epsilon$ , plus corrections involving the intrinsic curvatures of this surface. For instance, in  $3 + 1$  bulk dimensions this can be written as

$$T^{ab} = \frac{1}{8\pi G} \left( K^{ab} - K\gamma^{ab} - \frac{2}{\ell}\gamma^{ab} - \ell G^{ab} \right), \quad (1.28)$$

where  $\gamma_{ab}$ ,  $K_{ab}$  and  $G_{ab}$  are the induced metric, extrinsic curvature, and Einstein tensor on the surface on which this quantity is evaluated. To extract  $\langle T_{ab} \rangle$ , this surface needs to be taken to the conformal boundary. Depending on the set of surfaces taken in this limit, different conformal frames will be approached on the boundary. To match a given conformal frame for which we've taken FG coordinates as in (1.25), we can choose constant  $z$  surfaces and take  $z \rightarrow 0$ . In fact, written in terms of these coordinates, the CFT stress tensor becomes in general dimensions[23, 30]

$$T_{ab} = dc_{\text{eff}}t_{ab} + X_{ab}. \quad (1.29)$$

where  $X_{ab}$  is a dimension dependent, local function of the boundary geometry. Its presence is related to the conformal anomaly, and leads to scheme dependence<sup>6</sup> in even boundary spacetime dimensions, but vanishes for odd boundary dimensions[23, 30]. We will be dealing almost exclusively with odd boundary dimensions, so we won't have to worry about this term.

As discussed above, this universal sector will be shared by all holographic CFTs. In this sector we can vary the CFT spacetime, and examine how the one point function of the stress-tensor varies as a result. As we will find, there is a lot of interesting physics already in this regime. Note that the stress tensor extracted in this way is proportional to  $c_{\text{eff}}$  from (1.7). As remarked above, this parameter plays the role of the effective number of degrees of freedom in the CFT, and classical gravity is valid only in a large  $c_{\text{eff}}$  limit. When the stress tensor extracted in this way vanishes, what we are saying is that the stress tensor is no longer  $O(c_{\text{eff}})$ , but is  $O(1)$  instead[8].

## 1.6.2 Primary Scalar Operators

The simplest deformation we can consider adding to the CFT is a source for a primary scalar operator. In order to do this we need to add a scalar field in the bulk. The scalar field will be described by the action

$$S_{\phi,m} = -\frac{1}{16\pi G} \int d^d x \sqrt{-g} \partial_\mu \phi \partial^\mu \phi + m^2 \phi^2. \quad (1.30)$$

Near the conformal boundary, we can solve the resulting Klein-Gordon equation in a series. Taking the metric to be written in Fefferman-Graham coordinates, the scalar field solving the equations of motion has the form[23]

$$\phi = z^{d-\Delta} \left( \phi_0 + z^2 \phi_2 + \dots z^{2\Delta-d} (\phi_{2\Delta-d} + \log z \phi_l) \right) + O(z^{\Delta+1}). \quad (1.31)$$

<sup>6</sup>An arbitrary coefficient in the stress tensor coming from a finite counter term you can add to the action [23].

Here  $\phi_0$  and  $\phi_{2\Delta-d}$  are the two free pieces of information in the boundary expansion.  $\Delta$  satisfies

$$\Delta(\Delta - d) = \ell^2 m^2. \quad (1.32)$$

We can consider the holographic interpretation of the theory consisting of this scalar field of mass  $m$  coupled to gravity. We define the generating function to be

$$W_{\text{CFT}}^\Delta[J(x)] = -S_{\phi,m}|_{\phi_0(x)=J(x)}. \quad (1.33)$$

So we've chosen to solve the bulk equations subject to boundary conditions that fix  $\phi_{d-\Delta}(x)$ . The calculation of the renormalized on-shell action in the bulk for this theory for the case where the scalar is on a fixed background of AdS is described in [17], with the more general case where it is coupled to gravity in [23]. The vacuum expectation value of the operator  $\Phi(x)$  conjugate to the source  $J(x)$  in the CFT is<sup>7</sup>

$$\langle \Phi(x) \rangle_J \equiv \frac{\delta W_{\text{CFT}}^\Delta[J]}{\delta J(x)} = 2c_{\text{eff}} (2\Delta - d) \phi_{(2\Delta-d)}(x). \quad (1.34)$$

The one-point function of the dual field is therefore given by the  $z^\Delta$  term in the expansion of the solution. It is clear from construction that this operator is a scalar, in fact it is a primary scalar field of dimension  $\Delta$  (sourced by a primary scalar classical source  $J$  of dimension  $d - \Delta$ ). We can see this by noting that a Weyl scaling is generated by  $z \rightarrow z/\lambda$ , under which  $h^{(0)} \rightarrow \lambda^2 h^{(0)}$ , and our fields transform as

$$\begin{aligned} \Phi(x) &\rightarrow \lambda^{-\Delta} \Phi(x) \\ J(x) &\rightarrow \lambda^{\Delta-d} J(x) \end{aligned} \quad (1.35)$$

which are the scaling transformation laws for the field and a source for a primary scalar field of scaling dimension  $\Delta$ .

### 1.6.3 Global U(1) symmetry - a Chemical Potential

A situation that often arise in AdS/CMT is when we have a conserved particle number or charge density in the condensed matter system. We may then want to consider states that are 'finite density' with respect to this. This can be done by adding a chemical potential as a source term for this current density on the boundary<sup>8</sup>.

This vector chemical potential has to be the boundary condition for a bulk field. In fact the bulk field is a gauge field. As discussed in [13], we add a gauge field to the bulk action leaving us with Einstein-Maxwell

$$S_{\text{EYM}} = \int \frac{1}{16\pi G} \left( R + \frac{d(d-1)}{\ell^2} \right) - \frac{F^2}{4g^2}. \quad (1.36)$$

<sup>7</sup>This differs by a factor of  $\frac{1}{8\pi G}$  from the value in [23] because we've normalized our scalar field differently here.

<sup>8</sup>In other words, we are now considering a Grand Canonical Ensemble.

The global  $U(1)$  symmetry associated to the conserved current on the boundary is the global part of the local  $U(1)$  gauge symmetry in the bulk. If we restrict ourselves to static, electric configurations, then the gauge field can be written in terms of an electric potential  $A_t = \phi$ , and has a near boundary expansion

$$\phi = \chi(x) + \dots - \psi(x)z^{d-2} + \dots \quad (1.37)$$

where both  $\chi$  and  $\psi$  are free from the point of view of this expansion.

The holographic interpretation of this Einstein-Maxwell theory is to consider the generating function

$$W_{\text{CFT}}[h_{\mu\nu}, \Xi] = -S_{\text{EYM}}|_{\chi=\Xi, h^{(0)}=h}. \quad (1.38)$$

The one-point function of the conserved current is given by  $\langle \rho(x) \rangle = \frac{\delta W_{\text{CFT}}}{\delta \Xi(x)} \sim \psi(x)$ .

## 1.7 Holography on Simple Spaces

We shall now describe the simplest examples of holographic CFT states. We will consider universal sector states on flat space, a sphere, and a torus, and we will then give a basic example beyond the universal sector.

### 1.7.1 Flat Space: Poincaré AdS and the AdS Black Brane

The simplest bulk spacetime where the boundary is flat Minkowski space is Poincaré AdS [14]

$$ds^2 = \left(\frac{\ell^2}{z^2}\right) \left(dz^2 + \eta_{ab}dx^a dx^b\right). \quad (1.39)$$

The conformal boundary is at  $z = 0$ , and the  $x^a$  are the coordinates in the boundary. This bulk geometry represents a maximally symmetric CFT vacuum state. The global Poincaré symmetry in the boundary  $x^\mu$  coordinates is manifest, as is the scale invariance through  $z \rightarrow \lambda z$  and  $x^a \rightarrow \lambda x^a$ . In fact, this geometry is invariant under the full  $d$  dimensional conformal group  $\text{SO}(d,2)$ . We can also immediately see that the one-point function of the stress tensor  $T_{ab} = 0$ , as this metric is already in Fefferman-Graham coordinates.

An alternative bulk geometry which breaks the scale invariance is given by [13]

$$ds^2 = \left(\frac{\ell^2}{z^2}\right) \left(\frac{dz^2}{f(z)} - f(z)dt^2 + \delta_{ij}dx^i dx^j\right) \quad (1.40)$$

with  $f(z) = 1 - z^d/z_0^d$ . The indices  $i, j$  run over the spatial directions on the boundary and the  $x^i$  are coordinates on these spatial sections. There is a planar black hole horizon at  $z = z_0$ . The presence of this horizon means that the CFT partition function is at finite temperature. To find this temperature, we transform to Euclidean signature and demand that the axis where the time circle shrinks is regular. The resulting size of the time circle gives the inverse temperature. Near the horizon, writing  $z = z_0 + \epsilon\rho^2$  the metric takes the

form

$$ds^2 = \frac{\ell^2}{z^2} \delta_{ij} dx^i dx^j + \epsilon \left( \frac{4d\rho^2}{-f'(z_0)} + \rho^2 dt^2 f'(z_0) \right) + O(\epsilon^2). \quad (1.41)$$

For this to be smooth, the time coordinate has to have period  $\beta = -\frac{4\pi}{f'(z_0)} = \frac{4\pi z_0}{d}$ . The CFT temperature is then  $T = 1/\beta$ .

Unsurprisingly, for these finite temperature states the stress tensor does not vanish. To transform to Fefferman-Graham coordinates we write

$$z = Z \left( 1 - \frac{Z^d}{2dz_0^d} + O(Z^{d+1}) \right) \quad (1.42)$$

which yields a stress tensor with non-vanishing diagonal elements. In particular,  $T_{tt} = c_{\text{eff}} \frac{d-1}{z_0^d}$ .

These black-brane spacetimes (1.40) have a conformal boundary at  $z = 0$ , and end on a black-brane horizon at  $z = z_0$ . In Poincaré AdS (1.39) there is also a horizon, although it's less obvious in this case. There is an extremal horizon, that in these coordinates can be reached by taking  $z, x^i \rightarrow \infty$  while keeping their ratios finite[31]. An extremal horizon is a type of black hole horizon with vanishing surface gravity, and so vanishing temperature.

### 1.7.2 The Sphere: Global AdS and the Hawking Page Transition

The universal sector vacuum state with a round sphere on the boundary is global AdS as in (1.11). This is a unit sphere, but we can vary the radius simply by rescaling  $t \rightarrow \frac{t}{\mathcal{R}}$ ,  $r \rightarrow \mathcal{R}r$  to get

$$g_{\text{AdS}} = - \left( \frac{\ell^2}{\mathcal{R}^2} + r^2 \right) dt^2 + r^2 \mathcal{R}^2 d\Omega_{d-1}^2 + \ell^2 \frac{dr^2}{\frac{\ell^2}{\mathcal{R}^2} + r^2}. \quad (1.43)$$

At finite temperature, things get a bit more complicated. As discussed in [8], unlike the flat space case, on a sphere there are two possible competing finite temperature spacetimes which preserve the spherical symmetry. One is simply to take (1.43) at finite temperature, thermal AdS, and the alternative is a black hole spacetime, AdS-Schwarzschild

$$ds^2 = -f(r)dt^2 + \frac{\ell^2 dr^2}{f(r)} + r^2 d\Omega_{d-1}^2 \quad (1.44)$$

with

$$f(r) = \frac{\ell^2}{\mathcal{R}^2} + r^2 - \frac{r_h^{d-2} \left( \frac{\ell^2}{\mathcal{R}^2} + r_h^2 \right)}{r^{d-2}}. \quad (1.45)$$

To figure out which one dominates in the saddle point approximation for the partition function at a given temperature, you have to compare their free energies. To compute this, we need to extract the holographic stress energy tensors of the two spacetimes. Now, in even dimensions we would in principle have to worry about the contribution of the conformal anomaly. However this term is just a function of the background metric in the

CFT, and so since we are going to be only interested in the difference of free energy in two solutions with the same boundary metric we can drop it.

The AdS-Schwarzschild black holes are a one-parameter family of solutions that we can label by their horizon size,  $r_h$ . The temperature as a function of horizon size is given by

$$T = \frac{dr_h^2 + (d-2)\ell^2}{4\pi r_h \mathcal{R} \ell^2}. \quad (1.46)$$

This diverges for small or large radius, and has a minimum value  $T_{\min} = \frac{\sqrt{d(d-1)}}{2\pi\ell}$ . In the Euclidean picture, this temperature is the inverse size of the Euclidean time circle, and this is fixed by smoothness when this circle shrinks at the horizon. In thermal AdS on the other hand, this thermal circle never shrinks, so there is no constraint from smoothness, and so it makes a contribution to the partition function at any temperature.

For  $T < T_{\min}$ , thermal AdS is therefore the only saddle point. For  $T > T_{\min}$  on the other hand there are three possibilities, thermal AdS, and a small or large black hole. The free energy of the black hole solution as a function of horizon size, compared to thermal AdS of the same temperature is

$$F = c_{\text{eff}} \frac{\Omega_{d-1}}{\ell \mathcal{R}} \left(1 - \frac{r_h^2}{\ell^2}\right) \left(\frac{r_h}{\ell}\right)^{d-2}. \quad (1.47)$$

This is positive, so the free energy is greater than thermal AdS, for  $r_h < \ell$ . A transition happens at  $r_h = \ell$ , which corresponds to the larger black hole at the Hawking-Page temperature  $T_{\text{HP}} = \frac{d-1}{2\pi\ell\mathcal{R}}$ .

At  $T = T_{\text{HP}}$  we therefore undergo a phase transition, and the large black hole branch describes the state of the field theory. This is interpreted as a confinement/deconfinement transition in the CFT, with thermal AdS for  $T < T_{\text{HP}}$  describing a confined phase[3, 32]. There are several ways this interpretation can be motivated, but the simplest is just to look at the behaviour of the energy. The energy extracted from the holographic stress tensor in the confined phase is independent of  $T$ , since the bulk spacetime is just global AdS. Because of the large  $N$  limit, this energy should really be interpreted as the  $O(c_{\text{eff}})$  component of the energy in the field theory, so what this is saying is that, for  $T < T_{\text{HP}}$ ,  $E - E_{\text{vac}} \sim O(1)$ . For  $T > T_{\text{HP}}$ , the spacetime is a black-hole spacetime that varies with temperature, so the holographic stress tensor varies, and so  $E(T) - E_{\text{vac}} \sim O(c_{\text{eff}})$ . This is consistent with a deconfined phase at high temperature, and a phase transition to a confined phase at low temperature. For instance, in the  $\mathcal{N} = 4$  SYM example, the effective number of degrees of freedom in a deconfined phase is the number of ‘quarks’ which goes as  $N^2$ , and in a confined phase the quarks are restricted to an  $O(1)$  number of singlet states [8].

### 1.7.3 The Torus

There are two different vacuum solutions which we can consider when the boundary is a torus. The simplest thing we can do is take the Poincaré patch of AdS

$$ds^2 = \frac{dz^2 - dt^2 + \delta_{ij} dx^i dx^j}{z^2} \quad (1.48)$$

and periodically identify the  $x^i$  coordinates. The resulting geometry is smooth except for a null singularity in the place of the extremal horizon in the IR, which we will explain in Chapter 3.5. There is an alternative geometry given by the AdS-Soliton, which is a double wick rotated black brane[33]

$$ds^2 = r^2(-dt^2 + \delta_{ij} dx^i dx^j) + \frac{\ell^2 dr^2}{f(r)} + f(r) \mathcal{R}^2 d\theta^2. \quad (1.49)$$

with  $f(r) = r^2 \left(1 - \frac{r_0^d}{r^d}\right)$ ,  $r_0 = \frac{2\ell}{d\mathcal{R}}$ , and the  $\theta$  coordinate has canonical period  $2\pi$ . One of the  $S_1$  factors in the boundary, the one described by  $\theta$ , now plays a special role. On the boundary this circle has radius  $\mathcal{R}$ , but into the bulk its radius shrinks compared to the other dimensions of the torus, until it smoothly caps off at  $r = r_0$ . This point where it shrinks is the double wick rotation of the horizon from the black brane. This solution is only allowed if we take antiperiodic boundary conditions for the fermions around this shrinking circle[8].

If we take the AdS black brane which describes finite temperature states on flat space and periodically identify it we get a smooth bulk geometry which can describe finite temperature states on the Torus. However, as in the case of the sphere, we can also simply take the zero temperature vacuum and trivially put it at finite temperature, giving a confining finite temperature bulk state. There is a thermodynamic competition between these three possibilities which we resolve by comparing their free energy densities[8]

$$\begin{aligned} f_{\text{Thermal AdS}} &= 0 \\ f_{\text{AdS Soliton}} &= -c_{\text{eff}} \ell \left(\frac{4\pi}{d\mathcal{R}}\right)^d \\ f_{\text{Black Brane}} &= -c_{\text{eff}} \ell \left(\frac{4\pi T}{d}\right)^d. \end{aligned} \quad (1.50)$$

We see that, while thermal AdS is never preferred, there is a phase transition between the black brane and the AdS-Soliton at  $T = \frac{1}{\mathcal{R}}$ . This phase transition only happens if the AdS-Soliton is allowed by the boundary conditions on the fermions.

### 1.7.4 Chemical-Potential - Reissner-Nordstrum Black Branes

To add a chemical potential to the boundary, we add a Maxwell field to the bulk, and solve the equations of motion corresponding to the action  $S_{\text{EYM}}$  (1.36). There are translationally symmetric electrically charged black-brane solutions, where the metric is of the

form (1.40), but with[13]

$$f(z) = 1 - \left(1 + \frac{z_+^2 \mu^2}{\gamma^2}\right) \left(\frac{z}{z_+}\right)^d + \frac{z_+^2 \mu^2}{\gamma^2} \left(\frac{z}{z_+}\right)^{2(d-1)} \quad (1.51)$$

where  $\gamma^2 = \frac{(d-1)g^2 \ell^2}{(d-2)8\pi G}$ . These solution has in addition a gauge field<sup>9</sup>

$$A = \mu \left(1 - \left(\frac{z}{z_+}\right)^{(d-2)}\right) dt. \quad (1.52)$$

The chemical potential on the boundary is  $\mu$ , and there is a resulting charge density in the CFT  $\rho \sim \frac{\mu}{z_+^{d-2}}$ . These solutions have a temperature[13]

$$T = \frac{1}{4\pi z_+} \left(d - \frac{(d-2)z_+ \mu^2}{\gamma^2}\right). \quad (1.53)$$

## 1.8 Applications of the correspondence

### 1.8.1 Condensed Matter - AdS/CMT

One promising application of this correspondence is in Condensed Matter systems. This is reviewed in [13]. There are real world physical systems with quantum critical points (zero temperature phase transitions), where near the critical point, the effective degrees of freedom are strongly interacting. The lack of weakly coupled quasi-particles means that the usual effective field theory methods of condensed matter cannot be applied.

Using AdS/CFT, strongly coupled systems with properties similar to these quantum critical systems can be constructed. An example of this is the construction of holographic models of superconductors, reviewed in [34, 35]. S-wave models can be constructed by considering gravitational bulks which are black hole solutions which develop scalar ‘hair’, a non-trivial static scalar field outside of the horizon, below some critical temperature. This scalar field is dual to a primary scalar operator in the CFT, as in Section 1.6.2. When the black hole develops hair, the dual scalar operator picks up a non-zero expectation value. This is the analogue of the bosonic condensate in BCS superconductors. Along with the scalar field, these bulk black holes also involve a Maxwell field, which is dual to a conserved current on the boundary as in 1.6.3. By adding an  $SU(2)$  yang-mill’s field, or a charged rank 2 tensor, p-wave and d-wave models can also be constructed, with corresponding vector or spin-2 condensates[35].

By looking at linear fluctuations of this Maxwell field, you can find how the dual current in the CFT responds to an applied potential, and so study the conductivity of these holographic superconductors[34]. This is one way that it is hoped to be able to make comparisons with real world superconductors, and so gain a better understanding of their physics. An important feature of real world superconductors is that they are not

<sup>9</sup>The gauge field vanishes on the horizon, which is required by smoothness[13].

necessarily homogeneous and isotropic, often with lattice structures that break the symmetry. This can be achieved by breaking the symmetry in our gravitational bulks. For instance, in [36], bulk spacetimes are numerically constructed with a periodic chemical potential on the boundary. This periodic chemical potential is a model for the lattice background for the superconductor, and the dependence of conductivities on the structure of this lattice can be explored.

### 1.8.2 Heavy Ion Collisions, QGP, and the Fluid/Gravity Correspondence

Another example of a strongly coupled field theory that AdS/CFT might shed some light on is QCD. While QCD itself does not have a known holographic dual, you can still hope to explore qualitative features by studying theories which do have gravitational duals, like  $\mathcal{N} = 4$  SYM [37]. In particular, the quark-gluon plasma (QGP), in which QCD is in a deconfined phase, is a regime that is not very well understood using other techniques.

The QGP is produced soon after heavy ion collisions in detectors like RHIC, and is very quickly in local thermodynamic equilibrium (LTE), with the temperature and local densities<sup>10</sup> sufficiently slowly varying functions of position for a hydrodynamic description to be valid[38]. This regime can be described in the gravitation bulk with a corresponding long wavelength expansion of solutions Einstein's equation, which was introduced in [39] and is reviewed in [38, 40]. This is called the Fluid/Gravity correspondence. The long wave-length expansion allows you to construct bulk geometries that can describe LTE by starting with global thermodynamic equilibrium solutions (like the AdS black brane (1.40)), allowing parameters like the temperature to be slowly varying functions of position, and adding corrections with increasing numbers of gradients of these parameters. Among the properties that can be considered in this way is a local entropy current [41], the viscosity to entropy ratio [42] and the behaviour of shock waves [43, 44]. The correspondence has also been generalized to charged fluids[45, 46].

The applicability of AdS/CFT to heavy ion collisions isn't limited to the hydrodynamic regime of QGP. For example in [47, 48], they studied boost invariant solutions to Einstein's equation to try to understand how fast a QGP should thermalize and admit a hydrodynamic description after a collision. Another avenue of study involves looking at single quarks travelling through a homogeneous QGP, which is described in the bulk by a string on the background of an AdS-Schwarzschild black brane(1.40). This example is described in detail in the review[37]. The string ends on the conformal boundary, and this end point of the string corresponds to the location of the quark in the QGP. The back-reaction of this string on the bulk geometry can be used to extract the linear response of the QGP to the moving quark. This interaction between the QGP and the quark may be crucial in understanding features of heavy ion collision events like jet splitting.

<sup>10</sup>energy densities, charge densities, etc...

## 1.9 Evidence for the Correspondence

Of course, there is no complete proof of the AdS/CFT correspondence, it is a conjecture; so we conclude this introduction with a few reasons why this duality is believed to hold. Firstly, as we pointed out in Section 1.4.1, a partition function on AdS, written in terms of a Lagrangian which is a scalar, and supplemented with boundary conditions at the conformal boundary, has the right symmetries to be viewed as the generating function of a CFT on this conformal boundary. The question is whether this is a consistent CFT, and if so what specific theory it is.

Maldacena's argument from Section 1.1.1 tells us that we can use the low energy description of a stack of D-branes to tell us what theory this is. It is then possible to compare quantities on both sides of the correspondence. For instance, the global symmetries, and the spectra of supersymmetric states[7] have been matched up. However, most physical observables are functions of parameters in the theory, and often calculations of these quantities use perturbative expansions that rely on some coupling constant or similar parameter being small. This means that there is no reason to expect all quantities to agree unless there is some symmetry that determines their dependence on coupling. For instance, in [33] the AdS-Soliton (1.49) bulk is used to calculate the Casimir energy of a non-supersymmetric vacuum state. This is compared to a corresponding calculation in the field theory, and the two are found to differ by an overall factor. This is not unexpected, because the field theory calculation in question is only valid when the CFT is weakly coupled, while we can only ignore quantum corrections to the gravitational description when the CFT is strongly coupled. However, there are cases when you can use symmetries to compute quantities exactly. For instance, in [49] they were able to match the large  $N$  limit of the free energy on a class of deformed 3-spheres with rigid supersymmetry, computed exactly using a technique called localization, to the corresponding calculation of the renormalized action in a dual gravitational bulk.

One tool that allows a direct comparison between quantities in the CFT and in the string theory is integrability[50]. In the t'Hooft planar limit,  $\mathcal{N} = 4$  SYM becomes integrable. This is a very special property for a theory to have which means, for instance, that the spectrum of scaling dimensions of local operators can be computed exactly (in terms of solutions to algebraic equations) as a function of t'Hooft coupling  $\lambda = g_{YM}^2 N$ . At weak coupling, this can be compared to perturbative calculations in the planar gauge theory, while at strong coupling it can be compared to free classical strings. The quantities that have been compared in this way are found to agree[50].

## Chapter 2

# Numerical Methods for Gravity

What we have learnt is that we can calculate the leading order large ‘ $N$ ’ behaviour of certain strongly coupled CFTs by solving classical field equations. The classical field equations in question is Einstein’s equation of general relativity with negative cosmological constant, sometimes with additional matter fields. In  $d + 1$  dimensions, we write Einstein’s equation as

$$R_{\mu\nu} + \frac{d}{\ell^2}g_{\mu\nu} = \tilde{T}_{\mu\nu}, \quad (2.1)$$

where  $\tilde{T}_{\mu\nu} = T_{\mu\nu} - \frac{1}{2}Tg_{\mu\nu}$  is a source term coming from the stress tensor  $T_{\mu\nu}$  of any matter fields we consider.

Together with the equations of motion of these matter fields, these form a set of coupled, second order, non-linear PDEs. The problem of finding their general solution is of course unsolved, so in order to make progress you have to either

1. Assume sufficient symmetry to solve the problem analytically (typically enough symmetry to reduce to ODEs)
2. Assume less symmetry, and solve the resulting set of PDEs numerically.
3. Try and prove general statements about solutions

In this section we’re going to explain the numerical methods involved in option 2. In Chapters 4 and 7, we will be numerically solving the static Einstein’s Equation, sometimes coupled to a Maxwell field or a scalar field. In both cases, we will be assuming sufficient symmetry to reduce the problem to a set of two dimensional PDEs. The techniques I will discuss were developed for the static solutions in [51], and further developed in [52], with a generalization to the stationary case in [53]. We will restrict our discussion to static spacetimes, since our application of these methods will be limited to this case. In what follows, it will be convenient to analytically continue these static solutions to Euclidean signature (replacing the time coordinate  $t$  with  $\tau = it$ ), leaving us with a Riemannian metric. At finite temperature, the resulting Riemannian manifolds have a compact time coordinate with a period given by the inverse temperature[54].

### 2.1 Coming up with a well-posed Problem

When faced with a numerical problem like finding a solution of Einstein’s equation, the first thing that needs to be done is to state the problem in such a way that there is a

unique solution. Part of this is making sure you've fixed enough boundary conditions. This can sometimes be a subtle problem, and we won't attempt to address it in general, but we will go into more specifics when we come to the explicit cases in the thesis. The spacetimes we consider have a conformal boundary, and we will fix data for the bulk metric and other fields at this boundary. This fixed data will determine the metric on the conformal boundary and the sources for the CFT operators dual to any matter fields we consider as in 1.6.

The other part of posing the problem unambiguously is getting rid of any gauge symmetry. In particular, GR has coordinate invariance. This means that for any metric that solves our equations with the boundary conditions we've applied, we can perform any one of an infinite number of coordinate redefinitions to get another, physically equivalent, but numerically different solution to the problem.

### 2.1.1 The Harmonic Einstein Method

In order to completely specify the problem of solving the static Einstein's equation, we need to get rid of the coordinate freedom by imposing a gauge condition. Instead of doing this directly, we are going to circumvent this problem using the following gauge fixing trick first developed in [51].

The problem of the gauge freedom manifests itself in the fact that the differential equations are only weakly elliptic[51]. By this we mean that if we take the principal symbol (two derivative terms) in  $R_{\mu\nu}$  and look at its linear shift about some background  $g_{\mu\nu} \rightarrow g_{\mu\nu} + h_{\mu\nu}$ , then there are unphysical wavelike modes in  $h_{\mu\nu}$  for which this vanishes. More concretely, the shift in the Ricci tensor is given by

$$\delta R_{\mu\nu} = -\frac{1}{2}g^{\alpha\beta}\partial_\alpha\partial_\beta h_{\mu\nu} - \frac{1}{2}\partial_\mu\partial_\nu h + g^{\alpha\beta}\partial_\alpha\partial_{(\nu}h_{\mu)\beta} + \dots \quad (2.2)$$

where ... refers to lower derivative terms. Note that the  $\partial_\alpha$  are just partial derivatives, not covariant derivatives, because we are only interested here in the two derivative terms. Then if we take  $h_{\mu\nu} = \partial_{(\mu}\chi_{\nu)}$  for some vector  $\chi$ , this principal part vanishes. In fact, if we take  $h_{\mu\nu} = \nabla_{(\mu}\chi_{\nu)}$ , then this is precisely a coordinate transformation. It's these gauge degrees of freedom that we need to get rid of.

The trick is instead of solving Einstein's equation, to solve

$$R_{\mu\nu}^H \equiv R_{\mu\nu} - \nabla_{(\mu}\xi_{\nu)} - \frac{d}{\ell^2}g_{\mu\nu} = 0, \quad (2.3)$$

where we have defined  $\xi^\mu = g^{\alpha\beta}(\Gamma_{\alpha\beta}^\mu - \bar{\Gamma}_{\alpha\beta}^\mu)$ , for  $\bar{\Gamma}_{\alpha\beta}^\mu$  as some fixed reference connection. This is referred to as the Harmonic Einstein's equation. If it so happens that in solving this equation, we find a solution such that  $\xi = 0$  then we have in addition solved Einstein's equation. These equations are elliptic for Riemannian metrics[51]. This follows from the fact that the two derivative term in the linearised equation now looks like

$$\delta R_{\mu\nu}^H = -\frac{1}{2}g^{\alpha\beta}\partial_\alpha\partial_\beta h_{\mu\nu} + \dots \quad (2.4)$$

which does not have any equivalent to the gauge modes above. The Harmonic Einstein's equation 2.3 is still covariant, because  $\xi^\mu$  being constructed from the difference of two connections is a proper vector. The coordinate invariance is broken by the fact that when we solve the equations we will choose an explicit form for the components of  $\bar{\Gamma}_{\beta\gamma}^\alpha$ .

## 2.2 Asymptotics of the reference connection and a maximum principle for $\xi$

The method outlined above is to solve the Harmonic Einstein's equation and 'hope' that the solution we find satisfies  $\xi = 0$ , and so is a solution of Einstein's equation. In fact, in certain situations it has been proved that this is exactly what will happen[52]. We reproduce this proof here because we will make use of it later on.

Let's assume we've managed to find a (Euclidean) static solution with no matter fields

$$R_{\mu\nu} - \nabla_{(\mu}\xi_{\nu)} - \Lambda g_{\mu\nu} = 0, \quad (2.5)$$

such that  $\xi \neq 0$  (such solutions are called Ricci Solitons). Using the contracted Bianchi identities one can show

$$\nabla^2 \xi_\mu + R_{\mu\nu} \xi^\nu = 0 \quad (2.6)$$

$$(\nabla^2 + \xi^\mu \partial_\mu) \phi = -2\Lambda \phi + 2(\nabla^\mu \xi^\nu)(\nabla_\mu \xi_\nu), \quad (2.7)$$

where  $\phi = \xi^\mu \xi_\mu$ . The right hand side of (2.7) is positive definite. This means we have the inequality

$$(\nabla^2 + \xi^\mu \partial_\mu) \phi > 0. \quad (2.8)$$

For Riemannian metrics, this inequality obeys a maximum principle. Any function  $\phi$  that satisfies (2.8) in some region  $\mathcal{M}$ , attains its maximum on the boundary of that region  $\partial\mathcal{M}$ . For static solutions  $\phi \geq 0$ , so if  $\phi = 0$  on  $\partial\mathcal{M}$  then  $\phi = 0$  throughout  $\mathcal{M}$ .

This boundary includes the conformal boundary, but the spacetime domains we consider will sometimes have other boundaries, such as for instance finite temperature horizons. However, since we are considering static solutions, the analytically continued Euclidean geometry in fact no longer has a boundary at the horizon[54]. It is instead just a fixed point of Euclidean time translations generated by  $\frac{\partial}{\partial\tau}$ . From the point of view of this maximum principle, therefore,  $\phi$  cannot be maximized on a horizon<sup>1</sup>.

In certain cases we will consider, there will also be boundaries that aren't finite temperature horizons, but in those cases we will have symmetries that prevent  $\phi$  from being maximized there. Therefore, for the cases we will be interested in, the only relevant

<sup>1</sup>This also means that we don't need to treat the horizon as a boundary from the point of view of our PDEs. We need to make sure it is smooth, but so long as this Euclidean picture gives a smooth geometry at the horizon the horizon is regular. We can build our metric ansatz in such a way that this happens automatically and no explicit boundary conditions need to be applied.

boundary will be the conformal boundary of the spacetime. If we choose boundary conditions such that  $\phi = 0$  on the conformal boundary, Ricci Solitons are in this way ruled out.

When we choose our reference connection  $\bar{\Gamma}^e_{\mu\nu}$ , we can choose it in such a way that our boundary conditions on the metric at the conformal boundary imply that  $\phi = \xi^\mu \xi_\mu$  vanishes on this boundary. For convenience, we will construct the reference connection from a reference metric  $\bar{g}$ . At the conformal boundary, the vanishing of  $\phi$  is then assured by making sure that the leading order behaviour in the reference metric matches the solution.

As discussed in 1.4.1, near the conformal boundary, the metric can be written in the form

$$g_{\mu\nu} = \frac{G_{\mu\nu}}{z^2}, \quad (2.9)$$

for some regular metric  $G_{\mu\nu}$ , where the conformal boundary is at  $z = 0$ . The boundary conditions we apply to  $g_{\mu\nu}$  will fix  $G_{\mu\nu}$  at  $z = 0$ . If we choose a reference metric that also has a conformal boundary in the same place,

$$\bar{g}_{\mu\nu} = \frac{\bar{G}_{\mu\nu}}{z^2}, \quad (2.10)$$

then so long as  $\bar{G}_{\mu\nu} = G_{\mu\nu}$  at  $z = 0$ ,  $\phi$  vanishes at the conformal boundary. This means that if we choose our reference connection to satisfy the same boundary conditions here as the solution, we can rule out Ricci Solitons. This result no longer holds automatically with the addition of matter fields, so in the most general case we need to check that  $\phi = 0$  on our solutions.

## 2.3 Choosing an Ansatz

We now have a well defined problem to solve, so the next step is choosing an ansatz for the metric. This ansatz has to be the most general metric corresponding to the symmetries, because all the coordinate fixing is done by the choice of reference connection in the Harmonic Einstein's equation (2.3). Another useful property is for smoothness of the metric to translate into smoothness of the functions in the ansatz.

An example where smoothness of the functions does not translate into smoothness of the corresponding metric is 2-d polar coordinates

$$ds^2 = A(r, \phi)dr^2 + B(r, \phi)r^2d\phi^2. \quad (2.11)$$

Here the  $\phi$  coordinate is compact, and there is a point  $r = 0$  where the circle described by  $\phi$  shrinks to zero. The coordinates therefore break down here, so smoothness of the functions  $A$  and  $B$  at  $r = 0$  does not translate into smoothness of the metric. For instance, if  $A(r, \phi) = 1$ , and  $B(r, \phi) = \alpha^2$ , this is the metric of a cone, and unless  $\alpha = 1$ , there is a conical singularity at the tip  $r = 0$ . Once  $\phi$  dependence gets introduced, the conditions for the geometry to be smooth at  $r = 0$  become much more complicated, so diagnosing

whether a given choice of  $A$  and  $B$  corresponds to a smooth choice of metric becomes cumbersome.

On the other hand, writing the problem in a Cartesian coordinate system

$$ds^2 = \tilde{A}(x, y)dx^2 + \tilde{B}(x, y)dy^2 \quad (2.12)$$

where both coordinates are now non-compact, means that smoothness of the functions automatically translates into smoothness of the corresponding metric, so long as  $A \neq 0$  and  $B \neq 0$  everywhere<sup>2</sup>.

## 2.4 Discretize

Having chosen coordinates and an ansatz, the differential equations then need to be discretized. This involves choosing a lattice of points to replace the continuous domain, and constructing approximations of the derivative operators on these lattices. Our continuous functions become a vector of values, with each element corresponding to the value of the function at a point in the lattice. The discretized version of derivative operators are matrices that act on these vectors. There are various methods for constructing these derivative matrices, and through the work presented in this thesis we make use of a few different ones. Which one we use depends on the smoothness of the solutions we are looking for, and on the boundary conditions.

We will be solving two dimensional problems on square lattices, so we can discretize each coordinate separately. Namely we take a pair of coordinates,  $x, y$ , discretize each using one of the methods described here, and then the full 2d lattice is simply the outer product of those two 1d lattices. Mixed derivatives like  $\frac{\partial^2}{\partial x \partial y}$  are simply calculated by applying the derivative matrices for each of the 1d lattices one after the other.

Perhaps the most straight forward discretization method is finite difference described, for instance, in section 5.7 of [55]. In this case we take a regularly spaced<sup>3</sup> grid of points. Derivatives are then approximated locally. For order  $n$  finite difference, at each point, we effectively find the order  $n$  polynomial that passes through the point and the  $n/2$  points to either side. The approximation for the derivatives is then the explicit values of the derivatives of this polynomial. At each point in the lattice we're fitting a separate polynomial. The resulting derivative matrices only take values in a band  $n + 1$  columns wide around the diagonal<sup>4</sup>.

With periodic boundary conditions, Fourier methods are natural. Instead of a separate fit to the function around each point in the lattice, we approximate our function by an expansion in Fourier modes. There are as many modes as lattice points so that the

<sup>2</sup>Equivalently  $\frac{\partial}{\partial x}$  and  $\frac{\partial}{\partial y}$  are a well defined set of basis vector fields everywhere, so a metric that acts on them smoothly acts on all vector fields smoothly. In contrast,  $\frac{\partial}{\partial r}$  and  $\frac{\partial}{\partial \phi}$  are not well defined at the origin, so even if the metric acts on these vector fields smoothly everywhere they are defined, that isn't enough to guarantee smoothness at the origin.

<sup>3</sup>Regularly spaced in coordinate distance. The physical distance between the points will of course be determined by the metric, which is what we are solving for, so is initially unknown.

<sup>4</sup>This is true in the middle of the lattice, towards the boundary the story is a bit more complicated.

function values at the lattice points uniquely specify the expansions and vice-versa. The Fourier expansion then determines the derivative operators. Because we are expanding the whole function in a basis of functions, we are effectively doing a global rather than a local fit, and as such the resulting derivative matrices have non-zero entries everywhere.

If you expect your solution functions to be infinitely differentiable, then pseudospectral interpolation can be used. This makes use of the Chebyshev polynomials[55]

$$T_n(x) = \cos(n \arccos x), \quad (2.13)$$

for integer  $n \geq 0$ . Like the Fourier interpolation this involves an expansion in a basis of functions. The functions  $T_n$  can be used as a basis for the domain  $-1 \leq x \leq 1$ <sup>5</sup>. The lattice consists of the Chebyshev points

$$x_n = \cos\left(\frac{n\pi}{N}\right) \quad (2.14)$$

for  $n = 0, 1, 2, \dots, N$ . A set of values at these points  $f_n$ , determines a function of the form

$$f(x) = \sum_{n=0}^N \tilde{f}_n T_n(x) \quad (2.15)$$

which takes these values at these points,  $f(x_n) = f_n$ <sup>6</sup>. This expansion is used to determine the derivative matrices. This interpolation method is described in Chapter 5 of [55], but the way in which we use it with a Chebyshev lattice is described in Chapter 6 of [56].

In the same way that the spectral methods build in periodic boundary conditions, we can build other types of symmetry into our discretization method. One which we will make use of quite a lot is a parity symmetry. It is often convenient to limit ourselves to functions  $f(x)$  which are either even or odd under  $x \rightarrow -x$ . Say we are solving for such functions in the domain  $-1 \leq x \leq 1$ , then we can simply construct a lattice and derivative operators that build this in, and reduce the memory cost. First we construct a lattice that runs over the whole domain, and then we project our derivative operators on to functions with the correct symmetry, giving us an effective lattice that runs only over half the points  $0 < x \leq 1$ . More explicitly, we start with  $n$  points running between  $-1$  and  $1$  (with  $n$  even). We construct our  $n \times n$  derivative matrices using whichever method we choose. We then construct  $n/2 \times n/2$  versions of these derivatives, that act just on the  $n/2$  points between  $0$  and  $1$ , by assuming that the other points on the other half of the lattice have the values they should have based on the parity symmetry.

## 2.5 Solution of Discretized System

Once we've discretized these equations, we are left with a set of non-linear simultaneous equations for the function values at the lattice sites. Think of the set of function values as

<sup>5</sup>We will map this domain linearly to the domains we end up using in our problems.

<sup>6</sup>The vectors  $f_n$  and  $\tilde{f}_n$  are related by a discrete cosine transformation.

a vector  $\phi_i$  and the set of equations as a vector function of this vector

$$R^a(\phi_i) = 0. \quad (2.16)$$

We will solve these systems using Newton-Raphson iteration. The one dimensional version of this is described in section 9.4 of [55]. Start by making an initial guess  $\phi_i = \phi_i^{(0)}$ . Then linearise the system about this guess,

$$R^a(\phi_i^0 + \delta\phi_i) \approx R^a(\phi_i^0) + \frac{\partial R^a}{\partial \phi_i} |_{\phi^0} \delta\phi_i = 0. \quad (2.17)$$

We then solve this linear system to get an improved guess  $\phi_i^1 = \phi_i^0 + \delta\phi_i$ , and proceed iteratively. In this way you, hopefully, converge on the solution.

## 2.6 Implementation in C++

I implemented the PDE solver itself in C++, while the problems are set up in Mathematica[57]. The C++ program is modular, and roughly speaking can be divided into the following sections

- The *Field* section that looks after the discretized functions. The initial guesses are read in from a file, and the final solutions are written back out.
- The *Lattice* section that uses the methods discussed in 2.4 to take the *Fields* and calculate the derivatives. The points in the lattice, and the derivative matrices to use (and so implicitly the discretization method) are provided to the program in an input file generated in Mathematica. Mathematica has built in methods for generating the derivative matrices given a choice of lattice points and discretization method.
- The *Geometry* section that calculates the equations of motion based on the discretized functions. This section changes depending on the precise geometric setup in which we are searching for solutions. Much of the C code in this section is generated by Mathematica, and contains the formulae for the metric, connection, and curvature in terms of the functions in our ansatz for the metric. I have written Mathematica code that automatically generates this section of C code given the ansatz we are using for the metric in terms of component functions.
- The *Linear System Solver* section is a wrapper for the library we use to solve the linearised systems as part of the Newton-Raphson method. Under the covers it uses the UMFPACK solver from SuiteSparse [58]. This solver is particularly suited to sparse systems where most of the matrix entries are 0. This allows us to be much more memory efficient when we use finite difference interpolation.

- The *Solver* that brings all of the above together and solves the non-linear PDE by implementing Newton's method. At each step in the iterative method, the linearisation (2.17) is done numerically, this linear system is solved, and the solution is used to update our guess. This process continues until the maximum residual on the solution is small enough that we can conclude that we have solved the discretized system to within numerical error. We also track the change in solution from step to step, and cut-off the process if this becomes too small or too large.

The Solver has several parameters you can tweak. One of these is the step-size  $\epsilon$ . If the linear system tells us that we should update our solution to  $\phi_i^{n+1} = \phi_i^n + \delta_i$ , then we modify this update step to

$$\phi_i^{(n+1)} = \phi_i^{(n)} + \epsilon \delta_i$$

typically for  $0 < \epsilon \leq 1$ . This helps mitigate the fact that you might land on a particular configuration  $\phi_i$  where one of the eigenvalues of the linearised system becomes very small. This would lead to you updating your field to somewhere far away in configuration space.

## Chapter 3

# Extremal Horizons and the Infrared in AdS/CFT

The bulk spacetimes in AdS/CFT all have conformal boundaries. This fixes one asymptotic region in these geometries (the AlAdS region). However, as you move into the bulk away from the conformal boundary, the spacetime can do many different things. These behaviours are not completely unconstrained, and often reflect features of the dual CFT state. For instance, if there is a black hole horizon in the bulk with finite surface gravity, the CFT is at finite temperature. However, as we saw in 1.7.2, finite temperature bulks don't have to have a black hole horizon, and whether or not the bulk has a horizon can be a signal of confinement or deconfinement in the CFT.

At zero temperature, there are also different types of possible behaviour. The bulk may smoothly round off, with no other asymptotic regions other than the conformal boundary. Examples of this include global AdS, and the AdS-Soliton and we will discuss these type of bulks in Chapters 5 through 7.

The case we will be interested in here is when the bulk has another asymptotic region away from the conformal boundary. In this region the redshift diverges, so it is known as the infrared (IR) (with the conformal boundary where the redshift goes to zero often called the UV). Just like the conformal boundary region, this IR region can have non-trivial geometry. The geometry at the conformal boundary is related to the space-time the CFT lives on, so an interesting question is whether the geometry in the IR is similarly fixed, and what it corresponds to from the perspective of the CFT. What we will find is that there is a class of IR geometries that are related to a large scale, scale-invariant limit in the CFT. The relation goes two ways. To a certain extent the IR geometry is determined by the large-scale limit of the boundary geometry and source terms, and then, given the IR geometry, the large scale limit of the one-point function of the stress tensor and corresponding operators can be read off.

We will begin by discussing scale-invariance in CFTs. We will then introduce a class of AlAdS Einstein spacetimes that can be used to describe scale-invariant CFT states holographically via AdS/CFT. These are the near-horizon geometries of AlAdS extremal horizons, and we will provide a few examples of such spacetimes, and the scale-invariant states they can describe.

We will then discuss holographic CFT states that are not scale-invariant, but where scale-invariance can be recovered in a large scale limit. We will find that we can describe

such states holographically using bulk spacetimes with an IR region, with this IR region being described by an extremal horizon. The key result of this chapter, from [59], is then that the near-horizon geometry of this extremal-horizon, which is what we mean by the geometry of the IR, describes a scale-invariant state which is precisely the large scale limit of the CFT state we started with. However, we will also find that only a particular class of scale-invariant states can be described using these near-horizon geometries. This will lead us to discuss a more general type of IR geometry in Chapter 4. The work discussed in this chapter was done in collaboration with Toby Wiseman and James Lucietti.

### 3.1 Scale-invariant CFT states

CFTs on  $(d-1) + 1$  dimensional Minkowski space have global symmetry group  $SO(d, 2)$ , which is the  $(d-1) + 1$  dimensional conformal group. This is a symmetry of the theory, and particular states in this CFT may respect or break it. Typically, the vacuum will preserve this symmetry which has consequences for vacuum correlators of the fields in these theories - they are highly constrained, with the two-point and three-point functions in particular completely determined up to constants[19].

Other states may break the symmetry to a subgroup. For instance, the finite temperature state which we can describe holographically by the AdS-Schwarzschild black brane bulk breaks the group down to the  $d - 1$  dimensional Euclidean group[13]. The temperature picks out an energy scale and so breaks the scale invariance. You can also explicitly deform the CFT, for instance by adding external sources to the action, or by taking the theory and putting it on a curved space time. These deformations may break some or all of the symmetries, and so the symmetry group of the vacuum will then be reduced.

In this chapter and the next we are going to be interested in CFTs that have been deformed so that the conformal group is broken down to just staticity and scale-invariance. This can be achieved by putting the CFT on a curved space time which preserves these symmetries, or by deforming the CFT by appropriate source terms. In this section we will introduce these spacetimes and CFT deformations, as well as discussing features of CFT states that preserve these symmetries.

#### 3.1.1 Spacetimes consistent with static, scale-invariance

To start with let's consider what the static and scale-invariance symmetries look like on flat space. Writing Minkowski as

$$ds^2 = -dt^2 + dr^2 + r^2 d\Omega_{d-2}^2, \quad (3.1)$$

then the symmetries corresponding to staticity and scale-invariance are generated by the vectors<sup>1</sup>

$$\begin{aligned}\chi^t &= \frac{\partial}{\partial t} \\ \chi^s &= r \frac{\partial}{\partial r} + t \frac{\partial}{\partial t}.\end{aligned}\tag{3.2}$$

Taken together, these generate the algebra of one-dimensional affine transformations[60]. The corresponding finite transformations are

$$\begin{aligned}t &\rightarrow \mu t + \lambda \\ r &\rightarrow \mu r.\end{aligned}\tag{3.3}$$

Note that, while  $\chi^t$  is a Killing vector, which satisfies the Killing equation

$$\nabla_{(\mu} \chi_{\nu)}^t = 0,\tag{3.4}$$

$\chi^s$  is a conformal Killing vector satisfying,

$$\nabla_{(\mu} \chi_{\nu)}^s = g_{\mu\nu}\tag{3.5}$$

and which generates Weyl scaling of the metric. This means that the transformation 3.3 leads to

$$g \rightarrow \mu^2 g\tag{3.6}$$

Because of the conformal invariance, this type of symmetry is a symmetry of the theory. In fact, we can make use of this freedom to Weyl transform this metric to an alternative conformal frame where it becomes  $AdS_2 \times S_{d-2}$

$$\bar{d}s^2 = \frac{ds^2}{r^2} = \frac{-dt^2 + dr^2}{r^2} + d\Omega_{d-2}^2.\tag{3.7}$$

In this frame both  $\chi^t$  and  $\chi^s$  are Killing vectors.

A more general class of space-times we will consider which have this symmetry take the form

$$g = -A(x^i)dt^2 + B(x^i)dr^2 + 2\xi_i(x^k)r dx^i dr + r^2 h_{ij}(x^i) dx^i dx^j,\tag{3.8}$$

where the  $x^i$  are a set of  $d - 2$  spatial coordinates. When  $A(x^i) = 1$ ,  $B(x^i) = 1$  and  $\xi_i = 0$ , this is a generalized cone with base  $h_{ij}(x^i)$ . We will refer to these more general metrics as twisted cones. In fact, this form of the metric has some degeneracy, in that our freedom to choose coordinates and our freedom to choose a conformal frame can allow us to remove some of the functions in this ansatz. It is often natural, for instance, to do a conformal transformation to an ultrastatic frame defined by  $A(x^i) = 1$ , but we'll discuss these choices when we come to specific examples.

<sup>1</sup>We are considering relativistic scaling, where space and time get scaled in the same way together. For an introduction to the holographic treatment of more general scaling laws, see [13].

We can again use the conformal freedom to transform to a frame where the conformal Killing vector  $\chi^s$  becomes a regular Killing vector

$$\bar{g} = \frac{g}{r^2} = \frac{-A(x^i)dt^2 + B(x^i)dr^2}{r^2} + 2\xi_i(x^k)dx^i \frac{dr}{r} + h_{ij}(x^i)dx^i dx^j. \quad (3.9)$$

Note that this conformal transformation is singular at  $r = 0$ , and the inverse transformation is singular as  $r \rightarrow \infty$ ; correspondingly  $\bar{g}$  ends up with a conformal boundary at  $r = 0$ , and the  $r, t \rightarrow \infty$  null infinity of  $g$  has been conformally compactified to a null surface in  $\bar{g}$ . This frame, along with this null surface, will be central when we come to talk about these CFTs holographically because it will emerge naturally when we take coordinates in the gravitational bulk where the scale-invariance is manifest. We will refer to (3.8) as the cone frame, and (3.9) as the scale-invariant frame.

### 3.1.2 Fields that preserve the static, scale-invariance

In addition to deforming the metric, we can also add sources for other fields, and consider states where these fields take non-zero expectation values.

What a scale-invariant source term or expectation value looks like depends on whether we take the frame (3.8) or (3.9). In the frame (3.8), we need to take into account of the fact that the coordinate transformation (3.3) leads to the Weyl scaling (3.6).

It's therefore more straightforward to write down the scale-invariant terms in (3.9) where they are simply invariant under the transformations (3.3), and then Weyl transform them to the frame (3.8). Under a Weyl scaling of the metric

$$g_{\mu\nu} \rightarrow \frac{g_{\mu\nu}}{\mu^2} \quad (3.10)$$

operators transform according to their scaling dimension. For the transformation from the scale-invariant to the cone frame,  $\mu = \frac{1}{r}$ .

Let's first consider the simplest case of a scalar operator of dimension  $\Delta$ . A scale-invariant vev in the scale-invariant frame (3.9) simply needs to be independent of  $t$  and  $r$ , so it takes the form

$$\langle \Phi_\Delta(r, x^i) \rangle_{\text{scale invariant}} = f_\Delta(x^i). \quad (3.11)$$

The Weyl transformation of a primary scalar field is [19]

$$\Phi_\Delta(r, x^i) \rightarrow \mu^\Delta \Phi_\Delta(r, x^i), \quad (3.12)$$

so in the cone frame (3.8) it becomes

$$\langle \Phi_\Delta(r, x^i) \rangle_{\text{cone}} = r^{-\Delta} f_\Delta(x^i). \quad (3.13)$$

An operator that we will be particularly interested in is the stress tensor  $T^{\mu\nu}$ . In the scale-invariant frame, this is static and scale invariant if the lie derivatives  $\mathcal{L}_{\chi^t} T_{\mu\nu} =$

$\mathcal{L}_{\chi^s} T_{\mu\nu} = 0$ . This means that

$$\begin{aligned} \langle T_{\mu\nu}(r, x^i) \rangle_{\text{scale invariant}} &= \frac{T_{tt}(x^i)dt^2 + T_{rr}(x^i)dr^2}{r^2} + 2T_{ri}(x^i)\frac{dr}{r}dx^i \\ &\quad + T_{ij}(x^i)dx^i dx^j. \end{aligned} \quad (3.14)$$

The stress tensor has scaling dimension  $d$ [61], which means that it transforms as<sup>2</sup> so that we have

$$T_{\mu\nu} \rightarrow \mu^{d-2} T_{\mu\nu} \quad (3.15)$$

and so transforming to the cone frame (3.8)

$$\langle T_{\mu\nu}(r, x^i) \rangle_{\text{cone}} = \frac{T_{tt}(x^i)dt^2 + T_{rr}(x^i)dr^2}{r^d} + 2T_{ri}(x^i)\frac{dr}{r^{d-1}}dx^i + \frac{T_{ij}(x^i)dx^i dx^j}{r^{d-2}}. \quad (3.16)$$

The other case we will be interested in will be a static chemical potential and a corresponding conserved electric charge density. The scale invariant potential and current in the scale-invariant frame are of the form

$$\begin{aligned} A^{\text{scale-invariant}} &= \frac{\alpha(x^i)dt}{r} \\ \langle J \rangle_{\text{scale-invariant}} &= \rho(x^i)r \frac{\partial}{\partial t}, \end{aligned} \quad (3.17)$$

where note we are only considering electric and not magnetic charge. A conserved current has scaling dimension  $d - 1$ [61], which means that it and its source transform as

$$\begin{aligned} A_\mu &\rightarrow A_\mu \\ J^\mu &\rightarrow \mu^d J^\mu \end{aligned} \quad (3.18)$$

and so in the cone frame we get

$$\begin{aligned} A^{\text{cone}} &= \frac{\alpha(x^i)dt}{r} \\ \langle J \rangle_{\text{cone}} &= \rho(x^i)r^{1-d} \frac{\partial}{\partial t}. \end{aligned} \quad (3.19)$$

## 3.2 Introduction to Extremal Horizons

Here we review only those features of extremal horizons necessary for this work. For a more comprehensive review of extremal horizons and their near horizon geometries see [31]. An extremal horizon is a degenerate Killing horizon. Geometrically, the fact that it is a Killing horizon means that we have a Killing vector  $k^\mu$ , which becomes null specifically on the horizon. In addition,  $k_\mu$  is normal to the horizon.

<sup>2</sup>It is  $\mu^{d-2}$  rather than  $\mu^d$  because of the two lowered indices. If we did a conformal transformation rather than just a Weyl scaling, then another two factors of  $\mu$  would come from the accompanying coordinate transformation.

The fact that its norm vanishes on the horizon means that the derivative of its norm must be proportional to the normal vector

$$\partial_\mu(g_{\nu\rho}k^\nu k^\rho) = 2\kappa k_\mu, \quad (3.20)$$

for some  $\kappa$ , and using the Killing equation for  $k$  this can be rearranged to yield

$$k^\mu \nabla_\mu k^\nu = \kappa k^\nu, \quad (3.21)$$

which tells us that the Killing vector generates geodesics along the horizon[62]. The parameter  $\kappa$  is called the surface gravity of the horizon, and it is constant for Killing horizons[63]<sup>3</sup>. Degenerate Killing horizons are those for which  $\kappa = 0$ , and so the parameter along the geodesics defined by the vector field  $k^\mu$  is affine.

A special feature of these horizons is their ‘near horizon geometry’. For a generic null Killing horizon (not necessarily degenerate) one can construct Gaussian null coordinates in an open neighbourhood, such that the metric takes the form[31]

$$g = rA(r, y)dv^2 + 2dvdr + 2rl_a(r, y)dy^a dv + h_{ab}(r, y)dy^a dy^b, \quad (3.22)$$

where  $A$ ,  $l_a$ , and  $h_{ab}$  are smooth functions for some open region including  $r = 0$ . The Killing vector is  $\frac{\partial}{\partial v}$  and the horizon is at  $r = 0$ . The coordinates  $y^a$  span the horizon. When it’s degenerate, the condition in (3.20) (with  $\kappa = 0$ ) implies that  $d(rA(r, y))|_{r=0} = A(0, y)dr = 0$ . This means we can write

$$g = r^2\tilde{A}(r, y)dv^2 + 2dvdr + 2rl_a(r, y)dy^a dv + h_{ab}(r, y)dy^a dy^b. \quad (3.23)$$

The metric in (3.23) has an important property not shared by that in (3.22), in that we are able to take an  $r \rightarrow 0$  limit of it in such away that we end up with a full-dimensional metric. Obviously, if you just set  $r = 0$ , in either case you get the  $n - 2$  dimensional metric  $h_{ab}(0, y^a)dy^a dy^b$  induced on the null hypersurface. However, in the second case you can consider the following limit which takes advantage of the Killing symmetry

$$\begin{aligned} r &\rightarrow \epsilon r \\ v &\rightarrow v/\epsilon \\ \epsilon &\rightarrow 0. \end{aligned} \quad (3.24)$$

In this limit we get

$$g \rightarrow g_{NH} = r^2\tilde{A}(0, y)dv^2 + 2dvdr + 2rl_a(0, y)dy^a dv + h_{ab}(0, y)dy^a dy^b. \quad (3.25)$$

This is the ‘near horizon geometry’ of the extremal horizon[31]. Since the transformation described in (3.24) is a coordinate transformation for any finite  $\epsilon$  (albeit a singular one in the limit  $\epsilon \rightarrow 0$ ), if the original metric satisfies some covariant condition (i.e. Einstein’s

<sup>3</sup>Subject to a dominant energy condition on the stress tensor for any matter fields.

equation for some cosmological constant  $\Lambda$ , and with some stress tensor), then, by continuity, the near horizon geometry satisfies this same condition on its own. The restriction of Einstein's equation to the specific case of a near-horizon geometry is referred to as the near-horizon equations.

### 3.3 Enhanced Symmetry of Static near-horizon Geometries

If the Killing field that generates the horizon is hypersurface orthogonal, then it turns out that the near-horizon geometry can be written in the form [31]

$$g_{NH} = \psi(y)^2 d\Sigma^2 + \gamma_{ab}(y) dy^a dy^b, \quad (3.26)$$

where

$$d\Sigma^2 = kr^2 dv^2 + 2dvdr. \quad (3.27)$$

for some constant  $k$ . Depending on the value of  $k$ ,  $d\Sigma^2$  is one of the two-dimensional constant curvature manifolds.  $k > 0$ ,  $k = 0$  and  $k < 0$  corresponds to deSitter, Minkowski, and Anti-deSitter respectively. We can scale coordinates so that  $k = 1$ ,  $k = 0$ , or  $k = -1$ . Note that while for  $k = 1$  or  $k = -1$  the near horizon geometry inherits the Killing horizon from the bulk, in the  $k = 0$  case there is no Killing horizon in the near horizon geometry. In this case the surface  $r = 0$  is just one null Killing surface among many, and the Killing vector that generates it is null everywhere. This case arises if  $|\frac{\partial}{\partial v}|^2$  falls off sufficiently quickly near  $r = 0$ .<sup>4</sup>

For  $k = 1, -1$  we can write  $t = v - \frac{k}{r}$  we then find that

$$d\Sigma^2 = k(r^2 dt^2 - \frac{dr^2}{r^2}). \quad (3.28)$$

In these coordinates, the Killing vector is  $\frac{\partial}{\partial t}$ . For the  $AdS_2$  case, this Killing vector is timelike outside the horizon, so that the near horizon geometry is static.

We can see from (3.26) that when the Killing vector is hypersurface orthogonal, the near horizon geometry has more symmetries than we might have have a priori expected.<sup>5</sup> It was guaranteed to inherit the Killing symmetry associated with the Killing horizon and, in addition, since it is the end point of the flow defined by (3.24), it is automatically invariant under that flow. However, we now have the full symmetry of  $d\Sigma^2$ . So, in addition to these symmetries generated by

$$\frac{\partial}{\partial v}, v \frac{\partial}{\partial v} - r \frac{\partial}{\partial r}, \quad (3.29)$$

<sup>4</sup>Generically, we see from Equation 3.65 that  $|\frac{\partial}{\partial v}|^2 \sim r^2$ , but if  $|\frac{\partial}{\partial v}|^2 \sim r^3$  or higher, we will end up with this Minkowski case in the near-horizon limit.

<sup>5</sup>In fact, it is shown in [64], that if sufficient rotational symmetries are assumed, you get this extended symmetry as well.

we have an extra symmetry generated by

$$\frac{\partial}{\partial r} + k \left( \frac{1}{2} v^2 \frac{\partial}{\partial v} - r v \frac{\partial}{\partial r} \right). \quad (3.30)$$

For  $k \neq 0$ , these three symmetries taken together form  $SO(2,1)$ , and for  $k = 0$  they are the two dimensional Lorentz group.

Even without the stipulation that  $\frac{\partial}{\partial v}$  was hypersurface orthogonal, we see in (3.25) that we don't have the most generic metric compatible with the Killing and scaling symmetry. We are missing the potential  $dr dy^a$  terms<sup>6</sup>

$$g = r^2 \tilde{A}(y) dv^2 + 2dvdr + 2r l_a(x^i) dy^a dv + 2p_a(y) \frac{dr}{r} dy^a + h_{ab}(y) dy^a dy^b. \quad (3.32)$$

If  $p_i(0, y) \neq 0$  this does not describe a smooth near horizon geometry, and we will have more to say about these singular geometries later.

### 3.4 Near Horizon Geometries with Conformal Boundaries

We now consider static near-horizon geometries  $\mathcal{M}$ , which are AlAdS solutions to Einstein's equation with negative cosmological constant. We discussed general AlAdS spacetimes and their conformal boundaries in 1.4.1. From, (3.26), it is clear that there must be a special class of defining functions  $Z(y)$  which is invariant over  $\Sigma$ , so doesn't depend on  $t$  or  $r$ <sup>7</sup>. The crucial thing to note is that, for such choices of defining function, the ambient metric,  $\bar{g}_{NH} = Z(y)^2 g_{NH}$  which we introduce as part of this construction is itself a near-horizon geometry. In particular, the surface in this ambient space corresponding to the conformal boundary has a metric of the form

$$g_{NH\bar{B}} = p(x)^2 d\Sigma^2 + h_{ij}(x) dx^i dx^j, \quad (3.33)$$

where the  $(d-2)$   $x^i$  coordinates span the  $Z(y^a) = 0$  subspace of the  $y^a$  coordinates. Explicitly, comparing with (3.26), we have

$$\begin{aligned} p(x) &= Z(y) \psi(y) \Big|_{Z=0} \\ h_{ij}(x) dx^i dx^j &= Z(y)^2 \gamma_{ab}(y) dy^a dy^b \Big|_{z=0}. \end{aligned} \quad (3.34)$$

We see, therefore, that the conformal boundary of a near-horizon geometry must, in some class of conformal frames, be a near horizon geometry itself.<sup>8</sup>

<sup>6</sup>Note that there were two coordinate freedoms

$$\begin{aligned} r &\rightarrow r \lambda(y) \\ v &\rightarrow v + \frac{k(y)}{r} \end{aligned} \quad (3.31)$$

which we fixed by demanding that the coefficient of  $dr^2$  vanishes and the coefficient of  $dvdr$  is 1.

<sup>7</sup>i.e.  $\gamma_{ab} dy^a dy^b$  taken on its own has to have a conformal boundary.

<sup>8</sup>This follows as well in the non-static case.

We focus now on the  $k = -1$ ,  $AdS_2$  case and examine this boundary. We see that the boundary metric is a special case of the general static scale-invariant geometries in (3.9). In fact, the generators of the static scale-symmetry, are just the restriction of the generators of the symmetries of the near horizon geometry (3.29) to the boundary. Transforming this to the frame (3.8) we get

$$\bar{g}_{NHB} = p(x) (-dt^2 + d\rho^2) + \rho^2 h_{ij}(x^i) dx^i dx^j. \quad (3.35)$$

We can always take the special conformal frame where  $p(x) = 1$ . If the  $x^i$  describe a compact manifold, this is then the product of time and a generalized cone. AlAdS near horizon geometries therefore describe static-scale invariant states on these generalized cones. Note that these geometries are a subset of (3.8), and don't include 'twisted' cones.

### 3.4.1 AdS Example

The simplest example of a near-horizon geometry in  $d + 1$  dimensions is the Poincaré patch of AdS described in 1.7. We can write the metric as

$$g = \frac{-dt^2 + dz^2 + d\rho^2 + \rho^2 d\Omega_{d-2}^2}{z^2}. \quad (3.36)$$

where the conformal boundary metric is at  $z \rightarrow 0$  and is simply flat space

$$h = -dt^2 + d\rho^2 + \rho^2 d\Omega_{d-2}^2. \quad (3.37)$$

In these coordinates it's not obvious that there is an extremal horizon, but we can perform the coordinate transformation[31]

$$\begin{aligned} z &= \frac{r'}{\psi} \\ \rho &= \frac{r' \sqrt{\psi^2 - 1}}{\psi}, \end{aligned} \quad (3.38)$$

to make this manifest. The metric is then

$$g = \psi^2 \left( \frac{-dt^2 + dr^2}{r^2} \right) + \frac{d\psi^2}{\psi^2 - 1} + (\psi^2 - 1) d\Omega_{d-2}^2. \quad (3.39)$$

Now the conformal boundary is at  $\psi \rightarrow \infty$ , and there is an axis at  $\psi = 1$ . This has the standard form of a static near horizon geometry, with the horizon at  $r \rightarrow \infty$ . Note from (3.38) that to get to the horizon, you don't just send  $z \rightarrow \infty$ , but  $\rho \rightarrow \infty$  to with the ratio  $\frac{z}{\rho}$  kept finite. The conformal boundary metric is now given by

$$\bar{h} = \left( \frac{-dt^2 + dr^2}{r^2} \right) + d\Omega_{d-2} \quad (3.40)$$

which is  $AdS_2 \times S_{d-2}$ . In doing this bulk coordinate transformation we see that we generated the Weyl transformation from the cone frame to the scale-invariant frame. In the

scale-invariant frame the boundary itself has an extremal horizon, and this horizon extends into the bulk as the Poincare horizon. Under the Weyl transformation that relates these two frames, this extremal horizon on the boundary gets mapped to null infinity, so in the cone frame we can say that the Poincare horizon meets the boundary at null infinity.

### 3.4.2 4d Einstein Near Horizon Geometries

In 4 dimensions, the complete set of AlAdS near horizon geometries is known analytically. The metrics take the form[31]

$$g = \frac{d\psi^2}{f(\psi)} + \alpha^2 f(\psi) d\phi^2 + \psi^2 \left( \frac{-dt^2 + dr^2}{r^2} \right) \quad (3.41)$$

where  $f(\psi) = \psi^2 - 1 - \frac{\psi_0(\psi_0^2 - 1)}{\psi}$ , and where  $\psi_0$  and  $\alpha$  are constants. The case  $\psi_0 = 1$  corresponds to AdS. More generally we can consider values of  $\psi_0 > \frac{1}{\sqrt{3}}$ , so that  $\psi = \psi_0$  is the largest zero of  $f(\psi)$ . The conformal boundary is again at  $\psi \rightarrow \infty$ , and now the axis of symmetry for the  $\phi$  coordinate in the bulk is at  $\psi = \psi_0$ . The parameter  $\alpha$  is fixed in terms of  $\psi_0$  by requiring that there is no conical singularity in the bulk along this axis<sup>9</sup>. This fixes  $\alpha = \frac{2\psi_0}{3\psi_0^2 - 1}$ , so we have a one parameter family of solutions corresponding to the full range of possible values of  $\alpha > 0$ . The conformal boundary metric is  $AdS_2 \times S_1$

$$h = \frac{-dt^2 + dr^2}{r^2} + \alpha^2 d\phi^2 \quad (3.42)$$

with  $\alpha$  controlling the size of the  $S_1$ . This is the scale-invariant frame, and transforming to the cone frame we have

$$\bar{h} = -dt^2 + dr^2 + \alpha^2 r^2 d\phi^2, \quad (3.43)$$

which is a cone with  $\alpha$  controlling the opening angle.

If we examine the limiting case  $\psi_0 \rightarrow \frac{1}{\sqrt{3}}$ , we find something a little different.  $\alpha(\psi)$  diverges in this limit, but this was just a factor inserted to keep the period of  $\phi$  canonical, and so can just be absorbed as a redefinition of  $\phi = \frac{\tilde{\phi}}{\sqrt{\alpha}}$ . In this solution, the  $\tilde{\phi}$  coordinate is no longer compact (since when  $\phi \rightarrow \phi + 2\pi$ ,  $\tilde{\phi} \rightarrow \tilde{\phi} + 2\pi\sqrt{\alpha}$  which diverges as  $\psi_0 \rightarrow \frac{1}{\sqrt{3}}$ ). This means that the natural choice of boundary is asymptotically the same as before but with a non-compact  $\phi$  coordinate. However, there is nothing to stop us from compactifying this coordinate to turn it into a circle of whatever size we want and so turn the boundary into a cone of any conical deficit we want. For each cone opening angle, there are therefore two possible bulk geometries we can choose.

These near-horizon geometries therefore describe static, scale-invariant CFT states on

---

<sup>9</sup>We take  $\phi$  to have canonical period.

a cone. The stress tensor can be extracted by moving to the Fefferman-Graham coordinates we discussed in 1.6.1, and in the two frames it takes the form

$$\begin{aligned} T_{\text{scale-invariant}} &= c \frac{\psi_0 (\psi_0^2 - 1)}{r^2} (-dt^2 + dr^2 - 2r^2 \alpha^2 d\phi^2) \\ T_{\text{cone}} &= c \frac{\psi_0 (\psi_0^2 - 1)}{r^3} (-dt^2 + dr^2 - 2r^2 \alpha^2 d\phi^2). \end{aligned} \quad (3.44)$$

### 3.4.3 4d Einstein-Maxwell Near-Horizon Geometries

We can add in a gauge field, in which case the solutions take the form[65]

$$\begin{aligned} g &= \frac{d\psi^2}{f(\psi)} + \alpha^2 f(\psi) d\phi^2 + \frac{\psi^2 (dr^2 - dt^2)}{r^2} \\ A &= e \frac{dt}{r} \end{aligned} \quad (3.45)$$

where  $f(\psi) = \psi^2 - 1 - \frac{\psi_0^3 - \psi_0 - e^2}{\psi} - \frac{e^2}{\psi^2}$ . There are now two free parameters  $\alpha$  and  $e$ <sup>10</sup>. In addition to the boundary metric as above, there is now a scale-invariant boundary chemical potential of the form  $e \frac{dt}{r}$ . These solutions (in the special case  $\alpha = 1$ ) are discussed in [66], where they are interpreted as point charge defects in the CFT. Fixing  $\alpha = 1$ ,  $e$  is given in terms of the largest zero  $\psi_0$  by

$$e^2 = \psi_0^2 (1 + 3\psi_0)(1 - \psi_0). \quad (3.46)$$

In this case  $\psi_0$  is the greatest positive zero of  $f$  so long as  $0.226... < \psi_0 < 1$ . The parameter  $\psi_0$  in this range labels a family of bulk solutions, and the dual CFT states are sourced by a potential with strength  $e$ . As pointed out in [66], the map,  $e \rightarrow \psi_0$ , from source to state is neither left-complete nor one-to-one. The range of  $e$  for which there is a corresponding state is bounded by  $e^2 < \frac{1}{288} (69 + 11\sqrt{33}) \equiv e_m^2$ , and, for  $e^2 > 0.066... \equiv e_c^2$ , there are two branches of states labelled by two different values of  $\psi_0$ . The two branches are,

- Branch 1: Runs from  $0 < e^2 < e_m^2$ . The  $e^2 = 0$  case is pure AdS.
- Branch 2: Runs from  $e_c^2 < e^2 < e_m^2$ . It meets Branch 1 at  $e^2 = e_m^2$ .

The boundary charge density corresponding to the chemical potential can be read off by looking at the series expansion of the gauge field near  $\psi \rightarrow \infty$ . Since the gauge field is independent of  $\psi$ , we find that this vanishes. However, as explained in [66] this isn't the whole story.

There are in fact two different components of the conformal boundary. There is a  $2 + 1$  dimensional component at  $\psi \rightarrow \infty$ , and a  $1 + 1$  dimensional component coming from the conformal boundary of the  $AdS_2$  factor as  $r \rightarrow 0$ . This comes from the fact that the conformal transformation relating the scale invariant frame to the cone frame is singular at  $r = 0$ . The effect of this can be seen in the explicit AdS example in 3.4.1.

<sup>10</sup> $\psi_0$  is again then determined by the requirement that the bulk has no conical singularity.

The bulk coordinate transformation (3.38) that generates this conformal transformation is degenerate at  $r = 0$ , which is why the origin of the cone frame conformal boundary has been blown up to lie along all values of  $\psi$  at  $r = 0$ .

To extract the full boundary charge, we need to take this additional component into consideration. In the cone frame, the charge that comes from this extra component can be thought of as a point charge defect at the origin on the boundary [66], and when that is taken into account, the total charge is  $Q = \frac{2e}{\psi_0}$ .

### 3.5 Extremal Horizons and Large Scale Limits in AdS/CFT

We have seen that we can describe certain static, scale-invariant, holographic CFT states in the bulk by AlAdS near horizon geometries. In 3.5.1 we will discuss more general CFT states which are only static, and scale-invariant in a large scale limit. In [59] we explore how AlAdS bulk spacetimes with extremal horizons describe these more general states in AdS/CFT, and we will now discuss this result. This work was in collaboration with James Lucietti and Toby Wiseman.

What is shown here is that when you have an extremal horizon in the infrared in the bulk, which meets the conformal boundary at null infinity, you cannot choose the near horizon geometry of this extremal horizon freely. This is because the geometry of the Extremal Horizon in the bulk determines the large scale limit of the geometry on the boundary. In fact, going the other way, the geometry of null infinity on the boundary forms the boundary conditions for an elliptic PDE whose solution is the geometry of the Extremal Horizon, which in turn determines the large scale limit of the CFT state on this geometry. After introducing large scale limits, we will discuss a non-trivial example of bulk spacetimes that contain the 4d extremal horizons with the near-horizon geometries discussed in 3.4.2. We'll see there explicitly the correspondence between the large scale limit on the boundary, and the near-horizon limit in the bulk. In Section 3.5.3 we provide a sketch of the proof of this result, and then in 3.5.4 we discuss potential generalizations.

#### 3.5.1 Large Scale Limit of a CFT state

An exactly scale-invariant state is quite special. However they arise naturally as a large scale limit of a large class of CFT states. To illustrate this, consider first an asymptotically flat spacetime. At large  $r$  the metric can be written in the form

$$g = - \left( 1 + O \left( \frac{1}{r} \right) \right) dt^2 + \left( 1 + O \left( \frac{1}{r} \right) \right) dr^2 + r^2 \left( 1 + O \left( \frac{1}{r} \right) \right) d\Omega^2. \quad (3.47)$$

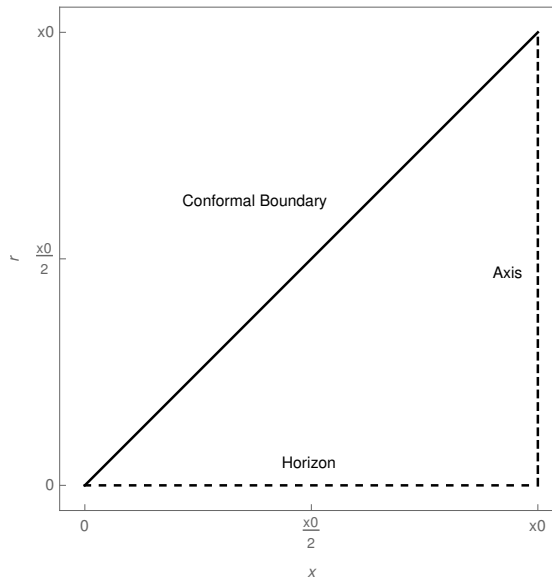


FIGURE 3.1: The C-Metric

We can think of this as a metric that becomes Minkowski in a ‘large scale limit’. To make this more precise, consider the combination of transformations

$$\begin{aligned} r &\rightarrow \lambda r \\ t &\rightarrow \lambda t \\ g &\rightarrow \frac{g}{\lambda^2}. \end{aligned} \tag{3.48}$$

Under these transformations, the metric becomes

$$g \rightarrow - \left( 1 + O\left(\frac{1}{\lambda r}\right) \right) dt^2 + \left( 1 + O\left(\frac{1}{\lambda r}\right) \right) dr^2 + r^2 \left( 1 + O\left(\frac{1}{\lambda r}\right) \right) d\Omega^2. \tag{3.49}$$

We see that if we then take  $\lambda \rightarrow \infty$  limit this becomes Minkowski. This is what we will call the large scale limit.

We can consider more general spacetimes that admit a large scale limit (3.48) which are not necessarily asymptotically flat. Spacetimes that at large  $r$  are of the form (3.8) plus contributions that fall off faster with  $r$  admit such a limit. We can similarly consider other sources and the expectation values of fields in CFT states. The state has a large scale limit if the leading order in  $r$  behaviour at large  $r$  of sources and vevs is the scale-invariant form we discussed in 3.1.2. Any fields that fall off faster than this disappear in the scale-invariant limit, while any that do not fall off fast enough obstruct the construction of this limit.

### 3.5.2 Holographic CFT on 2+1 dimensional resolved cones

Before we move on to the more general result, we will start with a non-trivial explicit four dimensional example. We consider a class of static, rotationally symmetric, 4-d bulk

AdS C-Metrics[67]. These spacetimes take the form

$$\begin{aligned}
g_C &= \frac{1}{(x-r)^2} \left( -r^2 f(r, x_0) dt^2 + \frac{dr^2}{r^2 f(r, x_0)} + \frac{dx^2}{g(x, x_0)} + g(x, x_0) \alpha(x_0) d\phi^2 \right) \\
f(r, x_0) &= 1 - \frac{x_0^2 - 1}{x_0^3} r \\
g(x, x_0) &= 1 - x^2 - \frac{x^3}{x_0^3} (1 - x_0^2) \\
\alpha(x_0) &= \frac{4x_0^2}{(x_0^2 - 3)^2},
\end{aligned} \tag{3.50}$$

forming a one-parameter family parametrized by the constant  $x_0$ . The bulk is described by the domain

$$0 < r < x \leq x_0. \tag{3.51}$$

The  $x-r$  dependence of this spacetime is illustrated in 3.1. It has a conformal boundary at  $x = r$ , and an extremal horizon at  $r = 0$  that meets the conformal boundary at  $x = r = 0$ . There is an axis of symmetry running from the horizon to the boundary at  $x = x_0$ . For this bulk to be smooth  $x_0$  needs to be the smallest positive root of  $g(x, x_0)$ . This implies the condition

$$0 < x_0 \leq \sqrt{3}. \tag{3.52}$$

The constant  $\alpha(x_0)$  simply rescales the  $\phi$  coordinate, and is inserted so that  $\phi$  is taken to have canonical period  $2\pi$  with there being no conical singularity on the axis at  $x = x_0$ . Explicitly, writing  $x = x_0 - \epsilon\rho^2$ , and looking at the  $x-\phi$  part of the metric for small  $\epsilon$  we find

$$g_C|_{r,t=\text{const}} = \frac{2\sqrt{\alpha(x_0)}}{(x-r)^2} (d\rho^2 + \rho^2 d\phi^2) \epsilon + O(\epsilon^2). \tag{3.53}$$

Let's examine the conformal boundary  $x = r$ . A representative of the induced conformal structure is given by

$$\begin{aligned}
\bar{h}_C &= (x-r)^2 g_C|_{x=r} \\
&= -x^2 f(x, x_0) dt^2 + dx^2 \left( \frac{1}{x^2 f(x, x_0)} + \frac{1}{g(x, x_0)} \right) + g(x, x_0) \alpha(x_0) d\phi^2.
\end{aligned} \tag{3.54}$$

To understand what spacetime the conformal boundary is, let's look at two limits. If we look at small  $x$ , or large  $\rho = \frac{1}{x}$  the metric becomes

$$\begin{aligned}
\bar{h}_C &\rightarrow x^2 \left( -dt^2 + \frac{dx^2}{x^4} + \frac{\alpha(x_0)}{x^2} d\phi^2 \right) \\
&= \frac{-dt^2 + d\rho^2 + \rho^2 \alpha(x_0) d\phi^2}{\rho^2}.
\end{aligned} \tag{3.55}$$

On the other end if we look at the region approaching  $x = x_0$  and again write  $x = x_0 - \rho^2$  we find

$$\bar{h}_C \rightarrow x_0^2 \left( -dt^2 + 2\sqrt{\alpha(x_0)} (d\rho^2 + \rho^2 d\phi^2) \right). \tag{3.56}$$

So at small  $x$  it is an example of the scale-invariant metric of the form (3.9), and at  $x = x_0$  it caps off smoothly. We can perform a Weyl scaling to instead put the metric in a form so it is asymptotically like (3.8)

$$\begin{aligned} h_C &= \frac{\bar{h}_C}{x^2} \\ &= -f(x, x_0)dt^2 + dx^2 \left( \frac{1}{x^4 f(x, x_0)} + \frac{1}{x^2 g(x, x_0)} \right) + \frac{g(x, x_0)}{x^2} \alpha(x_0) d\phi^2. \end{aligned} \quad (3.57)$$

Then the two limits become

$$h_C \rightarrow -dt^2 + d\rho^2 + \rho^2 \alpha(x_0) d\phi^2 \quad (3.58)$$

and

$$h_C \rightarrow -dt^2 + 2\sqrt{\alpha(x_0)} (d\rho^2 + \rho^2 d\phi^2). \quad (3.59)$$

This is a resolved cone. At large  $\rho$  there is an opening angle determined by  $\alpha(x_0)$ , but instead of a conical singularity, the geometry rounds off smoothly.

Now let's look at the extremal horizon at  $r = 0$  which meets the conformal boundary at  $x = 0$ , or  $\rho \rightarrow \infty$ . We can find the associated near horizon geometry. We do this by taking  $r \rightarrow \epsilon r$ ,  $t \rightarrow \frac{t}{\epsilon}$  and taking the limit  $\epsilon \rightarrow 0$ . This yields

$$\mathcal{G}_C^{nh} = \frac{1}{x^2} \left( -r^2 dt^2 + \frac{dr^2}{r^2} + \frac{dx^2}{g(x, x_0)} + g(x, x_0) \alpha(x_0) d\phi^2 \right), \quad (3.60)$$

which through the change of variables  $x = \frac{1}{\psi}$ , recovers the 4-d near horizon geometries from (3.41).

Having taken this limit we can, if we choose, simply forget about the rest of the geometry, and take this metric to describe a new complete spacetime. Recall from Section 3.4.2 that the conformal boundary is now given by

$$h = -dt^2 + d\rho^2 + \rho^2 \alpha(x_0) d\phi^2. \quad (3.61)$$

This is precisely what we got as the large scale limit of the C-Metric boundary in (3.58). As we've taken a near-horizon limit in the bulk, we've found that we've taken a large scale limit on the boundary, and thrown away all other information. This principle also extends to observables like the stress energy tensor.

### 3.5.3 The General Statement

What we saw in Section 3.5.2 was an example of a bulk spacetime with an extremal horizon that met the conformal boundary. In an appropriate conformal frame as in (3.8), this extremal horizon meets the boundary at null infinity. What we found was that there was a connection between the near horizon geometry of extremal horizon, and the large scale limit of the conformal boundary. The main result of [59] was to prove the statement about this connection in general.

### FG Coordinates for Near Horizon Geometries

The near-horizon equations for static extremal horizons of this form are just a set of elliptic equations, with the boundary conditions given by the metric on the conformal boundary. Following from (3.26), we know that these solutions take the form

$$g_{NH} = \psi(y)^2 \left( \frac{-dt^2 + dr^2}{r^2} \right) + \gamma_{ab}(y) dy^a dy^b. \quad (3.62)$$

If they are AlAdS, then the conformal boundary is a cone

$$g_c = -dt^2 + dr^2 + r^2 h_{ij}(x^i) dx^i dx^j. \quad (3.63)$$

We will write  $g_{NH}[h(x)]$  as a (not necessarily unique) solution to the near-horizon equations, with a conformal boundary that in some frame is this cone specified by  $h_{ij}$ .

As usual, we can take Fefferman-Graham coordinates near the conformal boundary. The bulk coordinates  $y^a$  on the horizon get replaced by  $z, x^i$ , where the  $x^i$  are boundary coordinates, and the coordinate  $z = 0$  on the boundary, and increases in to the bulk. Adapted to an AlAdS near-horizon geometry this takes the form

$$g_{NH}[h(x)] = \frac{1}{z^2} \left( \psi(x, z) \left( \frac{-dt^2 + dr^2}{r^2} \right) + H_{ij}(x, z) dx^i dx^j + dz^2 \right). \quad (3.64)$$

If we choose the frame where  $\psi(x, 0) = 1$ , then we will have  $H_{ij}(x, 0) = h_{ij}(x)$ . The FG expansion from 1.6.1 then determines  $\psi$  and  $\gamma_{ij}$  in a series expansion in  $z$ , until at order  $z^d$  there is information corresponding to the stress tensor in the CFT that is not fixed by the boundary expansion. To find this, we need to solve the full near-horizon equations for  $g_{NH}[h(x)]$ .

### Large Scale limits and Near Horizon limits related through the Fefferman Graham Expansion

We now argue that if there is an extremal horizon in the bulk, that meets the boundary at null infinity, then the conformal boundary of the Near Horizon Geometry of the bulk horizon is the large scale limit of the boundary. Thus, this large scale limit forms the boundary conditions of the near horizon Einstein equations described above. This argument was come up with collaboratively, but the slightly more general presentation in [59] which holds as well when the near horizon geometry as written in (3.26) has  $k = 1$  or  $k = 0$  is due to James Lucietti.

We do this by illustrating the relationship between extracting the large scale limit on the boundary and taking the near horizon limit in the bulk for the case where the extremal horizon meets the boundary at null infinity. Consider a static spacetime with an extremal

horizon. In a region containing the horizon we can write the metric as[52]<sup>11</sup>

$$g = \frac{-A(r, y^a)dt^2 + B(r, y^a)(dr + \omega_a(y^a)dy^a)^2}{r^2} + \gamma_{ab}(r, y^a)dy^a dy^b, \quad (3.65)$$

where  $\lim_{r \rightarrow \infty} A(r, x^a) = \lim_{r \rightarrow \infty} B(r, x^a) = \psi(x^a)$ ,  $\lim_{r \rightarrow \infty} \gamma_{ab}(r, y^a) = \gamma_{ab}(y^a)$ , and all other functions are smooth and bounded. Unless otherwise stated, in everything that follows  $f(y) \equiv \lim_{r \rightarrow \infty} f(r, y)$ . The near-horizon geometry of this extremal horizon is thus (3.62).

If this extremal horizon meets a conformal boundary, we can transform this to Fefferman-Graham coordinates in some open region which includes the conformal boundary. Compared to (3.64), it's complicated slightly by the  $r$  dependence of the metric functions

$$g = \frac{-\bar{A}(r, z, x^i)dt^2 + \bar{B}(r, z, x^i)dr^2 + 2\alpha_i(r, z, x)drdx^i}{z^2 r^2} + \frac{H_{ij}(r, z, x^i)}{z^2} dx^i dx^j + \frac{dz^2}{z^2}. \quad (3.66)$$

The conformal boundary metric is given by

$$g^b = \frac{-\bar{A}(r, 0, x^i)dt^2 + \bar{B}(r, 0, x^i)dr^2 + 2\alpha_i(r, z, x)drdx^i}{r^2} + H_{ij}(r, 0, x^i)dx^i dx^j \quad (3.67)$$

which we can see is an asymptotically scale-invariant boundary metric written in the scale-invariant frame. We can transform this to the cone frame by performing a coordinate redefinition in the bulk. We can write

$$g = \frac{-\tilde{A}(r', Z, x^i)dt^2 + \tilde{B}(r', Z, x^i)dr'^2 + 2\tilde{\alpha}_i(r, Z, x)drdx^i}{Z^2} + \frac{r'^2 \tilde{H}_{ij}(r', Z, x^i)}{Z^2} dx^i dx^j + \frac{dZ^2}{Z^2} \quad (3.68)$$

where  $Z = zr + O(z^3)$  and  $r' = r + O(z^2)$ , where the higher order terms are determined by forcing the metric to take this FG form. The boundary metric is now in the cone frame

$$g_f^b = -\bar{A}(r, 0, x^i)dt^2 + \bar{B}(r, 0, x^i)dr^2 + 2\alpha_i drdx^i + r^2 H_{ij}(r, 0, x^i)dx^i dx^j. \quad (3.69)$$

The near horizon limit in (3.66) amounts to taking  $r \rightarrow \mu r$ ,  $t \rightarrow \mu t$  and then  $\mu \rightarrow \infty$ . To leading order in  $z$ , this means in (3.68) that  $Z \rightarrow \mu Z$ , and so for the boundary metric in flat frame  $g_f^b \rightarrow \frac{g_f^b}{\mu^2}$ . This is precisely the large scale limit from 3.5.1.

What's more, by considering the FG expansion, the expansion in  $z$  or  $Z$  of (3.66) or (3.68), we can see that we've also taken the large scale limit of the state. It's simplest to consider the cone frame (3.66). The stress tensor is the  $O(z^d)$  component of the expansion,

<sup>11</sup>Crucially, these coordinates hold over the entire horizon.

$$\langle T \rangle = dc \left( \frac{-\bar{A}^{(d)}(r, 0, x^i) dt^2 + \bar{B}^{(d)}(r, 0, x^i) dr^2 + 2\alpha_i^{(d)}(r, 0, x) dr dx^i}{r^2} \right) + dc \left( H_{ij}^{(d)}(r, 0, x^i) dx^i dx^j \right), \quad (3.70)$$

where  $\bar{A}(r, z, x^i) = \bar{A}^{(0)}(r, 0, x^i) + z^2 \bar{A}^{(2)}(r, 0, x^i) + \dots z^d \bar{A}^{(d)}(r, 0, x^i) + \dots$ , and similarly for the other functions. The crucial point is that the near-horizon limit and this expansion in  $z$  commute, so we can take the near-horizon limit independently at each order in  $z$ . Applied at this order in  $z$ , the near horizon limit is simply the large scale limit of this stress tensor, and so this large scale limit must be equal to the stress tensor from the near horizon geometry  $g_{nh} [h_{ij}(x)]$ .

In summary we conclude that if the bulk contains an extremal horizon that meets the boundary at null infinity, it's near horizon geometry is a solution to the near horizon equations with conformal boundary given by the large scale limit of the boundary geometry. In addition, the above argument tells us that the large scale limit of the one-point function of the stress tensor can be extracted from the near-horizon geometry.

### Obstructions to Null Infinity extending to an Extremal Horizon

So far we have discussed what must happen if there is an extremal horizon that meets the boundary at null infinity. We now turn that on it's head, and ask under what conditions null infinity **can** extend to an extremal horizon in the bulk.

First of all, it follows from (3.33), that any null infinity that extends to an extremal horizon in the bulk must be conformally related to an extremal horizon. It must therefore have the corresponding enhanced SO(2,1) symmetry. We call this an 'extremal null infinity'. We will discuss what happens in the interesting more generic case where null infinity is non-extremal in Chapter 4. For now, we can construct an example by taking a Minkowski boundary and periodically identifying one of it's spatial directions. For instance, for a 2 + 1 dimensional boundary we would write

$$g = -dt^2 + dr^2 + \alpha^2 d\phi^2 \quad (3.71)$$

where  $\phi$  has period  $2\pi$ . We can see that the scale-invariant limit of this is in fact singular. The transformation (3.48) leaves

$$\bar{g} = -dt^2 + dr^2 + \alpha^2 \frac{d\phi^2}{\mu^2}. \quad (3.72)$$

so the  $\phi$  circle vanishes in this limit. This, therefore, cannot be the boundary of a bulk which has an extremal horizon that meets the boundary at infinity. Indeed, as we discussed in 1.7.3, there are two bulk vacuum solutions we could consider here, the AdS-Soliton or periodically identified Poincaré AdS. Neither of these has an extremal horizon. Periodically identified Poincaré AdS actually has a region that looks like an extremal horizon, but has a singularity in place of the horizon. To illustrate this, we can add a

compact direction to Poincare AdS (3.73)

$$g = \frac{-dt^2 + dz^2 + d\rho^2 + \rho^2 d\Omega_{d-3}^2 + d\theta^2}{z^2}. \quad (3.73)$$

Performing the coordinate transformation (3.38)

$$g = \psi^2 \left( \frac{-dt^2 + dr^2 + d\theta^2}{r^2} \right) + \frac{d\psi^2}{\psi^2 - 1} + (\psi^2 - 1) d\Omega_{d-3}^2. \quad (3.74)$$

The near-horizon limit of this looks like a near-horizon geometry, except the  $\theta$  circle shrinks, making it singular.

Given a boundary geometry that does have an extremal null infinity further constraints are provided by the conditions that the near-horizon limit of (3.66) is well-defined. Since the FG coordinate  $z$  is not touched by this limit, this should be true order by order in  $z$ . For instance, the  $z^d$  component of this expansion tells us the stress tensor needs to be finite in this limit, which means it has the scale-invariant form (3.14). Transforming to the flat frame, it's leading order fall off needs to be (3.16), otherwise null infinity cannot extend to an extremal horizon in the bulk. This is precisely the condition that the CFT state has a well defined large scale limit as in 3.5.1.

We can illustrate what changes holographically when the state does not have a large scale limit by, for instance, considering a finite temperature homogeneous state in Minkowski. The stress tensor here has a constant energy density, and so does not fall off as fast as (3.16). The bulk dual to this state is AdS-Schwarzschild (1.40) We can take coordinates like we do for the near horizon geometry by setting  $z = \bar{z}r$

$$g = \frac{d\phi^2 + \frac{dr^2}{r^2} - \left(1 - \frac{\bar{z}^d r^d}{z_0^d}\right) \frac{dt^2}{r^2} + \frac{(rd\bar{z} + \bar{z}dr)^2}{r^2 \left(1 - \frac{\bar{z}^d r^d}{z_0^d}\right)}}{\bar{z}^2}. \quad (3.75)$$

However now we cannot take the  $r \rightarrow \infty, t \rightarrow \infty$  limit. Note that, in these coordinates, the black-hole horizon is at

$$r = \frac{z_0}{\bar{z}}, \quad (3.76)$$

which does meet the boundary at null infinity, but is not an extremal horizon.

### 3.5.4 Beyond the universal sector

The proof in [59] was in the universal sector, but we would expect a similar story with the addition of extra fields. In particular, the argument relating the near horizon limit to the large scale-limit holds just as well with the addition of extra bulk fields. Taking the near horizon limit of additional bulk fields is therefore equivalent to taking the large scale limit of the corresponding dual CFT operators.

An example has been demonstrated numerically in [66]. Here they considered the addition of a gauge field in the  $3 + 1$  dimensional bulk, and so an electric potential on the

2 + 1 dimensional boundary. The boundary electric potential was asymptotically scale-invariant, but had non-trivial rotationally invariant profiles as a function of radius. The large scale, scale-invariant limit of this electric potential determined the resulting near horizon geometry of the extremal horizon in the bulk. These near horizon geometries are the ones we discussed in 3.4.2.

### 3.6 Discussion

In this chapter, we started with the simple observation that near-horizon geometries in the bulk describe a certain class of scale-invariant states in holographic CFTs. We then argued more generally that spacetimes with extremal horizons in the bulk can be used to describe holographic CFT states with well defined large scale limits. The large scale limit of the state is then described by the near-horizon geometry. The power of this result lies in its universality. This holds for any universal-sector state with an extremal horizon that meets the conformal boundary in this way. We would argue that similar results should hold with the addition of matter fields. The existence of the near-horizon limit in the bulk, which satisfies its own near-horizon equations means that the large-scale limit of the corresponding CFT states can also be treated apart from the full states.

In certain cases, this could even apply to integrated quantities like charges, when those quantities are tied to the asymptotic fall-off of corresponding densities. For instance in [66] they considered a CFT with no chemical potential and then smoothly turn one on with arbitrary profile  $V(r)$ . They found that the total charge only depended on the scale-invariant large scale fall-off of the chemical potential. Hence, if this large scale fall-off is described by a near-horizon geometry, this near horizon-geometry tells you the total charge, independent of what happens away from the large scale limit. Holographically, you can argue this by considering a non-scale-invariant bulk with a gauge field and an extremal horizon in the infrared. If the bulk spacetime is bounded only by this null surface and the conformal boundary, and there is no charged matter or horizons in the bulk, then Gauss's law tells us that the electric flux through the boundary (which is the total charge in the CFT), is equal to the charge on the horizon. This charge can be calculated just as well on the near-horizon geometry, and so would be unchanged as you take the large scale limit.

However, this story is by no means all encompassing. From the discussion in 3.3 of the enhanced symmetry of static extremal horizons, we know that they cannot describe the most generic static, scale-invariant states. Since a conformal boundary that breaks this symmetry is a perfectly legitimate choice of boundary conditions for Einstein's equations, there should exist static, scale-invariant bulks without this extra symmetry. These bulks are the subject of Chapter 4.

## Chapter 4

# Singular Scale Invariant Geometries

In the previous chapter we explored the role of extremal horizons in describing (asymptotically) static scale-invariant states in Holographic CFTs. The observation we now want to make is that these bulk space-times can only get us so far. As remarked in Section 3.3 static near-horizon geometries have enhanced symmetry. The static and scale-symmetry are part of a larger  $SO(2, 1)$  symmetry due to the  $AdS_2$  factor in their metric.

This means that AlAdS extremal horizons cannot describe the most generic static scale-invariant states. In this chapter we discuss work that was published in [68] in which we discussed bulk spacetimes that generalize the notion of extremal horizons, and which allow us to describe more generic static scale-invariant states holographically. We demonstrate their existence by constructing them numerically using the techniques described in Chapter 2. Our claim is then that these are possible IR geometries in the case that the CFTs have a large scale limit of this more general form, in the same way that extremal horizons can lie in the IR when the large scale limit has the appropriate enhanced symmetry. This would mean that the enhanced symmetry that's often observed in the IR in AdS/CFT is only there because we are considering a subset of the possible IR geometries.

The examples we will construct will have  $3 + 1$  dimensional bulks, and we will consider both the universal sector, and the addition of a bulk gauge field. From the discussion in 3.4.2, we know that the most general static scale-invariant boundary metric and chemical potential that is consistent with a near-horizon geometry in the bulk is

$$\begin{aligned} h &= -dt^2 + dr^2 + \alpha^2 r^2 d\phi^2 \\ A &= e \frac{dt}{r}. \end{aligned} \tag{4.1}$$

The metric is a cone, and the chemical potential has a scale-invariant, isotropic (i.e. independent of  $\phi$ ), fall off. However, a more generic scale-invariant set of sources we might consider is

$$\begin{aligned} h &= -dt^2 + dr^2 + 2\chi(\phi)rdrd\phi + \alpha^2 r^2 d\phi^2 \\ A &= V(\phi) \frac{dt}{r}. \end{aligned} \tag{4.2}$$

Here, the cone metric has been replaced by what we will call a twisted cone, and the chemical potential is no longer isotropic. These sources are still static and scale-invariant, but they break the extra generator of the  $SO(2, 1)$  symmetry. As before, we can also write

this in a conformal frame where the scale invariance is manifest

$$\begin{aligned}\bar{h} &= \frac{-dt^2 + dr^2}{r^2} + 2\chi(\phi)\frac{dr}{r}d\phi + \alpha^2 d\phi^2 \\ A &= V(\phi)\frac{dt}{r}.\end{aligned}\tag{4.3}$$

The bulk Einstein-Maxwell equations are

$$\begin{aligned}R_{\mu\nu}^{(n)} &= -\frac{3}{\ell^2}g_{\mu\nu}^{(n)} + 2\left(F_{\mu\alpha}F_{\nu}{}^{\alpha} - \frac{1}{4}g_{\mu\nu}(F_{\alpha\beta}F^{\alpha\beta})\right) \\ \nabla_{\mu}F^{\mu\nu} &= 0.\end{aligned}\tag{4.4}$$

where we will take units with  $\ell = 1$ . The bulk spacetime is four dimensional, but the staticity and scale-invariance will leave us with a set of two dimensional PDEs.

We will start by constructing these bulks as linear perturbations of AdS, then we will proceed to the numerical construction of examples of bulk solutions to the full equations, and then we will discuss their properties and the singularity more generally.

## 4.1 Linearised Construction of Solutions

Here we present the linearised construction of the bulks we are interested in as perturbations of AdS. This calculation was first presented without a gauge field in [59], and then the gauge field was added in [68].

We write down a linearised perturbation of AdS, and a linearised gauge field

$$\begin{aligned}g &= g_{AdS} + h \\ A &= \alpha,\end{aligned}\tag{4.5}$$

substitute into (4.4), and expand to linear order in  $h$  and  $\alpha$ . Since the gauge field only enters quadratically in the equations, it decouples and simply satisfies Maxwell's equations on  $AdS_4$  and the perturbation  $h$  separately satisfies the linearised Einstein's equation on this background. The perturbations are going to preserve the staticity and the scaling symmetry, but break the other symmetries of AdS. To take advantage of this symmetry we will write  $AdS_4$  as

$$g_{AdS} = \frac{\psi^2}{r^2}(-dt^2 + dr^2) + \frac{1}{\psi^2 - 1}d\psi^2 + (\psi^2 - 1)d\phi^2.\tag{4.6}$$

Because of the rotational symmetry of the background, we can expand our perturbation in Fourier modes in  $\phi$ . For each mode we write an ansatz

$$\begin{aligned}
h &= \cos n\phi \left( p_n(\psi) \left( \frac{-d\psi^2}{\psi^2 - 1} + (\psi^2 - 1) d\phi^2 \right) \right) \\
&\quad + \cos n\phi \left( 2l_n(\psi) \frac{dr}{r} d\psi \right) \\
&\quad + \sin n\phi \left( 2f_n(\psi) \frac{dr}{r} d\phi \right) \\
&\quad + \sin n\phi (2h_n(\psi) d\psi d\phi) \\
\alpha &= v_n(\psi) \cos n\phi \frac{dt}{r}
\end{aligned} \tag{4.7}$$

with integer  $n \geq 0$ . We then have a set of ODEs in  $\psi$ . The solution for the gauge field is

$$v_n(\psi) = \begin{cases} B_1 + B_2 \operatorname{arcCoth} \psi & n = 0 \\ B_1 \left( \frac{\psi-1}{\psi+1} \right)^{n/2} + B_2 \left( \frac{\psi+1}{\psi-1} \right)^{n/2} & n > 0 \end{cases} \tag{4.8}$$

where  $B_1$  and  $B_2$  are constants, and the Einstein's equation for the other functions can be reduced to a single second order ODE for  $p_n$  with solution

$$p_n(\psi) = \begin{cases} C_1 + C_2(\psi + 2 \operatorname{arcCoth} \psi) & n = 0 \\ \frac{1}{\psi(\psi^2-1)} \left( C_1 \left( \frac{\psi-1}{\psi+1} \right)^{n/2} (n\psi - 1) + C_2 \left( \frac{\psi+1}{\psi-1} \right)^{n/2} (n\psi + 1) \right) & n > 0 \end{cases} \tag{4.9}$$

Imposing smoothness at  $\psi = 1$  implies  $B_2 = C_2 = 0$ .

The  $n = 0$  modes aren't very interesting, they simply move us along the 2 parameter family of near-horizon geometries from 3.4.2. For  $n > 0$  the other metric functions take the form

$$\begin{aligned}
l_n(\psi) &= -C_1 n \psi (\psi - 1)^{\frac{n}{2}-1} (\psi + 1)^{-\frac{n}{2}-1} \\
f_n(\psi) &= C_1 \left( \frac{\psi - 1}{\psi + 1} \right)^{n/2} (n\psi + \psi^2 - 1) \\
h_n(\psi) &= C_1 \frac{(\psi - 1)^{\frac{n}{2}-1} (\psi + 1)^{-\frac{n}{2}-1} (n\psi - 1)}{\psi}.
\end{aligned} \tag{4.10}$$

To interpret these deformations we look at the conformal boundary. For the perturbation to the gauge field, the boundary chemical potential is of the form (4.3) with

$$V(\phi) = B_1 \cos n\phi. \tag{4.11}$$

From the asymptotic expansion of the solution we can extract the VEV of the dual charge density

$$\rho(\phi) = -nB_1 \cos n\phi. \tag{4.12}$$

For the metric perturbation we can see that the boundary metric gets deformed to

$$g_{\partial} = \frac{-dt^2 + dr^2}{r^2} + d\phi^2 + 2\epsilon C_1 \sin n\phi \frac{dr}{r} d\phi, \quad (4.13)$$

which is a twisted cone from (4.3). Through the Fefferman-Graham expansion[30], we can extract the boundary stress tensor

$$T_{\mu\nu} = cC_1 \left( \frac{(n^2 - 1) dt^2 \cos(n\phi)}{r^2} + \frac{(n^2 + 1) dr^2 \cos(n\phi)}{r^2} + \frac{4ndr d\phi \sin(n\phi)}{r} - 2d\phi^2 \cos(n\phi) \right). \quad (4.14)$$

These modes can be added together to give any choice of  $V(\phi)$  or  $\chi(\phi)$  we want, while an extremal horizon in the bulk would require  $\chi(\phi) = 0$  and  $V(\phi) = e$  for some constant  $e$ . This linearised calculation therefore suggests that the near-horizon geometries are only a very special subset of a more generic class of scale-invariant IR geometries.

## 4.2 Setup for Numerical Construction of Solutions

The best way to demonstrate that these scale-invariant bulk geometries exist would be to find an explicit analytic solution. Unfortunately, we haven't yet found one, so all we can do is construct them numerically. In this section we present the setup for finding these solutions, what boundary conditions we choose to consider, and aspects of how we can demonstrate that these are genuine solutions. We will then discuss the explicit solutions in 4.3.

### 4.2.1 The Harmonic Einstein's Equation and our Ansatz

For the numerical computation, we take coordinates like (4.6) but we replace the holographic coordinate  $\psi$  with a new coordinate  $X$  which ranges from  $0 \leq X \leq 1$ , with  $X = 1$  being the conformal boundary, and  $X = 0$  being the axis of symmetry. The domain of the problem has therefore been compactified to a unit-disk  $\mathcal{D}$ , with  $X$  the radial coordinate, and  $\phi$  the angular one.

We will take an ansatz for the most general metric and gauge field compatible with the symmetries, written in terms of these coordinates

$$g = \frac{1}{(1-X^2)^2} \left( S_1(X, \phi) \frac{dt^2}{r^2} + S_2(X, \phi) \frac{dr^2}{r^2} + 2 \frac{dr}{r} \omega_i(X, \phi) dy^i + g_{2ij}(X, \phi) dy^i dy^j \right) \\ A = S_3(X, \phi) \frac{dt}{r}, \quad (4.15)$$

where  $y$  runs over  $(X, \phi)$ . From the perspective of  $\mathcal{M}$ ,  $S_1$ ,  $S_2$ , and  $S_3$  are scalars,  $\omega$  is a one-form, and  $g_2$  is a symmetric rank 2 tensor. Note that as we have explicitly factored out the divergent conformal factor  $\frac{1}{(1-X^2)^2}$ , we can choose coordinates such that these are all smooth objects on  $\mathcal{D}$ . While, as we will discuss, the surface  $r \rightarrow 0$  is singular, we still

want the geometry on constant  $r$  surfaces to be smooth which means, for instance, that the induced metric  $g_{ij}^2$  will be non-degenerate.

Building the symmetries into the ansatz goes some way towards fixing the gauge freedom in (4.4). In particular, we have chosen to focus on a pure electric solution, so we are able to fix the  $U(1)$  gauge freedom by setting the spatial components of  $A$  to zero,  $A_i = A_r = 0$ . However, we still have coordinate freedom over  $\mathcal{D}$  corresponding to the transformations

$$\begin{aligned} t &\rightarrow \mu t \\ r &\rightarrow r\lambda(X, \phi) \\ X &\rightarrow \tilde{X}(X, \phi) \\ \phi &\rightarrow \tilde{\phi}(X, \phi). \end{aligned} \tag{4.16}$$

The first of these is fixed by the boundary conditions, but to fix the others we will need to make use of the method described in Chapter 2. We will use the Harmonic Einstein's equation, which in our case take the form

$$\begin{aligned} R_{\mu\nu} &= -\frac{d}{\ell^2}g_{\mu\nu} + 2\left(F_{\mu\alpha}F_{\nu}^{\alpha} - \frac{1}{4}g_{\mu\nu}\left(F_{\alpha\beta}F^{\alpha\beta}\right)\right) + \nabla_{(\mu}\xi_{\nu)} \\ \nabla_{\mu}F^{\mu\nu} &= 0. \end{aligned} \tag{4.17}$$

where  $\xi$  is defined as usual in terms of some reference connection  $\bar{\Gamma}$

$$\xi(x)^{\alpha} \equiv g^{\mu\nu}\left(\Gamma^{\alpha}_{\mu\nu} - \bar{\Gamma}^{\alpha}_{\mu\nu}\right). \tag{4.18}$$

This reference connection will be derived from a reference metric  $\bar{g}$  which we will write in the same ansatz (4.15). The choice of  $\bar{g}$  is implicitly a choice of coordinate system, and we'll discuss this choice in 4.2.5.

## 4.2.2 A Generalization of the Maximum Principle

In the absence of a gauge field, the maximum principle discussed in 2.2 ensures that so long as we choose boundary conditions such that  $\phi = \xi^{\alpha}\xi_{\alpha}$  vanishes on  $\partial\mathcal{D}$ , then solutions to (4.17) are automatically solutions to (4.4). Note that the scaling symmetry means that  $\phi$  is independent of  $r$ , so we don't need to worry about it being maximized for  $r \rightarrow 0$  or  $r \rightarrow \infty$ . For  $F_{\mu\nu} \neq 0$  however we do not have such a maximum principle. This presents a potential difficulty. In order to demonstrate that a particular solution to (4.17) is a solution to (4.4) we need to show that  $\xi = 0$  everywhere. While this would be straight forward for analytic solutions, we will be producing numerical solutions to discretized versions of (4.17) evaluated on a finite lattice. At any finite lattice spacing, we would not expect to find  $\xi = 0$ . Rather, we would expect that as the lattice spacing is taken to zero, and our numerical solutions are becoming ever better approximations to continuum solutions, we should find  $\xi \rightarrow 0$ . The problem of demonstrating  $\xi = 0$

is therefore tied up with the issue of demonstrating the numerical convergence of our solutions to continuum, and it becomes hard to rule out finite but small  $\xi$ .

In some cases, we can show  $\xi = 0$  more robustly by an indirect method. This involves a slight generalization of the maximum principle from 2.2. From the contracted Bianchi identity applied to (4.17) we can show

$$\nabla^2 \phi + \xi^\mu \partial_\mu \phi = 2 \frac{d}{\ell^2} \xi^\alpha \xi_\alpha + 2(\nabla^\mu \xi^\nu)(\nabla_\mu \xi_\nu) - 2\tilde{T}_{\mu\nu} \xi^\mu \xi^\nu, \quad (4.19)$$

where  $\tilde{T}_{\mu\nu} = 2(F_{\mu\alpha} F_\nu^\alpha - \frac{1}{4} g_{\mu\nu} (F_{\alpha\beta} F^{\alpha\beta}))$  and  $\phi = \xi^\alpha \xi_\alpha$ . Because of the static symmetry, we will have that  $(\nabla^\mu \xi^\nu)(\nabla_\mu \xi_\nu) \geq 0$ <sup>1</sup>. We can therefore write

$$\nabla^2 \phi + \xi^\mu \partial_\mu \phi \geq 2 \left( \frac{d}{\ell^2} g_{\mu\nu} - \tilde{T}_{\mu\nu} \right) \xi^\mu \xi^\nu, \quad (4.20)$$

If the right hand side of this equation is positive for any  $\xi$ , then we have  $\nabla^2 \phi + \xi^\mu \partial_\mu \phi \geq 0$  which is the inequality from which the usual maximum principle follows. Therefore, if the spatial part of the tensor  $\frac{d}{\ell^2} g_{\mu\nu} - \tilde{T}_{\mu\nu}$  is positive definite, the same maximum principle holds as before, and so long as  $\phi = 0$  on  $\partial D$ ,  $\phi$  vanishes everywhere.

While the spatial part of  $g_{\mu\nu}$  is positive definite on an arbitrary spacetime, the properties of  $\frac{d}{\ell^2} g_{\mu\nu} - \tilde{T}_{\mu\nu}$  depend on the precise solution. This is therefore something we have to test on each explicit numerical solution. However, this test can be easier than demonstrating  $\phi = 0$  directly. This is because we just need to test that the eigenvalues of this matrix are positive, and if these eigenvalues are reasonably large, this disentangles the problem from issues of numerical convergence. For some of our solutions we find this is true, and in others we don't. For instance, if we look at the near horizon solutions from Section 3.4.2 we find that sometimes this matrix is positive definite, and sometimes it isn't. This is illustrated in Figure 4.1.

In the cases where this matrix is not positive definite, we have to check  $\xi_\mu = 0$  directly. As mentioned, at any finite lattice resolution this won't be the case, but rather what we should have is  $\xi_\mu \rightarrow 0$  as the number of lattice points is increased. This is checked in 4.3.4.

### 4.2.3 Boundary Conditions

We have a set of two dimensional PDEs which are elliptic on  $\mathcal{D}$ . In order to have a well-posed problem, we need to provide boundary conditions on  $\partial\mathcal{D}$ , which is  $X = 1$ . These boundary conditions fix the metric and chemical potential on the conformal boundary. As long as we impose these constraints on our boundary conditions for the ansatz (4.15) here

$$\begin{aligned} \omega(1, \phi) &= \omega_\phi(1, \phi) d\phi \\ g_2(1, \phi) &= 4dX^2 + g_{\phi\phi}(1, \phi) d\phi^2, \end{aligned} \quad (4.21)$$

<sup>1</sup>This can be seen most easily by analytically continuing to Euclidean signature.

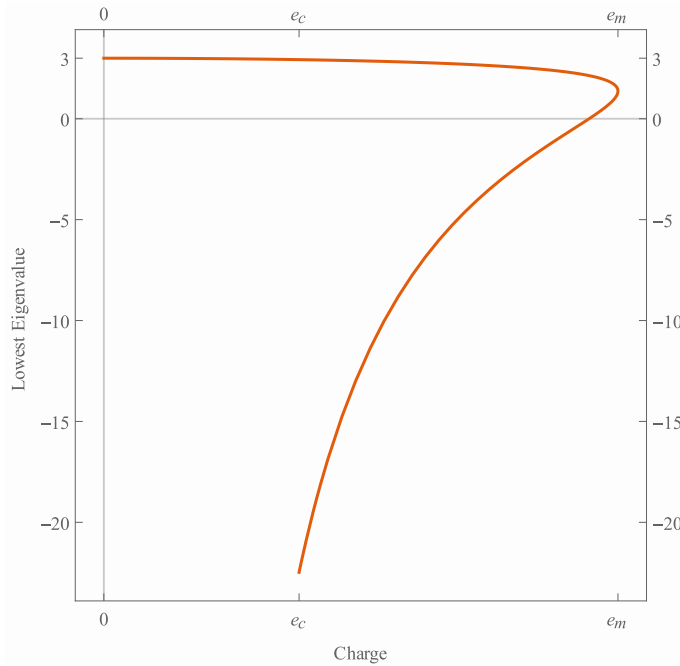


FIGURE 4.1: Minimum value of the minimum eigenvalue of the spatial matrix  $\frac{d}{d^2}g_{\mu\nu} - \tilde{T}_{\mu\nu}$  for the near-horizon geometries from (3.45) (with no conical deficit) as a function of charge. For the entirety of Branch 1, as defined in 3.4.2, this eigenvalue is positive, meaning that the matrix is positive definite.

which is required so that the metric satisfies Einstein's equation to leading order, then the remaining boundary conditions fix the metric and potential on the conformal boundary to be

$$\begin{aligned} h &= S_1(1, \phi) \frac{dt^2}{r^2} + S_2(1, \phi) \frac{dr^2}{r^2} + 2\omega_\phi(1, \phi) \frac{dr}{r} d\phi + g_{\phi\phi}(1, \phi) d\phi^2 \\ A &= S_3(1, \phi) \frac{dt}{r}. \end{aligned} \quad (4.22)$$

We presented the boundary metric and chemical potential in which we will be interested in (4.2). This choice of boundary conditions corresponds to

$$\begin{aligned} S_1(1, \phi) &= S_2(1, \phi) = 1 \\ \omega_\phi(1, \phi) &= \chi(\phi) \\ g_{\phi\phi}(1, \phi) &= \alpha^2 \\ S_3(1, \phi) &= V(\phi). \end{aligned} \quad (4.23)$$

In fact, up to coordinate transformations and Weyl scaling, (4.2) is the most generic static, scale-invariant boundary condition. Starting from a general static-scale invariant metric and chemical potential

$$\begin{aligned} h &= -S_1(\phi) \frac{dt^2}{r^2} + S_2(\phi) \frac{dr^2}{r^2} + \psi(\phi)^2 d\phi^2 + 2\chi(\phi) d\phi \frac{dr}{r} \\ A &= V(\phi) \frac{dt}{r}, \end{aligned} \quad (4.24)$$

we can eliminate functions by a appropriate choice of coordinates and frame. Just like we had in the bulk in (4.16) we have coordinate transformations

$$\begin{aligned} t &\rightarrow \mu t \\ r &\rightarrow \lambda(\phi)r \\ \phi &\rightarrow \tilde{\phi}(\phi) \end{aligned} \tag{4.25}$$

and in addition we have a freedom of conformal frame under which

$$g \rightarrow \Omega(\phi)g. \tag{4.26}$$

Due to the scaling symmetry,  $t \rightarrow \mu t$  with  $r \rightarrow \mu r$  leaves the metric invariant, so only the second two of the coordinate transformations in (4.25) can help us.

The requirement that the signature of the metric is fixed means that  $S_1(\phi) > 0$  and  $S_2(\phi)\psi(\phi)^2 > \chi(\phi)^2 \geq 0$ . This means that the Weyl transformation where  $g \rightarrow \frac{g}{S_2(\phi)}$  is non-singular, and we can use it to send  $S_2(\phi) \rightarrow 1$ . Having done that, we can then perform the transformation  $r \rightarrow \sqrt{S_1(\phi)}r$  to send  $S_1(\phi) \rightarrow 1$ .

This just leaves three degrees of freedom  $\psi(\phi)$ ,  $\chi(\phi)$  and  $V(\phi)$ , and one gauge symmetry  $\phi \rightarrow \tilde{\phi}(\phi)$ . We need to be a little bit careful when using this freedom because the  $\phi$  coordinate is periodic, so we require

$$\tilde{\phi}(\phi + 2\pi) = \tilde{\phi}(\phi) + 2\pi. \tag{4.27}$$

A consistent choice is

$$\tilde{\phi}(\phi) = \frac{2\pi \int_0^\phi \psi(\phi')d\phi'}{\int_0^{2\pi} \psi(\phi')d\phi'} \tag{4.28}$$

which allows us to set  $\psi(\phi) \rightarrow \alpha = \frac{Vol(S_1)}{2\pi}$ . This leaves us with the general form (4.2). One subtlety is that if both  $V(\phi)$  and  $\chi(\phi)$  are constants the resulting rotational symmetry allows us to get rid of  $\chi$ . If  $\chi(\phi) = \mu$ , we can set  $\phi \rightarrow \phi - \frac{\mu}{\alpha^2} \log r$  to get rid of it. In addition the requirement that the metric is non-degenerate adds an additional constraint to (4.2). We require  $\alpha^2 > \chi(\phi)^2$ .

Having used up all this freedom, we can confirm that the the metric in (4.2) is conformally non-trivial by looking at it's Cotton tensor. The non-vanishing components are

$$\begin{aligned} C^{tr} &= \frac{2\chi(\phi)\chi'(\phi)^2}{\alpha(\chi(\phi)^2 - 1)^3} - \frac{\chi''(\phi)}{2\alpha(\chi(\phi)^2 - 1)^2} \\ C^{t\phi} &= -\frac{\chi'(\phi)}{\alpha r(\chi(\phi)^2 - 1)^2}. \end{aligned} \tag{4.29}$$

The fact that it is non-zero means that the metric is not conformally flat[69].

The set of possible boundary deformations forms an infinite dimensional function space, so we need to choose some finite set of deformations to focus on. We will, for simplicity, consider deformations to the metric and to the gauge field separately. So we

will consider a two parameter family of deformations where

$$\begin{aligned}\chi(\phi) &= \lambda \sin 2\phi \\ V(\phi) &= 0\end{aligned}\tag{4.30}$$

for varying values of  $\alpha$ , and another where

$$\begin{aligned}\chi(\phi) &= 0 \\ V(\phi) &= a + b \cos(2\phi),\end{aligned}\tag{4.31}$$

with  $\alpha = 1$ . For  $\lambda = 0$  in (4.30) and for  $b = 0$  in (4.31), we have the enhanced  $\text{SO}(2,1)$  symmetry, and the bulks are the near horizon geometries described in 3.4.2. For reasons which we will explain in 4.2.4, we have restricted ourselves here to deformations with a  $\phi \rightarrow \phi + \pi$  symmetry. In fact, they also have a  $\phi \rightarrow -\phi$  symmetry, and we'll see both symmetries are preserved in our solutions.

#### 4.2.4 Discretization

Having fixed the domain, ansatz, and boundary conditions, the equations (4.17) become a well posed set of 8 coupled PDEs to solve for 8 functions ( $S_1, S_2, S_3$ , the two components of  $\omega$ , and the three components of  $g_2$ ). In order to solve this numerically we now need to discretize the PDE as described in 2.4.

The difficulty is that the disk domain isn't really suited to a square lattice. We will take as our two coordinates the  $X$  and  $\phi$  radial and angular coordinates described above. These coordinates break down at the origin, so even if the functions in our ansatz are smooth functions of  $X$  and  $\phi$ , that doesn't imply that the geometric objects built up from them are smooth on  $\mathcal{D}$ .

The requirements of smoothness can be thought of as a set of differential constraints at  $X = 0$ . The objects are smooth if we can write them as smooth functions of some coordinates that are well defined at  $X = 0$ . A simple choice of such coordinates are the Cartesian type coordinates  $x, y$  related to  $X, \phi$  through

$$\begin{aligned}x &= X \cos \phi \\ y &= X \sin \phi.\end{aligned}\tag{4.32}$$

The requirement is then that in an open region around  $X = 0$

$$\begin{aligned}S_i(X, \phi) &= \tilde{S}_i(x, y) \\ \omega_X(X, \phi)dX + \omega_\phi(X, \phi)d\phi &= \tilde{\omega}_x(x, y)dx + \tilde{\omega}_y(x, y)dy \\ g_{XX}^2(X, \phi)dX^2 + 2g_{X\phi}^2(X, \phi)dXd\phi &= \tilde{g}_{xx}^2(x, y)dx^2 + 2\tilde{g}_{xy}^2(x, y)dxdy \\ &+ g_{\phi\phi}^2(X, \phi)d\phi^2 + \tilde{g}_{yy}^2(x, y)dy^2,\end{aligned}\tag{4.33}$$

where all the functions of  $x$  and  $y$  on the right hand side are smooth. Using the coordinate transformation, we can write out these equations component by component

$$\begin{aligned}
S_i(X, \phi) &= \tilde{S}_i(X \cos \phi, X \sin \phi) \\
\omega_X(X, \phi) &= \tilde{\omega}_x(X \cos \phi, X \sin \phi) \cos \phi + \tilde{\omega}_y(X \cos \phi, X \sin \phi) \sin \phi \\
\omega_Y(X, \phi) &= X (\tilde{\omega}_y(X \cos \phi, X \sin \phi) \cos \phi - \tilde{\omega}_x(X \cos \phi, X \sin \phi) \sin \phi) \\
g_{XX}^2(X, \phi) &= \tilde{g}_{xx}^2(X \cos \phi, X \sin \phi) \cos^2 \phi + \tilde{g}_{yy}^2(X \cos \phi, X \sin \phi) \sin^2 \phi \\
&\quad + \tilde{g}_{xy}^2(X \cos \phi, X \sin \phi) \sin 2\phi \\
g_{X\phi}^2(X, \phi) &= X \left( \tilde{g}_{xy}^2(X \cos \phi, X \sin \phi) \cos 2\phi \right. \\
&\quad \left. + \frac{\tilde{g}_{yy}^2(X \cos \phi, X \sin \phi) - \tilde{g}_{xx}^2(X \cos \phi, X \sin \phi)}{2} \sin 2\phi \right) \\
g_{\phi\phi}^2(X, \phi) &= X^2 (\tilde{g}_{yy}^2(X \cos \phi, X \sin \phi) \cos^2 \phi - \tilde{g}_{xy}^2(X \cos \phi, X \sin \phi) \sin 2\phi \\
&\quad + \tilde{g}_{xx}^2(X \cos \phi, X \sin \phi) \sin^2 \phi).
\end{aligned} \tag{4.34}$$

The differential constraints that impose smoothness at  $X = 0$  can be found by expanding the above in a power series in  $X$ . For instance the  $n$ -th  $X$  derivative of one of the scalars must satisfy

$$S_i^{(n,0)}(0, \phi) = \sum_{m=0}^n \cos^m \phi \sin^{n-m} \phi \tilde{S}_i^{(m, n-m)}(0, 0) \tag{4.35}$$

which is equivalent to the requirement that if you expand it in modes  $e^{im\phi}$ , the only non-zero ones are in the range  $-n \leq m \leq n$ .

This, and the corresponding constraints for the vector and tensor are tricky to apply as boundary conditions, so instead we avoid treating the point  $X = 0$  as a boundary. We will extend the  $X$  coordinate to the domain  $-1 \leq X \leq 1$ , so that we are covering the whole disk twice. The extension is defined so that the relation (4.32) continues to hold for negative  $X$ . When putting a lattice on this extended domain, we will avoid putting a point at  $X = 0$  as the equations are singular here.

Solutions on this extended domain must be invariant under

$$\begin{aligned}
X &\rightarrow -X \\
\phi &\rightarrow \phi + \pi
\end{aligned} \tag{4.36}$$

for consistency. This identification mixes  $X$  and  $\phi$  together, and so we wouldn't be able to construct separate derivative matrices for each coordinate. To avoid this complication, we will consider only solutions that are even about  $X = 0$ , so they are invariant under

$$\begin{aligned}
x &\rightarrow -x \\
y &\rightarrow -y.
\end{aligned} \tag{4.37}$$

The symmetry then implies that our solution is invariant under each of

$$\begin{aligned} X &\rightarrow -X \\ \phi &\rightarrow \phi + \pi \end{aligned} \quad (4.38)$$

taken separately. This obviously does not automatically mean that the conditions for smoothness are satisfied at  $X = 0$ , but since we are no longer treating the point as a boundary, we don't apply boundary conditions there. Instead, we simply check that our solutions are smooth there after finding them, by checking the conditions implied by (4.34). This is discussed in 4.3.4.

We therefore construct a lattice for  $X$  that builds in this even symmetry as described in 2.4, and similarly we construct a periodic lattice with period  $\pi$  for  $\phi$ . In the  $X$  direction we use 6th order finite difference, and in the  $\phi$  direction we use Fourier differencing. Crucially there is no point at  $X = 0$  where the equations would be singular.

We then specialize some of our functions in the ansatz to take advantage of this symmetry and to build in some of the lowest order smoothness requirements near  $X = 0$

$$\begin{aligned} S_1(X, \phi) &= (1 + X^2)(1 + A(X, \phi)) \\ S_2(X, \phi) &= (1 + X^2)(1 + B(X, \phi)) \\ \omega(X, \phi) &= F(X, \phi)d(X^2) + X^2H(X, \phi)d\phi \\ g(X, \phi) &= 4(1 + L(X, \phi))(dx^2 + dy^2) + 2M(X, \phi)dx dy + S(X, \phi)(dx^2 - dy^2). \end{aligned} \quad (4.39)$$

#### 4.2.5 The Reference Metric

The final thing that needs to be specified is the fixed reference metric in (4.17). Some care needs to be taken in choosing this because it needs to be consistent with the gauge condition  $\phi = \xi_\mu \xi^\mu = 0$  on the boundary. From the discussion in Section 2.2 we know that this means that the reference metric should satisfy the same boundary conditions as our solution.

For the gauge field deformations (4.31), for given  $a, b$  we will take as our reference metric the near-horizon geometry corresponding to the matching value of  $a$  with  $b = 0$ ,

$$\bar{g}_{\mu\nu} = \frac{1}{(1 - X^2)^2} \left( \psi_0^2 \frac{(1 + X^2)^2}{r^2} (-dt^2 + dr^2) + 4 \left( \frac{dX^2}{P(X)} + P(X)\psi_0^2 X^2 d\phi^2 \right) \right), \quad (4.40)$$

where  $P(X) = -\frac{\psi_0(X^2-1)^3 + X^2(X^2-1)^2 - 2\psi_0^2 X^2(X^4 - 2X^2 + 3)}{\psi_0^2(X^2+1)^2}$  and  $a^2 = \psi_0^2(1 + 3\psi_0)(1 - \psi_0)$ , which is simply (3.45) written in these coordinates.

However, for the metric deformations (4.30), we cannot take a near-horizon geometry as the reference metric, as that would be inconsistent with the boundary conditions. We

therefore choose

$$\begin{aligned} \bar{g}_{\mu\nu} = & h(X) \frac{(1+X^2)^2}{(1-X^2)^2 r^2} (-dt^2 + dr^2) \\ & + \frac{1}{(1-X^2)^2} \left( 4(dX^2 + X^2 d\phi^2) + 8\lambda X^2 k(X) \sin 2\phi \frac{drd\phi}{\alpha r} \right), \end{aligned} \quad (4.41)$$

with  $h(X) = 1 + \frac{1-\alpha^2}{\alpha^2} X^2$  and  $k(X) = 1 - (1 - X^2)^4$ . This has been chosen so that it satisfies the equations of motion for the first few orders near  $X = 1$ , and it satisfies the right boundary conditions so that  $\phi \rightarrow 0$  on the boundary.

#### 4.2.6 Computational Resources

While initial solutions were found using a desktop PC, in order to do a full parameter scan I made use of Imperial College's High Performance Computing (HPC) cluster[70]. This meant that I could make use of multiple nodes to run many different values of the parameters simultaneously. It also allowed me to use the increased memory resources to run at a higher resolution than would have been obtainable on the desktop.

#### 4.2.7 Aside on Calculation of Boundary Charge

Before we proceed to actual solutions, we will discuss a particular observable which we are going to be interested in, which is the total integrated charge on the boundary. As discussed in Section 3.4.2, in these scale-invariant coordinates there are two components to the conformal boundary, one at  $X = 1$  and another at  $r = 0$ .

In the cone frame the  $r = 0$  component corresponds to the origin, so the contribution to the total charge from this component is interpreted as a point charge at the origin. The additional contribution from  $X = 1$  corresponds to a charge density distributed away from the origin.

In fact, we can show that this distributed density integrates to 0, and the only overall contribution to the charge is the point charge at the origin. We've shown a slice of our spacetime at constant  $\phi$  and  $t$  in figure 4.2. The charge from each component of the conformal boundary can be written as[66]

$$Q_a = \lim_{z_a \rightarrow 0} \frac{1}{4\pi} \int_{\mathcal{S}(z_a)} *F, \quad (4.42)$$

where  $z_a$  is some function that goes to 0 on the boundary component in question,  $\mathcal{S}(z_a)$  is a constant time-slice of the surface  $z = z_a$ , and  $*$  is the Hodge star operator. The two components of the conformal boundary in the diagram are at the right and the top. Consider the cylinder in the bulk spatial slice enclosed by the surfaces  $\Sigma_{r_0}$ ,  $\Sigma_{r_1}$ , and  $\Sigma_X$  (the surfaces extend over the  $\phi$  coordinate, but on a constant time slice). We can consider a limit where this cylinder grows to fill the entire spacial slice. In this limit,  $\Sigma_{r_0 \rightarrow \infty}$  becomes the extremal horizon,  $\Sigma_{r_1 \rightarrow 0}$  the component of the conformal boundary corresponding to the origin, and  $\Sigma_{X \rightarrow 1}$  becomes the other component of the conformal boundary. The total

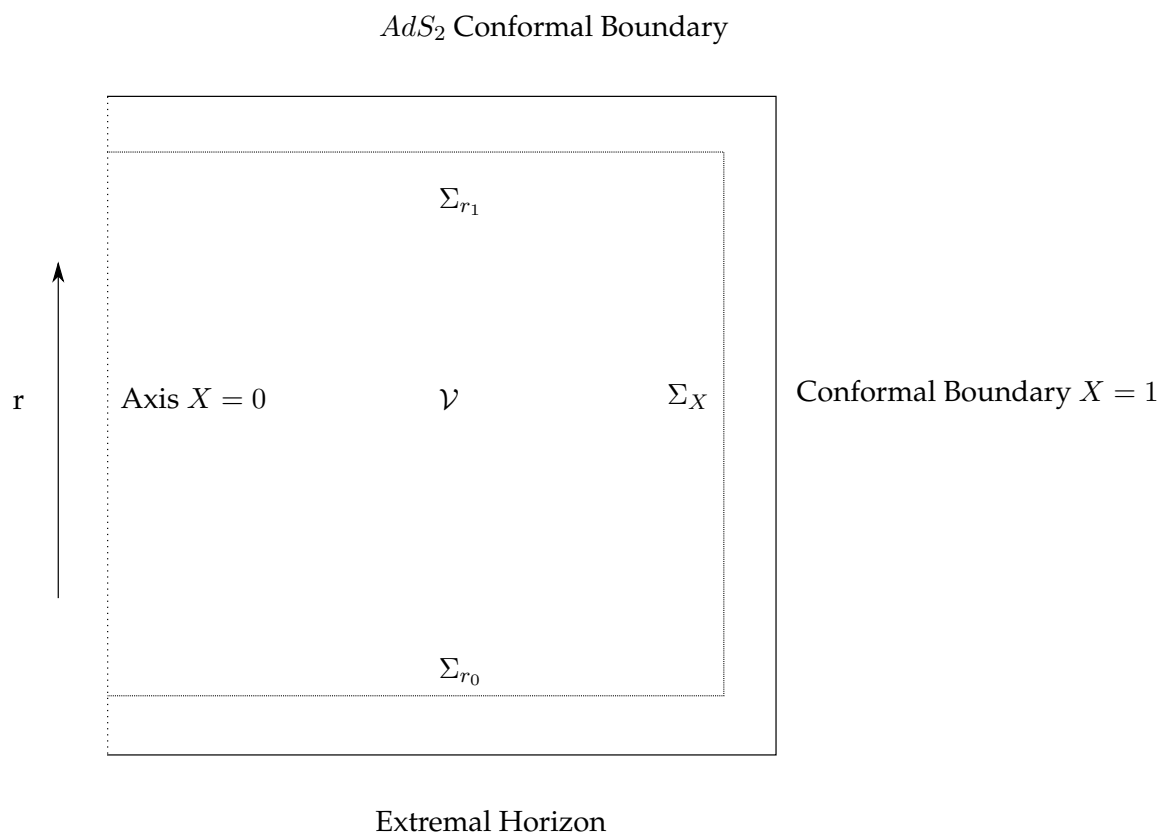


FIGURE 4.2: A Constant Time slice of the Bulk

charge can be extracted using this limit through

$$Q = \lim_{X \rightarrow 1, r_1 \rightarrow 0} \frac{1}{4\pi} \left( \int_{\Sigma_{r_1}} *F + \int_{\Sigma_X} *F \right). \quad (4.43)$$

where the surface integrals are oriented outwards.

To show that the contribution  $\int_{\Sigma_X} *F$  vanishes, note that the bulk gauge field satisfies Maxwell's equation, which can be written as

$$d * F = 0. \quad (4.44)$$

When this is integrated over the region enclosed by the cylinder,  $\mathcal{V}$ , and Stoke's theorem is applied we find,

$$\int_{\mathcal{V}} d * F = \int_{\Sigma_X} *F + \int_{\Sigma_{r_0}} *F + \int_{\Sigma_{r_1}} *F = 0, \quad (4.45)$$

From the scaling symmetry<sup>2</sup>

$$\int_{\Sigma_{r_1}} *F = - \int_{\Sigma_{r_0}} *F, \quad (4.46)$$

where the minus sign comes from the fact that the integrals are oriented outwards. Hence,

$$\int_{\Sigma_X} *F = 0, \quad (4.47)$$

and the overall charge contribution comes from the origin

$$Q = \lim_{r_1 \rightarrow 0} \frac{1}{4\pi} \int_{\Sigma_{r_1}} *F. \quad (4.48)$$

## 4.3 Numerical Solutions

### 4.3.1 Gauge Field Solutions

We will start by presenting bulk solutions corresponding to the gauge potential deformations (4.31). These were found up to a resolution of  $25 \times 65$  ( $\phi \times X$ ). By expanding these solutions near the conformal boundary, we are able to extract the boundary charge and energy densities.

#### Dependence of Charge on Boundary Parameters

Recall from Section 3.4.2, that for the extremal solutions, corresponding to  $b = 0$  in 4.31, depending on the value of  $a$  there are 0, 1 or 2 bulk solutions. We are able to observe this as well when  $b \neq 0$ . Some examples of the dependence of the point charge at the origin on boundary source parameters is shown in Figure 4.3. In order to find these solutions

<sup>2</sup>Like everything else,  $*F$  must be scale-invariant. Its pull-back to a constant  $(r, t)$  surface is therefore independent of  $r$ .

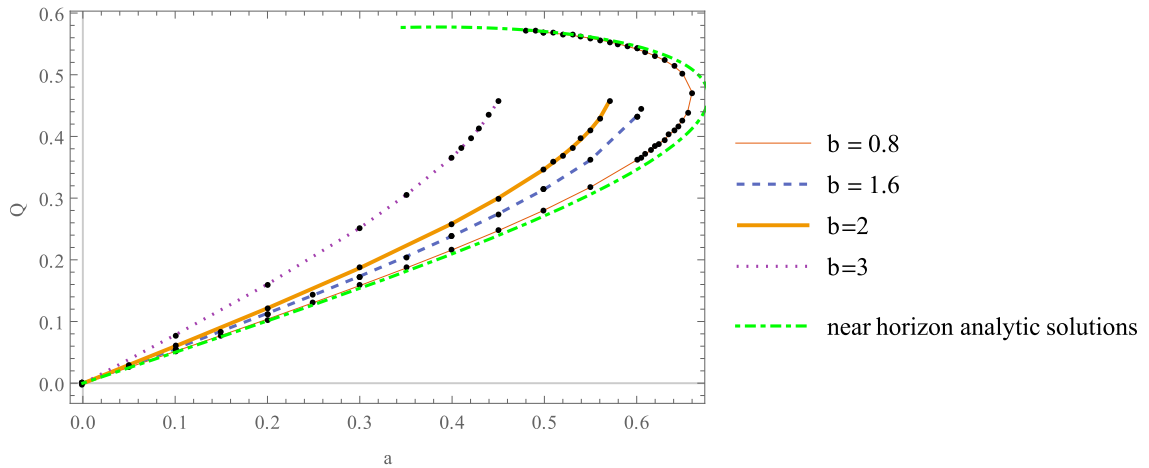
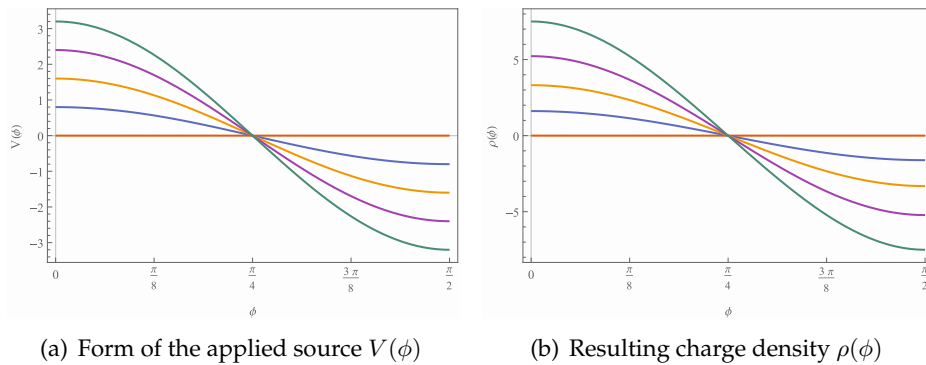


FIGURE 4.3: Overall charge on solutions as a function of the parameters  $a$  for a section of choices of  $b$  in the electric potential source term  $V(\phi) = a + b \cos 2\phi$  for which we find solutions. Note that at  $a = 0$  the total charge is always zero, which we would expect from symmetry.



(a) Form of the applied source  $V(\phi)$

(b) Resulting charge density  $\rho(\phi)$

FIGURE 4.4: Charge density resulting from an electric potential source term  $V(\phi) = \frac{b \cos 2\phi}{r}$ , for  $b = \{0, 0.8, 1.6, 2.4, 3.2\}$ . The induced charge density integrates to zero. Viewed in the cone frame the potential goes as  $1/r$ , the charge density as  $1/r^2$ , and both have been evaluated at  $r = 1$ .

we use the Newton-Raphson iteration described in 2.5. This requires an initial guess, and for that we use the reference metric (4.40). In order to find the two branches of solutions, for instance for the  $b = 0.8$  curve we take as the initial guess (and reference metric) each of the two different branches of the analytic near-horizon solutions. When we are talking about larger values of  $b$ , we only find one branch of solutions. There is, however, no reason to rule out the second branch. Additionally, for the larger values of  $a$  for which there is no  $b = 0$  near-horizon geometry, we weren't able to find any solution for non-zero  $b$  either.

### Dependence of Charge Density on Boundary Parameters

In addition to the point charge at the origin, there is also an induced charge density away from the origin, which in this case means on the  $X = 1$  conformal boundary. The

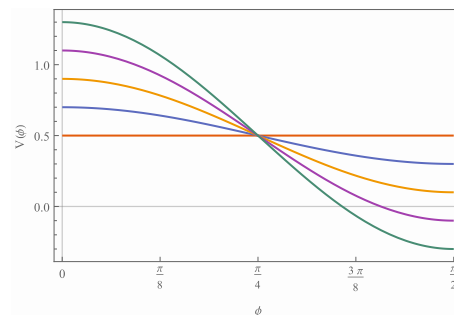
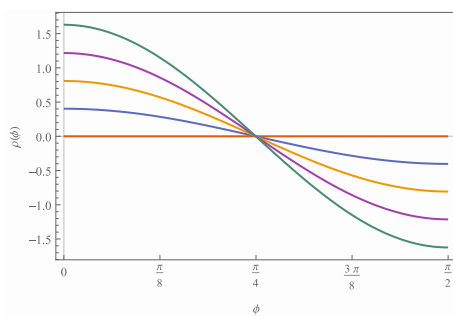
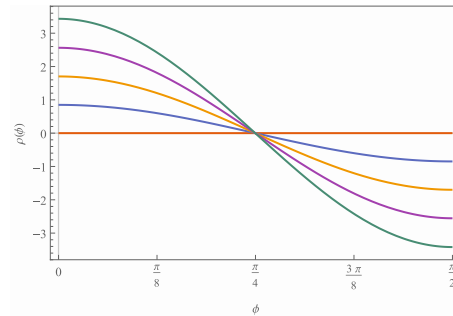
(a) Form of the applied source  $V(\phi)$ (b) Resulting charge density  $\rho(\phi)$  for branch 1(c) Resulting charge density  $\rho(\phi)$  for branch 2

FIGURE 4.5: Charge density resulting from an electric potential source term  $V(\phi) = \frac{0.5+b\cos 2\phi}{r}$  for  $b = \{0, 0.2, 0.4, 0.6, 0.8\}$ . In this case we found two branches of solutions. Note that even though the potential  $V(\phi)$  is no longer centred about zero, unlike in Figure 4.4, the charge density still is, and it still integrates to zero. Again, they have all been evaluated at  $r = 1$ .

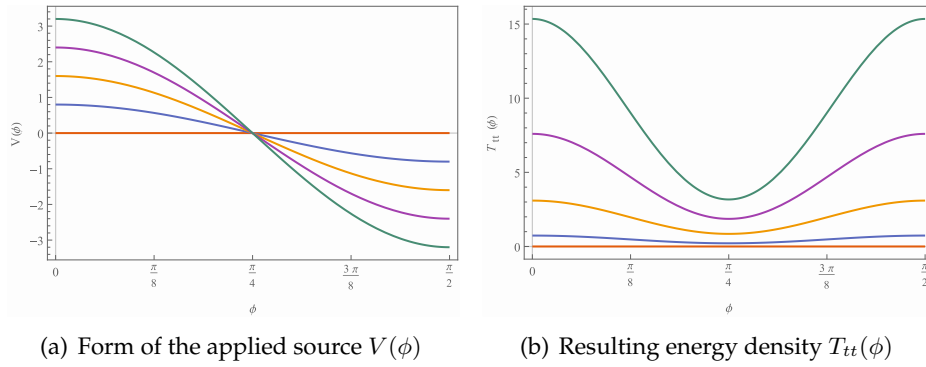


FIGURE 4.6: Energy density resulting from an electric potential source term  $V(\phi) = \frac{b \cos 2\phi}{r}$ , for  $b = \{0, 0.8, 1.6, 2.4, 3.2\}$ . Note that, quite intuitively, the energy density is peaked when the magnitude of the charge density in Figure 4.4 is largest. Also, there is a symmetry in the energy density between the regions of positive and negative charge, which makes sense because there is no overall charge at the origin. Again, everything is evaluated at  $r = 1$ .

dependence of this charge density on  $r$  is fixed by scaling symmetry<sup>3</sup>, but it has a non-trivial dependence on  $\phi$ . By the arguments in Section 4.2.7, the integral of the charge density vanishes, and this indeed is confirmed numerically (in the data it doesn't go above order  $10^{-6}$ , we'll discuss errors in more detail below). A few examples of the charge densities found are shown for  $a = 0$  in Figure 4.4 and for  $a = 0.5$  in Figure 4.5.

### Dependence of Energy Density on Boundary Parameters

Another observable we can look at is the boundary energy density, extracted from the stress tensor in the Fefferman-Graham expansion of the metric[28, 30]. Again, the  $r$  dependence is fixed by scale invariance (as  $1/r^2$  in the scale-invariant frame and  $1/r^3$  in the cone frame), but there is non-trivial dependence on  $\phi$ . The energy densities resulting from the same applied potential as above are shown in Figures 4.6 and 4.7.

### 4.3.2 Metric Deformation Solutions

For the case of the purely metric deformations (4.30), there is no gauge field, and so there is no charge density on the boundary. In this case we just focus on the energy density. The solutions were found up to a resolution of  $25 \times 145$ . The resulting plots are shown in Figure 4.8. The main difference is that the energy density is no longer positive definite, but this feature was already present in the extremal solutions corresponding to  $\lambda = 0$ . In this case, the boundary was a cone and the energy density was a constant which is positive for  $\alpha > 0$  and negative for  $\alpha < 0$ . Once we move to our more general case, we can find solutions that have regions of positive and negative energy density.

<sup>3</sup>In the scale-invariant frame it goes like  $1/r$ , and in the flat frame like  $1/r^2$

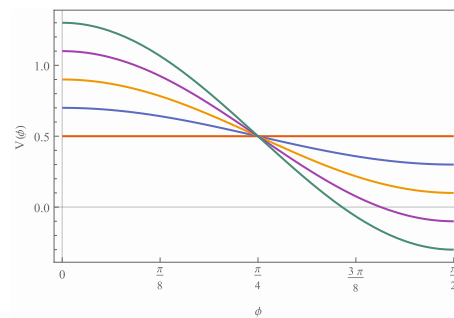
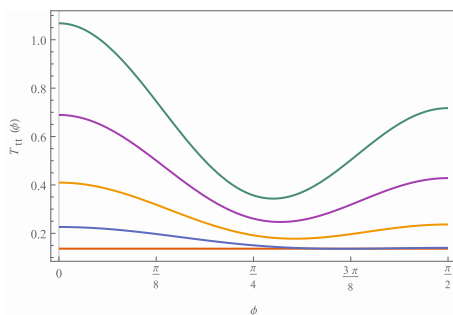
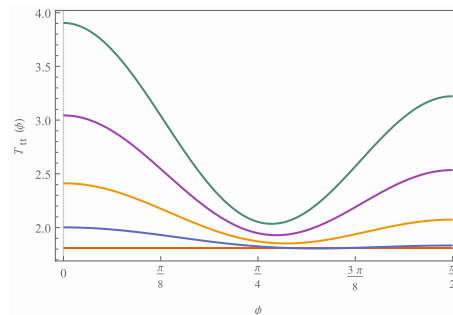
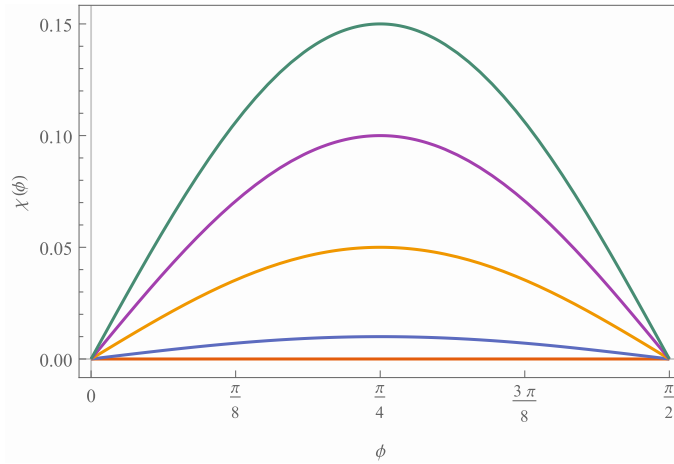
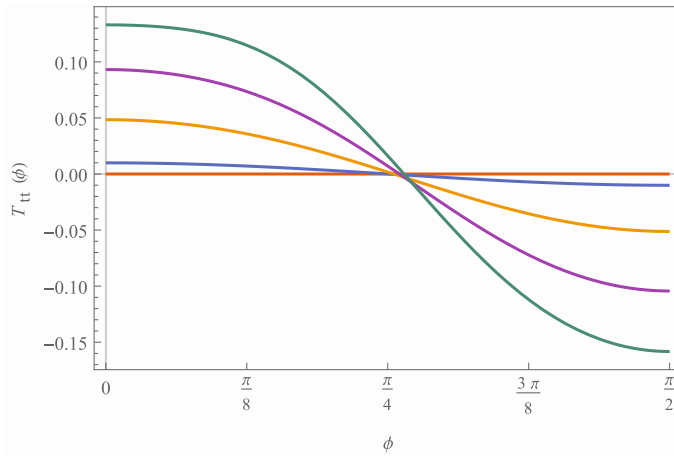
(a) Form of the applied source  $V(\phi)$ (b) Resulting energy density  $T_{tt}(\phi)$  for branch 1(c) Resulting energy density  $T_{tt}(\phi)$  for branch 2

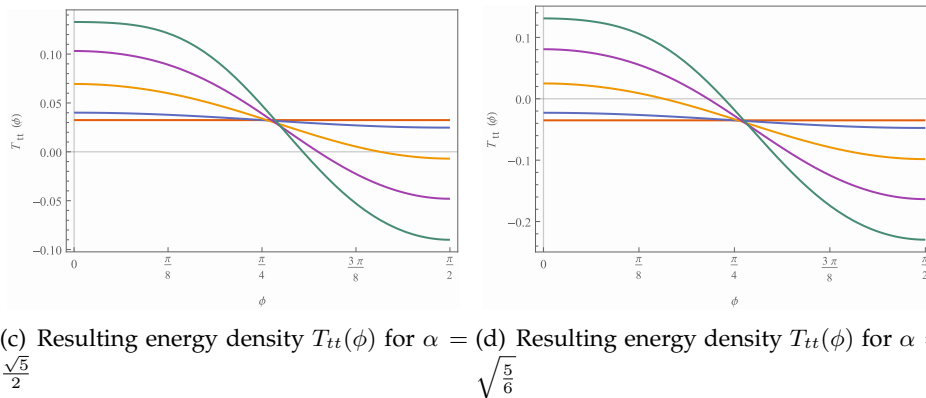
FIGURE 4.7: Energy density resulting from an electric potential source term  $V(\phi) = \frac{0.5+b\cos 2\phi}{r}$  for  $b = \{0, 0.2, 0.4, 0.6, 0.8\}$ . In this case we found two branches of solutions. The main difference now is that we no longer have a symmetry in the energy density between regions of positive charge and regions of negative charge. This is because these solutions have an overall (positive) charge at the origin. Again, they have all been evaluated at  $r = 1$ .



(a) Form of the off-diagonal SO(2,1) breaking  $drd\phi$  term in the boundary metric  $\chi(\phi)$



(b) Resulting energy density  $T_{tt}(\phi)$  for  $\alpha = 1$



(c) Resulting energy density  $T_{tt}(\phi)$  for  $\alpha = \frac{\sqrt{5}}{2}$  (d) Resulting energy density  $T_{tt}(\phi)$  for  $\alpha = \frac{\sqrt{5}}{6}$

FIGURE 4.8: Large scale energy density for a boundary metric with  $\chi(\phi) = \frac{\lambda \sin 2\phi}{r}$ , for  $\lambda = \{0, 0.01, 0.05, 0.1, 0.15\}$ , with 3 different conical deficits  $\alpha = \left\{ \sqrt{\frac{5}{6}}, 1, \frac{\sqrt{5}}{2} \right\}$ . The energy densities go as  $1/r^3$ , and we've evaluated them at  $r = 1$ . Now that we've deformed the boundary metric, the energy density is no longer positive definite. This is not a feature that is peculiar to our solutions as it was already the case in the near horizon solutions that some had positive energy density, and others negative. Roughly speaking the energy density follows the gradient of  $\chi(\phi)$ , and it always intersects the near-horizon energy density for the corresponding value of  $\alpha$  close to when  $\chi'(\phi) = 0$ .

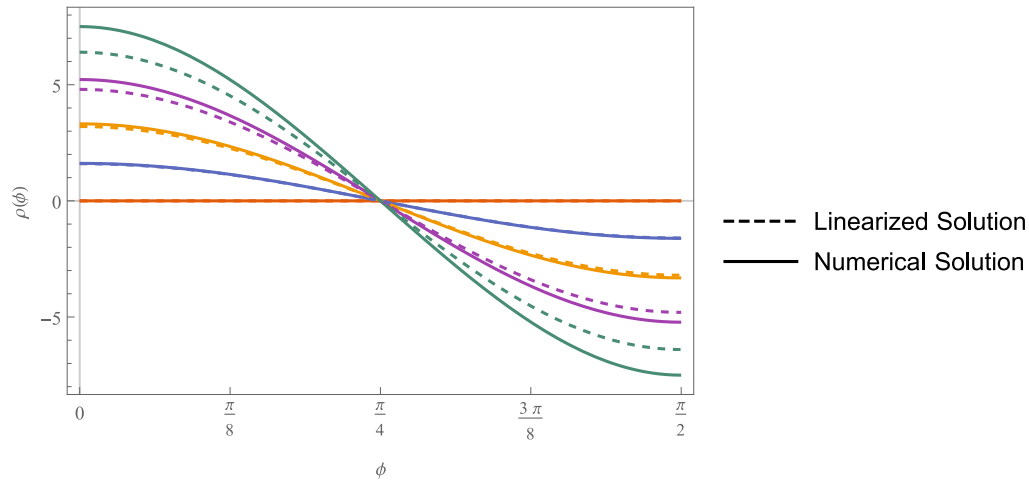


FIGURE 4.9: Charge density with an electric potential source term  $V(\phi) = \frac{b \cos 2\phi}{r}$  for a range of values of  $b$  compared to that of the linearised solution

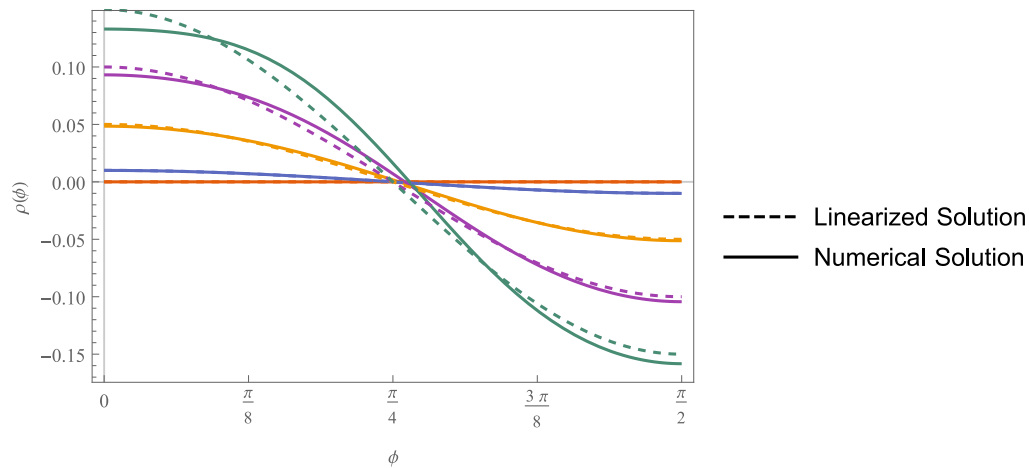


FIGURE 4.10: Energy density for a boundary metric with  $\chi(\phi) = \frac{\lambda \cos 2\phi}{r}$  compared with the linearised solution.

### 4.3.3 Comparison with Linearised Solutions

As a check on our solutions, we can compare them to the linearised solutions constructed in 4.1. In Figures 4.9 and 4.10, we look at a comparison between the charge densities and energy densities for the linearised solutions and the numerical ones. As one would expect, initially they agree well, but there is a disagreement that grows once the perturbation becomes too big.

### 4.3.4 Convergence and Smoothness

In sections 4.3.1 and 4.3.2 we presented a parameter scan of solutions. There is always the danger that these solutions to the discretized systems are not approximations to smooth solutions of the continuum equations. In this section we discuss our analysis of this issue.

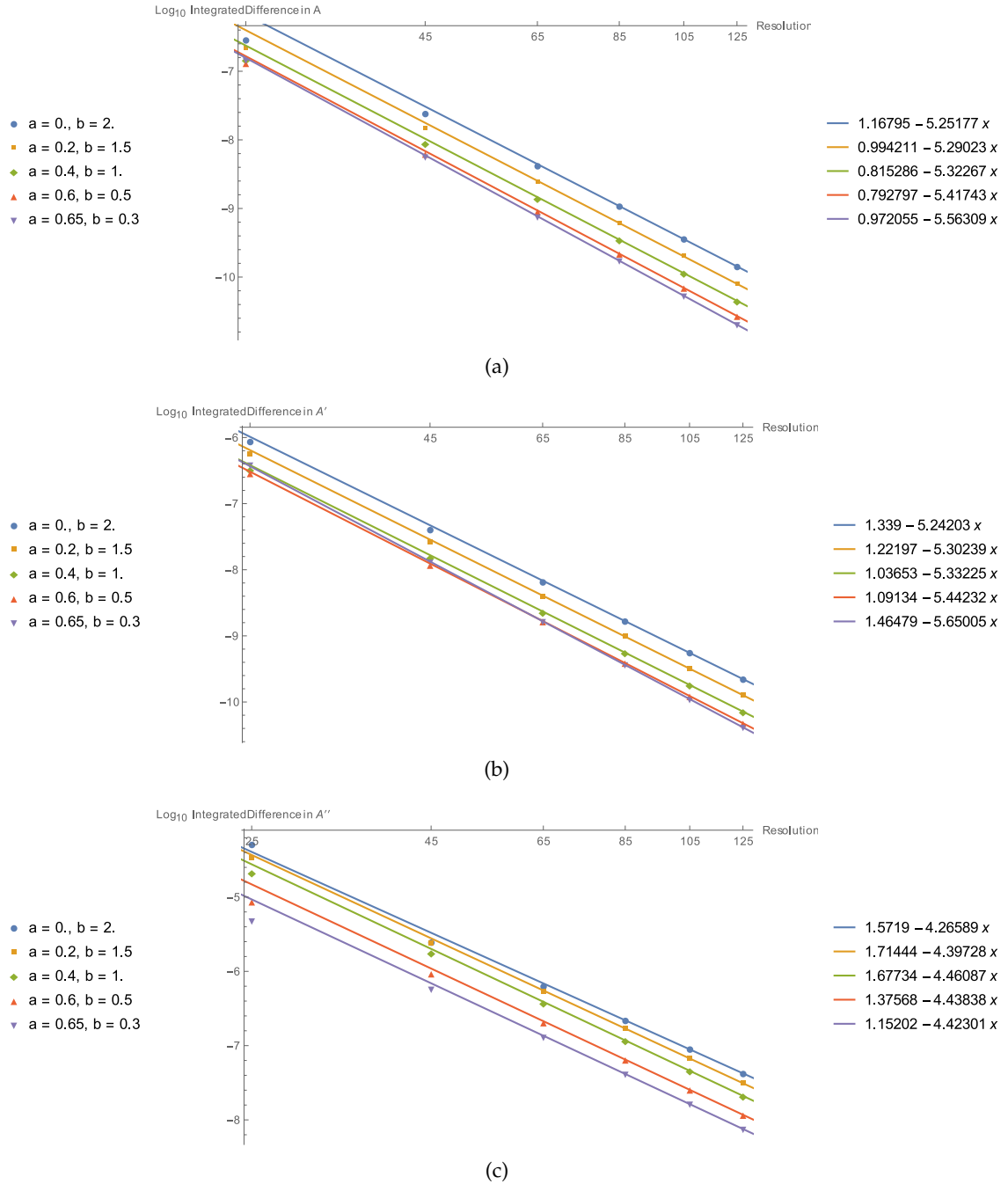


FIGURE 4.11: Integrated absolute value of the shift in the solutions between subsequent  $X$  resolutions with 20 points in the  $\phi$  direction, taken on the slice  $\phi = \frac{\pi}{8}$ . We take the case of the function  $A$  and we plot the shifts in (a) it's value, (b) it's first derivative, and (c) it's second derivative. These are log-log plots, and our linear fit to the final few points give us an estimate of the order of convergence. In these fits,  $x = \log_{10}$ Resolution. These seem to indicate fourth order convergence for the function and it's first derivative, and second order convergence for it's second derivative.

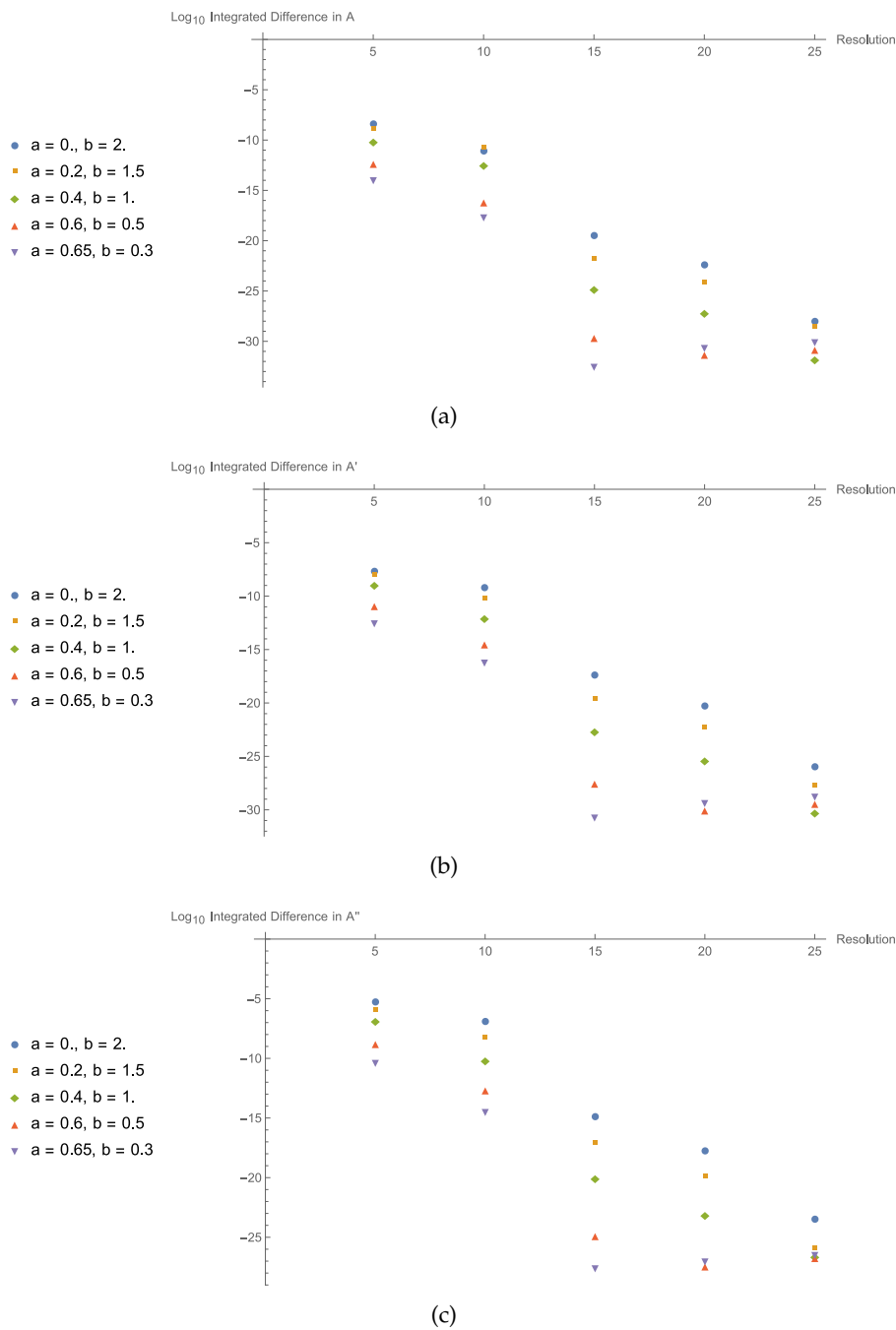


FIGURE 4.12: Integrated absolute value of the shift in the solutions between subsequent  $\phi$  resolutions, with 65 points in the  $X$  direction, taken on the slice  $\phi = \frac{\pi}{8}$ . We take the case of the function  $A$  and we plot the shifts in (a) its value, (b) its first derivative, and (c) its second derivative. These plots indicate approximately exponential convergence with  $\phi$  resolution. When you continue above a  $\phi$  resolution of 25 the  $X$  resolution becomes limiting.

### Direct Convergence

The first thing to check is the behaviour of our solutions as we vary the resolution of the discretization. As we increase the resolution, by raising the number of lattice points in the  $X$  and  $\phi$  directions, the solutions should converge. We should see this in the shift in the solutions from resolution to resolution shrinking. We take a selection of our parameters, and solve the discretized systems at various resolutions.

In Figures 4.11 and 4.12 we plot the integrated absolute value of the shift of one of the functions in our solutions at fixed  $\phi$  resolution and fixed  $X$  resolution respectively. In 4.11 the  $\phi$  resolution is fixed to 20 and in 4.12 the  $X$  resolution is fixed to 65. the first thing to note is that the shifts are definitely falling off with resolution, which is what we want. Also, in comparing these two plots we can see that its the dependence on  $X$  resolution that dominates as the shifts in this case are orders of magnitude bigger.

We can make this more numerically precise by estimating the order of convergence when the number of points in the  $X$  direction  $N$  is increased, while keeping the  $\phi$  resolution fixed. At high resolution, we expect some power law convergence. By this we mean that we expect our discretized solution to behave as

$$|f_N(x) - \tilde{f}(x)| \sim N^{-n} \quad (4.49)$$

where  $f_N(x)$  is the solution at this resolution, and  $\tilde{f}(x)$  is the continuum solution. This is called  $n$ -th order convergence. The ‘derivative’ of (4.49) tells us that the shifts we plot in 4.11 would obey

$$\begin{aligned} |f_N(x) - f_{N+1}(x)| &\sim N^{-n-1} \\ \log |f_N(x) - f_{N+1}(x)| &\sim -(n+1) \log N + c. \end{aligned} \quad (4.50)$$

We therefore try fitting lines to the log-plots in 4.11, and the resulting fits are included in the figure. Since we are using 6th order finite difference, we would typically expect 6th order convergence for the function itself, with lower order convergence for it’s derivatives. We find instead that our data is only consistent with 4th order convergence.

This is a signal that our solutions are not necessary smooth beyond 4th derivative, and in fact this lack of smoothness is a limitation stemming from our choice of reference metric which we will explain when we discuss the boundary expansions below.

### Harmonic Gauge Condition

Recall that these solutions to the discretized system are not converging to solutions to Einstein’s equation as the lattice size is increased unless the vector  $\xi^\mu = g^{\alpha\beta} \left( \Gamma^\mu_{\alpha\beta} - \bar{\Gamma}^\mu_{\alpha\beta} \right) \rightarrow 0$ . Since the static symmetry means that this is a space-like vector, it is sufficient to examine  $\phi = \xi^\mu \xi_\mu$ , since  $\phi = 0$  implies  $\xi_\mu = 0$ . It’s dependence on both  $X$  resolution and  $\phi$  resolution is shown in Figure 4.13. These demonstrate convergence, although in the latter part of 4.13(a), in which we plot dependence on  $X$  resolution, we are limited by the fixed  $\phi$  resolution, and vice versa for 4.13(b).

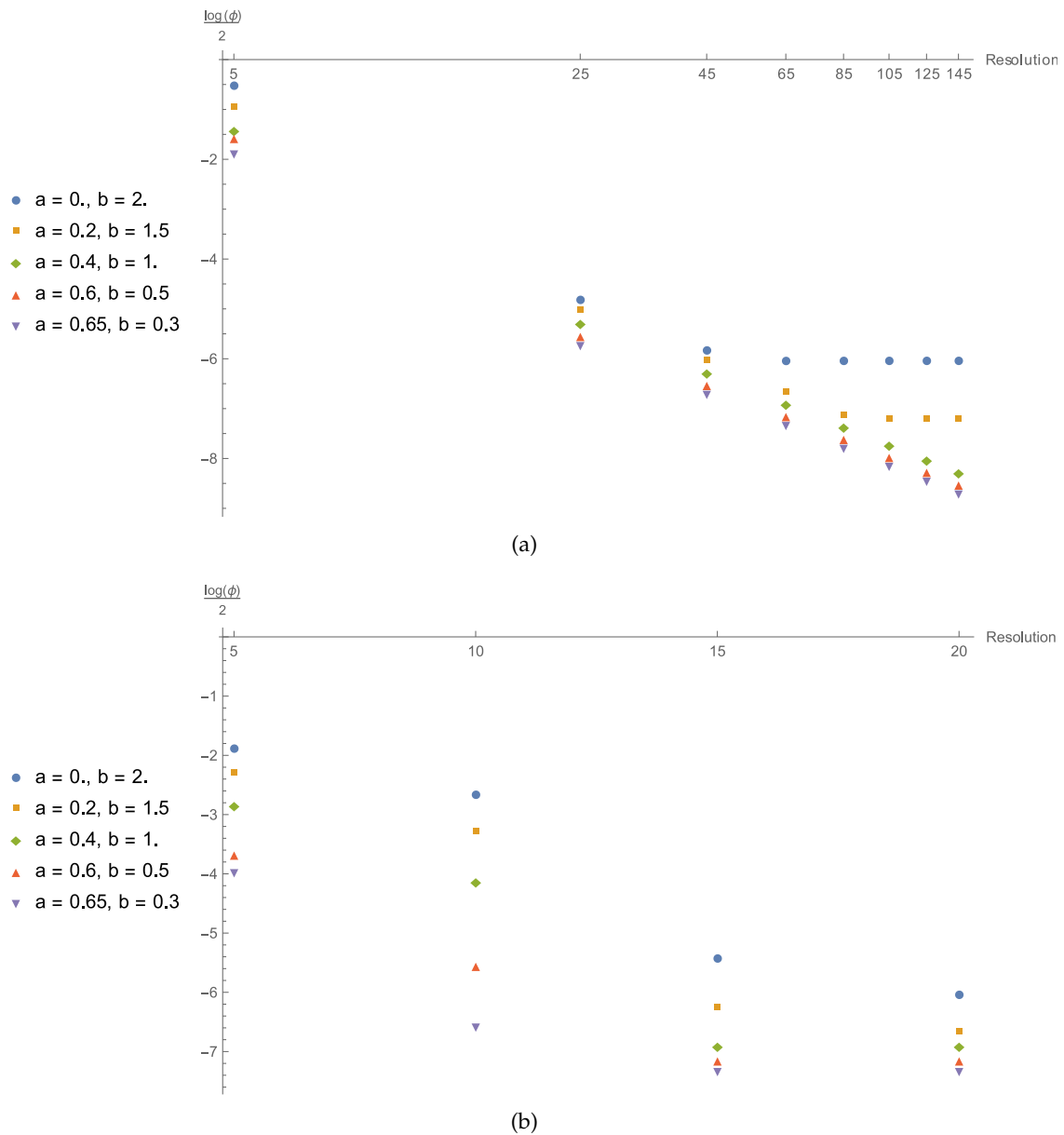


FIGURE 4.13: The maximum value of  $\phi = \xi^\mu \xi_\mu$  as a function of resolution. In (a) we see the dependence on  $X$  resolution at a fixed  $\phi$  resolution of 20 points. Initially we see what looks like power law behaviour in all these solutions, but a couple of them start to level off at around 65 points. This is where the  $\phi$  resolution is becoming the limiting factor. In (b) we plot the dependence on  $\phi$  resolution at a fixed  $X$  resolution of 65 points. Above the  $\phi$  resolution of 20 up to which we plot, the  $X$  resolution becomes the limiting factor. For the parts of (a) which look like a power law, the slope is about  $-3.9$ , which is consistent with the third order convergence seen in the second derivatives in Figure 4.11.

### Boundary Expansions

As remarked above, there is a limitation on the smoothness that we can trace back to our choice of reference metric and an expansion near the conformal boundary at  $X = 1$ . In Figure 4.14 we show the behaviour of a function at the boundary, and some of its normal derivatives, as the resolution is varied. Once we get to the 5th derivatives the functions aren't really converging at all.

This could be explained by a logarithm in our boundary expansion, but we think this logarithm just results from a poor choice of coordinates. We can argue that this logarithm is pretty much inevitably there as follows. If we think we have smooth solution to Einstein's equation, then we know at least one set of coordinates we can take, at least near the conformal boundary, where the solution is smooth, and that's the Fefferman-Graham expansion. Let's write our solution in these coordinates as

$$g = \frac{dz^2}{z^2} + \frac{g_{ab}(x)dx^a dx^b}{z^2} + h_{ab}(x, z)dx^a dx^b, \quad (4.51)$$

where the  $x^a$  coordinates are boundary spacetime coordinates. When we find our solution to the Harmonic Einstein's equation, these aren't the coordinates in which our solution will be written. Our reference metrics are themselves (for the first few orders in  $z$ ) solutions to Einstein's equation, so we can write our reference metric in FG coordinates as well

$$\bar{g} = \frac{dz^2}{z^2} + \frac{g_{ab}(x)dx^a dx^b}{z^2} + \bar{h}_{ab}(x, z)dx^i dx^j. \quad (4.52)$$

As described in Section 2.2, choosing our reference metric so that its boundary metric matches that of our solution insures that  $\phi = \xi^\mu \xi_\mu$  vanishes as  $z \rightarrow 0$ , however we will not generically have  $\xi^\mu = 0$  away from  $z = 0$  in these coordinates. The leading order behaviour of  $\xi$  is given by

$$\begin{aligned} \xi = & z^4 \left( \nabla_a \left( h^{ab}(x, z) - \bar{h}^{ab}(x, z) \right) \frac{\partial}{\partial x^b} \right) \\ & - z^4 \frac{1}{2} \left( \nabla^b (h(x, z) - \bar{h}(x, z)) \frac{\partial}{\partial x^b} - \frac{1}{2} \frac{\partial (h(x, z) - \bar{h}(x, z))}{\partial z} \frac{\partial}{\partial z} \right) + O(z^6). \end{aligned} \quad (4.53)$$

In fact, in this case, we have that  $h_{ab}(x, 0) = \bar{h}_{ab}(x, 0)$ . This is because the reference metric is itself a solution to Einstein's equation to this order, so the boundary expansion (1.25) guarantees agreement. Where the disagreement happens is at the order in  $z$  corresponding to the stress tensor. We therefore have

$$\begin{aligned} \xi^z &= \frac{z^4}{2} (\bar{T} - T) + O(z^5) \\ \xi^a &= z^5 \left( \nabla_b (T^{ba} - \bar{T}^{ba}) - \frac{1}{2} \nabla^a (T - \bar{T}) \right) + O(z^6), \end{aligned} \quad (4.54)$$

If we are considering the vacuum Einstein's equation (no gauge field), then the stress-tensor  $T_{ab}$  is traceless and conserved, and by choosing  $\bar{T}_{ab}$  to be so as well we can ensure

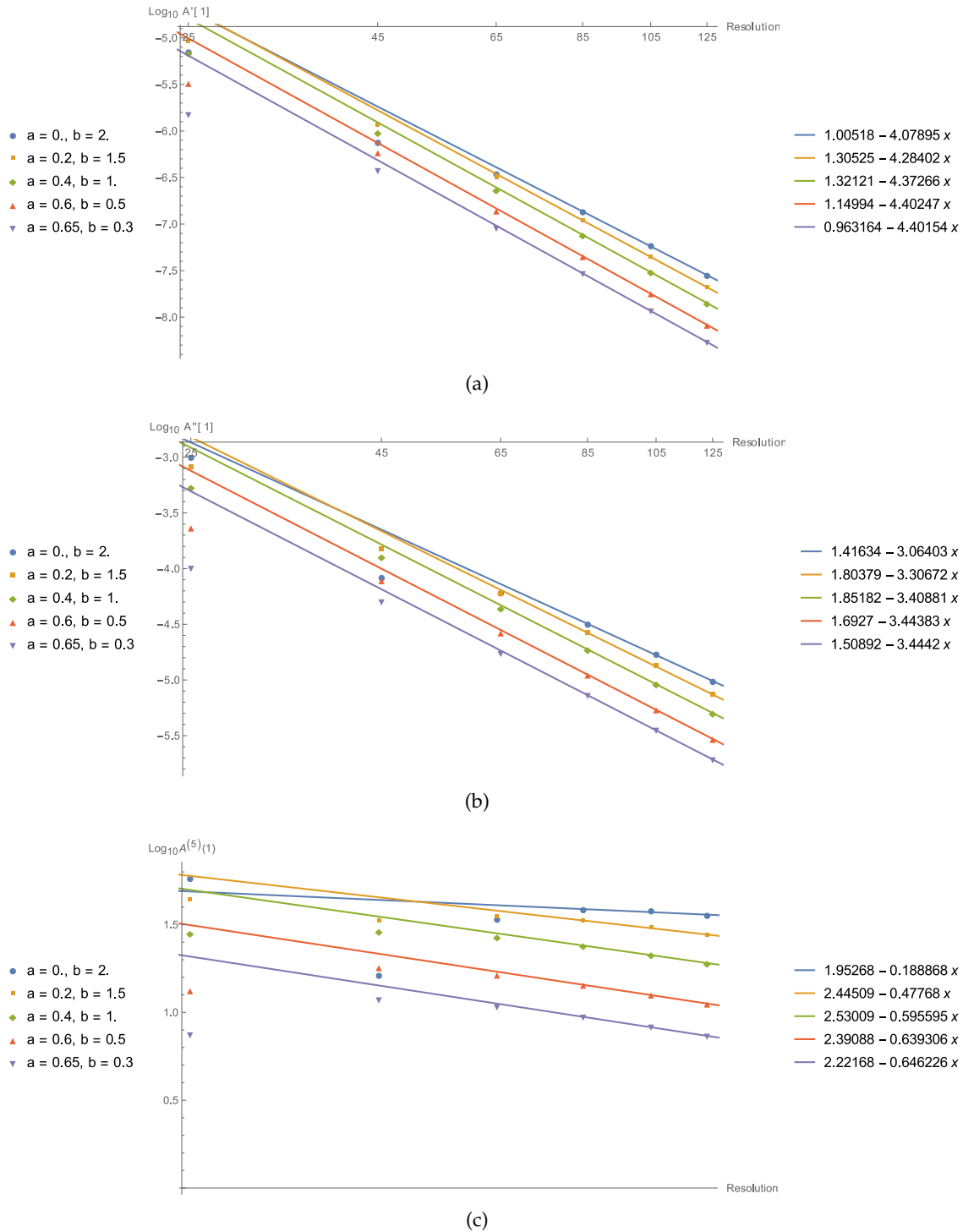


FIGURE 4.14: Absolute value shift in the boundary value of the solutions between subsequent  $X$  resolutions, taken at  $\phi = \frac{\pi}{8}$ . We take the case of the function  $A$  and we plot the shifts in (a) it's first derivative, (b) it's second derivative, and (c) it's fifth derivatives. Linear fits are made to the final few points with  $x = \log_{10} \text{Resolution}$ . Convergence is slower than the bulk convergence in Figure 4.11, and at fifth order we see the effect of the lack of smoothness discussed in the text.

that  $\xi$  vanishes to this order. However, when we add a chemical potential source to the boundary, the stress tensor is no longer conserved, but instead satisfies a sourced conservation equation. This can be seen by looking at how the argument for stress tensor conservation is modified by adding in the source term. The expectation values of the stress tensor and charge current are defined by the variation of the effective action

$$\delta W = \int \sqrt{g} \langle T_{ab} \rangle \delta g^{ab} + \langle J^a \rangle \delta A_a. \quad (4.55)$$

Coordinate invariance means that this should identically vanish for a diffeomorphism. This leads to the conservation equation

$$\nabla^b T_{ab} = -F_{ab} J^b, \quad (4.56)$$

which means that in our case

$$\begin{aligned} \xi^z &= O(z^5) \\ \xi^a &= z^5 \left( F_{ab} J^b - \bar{F}_{ab} \bar{J}^b \right) + O(z^6). \end{aligned} \quad (4.57)$$

While we can choose our reference metric such that  $\bar{F} = F$ , we can't choose  $\bar{J} = J$  because we don't know what  $J$  will be until we solve the equations. This means that there is a coordinate transformation between these smooth coordinates, and our coordinates in which  $\xi = 0$ , which is given to leading order by

$$x^a \rightarrow x^a + \frac{z^5 \log z}{5} \left( F_{ab} J^b - \bar{F}_{ab} \bar{J}^b \right) + O(z^6). \quad (4.58)$$

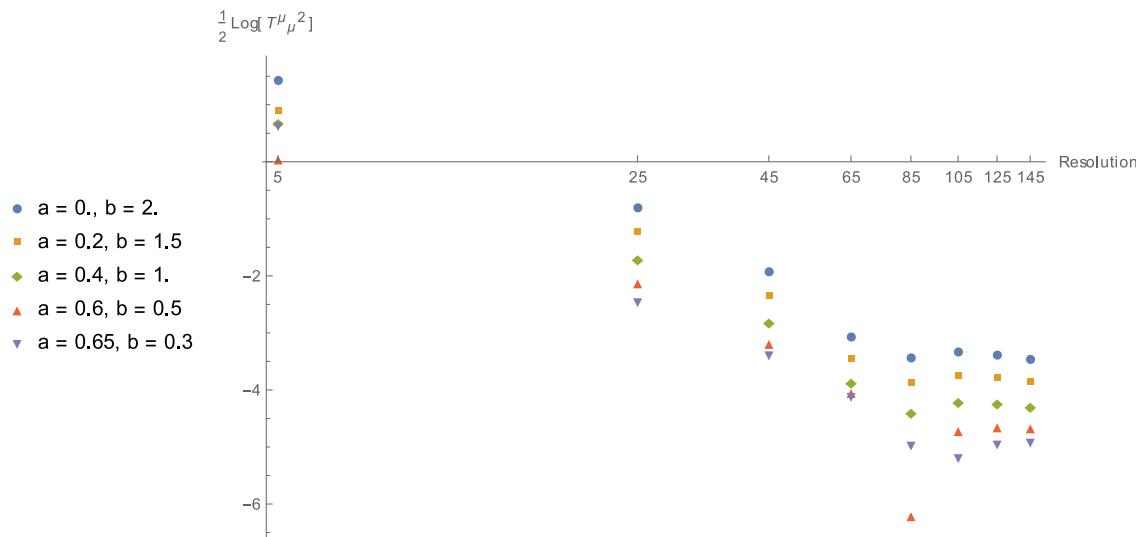
The presence of a logarithm in this transformation inevitably translates into a logarithm term in the boundary expansion of our numerical solutions at fifth order. This means that our solutions cannot be more than  $C^4$ , which would explain why we only get 4<sup>th</sup> order convergence.

The boundary expansion also gives us another check on our solutions, which is that the conservation condition (4.56)<sup>4</sup> and tracelessness of our stress tensor are satisfied. This is shown in Figure 4.15. We see that these quantities do not converge very rapidly, but, given the lack of smoothness on the boundary, we would not expect them to.

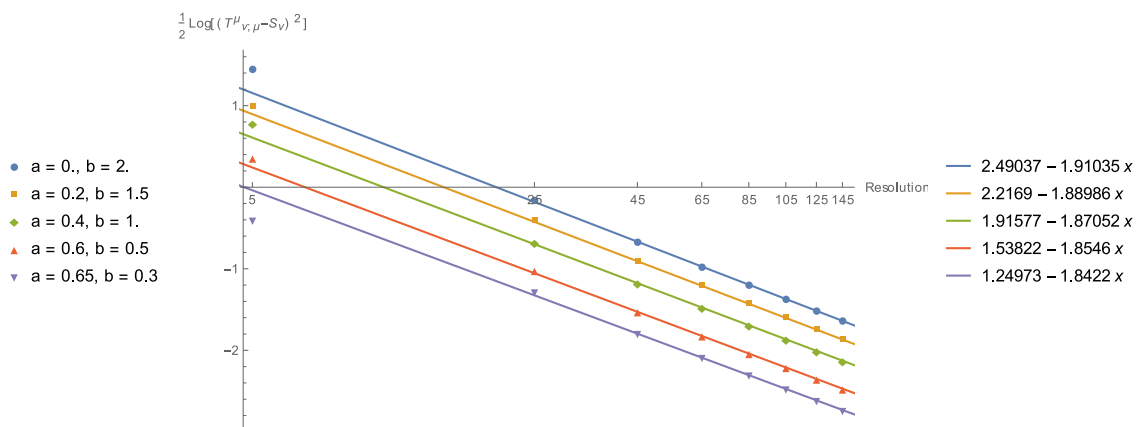
### Coordinate Axis Expansions

We've uncovered a limitation on the smoothness of our coordinate choice at the conformal boundary. Another place we might worry this could happen is at the axis  $X = 0$ . Even if our functions in the ansatz are perfectly smooth, the polar coordinates we've taken break down here, and we discussed in 4.2.4 how we go about constructing the

<sup>4</sup>In fact, the stress tensor we've been plotting is normalized in a non-standard way so the condition is  $\nabla_\mu T_\nu^\mu = -\frac{4}{3} F_{\mu\nu} J^\nu$ .



(a) Tracelessness



(b) Conservation

FIGURE 4.15: We plot how well the stress tensor satisfies the conservation and trace requirements. Neither converges very rapidly, but given the lack of smoothness on the boundary, we would not expect them to. In these plots, the  $X$  resolution is increased at fixed  $\phi$  resolution, so we can see a levelling off in the first plot corresponding to when the dependence on the  $\phi$  resolution has become the limiting factor.

conditions that impose smoothness. The symmetry we used means many of these conditions are satisfied automatically, but we still need to check smoothness order by order in powers of  $X$ .

As in (4.34) we transform into Cartesian coordinates here, and we impose order by order in  $X$  the condition following from (4.35) that at order  $X^n$  there is no Fourier mode in the  $\phi$  dependence beyond  $e^{in\phi}$ . This condition applies to components of the two-tensor and two-vector in the same way as the scalar. Half these modes are ruled out by our parity symmetry. In Figure 4.16 we check for Fourier modes that violate this condition at order  $X^0$ ,  $X$ , and  $X^4$ . We see very fast convergence in the first two plots, and even at order  $X^4$  we are still seeing fourth order convergence. This seems to indicate that the functions are well behaved at least up to fourth derivatives at the origin.

## 4.4 Analysis of the Singularity

Now we want to understand these scale-invariant bulk geometries more generally. The analytic,  $SO(2,1)$  invariant solutions had extremal horizons as  $r \rightarrow \infty$ , but in the more general solutions we've constructed in this chapter, the surface is singular. Pragmatically, we know that the surface is singular because you cannot take Gaussian null coordinates as in (3.65) in any open region around the surface, which you would be able to do for a codimension one smooth null hypersurface[31]. However, because of the scaling symmetry, no scalar curvatures can diverge as we approach this surface.

The physical nature of this singularity can be understood by examining how massive particles would behave in this spacetime. To this end, we look at timelike geodesics in these geometries. Moving now to general dimensions  $d$ , we choose coordinates where the metric takes the form

$$ds^2 = \psi(x)^2 \left( \frac{-dt^2 + dr^2}{r^2} \right) - 2\psi(x)^2 A_i(x) dx^i \frac{dr}{r} + (h_{ij}(x) + \psi(x)^2 A_i(x) A_j(x)) dx^i dx^j. \quad (4.59)$$

The  $x^i$  coordinates describe a  $d - 2$  dimensional subspace, on which  $h_{ij}(x)$  is a non-degenerate metric, and  $A_i(x)$  and  $\psi(x)$  are a one-form and scalar respectively. The geometry on constant  $r$  surfaces is smooth, but we will find singular behaviour as  $r \rightarrow 0$ . Near horizon solutions have  $A_i(x) = 0$  when written in this form, and the generalized solutions we found above have no-zero  $A_i(x)$  because they break the  $SO(2,1)$  symmetry. Using the remaining global scaling and time translation symmetries, we can integrate some of the geodesic equations using Noether's theorem. The equations we are left with are,

$$\begin{aligned} E &= \psi^2 r^2 \dot{t} \\ K &= Et + \psi^2 \left( \frac{A_i \dot{x}^i - \dot{r}}{r} \right) \\ \ddot{x}^i + \Gamma[h]^i_{jk} \dot{x}^j \dot{x}^k &= -\frac{\partial^i \psi}{\psi} \left( k^2 + h_{kl} \dot{x}^k \dot{x}^l \right) + EA^i \dot{t} - F^i_j \dot{x}^j (K - Et), \end{aligned} \quad (4.60)$$

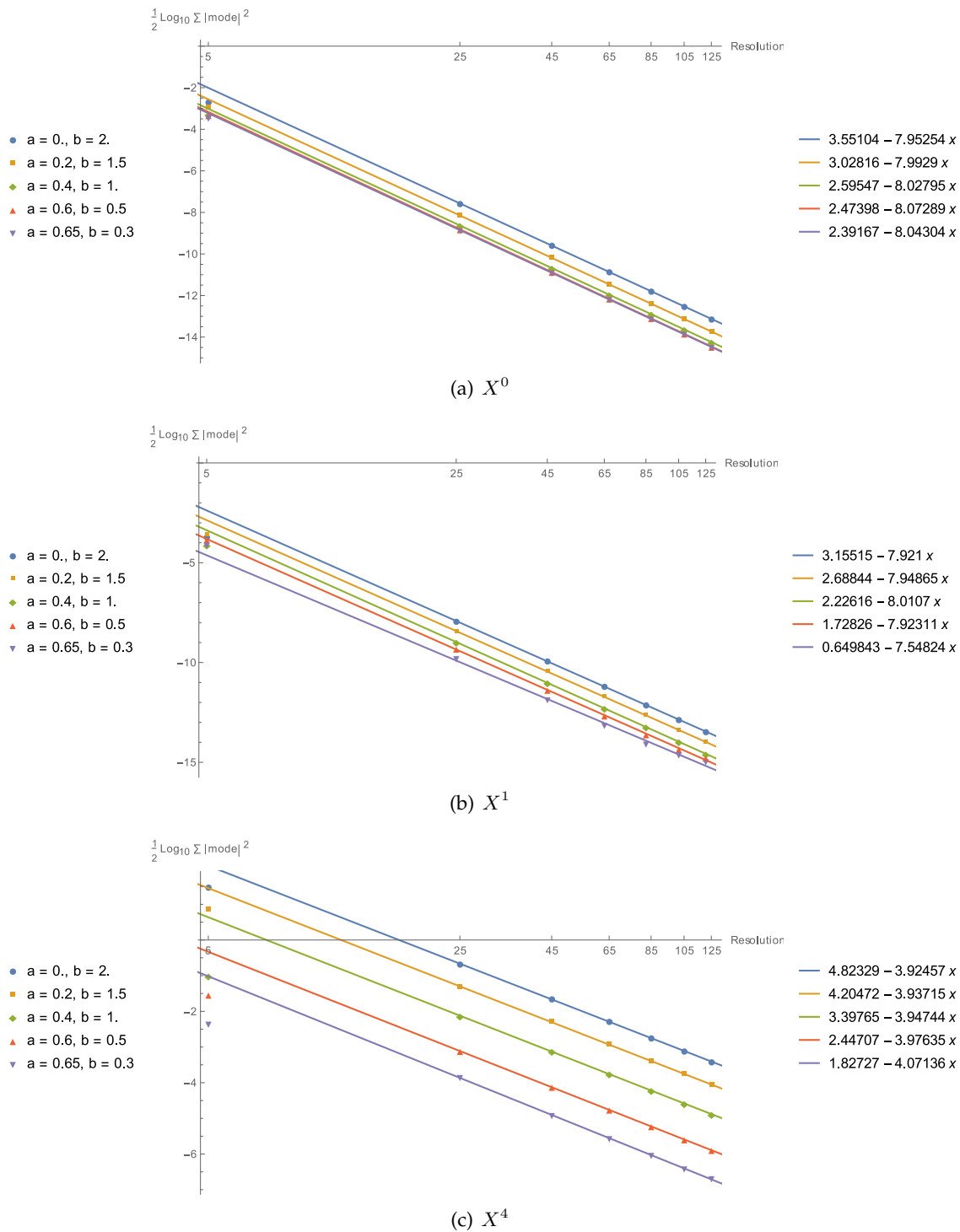


FIGURE 4.16: We've expanded our fields near the origin  $X = 0$  in a Cartesian basis  $(x,y)$  and checked that derivatives in  $x$  and  $y$  are well defined. Thanks to our parity symmetry, this amounts simply to checking that at each order  $X^n$ , if we expand the  $\phi$  dependence in Fourier modes, there are no modes above  $\cos n\phi$  and  $\sin n\phi$ . We plot here the sum of the squares of the modes  $\cos m\phi$  and  $\sin m\phi$  at order  $X^n$  for  $m > n$  summed over all the components of our fields, for (a)  $n = 0$ , (b)  $n = 1$  and (c)  $n = 4$ , at a series of  $X$  resolutions, at a fixed  $\phi$  resolution of 15 points. These show that the functions are well behaved at least up to fourth derivatives at the origin.

where a dot represents differentiation with respect to an affine parameter  $\lambda$ . Indices are raised and lowered using  $h_{ij}$ , and we have defined  $F_{ij} = A_{i,j} - A_{j,i}$ .  $K$  and  $E$  are conserved quantities due to the static and scaling symmetry, and the third equation is the geodesic equation in the  $x^i$  direction. The parameter  $k^2$  is a constant whose sign determines whether the geodesic is timelike, spacelike, or null. It is 0 for null geodesics, and otherwise if we take our affine parameter to be proper distance or time it will be 1 for timelike and  $-1$  for spacelike geodesics.

By dotting the third equation in with  $\dot{x}^i$  we can show that<sup>5</sup>

$$\frac{d}{d\lambda} (\psi^2(k^2 + \dot{x}_j \dot{x}^j)) = 2E^2 r^2 \dot{x}^i A_i. \quad (4.61)$$

Substituting this equation into the conservation equations, we find the differential equation

$$\frac{K}{E} = t - r \frac{dr}{dt} + \frac{1}{2E^2} \frac{d}{dt} (\psi^2(k^2 + \dot{x}_j \dot{x}^j)), \quad (4.62)$$

which can be solved to give

$$r^2(t) = \frac{(Et - K)^2 + C + \psi^2(k^2 + \dot{x}_j \dot{x}^j)}{E^2}. \quad (4.63)$$

The parameter  $C$  is a constant of integration. Using this result, we can rewrite the third equation as

$$\begin{aligned} \ddot{x}^i + \Gamma[h]^i_{jk} \dot{x}^j \dot{x}^k &= \left( A^i - \frac{\partial^i \psi}{\psi} \right) (k^2 + h_{kl} \dot{x}^k \dot{x}^l) \\ &+ \frac{A^i}{\psi^2} ((Et - K)^2 + C) + F^i_j \dot{x}^j (Et - K). \end{aligned} \quad (4.64)$$

Now, assume there exists some point on the  $n - 2$  dimensional  $x$  manifold,  $x_0$ , where  $A_i = d\psi_i = 0$ . Such a point exists, for instance, at the point  $X = 0$  in the solutions we constructed, because of the reflection symmetry we imposed. We can then consider freely falling particles at this point with  $\dot{x}^i = 0$ . In this case, the particles stay at  $x = x_0$ . Timelike geodesics satisfy

$$\begin{aligned} t(\lambda) &= -\frac{\cot \lambda}{B} + t_0 \\ r(\lambda) &= -\frac{\csc \lambda}{B}, \end{aligned} \quad (4.65)$$

$t_0$  and  $B$  being constant, while null geodesics are given by

$$\begin{aligned} t(\lambda) &= -\frac{1}{\lambda} + t_0 \\ r(\lambda) &= -\frac{1}{\lambda}, \end{aligned} \quad (4.66)$$

---

<sup>5</sup>This becomes an extra conservation law when  $A_i = 0$ , which is because the scaling/static symmetry gets enhanced to  $SO(2, 1)$  in this case.

where in both cases we have chosen  $\lambda = 0$  to be the time when the geodesic hits the surface. Note that they reach the horizon in finite affine parameter.

Define  $V^a$  to be the tangent vector  $\frac{d}{d\lambda}$ . The geodesic deviation tensor in the  $n - 2$  dimensional  $x^i$  space is then given by  $\tilde{R}_{ij} = R_{aibj}V^aV^b$  [62]. This means that if the vector  $X^i$  describes the infinitesimal displacement between a pair of geodesics both initially parallel to  $V^a$ ,

$$V^a\nabla_a\left(V^b\nabla_bX^i\right) = -h^{ij}\tilde{R}_{jk}X^k. \quad (4.67)$$

For both the timelike and null cases we find that this goes as

$$\tilde{R}_{ij} \sim \frac{1}{\lambda^2} \left( \psi^4 F_{ik} F_{jl} \gamma^{kl} - \psi^2 \nabla_{(i} A_{j)} \right). \quad (4.68)$$

We therefore see that, at least for this geodesic at  $x = x_0$ , the geodesic deviation diverges as you approach the surface.

More generally, away from  $x = x_0$  the geodesics seem to be very poorly behaved. From (4.63) it can be seen that any time-like or null geodesic will have  $t \rightarrow \infty$  as it approaches the horizon  $r \rightarrow \infty$ . By examining (4.64), if we project the trajectory of this particle onto a constant  $r$  surface, then the effect of the  $A^i$  and  $F_{ij}$  is like an electric and magnetic force on this particle. As we approach the horizon,  $t \rightarrow \infty$ , and the strength of these forces diverges. Unless there is some neat cancellation, which we don't expect generically, these particles will accelerate off to infinity in  $x$ . So while the scaling symmetry rules out any sort of curvature singularity as  $r \rightarrow \infty$ , we see the singular behaviour in the form of divergent tidal forces acting on test particles.

We haven't explicitly proven that this is what happens. We can, however, provide evidence for this numerically. We can take our numerically constructed bulk geometries (with no gauge-field), and shoot timelike geodesics towards the singularity. In Figure 4.17 we plot  $x(\tau)$ , and  $x'(\tau)$  for a selection of geodesics on pure-AdS and on one of our  $SO(2,1)$  symmetry breaking solutions. The coordinate  $x$  is one of a pair of Cartesian coordinates on our unit disk, and  $\tau$  is proper time. These geodesics were evolved using an adaptive step size Runge-Kutta method implemented in Mathematica, and we integrated until the step-size became too small to continue. From this we can see that, in the non-AdS case, as the geodesics get close to the singular surface there is a large transverse acceleration, and it looks like geodesics will have divergent  $x'$  by the time they hit the surface. It seems reasonable to conclude, based on examination of (4.64) above, that the large transverse acceleration observed in the singular case just before the end will continue and lead to a divergent  $x'$ .

## 4.5 Discussion and Generalizations

We have demonstrated the existence of bulk spacetimes that can describe static, scale-invariant CFT states without the enhanced symmetry required by extremal horizons. We conjecture that these geometries will also play the role of describing the large scale limit of more general CFT states. Such states could be described by bulk solutions where these

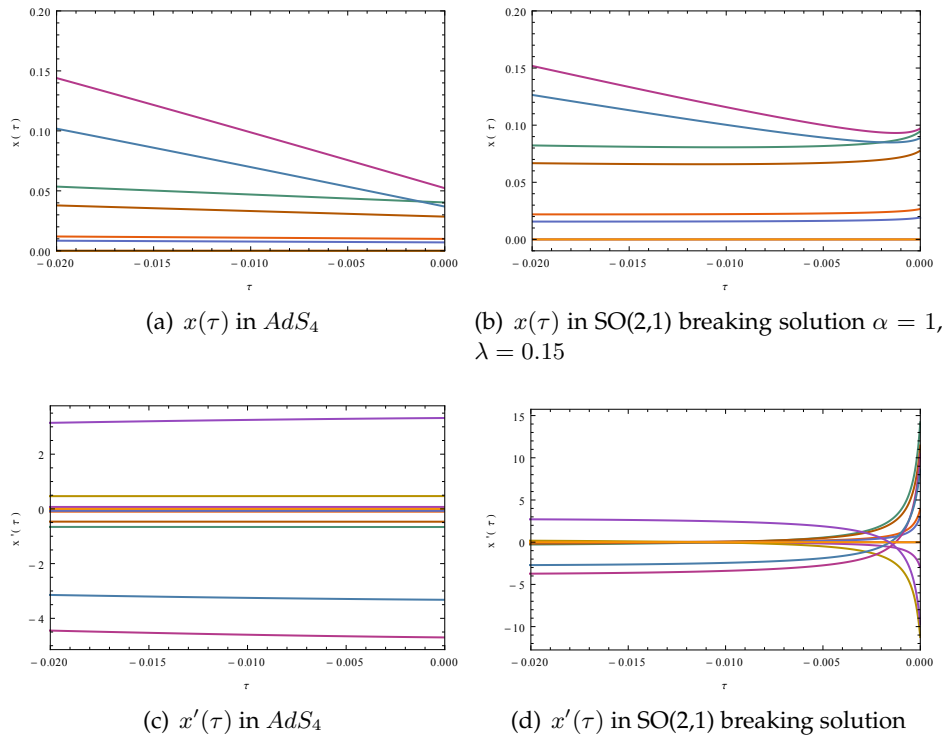


FIGURE 4.17:  $x(\tau)$  and  $x'(\tau)$  for various numerical timelike geodesics that head towards the  $r = 0$  surface. The proper time coordinate has been chosen so that it is 0 when they hit the surface. As they approach the surface, nothing happens in the case of the  $AdS_4$  and they just cross over a smooth extremal horizon. In the other case, all the geodesics start to swerve off as they approach the horizon, except a single geodesic that we've placed at the point  $x = y = 0$  with no transverse velocity ( $x' = y' = 0$ ). This is the point where  $A_i = d\psi_i = 0$  as discussed in the text.

geometries lie in the IR. The arguments from Chapter 3 make this compelling, and would relate this large scale-limit to a ‘near-geometry’<sup>6</sup> of these null singularities. However the general proof in [59] relies on results specific to spacetimes containing extremal horizons.

If this conjecture were true then it would mean that, like in the extremal horizon case, the large scale properties of the CFT state would decouple, and by knowing the scale-invariant bulks we have described here, you would be able to read off the large scale limit of expectation values given the large scale limit of sources. These large scale properties correspond to the leading order fall off of observables like the stress tensor and charge densities.

The scale-invariant IR geometries that are usually used in AdS/CFT are the near-horizon geometries of extremal horizons. The IR therefore usually has the corresponding enhanced symmetry associated with these spacetimes. The spacetimes we have constructed offer an answer to the interesting question of whether the enhanced symmetry that is often observed in the IR in AdS/CFT is actually just an artefact of considering a limited set of possible IR geometries. They suggest that there is a more generic case and, specifically, if the large scale limit in the CFT breaks this enhanced symmetry, in the IR in the bulk there will be a singular, scale-invariant geometry of the type we have studied here.

Finally, it is worth pointing out that while this is a singularity, at finite temperature we would expect bulk solutions to exist with smooth finite temperature horizons. So long as this is true, then these would be examples of ‘good’ singularities in the sense of [71], and so would be perfectly good for describing vacuum states. A useful piece of further work would be to demonstrate this explicitly.

---

<sup>6</sup>Like the near-horizon geometry of the extremal horizons.

## Chapter 5

# Holographic Description of Energy Gaps

So far we have been using AdS/CFT to discuss vacuum states and the expectation values of CFT operators on these states. We can also consider the spectrum of fluctuations about this state associated to given operators. This spectrum may be discrete or continuous, and it may be gapless or gapped, meaning that the lowest energy excitation may have zero energy, or positive energy<sup>1</sup>. If we move to a Euclidean signature, then a gap in the spectrum turns into an exponential fall-off of the two point function at large Euclidean time separations[32].

The CFT states we considered in the last two chapters had well defined large scale limits. The large scale scale-invariance generically implies that there is a gapless and continuous spectrum of excitations about this state, corresponding to arbitrarily long wavelength modes. From a bulk perspective, these modes can be thought of as living far down the ‘throat’ of the bulk extremal horizon, or scale-invariant null singularity. We would like to now explore the holographic description of vacuum states with gapped spectra. We will generate a gapped spectrum by putting the CFT on compact spacetimes. The length scales in the boundary provide the energy scale for the gap. The prototypical example is global AdS, where the boundary is a round sphere. As we will discuss, in this case there is indeed an energy gap.

We want to explore how the energy gap depends on the space the CFT lives on. We will start in 5.1 by computing the energy gap associated to an arbitrary primary scalar field on time  $\times$  sphere, where it is determined by conformal symmetry. We will then start to explore the dependence on geometry in 5.2, by deriving a bound on the gap in terms of the minimum value of the Ricci scalar  $R$  for a particular CFT corresponding to a single free scalar field. We will then use perturbation theory to describe more general CFTs on spacetimes that are small deformations of spheres. Finally, we will present the main results of [72] which is a bound on the energy gap associated to scalar operators for holographic CFTs. We will derive this bound using simple geometric properties of the classical gravitational bulk. This work was done in collaboration with Toby Wiseman, and the perturbation theory calculation in Section 5.3 was motivated by discussions with Paul McFadden.

---

<sup>1</sup>The energy won’t be negative since the vacuum is stable.

## 5.1 CFT on a Sphere - Radial Quantization

As a prototype for what can happen if you put a CFT on a compact space, let's consider a CFT on (time  $\times$ ) a sphere. Since this spacetime is conformally flat, we can simply take the flat space correlators and conformally transform them. This is the procedure used in radial quantization of a CFT on flat space, as discussed in [19].

On flat space, the conformal symmetry implies that the vacuum correlator of two (appropriately normalized) primary scalar fields of dimension  $\Delta$  is given by

$$\langle \phi(x_1)\phi(x_2) \rangle = \frac{1}{(x_1 - x_2)^{2\Delta}}. \quad (5.1)$$

Under a conformal transformation, the scalar field transforms as

$$\begin{aligned} g' &= b^2(x)g \\ \phi'(x') &= \frac{1}{b(x)^\Delta} \phi(x) \end{aligned} \quad (5.2)$$

where the second equation is an operator equation, which means it can be inserted in a path-integral together with other operators, and so this transformation carries directly through into correlators. If we write flat space in the form

$$\delta = d\rho^2 + \rho^2 d\Omega^2 \quad (5.3)$$

then we can conformally transform to (Euclidean) time  $\times$  sphere by taking  $b = 1/\rho$

$$\bar{g} = \frac{1}{\rho^2} (d\rho^2 + \rho^2 d\Omega^2) = d\tau^2 + d\Omega^2 \quad (5.4)$$

with  $\rho = e^\tau$ . We can therefore transform the two-point function (5.1) onto the sphere, taking  $x_2$  to be at the north pole

$$\langle \phi(x_1)\phi(x_2) \rangle^\Omega = \rho_1^\Delta \rho_2^\Delta \langle \phi(x_1)\phi(x_2) \rangle^\delta = \frac{\rho_1^\Delta \rho_2^\Delta}{((\rho_1 \cos \theta_1 - \rho_2)^2 + \rho_1^2 \sin^2 \theta_1)^\Delta}. \quad (5.5)$$

This is the propagator, and we can use it to get information about the energy spectrum. In particular, if we examine it at large (Euclidean) times, its fall off will be controlled by the lowest excited state. We find, taking  $\rho_1 \gg \rho_2$  ( $\tau_1 \gg \tau_2$ ) that

$$\langle \phi(x_1)\phi(x_2) \rangle^\Omega \sim e^{-\Delta(\lambda_1 - \lambda_2)}. \quad (5.6)$$

and so the energy gap for scalars is given by their scaling dimension

$$E = \Delta. \quad (5.7)$$

This relationship can be understood by noting that the euclidean time coordinate  $\tau$  is related to the radial coordinate on flat space, and the Hamiltonian on this sphere  $H_S =$

$\frac{\partial}{\partial \tau} = \rho \frac{\partial}{\partial \rho}$  generates dilations on flat space. This is closely related to the operator-state correspondence, where a scalar field inserted at the origin in flat space gets mapped to the far past on the cylinder, and so from (5.6) gives rise to a state of energy  $\Delta$ .

If we write flat space in Cartesian coordinates

$$\delta = dt^2 + \delta_{ij} dx^i dx^j \quad (5.8)$$

and think of  $t$  as a Euclidean time coordinate, then at large time separations we get

$$\langle \phi(x_1) \phi(x_2) \rangle^\delta \sim (t_1 - t_2)^{-2\Delta}. \quad (5.9)$$

Since this is a power law rather than an exponential falloff, this is an ungapped spectrum[32].

So, the spectrum of excitations of an arbitrary scalar operator in a CFT on flat space is gapless, while if we put the same theory on a sphere the spectrum is gapped, with the gap determined by conformal symmetry. To generate an energy gap you need some length scale to set its size. There is no inherent length scale to generate the gap on flat space, but when we put the theory on a sphere the finite volume, or non-zero curvature, of the space provides such a scale. To make this explicit, we can generalize (5.7) to a sphere of radius  $\mathcal{R}$ , and we find

$$E = \frac{\Delta}{\mathcal{R}}. \quad (5.10)$$

## 5.2 Free Scalar CFT

The example in 5.1 might lead us to conclude that while a CFT on an asymptotically flat space has a gapless spectrum, on a compact space the finite volume generates an energy gap, and it's the volume that controls the size of this gap. However, by studying the specific case of the free CFT introduced in Section 1.5.1, we will be lead to a different conclusion. To work out the spectrum of the theory on some static spacetime with metric  $\bar{g}$ , we would need to solve its equation of motion

$$\bar{\square} \phi = \frac{d-2}{4(d-1)} \bar{R} \phi \quad (5.11)$$

for energy eigenstates  $\phi = e^{iEt} \Phi(x)$ , where  $\bar{R}$  is the Ricci scalar and  $\bar{\square}$  is the Laplacian of the spacetime metric  $\bar{g}$ .

Consider first the torus,  $R \times T_{d-1}$ , with metric

$$\bar{g} = -dt^2 + \delta_{ij} d\theta^i d\theta^j. \quad (5.12)$$

In this case  $\bar{R} = 0$ , so  $\bar{\square} \phi = 0$  and the eigenmodes are simply

$$\Phi(x) = e^{i \sum_n k_n x_n} \quad (5.13)$$

with  $E^2 = \sum_n k_n^2$ . The wavenumbers in the different directions on the torus  $k_n$  are quantized by the size of the circles, so the spectrum is discrete, with the gaps between states set by the size of the torus cycles. However, there is a mode with  $k_n = 0$ , which corresponds to an excitation with  $E = 0$ , so the spectrum is ungapped. From this example we see that finite volume alone isn't enough to guarantee a gapped spectrum.

On the sphere, the free scalar CFT must obey (5.10) by symmetry, and so it has a gapped spectrum. Indeed for  $R \times S_{d-1}$ , with a sphere of radius  $\mathcal{R}$ , the energy eigenstates are spherical harmonics with  $Y_m^\ell(x)$  with  $E^2 = \left(\frac{d-2}{2\mathcal{R}}\right)^2 + \ell(\ell+1)$ . This is consistent with (5.10) since for the free scalar  $\Delta_f = \frac{d-2}{2}$ .

One difference between the torus and the sphere is that the sphere has a non-vanishing Ricci scalar, so we are going to explore to what extent we can argue that  $\bar{R}$  controls the gap. To that end, consider placing the free scalar CFT now on an arbitrary curved ultra-static spacetime

$$\bar{g} = -dt^2 + \bar{h}_{ij}dx^i dx^j, \quad (5.14)$$

where the spatial sections  $\bar{h}$  are compact.

The energy states are the solutions of the eigenvalue equation on the spatial section

$$\left(E^2 - \frac{d-2}{4(d-1)}\bar{R}\right)\Phi = -\bar{\nabla}^2\Phi, \quad (5.15)$$

where  $\bar{\nabla}^2$  is the Laplacian of  $\bar{h}$ , and we note that the Ricci scalar of  $\bar{g}$ ,  $\bar{R}$ , is also the Ricci scalar of  $\bar{h}$ . Since  $\bar{R}$  is not constant and  $\bar{\nabla}^2$  is the Laplacian of an arbitrary curved space, we can't solve this explicitly. However, we can quite simply extract an upper and lower bound on  $E$  in terms of the Ricci scalar.

To get the lower bound, multiply by  $\Phi$  and integrate over the compact space

$$\int \left(E^2 - \frac{d-2}{4(d-1)}\bar{R}\right)\Phi^2 = -\int \Phi\bar{\nabla}^2\Phi = \int (\bar{\nabla}\Phi)^2 \geq 0. \quad (5.16)$$

Rearranging yields

$$E^2 \geq \frac{d-2}{4(d-1)} \frac{\int \bar{R}\Phi^2}{\int \Phi^2} \geq \frac{d-2}{4(d-1)} \min \bar{R}. \quad (5.17)$$

This holds for any energy eigenstate, so in particular, this bounds the lowest energy mode, the energy gap  $E_{\min}$ .

To get an upper bound, we can use a variational method. Consider the functional

$$I[\phi] = \frac{\int (\bar{\nabla}\phi)^2 + \frac{d-2}{4(d-1)}\phi^2\bar{R}}{\int \phi^2}. \quad (5.18)$$

Stationary values of the functional are solutions to (5.15), and on these solution  $I[\phi] = E^2$ . Since this functional is invariant under rigid scaling of  $\phi \rightarrow \lambda\phi$ , we can restrict attention to unit normalized  $\phi$ . This leaves the quadratic form  $I_n[\phi] = \int (\bar{\nabla}\phi)^2 + \frac{d-2}{4(d-1)}\phi^2\bar{R}$ . Any given test function  $\phi$  can be expanded in terms of the eigenfunctions of (5.15) which diagonalize it, and so, so long as the functional is bounded from below,  $I_n(\phi)$  must be

greater than the minimum eigenvalue. This functional is bounded from below so long as  $\bar{R}$  is bounded from below, since then  $I[\phi] \geq \frac{d-2}{4(d-1)} \min \bar{R}$ . This means that if the functional is evaluated on an arbitrary test function, this value is then greater than the energy gap. Taking the test function  $\phi = 1$ , we find that

$$E_{\min}^2 \leq \frac{d-2}{4(d-1)} \frac{\int \bar{R}}{\text{vol}} \leq \frac{d-2}{4(d-1)} \max \bar{R}. \quad (5.19)$$

These bounds can be written in a neat way by noting that for a positive Ricci scalar we can define an associated length

$$\mathcal{R}^2(\bar{R}) = \frac{(d-2)(d-1)}{\bar{R}} \quad (5.20)$$

which is the radius of a sphere of constant Ricci scalar  $\bar{R}$ . If  $\bar{R}$  is positive everywhere, we can use this to rewrite the bound

$$\frac{\Delta_f}{\mathcal{R}(\max \bar{R})} \geq E_{\min} \geq \frac{\Delta_f}{\mathcal{R}(\min \bar{R})}. \quad (5.21)$$

Because of the scale-invariance in CFTs, only dimensionless ratios are physical. This means that we always need to choose a length scale with respect to which the energy is measured. What (5.21) therefore says is that, on spaces of positive definite  $\bar{R}$ , if we measure the energy gap with respect to a length scale given by the minimum value of  $\bar{R}$ , then this energy gap is bounded from below by the scaling dimension, and similarly it is bounded from above if we use the maximum Ricci scalar. This is our first indication that it is this scalar curvature, rather than the volume, that controls the size of the gap. By comparison with (5.10) we see that both bounds are saturated on a sphere, where it was determined by symmetry.

### 5.3 General Scalars - Conformal Perturbation Theory

We would like to begin to generalize the discussion in Section 5.2 for a free scalar CFT on an arbitrary compact space, to a general CFT with interacting scalars of arbitrary dimension  $\Delta$ . In 5.2 we could use the explicit Lagrangian for a free theory to tell us about the spectrum, so this method doesn't immediately generalize. We can, however, make use of the conformal symmetry. In Section 5.1, we used this symmetry to work out the energy gap for an arbitrary scalar on a sphere. This, however, relied on the fact that the space-time in question is conformally flat, so the symmetry allowed us to write down the two point function, and so read off the energy gap. A more general space-time will generically break this symmetry, and we won't have such a simple way to write down the correlator.

If we consider space-times that are small deformations of spheres, then by using perturbation theory we can continue to make use of the symmetry. Consider a conformal field theory defined by an action  $S[\bar{g}_{\mu\nu}, \phi_A]$  which is a functional of a spacetime  $\bar{g}$  and

some fields  $\phi_A$ . We take our spacetime to be

$$\bar{g} = d\tau^2 + d\Omega_{d-1}^2 + \epsilon h_{ij}(\theta_i) d\theta^i d\theta^j \quad (5.22)$$

where  $\epsilon$  is some small parameter. The coordinate  $\tau$  is a Euclidean time coordinate, the  $\theta^i$  span a  $d - 1$  dimensional sphere, and  $d\Omega_{d-1}^2$  is the usual round unit-sphere metric. The action can be expanded in a power series in  $\epsilon$

$$\begin{aligned} S[\bar{g}_{\mu\nu}, \phi_A] &= S[\bar{g}_{\mu\nu}^0, \phi_A] + \int \frac{\delta S}{\delta \bar{g}^{\mu\nu}} \delta \bar{g}^{\mu\nu} d\tau d\Omega_{d-1} \\ &= S_0[\phi_A] - \frac{\epsilon}{2} \int T_{ij} h^{ij} d\tau d\Omega_{d-1} + O(\epsilon^2) \equiv S_\epsilon[\phi_A]. \end{aligned} \quad (5.23)$$

where  $\bar{g}_{\mu\nu}^0$  is the  $\epsilon = 0$  sphere,  $S_0[\phi_A]$  is the  $\epsilon = 0$  action, and  $T_{ij}$  is the stress tensor on this sphere. The right hand side is written in terms of integrals over the sphere, so we can use it to define a deformed action on the undeformed sphere  $S_\epsilon[\phi^A]$ , which is equivalent to our theory on the deformed sphere to first order in  $\epsilon$ .

While, at  $\epsilon = 0$ ,  $S_0$  is conformally invariant, when we turn on the deformation  $S_\epsilon$  is no longer invariant. However, since  $\epsilon$  is a small parameter, we can use perturbation theory to rewrite expectation values in  $S_\epsilon$  in terms of correlators in  $S_0$  with additional insertions. This can be seen through the path integral

$$\begin{aligned} Z &= \int d[\phi_A] \exp(-S_\epsilon[\phi_A]) \\ &= \int d[\phi_A] \left( 1 + \frac{\epsilon}{2} \int T_{ij} h^{ij} d\tau d\Omega_{d-1} + O(\epsilon^2) \right) \exp(-S_0[\phi_A]). \end{aligned} \quad (5.24)$$

As we did on the  $\epsilon = 0$  sphere in Section 5.1 we consider the two point function of a scalar of dimension  $\Delta$ . This time it can be expanded in a series in  $\epsilon$

$$\begin{aligned} \langle \phi(\tau_1, \theta_1^i) \phi(\tau_2, \theta_2^i) \rangle_{S_\epsilon}^\Omega &= \langle \phi(\tau_1, \theta_1^i) \phi(\tau_2, \theta_2^i) \rangle_{S_0}^\Omega + \\ &\quad \frac{\epsilon}{2} \int \langle \phi(\tau_1, \theta_1^i) \phi(\tau_2, \theta_2^i) T_{ij}(\tau, \theta^i) \rangle_{S_0}^\Omega h^{ij}(\theta^i) d\tau d\Omega_{d-1} \\ &\quad + O(\epsilon^2). \end{aligned} \quad (5.25)$$

Since  $S_0$  is conformally invariant, the correlators on the right hand side above are correlators for a conformally invariant theory on time cross a sphere. Therefore, as in Section 5.1, we can conformally transform to flat space and use the conformal symmetry to constrain the correlators there<sup>2</sup>. Performing this same transformation here, noting the

<sup>2</sup>In fact we can reinterpret the whole perturbation in flat space, where it becomes the scale-invariant perturbation which sends the metric to

$$\tilde{g} = d\rho^2 + \rho^2 \left( d\Omega_{d-1}^2 + \epsilon h_{ij}(\theta^i) d\theta^i d\theta^j \right). \quad (5.26)$$

Note that this differs from the scale-invariant spatial deformations we considered in previous chapters since these had a separate time coordinate.

transformation of the stress tensor from (3.15),

$$\begin{aligned} \langle \phi(\tau_1, \theta_1^i) \phi(\tau_2, \theta_2^i) \rangle_{S_0}^\Omega &= \rho_1^\Delta \rho_2^\Delta \langle \phi(\rho_1, \theta_1^i) \phi(\rho_2, \theta_2^i) \rangle_{S_0}^\delta \\ \langle \phi(\tau_1, \theta_1^i) \phi(\tau_2, \theta_2^i) T_{ij}(\tau, \theta^i) \rangle_{S_0}^\Omega &= \rho_1^\Delta \rho_2^\Delta \rho^{d-2} \langle \phi(\rho_1, \theta_1^i) \phi(\rho_2, \theta_2^i) T_{ij}(\rho, \theta^i) \rangle_{S_0}^\delta. \end{aligned} \quad (5.27)$$

Putting this all together therefore yields

$$\begin{aligned} \langle \phi(\tau_1, \theta_1^i) \phi(\tau_2, \theta_2^i) \rangle_{S_\epsilon}^\Omega &= \rho_1^\Delta \rho_2^\Delta \langle \phi(\rho_1, \theta_1^i) \phi(\rho_2, \theta_2^i) \rangle_{S_0}^\delta + \\ &\quad \frac{\epsilon}{2} \rho_1^\Delta \rho_2^\Delta \int \langle \phi(\rho_1, \theta_1^i) \phi(\rho_2, \theta_2^i) T_{ij}(\rho, \theta^i) \rangle_{S_0}^\delta h^{ij}(\theta^i) \rho^{d-3} d\rho d\Omega_{d-1} \\ &\quad + O(\epsilon^2). \end{aligned} \quad (5.28)$$

The flat space two point function  $\langle \phi(\rho_1, \theta_1^i) \phi(\rho_2, \theta_2^i) \rangle_{S_0}^\delta$  is completely determined by conformal symmetry as we stated in (5.1), and also, as shown in [61] the conformal symmetry fixes the three point function with the stress tensor to be

$$\langle \phi(\rho_1, \theta_1^i) \phi(\rho_2, \theta_2^i) T_{\mu\nu}(\rho, \theta^i) \rangle_{S_0}^\delta = \frac{a (\hat{y}_\mu \hat{y}_\nu - \frac{1}{d} \delta_{\mu\nu})}{|x - x_1|^d |x - x_2|^d |x_1 - x_2|^{2\Delta-d}}, \quad (5.29)$$

with the constant  $a = -\frac{d\Delta}{\Omega_{d-1}(d-1)}$ .  $x^\mu$ ,  $x_1^\mu$  and  $x_2^\mu$  are Cartesian vectors corresponding to the points  $(\rho, \theta^i)$ ,  $(\rho_1, \theta_1^i)$  and  $(\rho_2, \theta_2^i)$  respectively, and the vector  $\hat{y}^\mu$  is the unit normalized vector parallel to

$$y^\mu = \frac{x^\mu - x_1^\mu}{|x - x_1|^2} - \frac{x^\mu - x_2^\mu}{|x - x_2|^2}. \quad (5.30)$$

We are interested in the limit where  $\tau_1 \gg \tau_2$ , and hence  $\rho_1 \gg \rho_2$ . In this limit  $|x_1 - x_2| \approx \rho_1$ , and (5.28) becomes

$$\langle \phi(\tau_1, \theta_1^i) \phi(\tau_2, \theta_2^i) \rangle_{S_\epsilon}^\Omega \approx \frac{\rho_2^\Delta}{\rho_1^\Delta} \left( 1 + \frac{a\epsilon\rho_1^d}{2} \int \frac{(\hat{y}_i \hat{y}_j - \frac{\rho_2^2}{d} \Omega_{ij})}{|x - x_1|^d |x - x_2|^d} h^{ij}(\theta^i) \rho^{d-3} d\rho d\Omega_{d-1} \right) + O(\epsilon^2). \quad (5.31)$$

Instead of diving into attempting to calculate this full integral, we can work out which bits of it are needed in order to calculate the shift in energy gap. Now, in flat space the correlator in this limit went as

$$\langle \phi(x_1) \phi(x_2) \rangle_{S_0}^\delta \approx \frac{1}{\rho_1^{2\Delta}} \quad (5.32)$$

which becomes, on conformally transforming to the sphere

$$\langle \phi(x_1) \phi(x_2) \rangle_{S_0}^\Omega \approx \frac{\rho_2^\Delta}{\rho_1^\Delta} = e^{-\Delta(\tau_1 - \tau_2)}. \quad (5.33)$$

Because of the scaling symmetry, the corrections to this will take the form

$$\langle \phi(x_1)\phi(x_2) \rangle_{S_\epsilon}^\Omega \approx \left( 1 + \epsilon f \left( \frac{\rho_2}{\rho_1} \right) \right) \frac{\rho_2^\Delta}{\rho_1^\Delta}. \quad (5.34)$$

We will find the function  $f$  will have an expansion of the form

$$f(x) = A + B \log x + \sum_{n>0} A_n x^n \quad (5.35)$$

at small  $x$ . Since  $\rho_1 \gg \rho_2$ , we can ignore all the positive powers of  $x$ , and we are left in the limit with

$$\langle \phi(x_1)\phi(x_2) \rangle_{S_\epsilon}^\Omega \approx (1 + \epsilon A) e^{-(\Delta + \epsilon B)(\tau_1 - \tau_2)} \quad (5.36)$$

so we see that it's the logarithm term  $B$  that shifts the energy. This is therefore the only term we need to calculate in the perturbation to the two point function, and we can ignore any finite contribution in the limit  $\frac{\rho_2}{\rho_1} \rightarrow 0$ .

At this point it is worth pointing out one subtlety. The integral as we have written it in (5.31) is not well defined due to the divergences as  $x \rightarrow x_1$  and  $x \rightarrow x_2$ . However, these divergences can be regulated, as discussed in [61], by replacing the divergent three point function with a distribution which is equivalent to (5.29) for  $x \neq x_1$  and  $x \neq x_2$ . This distribution then gives a finite constant contribution to these integrals at these points, so in terms of (5.36), these contributions modify the value of  $A$  and not  $B$ , and so we don't need to worry about them since they won't affect the energy shift.

In order to take advantage of this limit, we can split the  $\rho$  integral into two domains, one where  $\rho < \tilde{\rho}$  and another where  $\rho > \tilde{\rho}$ . If we choose  $\tilde{\rho}$  such that  $\rho_2 \ll \tilde{\rho}$  and  $\rho_1 \gg \tilde{\rho}$  then in each of these domains the integrand simplifies. In the first case  $\rho < \tilde{\rho}$  we have that

$$\begin{aligned} |x_1 - x| &\approx \rho_1 \\ \hat{y}^\mu &\approx \frac{x_2^\mu - x^\mu}{|x_2 - x|}. \end{aligned} \quad (5.37)$$

The components  $\hat{y}_i$  which will be contracted with  $h_{ij}(\theta^i)$  are the components normal to  $x$ . To separate the angular integral from the  $\rho$  integral we introduce a unit vector on the sphere  $\xi_2^i$ . This is a vector at the point  $x$  which is unit-normalized with respect to the sphere metric  $d\Omega^2$ , is perpendicular to  $x$ , and lies in the plane defined by  $x$  and  $x_2$ . This is illustrated in Figure 5.1. These normal components are then<sup>3</sup>

$$\hat{y}_i \approx \frac{\rho_2 \rho \xi_i^2 \sin \theta_2}{\sqrt{\rho^2 + \rho_2^2 - 2\rho\rho_2 \cos \theta_2}}. \quad (5.38)$$

<sup>3</sup>The indices of  $\xi$  are raised and lowered by the sphere metric  $\Omega_{ij}$ .

Using this, and introducing a dimensionless integration variable  $\alpha = \frac{\rho}{\rho_2}$

$$\begin{aligned}
I_1 &\equiv \frac{a\epsilon\rho_1^d}{2} \int_0^{\tilde{\rho}} \frac{(\hat{y}_i\hat{y}_j - \frac{\rho^2}{d}\Omega_{ij})}{|x-x_1|^d|x-x_2|^d} h^{ij}(\theta^i) \rho^{d-3} d\rho d\Omega_{d-1} \\
&\approx \frac{a\epsilon}{2} \int d\Omega_{d-1} \sin^2 \theta_2 \xi_2^i \xi_2^j h_{ij}(\theta^i) \left( \int_0^{\frac{\tilde{\rho}}{\rho_2}} d\alpha \frac{\alpha^{d-1}}{(1+\alpha^2 - 2\alpha \cos(\theta_2))^{d/2+1}} \right) \\
&\quad - \frac{a\epsilon}{2d} \int d\Omega_{d-1} \Omega^{ij} h_{ij}(\theta^i) \left( \int_0^{\frac{\tilde{\rho}}{\rho_2}} d\alpha \frac{\alpha^{d-1}}{(1+\alpha^2 - 2\alpha \cos(\theta_2))^{d/2}} \right).
\end{aligned} \tag{5.39}$$

If we send  $\frac{\tilde{\rho}}{\rho_2} \rightarrow \infty$ , then the first integral is finite, so by the above arguments we can ignore it. However, the second integral gives a divergent contribution

$$I_1 \sim -\frac{a\epsilon}{2d} \int d\Omega_{d-1} \Omega^{ij} h_{ij}(\theta_i) \log \frac{\tilde{\rho}}{\rho_2}. \tag{5.40}$$

For the second domain  $\rho > \tilde{\rho}$

$$\begin{aligned}
|x_2 - x| &\approx \rho \\
y^\mu &\approx \frac{x^\mu - x_1^\mu}{|x - x_1|^2} - \frac{x^\mu}{\rho^2}.
\end{aligned} \tag{5.41}$$

Proceeding as above, the normal component of  $\hat{y}$  is

$$\hat{y}_i \approx \frac{\rho^2 \xi_1^i \sin \theta_1}{\sqrt{\rho^2 + \rho_1^2 - 2\rho\rho_1 \cos \theta_1}}. \tag{5.42}$$

The integral is then

$$\begin{aligned}
I_2 &\equiv \frac{a\epsilon\rho_1^d}{2} \int_{\tilde{\rho}}^\infty \frac{(\hat{y}_i\hat{y}_j - \frac{\rho^2}{d}\Omega_{ij})}{|x-x_1|^d|x-x_2|^d} h^{ij}(\theta^i) \rho^{d-3} d\rho d\Omega_{d-1} \\
&\approx \frac{a\epsilon}{2} \int d\Omega_{d-1} \sin^2 \theta_1 \xi_1^i \xi_1^j h_{ij}(\theta^i) \left( \int_{\frac{\tilde{\rho}}{\rho_1}}^\infty d\alpha \frac{\alpha}{(1+\alpha^2 - 2\alpha \cos(\theta_1))^{d/2+1}} \right) \\
&\quad - \frac{a\epsilon}{2d} \int d\Omega_{d-1} \Omega^{ij} h_{ij}(\theta^i) \left( \int_{\frac{\tilde{\rho}}{\rho_1}}^\infty d\alpha \frac{1}{\alpha (1+\alpha^2 - 2\alpha \cos(\theta_1))^{d/2}} \right).
\end{aligned} \tag{5.43}$$

Now we send  $\frac{\tilde{\rho}}{\rho_1} \rightarrow 0$ . Again, the first integral is finite in this limit, but the second integral has a logarithmic divergence of the form

$$I_2 \sim \frac{a\epsilon}{2d} \int d\Omega_{d-1} \Omega^{ij} h_{ij}(\theta_i) \log \frac{\tilde{\rho}}{\rho_1}. \tag{5.44}$$

Combining all this together, we find

$$\langle \phi(\tau_1, \theta_1^i) \phi(\tau_2, \theta_2^i) \rangle_{S_\epsilon}^\Omega \approx \frac{\rho_2^\Delta}{\rho_1^\Delta} \left( 1 + \frac{a\epsilon}{2d} \int d\Omega_{d-1} \Omega^{ij} h_{ij}(\theta_i) \log \frac{\tilde{\rho}_2}{\rho_1} + \dots \right) + O(\epsilon^2). \tag{5.45}$$

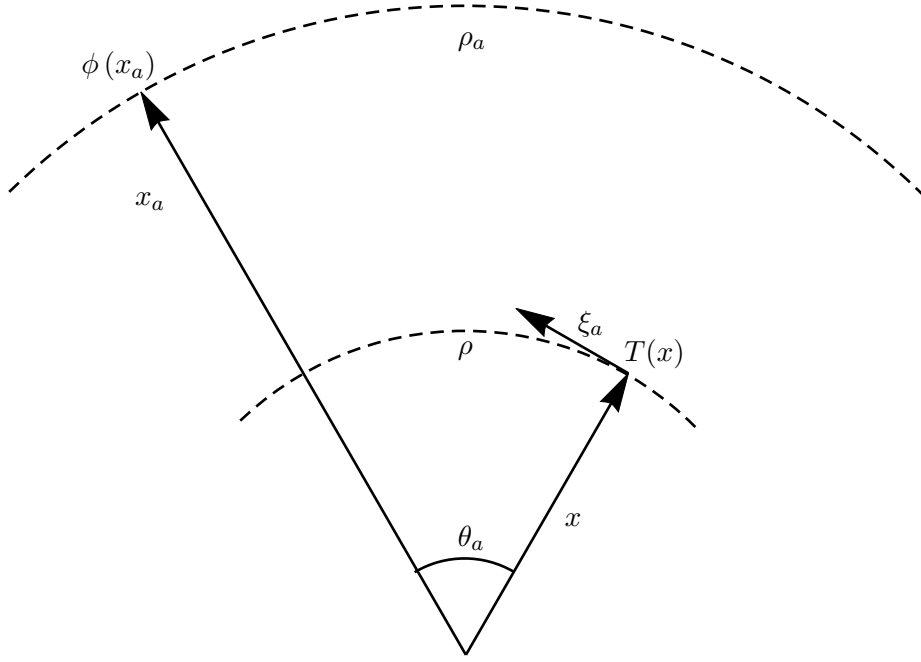


FIGURE 5.1: Illustration of the coordinate choice.

where the ... refer to terms that are finite as  $\frac{\rho_2}{\rho_1} \rightarrow 0$ . Noting that the shift in volume is  $\delta V = -\frac{\epsilon}{2} \int d\Omega_{d-1} \Omega^{ij} h_{ij}(\theta_i)$ , and substituting for  $a$ , we can therefore read off the shift in the energy gap

$$\delta E = \frac{\Delta \delta V}{(d-1)\Omega_{d-1}} = -\frac{E \delta V}{(d-1)V}, \quad (5.46)$$

where we have used the fact that we are perturbing a unit sphere where  $V = \Omega_{d-1}$  and  $E = \Delta$ . This is equivalent to the volume normalized temperature staying invariant to first order. To consider the energy gap normalized by the Ricci scalar, we can show that, for a sphere

$$\begin{aligned} \delta \min R &\leq \frac{\int \sqrt{g} \delta R}{V} = -2 \frac{R}{d-1} \delta V \\ \delta \max R &\geq \frac{\int \sqrt{g} \delta R}{V} = -2 \frac{R}{d-1} \delta V. \end{aligned} \quad (5.47)$$

Hence, to first order in perturbation theory,

$$\begin{aligned} \frac{\delta E}{E} &\geq \frac{\delta \min R}{2R} \implies \delta(E^2 \min R) \geq 0 \\ \frac{\delta E}{E} &\leq \frac{\delta \max R}{2R} \implies \delta(E^2 \max R) \leq 0. \end{aligned} \quad (5.48)$$

In other words, the energy gap normalized by the minimum(maximum) value of the Ricci scalar is minimized(maximized) on the sphere.

## 5.4 Holographic Energy Gap

What we've seen so far is that we can write down a bound on the energy gap for a primary scalar operator in two different cases. Firstly, for a free scalar, we can write a bound down on an arbitrary space of positive definite  $R$ , and secondly, for an arbitrary scalar, we can write down a bound that holds for small perturbations of a sphere. We will now move to holographic CFTs, and consider scalar fluctuations about universal sector vacuum solutions. What we'll find is that while we can derive precisely the same lower bound as in the other cases, the upper bound we will derive will not be as strong, and we will be able to find explicit counter examples to a straight forward generalization of the upper bound in (5.21) and (5.48).

### 5.4.1 The bulk equations and the optical geometry

We are going to consider scalar fluctuations about universal sector vacua where the CFT has  $(d - 1) + 1$  dimensions. The vacua will be described by  $d + 1$  dimensional static solutions to Einstein's equation

$${}^G R_{\mu\nu} = -\frac{d}{\ell^2} G_{\mu\nu}, \quad (5.49)$$

where we have used  $G_{\mu\nu}$  to denote the  $d + 1$  dimensional bulk metric, and  ${}^G R_{\mu\nu}$  is its Ricci tensor.

As discussed in Section 1.4.1, on the conformal boundary of this bulk spacetime, there isn't a single induced metric  $\bar{g}$ , but rather an induced conformal class of metrics

$$[\bar{g}] = \left\{ \tilde{g} \mid \tilde{g} = e^\phi \bar{g} \right\}. \quad (5.50)$$

where  $\bar{g}$  is some representative of the class. Each element of this set is called a choice conformal frame. If the geometry is static, then there is some class of representative metrics  $\tilde{g}$  that are static and take the form

$$\tilde{g} = -\omega^2(x^i) dt^2 + \alpha_{ij}(x^i) dx^i dx^j, \quad (5.51)$$

where the  $d - 1$   $x^i$  coordinates cover a spatial slice of the conformal boundary, and  $\alpha_{ij}(x^i)$  is some time-independent  $d - 1$  dimensional spatial metric. If there are no horizons, where we would have  $\omega^2 = 0$ , and the conformal boundary doesn't have any asymptotic regions where  $\omega^2 \rightarrow \infty$ , then we can Weyl scale to get rid of  $\omega$ . This yields a special conformal frame called the ultra-static frame where the metric takes the form

$$\bar{g} = -dt^2 + \bar{h}_{ij}(x^i) dx^i dx^j. \quad (5.52)$$

The results we have discussed above for CFTs on ultrastatic geometries therefore actually apply more generally to a wide class of static geometries. However, the Ricci scalar  $\bar{R}$  that enters into the bounds (5.21) is specifically the Ricci scalar of the spatial metric in

this ultrastatic frame, so in other conformal frames the bound won't take such a simple form.

We will consider bulk geometries where the static symmetry of the conformal boundary extends into the bulk, so we're considering a static CFT state. We can then write the bulk metric in a way that's adapted to this frame. We can write

$$G = \frac{\ell^2}{Z(y)^2} \left( -dt^2 + h_{ab}(y) dy^a dy^b \right) \quad (5.53)$$

where the  $dy^a$  coordinates span a spatial slice of the bulk, and  $h_{ab}(y)$  is a time-independent  $d$  dimensional spatial metric. The function  $Z(y)$  is called the redshift, because it relates time intervals measured by the scaled metric to ones measured by the physical metric. The metric  $h_{ab}$  is the optical geometry introduced in [73]. It's called the optical geometry because if you consider light rays following null geodesics in  $g$ , and project them on to constant time slices of the spacetime, the spatial paths they follow are the geodesics of  $h$ . If we take the redshift  $Z(y)$  as our defining function for the extraction of the conformal boundary metric, following 1.4.1, then the boundary metric will be in the ultrastatic frame (5.52). The conformal boundary of the physical metric at  $Z = 0$  becomes a regular smooth boundary of the optical metric  $h_{ab}$ , and the induced metric on this boundary is precisely  $\bar{h}_{ij}$ . Unlike the FG coordinates, we can write (5.53) everywhere in the bulk, not just in a region about the conformal boundary, so long as there are no horizons.

The bulk Einstein's equation written in terms of  $h_{ab}$  and  $Z$  takes the form

$$\begin{aligned} {}^h R_{ab} &= -(d-1) \frac{{}^h \nabla_a \partial_b Z}{Z} \\ {}^h R &= \frac{d(d-1)}{Z^2} (1 - \partial_a Z \partial^a Z) \end{aligned} \quad (5.54)$$

where  ${}^h R_{ab}$  and  ${}^h R$  are the Ricci tensor and scalar associated with the optical metric. A useful identity, which we will rely on heavily in what follows, can be derived from taking two derivatives of the first equation. After a bit of algebra, and application of the contracted Bianchi identity, it can be shown that (dropping the superscript)

$$\nabla^2 R = R^2 - d R_{ab} R^{ab} - \frac{d-3}{2} \frac{\partial_a Z}{Z} \partial^a R = -d \tilde{R}^{ab} \tilde{R}_{ab} - \frac{d-3}{2} \frac{\partial_a Z}{Z} \partial^a R. \quad (5.55)$$

where  $\tilde{R}_{ab} = R_{ab} - \frac{1}{d} h_{ab} R$  is the traceless component of the Ricci tensor. In what follows, we will drop the superscript  $h$ . Unless otherwise stated, unbarred quantities relate to the spatial optical geometry, and barred quantities relate to the spatial sections of the boundary geometry in ultrastatic frame.

For concreteness, let's consider two simple choices of boundary  $\bar{h}_{ij}$ , their dual bulk geometries, and the resulting optical metric. Firstly, for a sphere on the boundary, a bulk

vacuum is provided by global AdS (1.11). The optical metric is given by

$$h_{\text{AdS}} = \frac{r^2}{\ell^2 + r^2} d\Omega_{d-1}^2 + \frac{dr^2}{\ell^2 \left(1 + \frac{r^2}{\ell^2}\right)^2} = d\Omega_d^2 \quad (5.56)$$

where we have set  $r = \ell \tan \theta$  with  $\theta$  the angle to the pole in  $\Omega_d$ . The conformal boundary is at the equator  $\theta = \frac{\pi}{2}$ , so the optical geometry is a  $d$  dimensional hemisphere. This geometry has constant optical  $R = d(d-1)$ .

For flat space on the boundary, the simplest vacuum state we can consider is Poincaré AdS. In this case, the optical geometry is just

$$h_{\text{Poincaré AdS}} = dz^2 + \delta_{ij} dx^i dx^j \quad (5.57)$$

with the boundary at  $z = 0$ , and now optical  $R = 0$ . As remarked in Chapter 3, if we periodically identify the boundary into a torus this geometry is actually singular in the IR. An alternative bulk is the AdS-Soliton from (1.49), where the optical geometry is

$$h_{\text{AdS Soliton}} = \delta_{ij} dx^i dx^j + \frac{\ell^2 dr^2}{r^2 f(r)} + \frac{f(r)}{r^2} \mathcal{R}^2 d\theta^2. \quad (5.58)$$

Now, the optical Ricci scalar is  $R = \frac{4(d-1)r_0^{d-2}}{r^{d-2}(d\mathcal{R}^2)}$ , which starts from 0 on the boundary  $r \rightarrow \infty$ , and increases to a maximum value of  $\max R = \frac{4(d-1)}{d\mathcal{R}^2}$  when the geometry rounds off at  $r = r_0$ .

These special cases where the bulk solutions are known are the exception rather than the rule. In general, to find a solution with a given boundary  $\bar{h}_{ij}$ , we would have to solve (5.54) numerically using, for instance, the techniques from Chapter 2. Instead we will see what we can say simply by assuming a bulk geometry with certain properties exists, without specifying the precise form of the solution.

### 5.4.2 Scalar Fluctuations

To consider a primary scalar field in the CFT, we add a massive scalar field to the bulk. Since we are only interested in small fluctuations of the scalar, we can consider the scalar field on the background of the vacuum solution without worrying about its stress-tensor, and hence its back-reaction on the geometry. Also, this means we can restrict ourselves to a quadratic action for the scalar. The spectrum of linear fluctuations of this scalar field in the bulk then corresponds to the spectrum of excitations of the dual operator in the CFT. The most straightforward justification of this is the Hamiltonian formulation of the AdS/CFT correspondence, where the supergravity Hilbert space in the bulk is identified with the Hilbert space in the boundary CFT[3, 32].

Although strictly speaking the addition of this scalar field means we are no longer in the universal sector, our results are still very applicable. In any top-down two-derivative gravitational model, there will be a number of scalar degrees of freedom that have been truncated to get to the universal sector; some will come from scalars in the original action,

and some will be associated with internal spaces in the dimensional reduction. Small fluctuations of these scalar fields will behave as minimally coupled scalar fields, since at two derivatives there is nothing else they can covariantly couple to. On a general spacetime, they could couple to the Ricci scalar, but this is rendered trivial by Einstein's equation. We discussed these scalar fields in Section 1.6.2.

In order to find the spectrum, we need to solve for energy eigenmodes  $\phi = \phi_\omega(y)e^{i\omega t}$ . Written in terms of the optical metric, these satisfy

$$-Z(y)^{D-1}\nabla^a\left(\frac{1}{Z(y)^{D-1}}\partial_a\phi_\omega(y)\right)+\frac{\ell^2m^2}{Z(y)^2}\phi_\omega(y)=\omega^2\phi_\omega(y). \quad (5.59)$$

In order to think about solutions to these equations we need to decide on boundary conditions. We are interested in unsourced fluctuations, which, by comparison with (1.35) means that our solutions will go like  $Z^\Delta$  near the boundary, with the other leading order behaviour that goes as  $Z^{D-\Delta}$  set to 0.

It will be convenient to write the equation of motion in terms of a scaled field  $\psi_\omega = Z^{-\Delta}\phi_\omega$ . This is scaled in such a way that  $\psi_\omega$  is finite everywhere, and its boundary values on  $\partial\mathcal{M}$  are proportional to the expectation value of the field. This scaled field then satisfies the equation

$$\nabla^2\psi_\omega(y)+\frac{2\Delta-d+1}{Z(y)}\partial^aZ(y)\partial_a\psi_\omega(y)+\left(\omega^2-\frac{\Delta^2}{d(d-1)}R(y)\right)\psi_\omega(y)=0, \quad (5.60)$$

where  $R(y)$  is the Ricci scalar of the optical geometry.

In the simplest cases we can solve this equation explicitly. For instance, whenever optical  $R$  is constant, constant  $\psi_\omega$  is a solution. This is in fact the lowest energy solution<sup>4</sup>, so in these cases we have an energy gap  $\omega_{\min}^2 = \frac{\Delta^2 R}{d(d-1)}$ . For instance, in global AdS as shown above this is true, and we have an energy gap  $\omega_{\min} = \Delta$ . We had to find this value for the gap, since global AdS is the maximally symmetric vacuum which preserves the full conformal group in the boundary, so our arguments from 5.1 have to apply.

### 5.4.3 Bulk Assumptions

We are interested in scalar fluctuations about zero temperature vacuum states. These states are described by some bulk geometry, and we're going to make some assumptions about this bulk geometry. As we will see, these assumptions will give rise to a gapped spectrum of scalar fluctuations and allow us to put a bound on this gap. We are going to assume that the conformal boundary is compact and that the bulk geometry ends only on the conformal boundary, has no other asymptotic regions, and has no horizons. These assumptions have implications for the optical geometry we introduced in Section 5.4.1. Denote the Riemannian manifold consisting of the spatial section of our geometry and the optical metric by  $(\mathcal{M}, h_{ab})$ . Then it follows that

1. The redshift  $Z(y)$  is bounded on  $\mathcal{M}$ .

<sup>4</sup>This will follow from (5.63) derived below.

2.  $\mathcal{M}$  has finite volume, and ends only on a compact smooth boundary  $\partial\mathcal{M}$ , corresponding to the spatial section of the conformal boundary in ultrastatic frame.

Global AdS and the AdS-Soliton we discussed above satisfy these assumptions, and as a result their optical geometry has these properties, but periodically identified Poincaré AdS does not, because of the singular infrared region.

#### 5.4.4 Lower Bound on the Scalar Fluctuation Spectrum

We can proceed much as we did with the free conformal scalar. Let's first consider (5.59). We can multiply by  $\phi(x)$  and integrate. This yields

$$\omega^2 = \frac{\int_{\mathcal{M}} (Z^{1-d} \partial_a \phi_\omega \partial^a \phi_\omega + \ell^2 m^2 Z^{-1-d} \phi_\omega^2)}{\int_{\mathcal{M}} Z^{1-d} \phi_\omega^2} \quad (5.61)$$

so long as  $\Delta > \frac{d+1}{2}$  so that the integrals are finite and we can ignore boundary terms when we integrate by parts. We can extract a bound on  $\omega$  from this integral by noting that  $(\partial\phi_\omega)^2 \geq 0$  and  $\int_{\mathcal{M}} Z^{1-d} \phi_\omega^2 < (\max Z^2) \int_{\mathcal{M}} Z^{-1-d} \phi_\omega^2$  so that, if  $m^2 > 0$

$$\omega^2 > \frac{\ell^2 m^2}{(\max Z^2)}. \quad (5.62)$$

This inequality is unsatisfactory for a number of reasons. Firstly since  $Z$  is never constant, this bound can never be saturated. This is an indication that the bound is quite weak. Secondly, this bound only works if  $m^2 > 0$ , and hence  $\Delta > d$ . This in particular rules out any relevant operators. Finally, this bound as we've written it is not immediately written in terms of CFT data. Namely, while  $m^2$  can be determined by the scaling dimension of the dual operator in the CFT, the maximum redshift  $\max Z$  is a property of the vacuum solution of Einstein's equation. This means it is not something we would be able to immediately read off in the CFT, but instead is a property of the vacuum state.

In order to derive a better bound we can instead consider (5.60). We multiply by  $Z^{2\Delta-d+1} \psi_\omega$  and integrate by parts to find a bound on  $\omega$

$$\omega^2 = \frac{\int_{\mathcal{M}} \sqrt{g} Z^{2\Delta-d+1} \left( (\partial\psi_\omega)^2 + \frac{\Delta^2}{d(d-1)} \psi_\omega^2 R^2 \right)}{\int_{\mathcal{M}} \sqrt{g} Z^{2\Delta-d+1} \psi_\omega^2} \geq \frac{\Delta^2 \min R}{d(d-1)} \quad (5.63)$$

In order for these integrals to be finite, and for the boundary terms that arise from integrating by parts to vanish, the only condition is that  $\Delta > \frac{d-2}{2}$ <sup>56</sup>. This coincides with the unitarity bound [74], which is the lower bound on the scaling dimensions of scalar operators we can consider anyway. At first glance we haven't gained much compared to (5.62) beyond allowing ourselves to consider relevant operators. However, a series of observations will illustrate that this bound is much stronger. First of all, this bound can be

<sup>5</sup>This works for either quantization for  $\Delta < \frac{d+2}{2}$ .

<sup>6</sup>Recall from our assumptions that there are no boundary regions to consider in these integrals other than the conformal boundary.

saturated if  $R$  is constant, in which case lowest mode has  $\psi_\omega$  constant as well. This is indeed the case, for instance, on global AdS. Secondly, while we've written it here in terms of a bulk geometric quantity, this bound can be recast in terms of boundary quantities without making it any weaker.

This is because we can derive a maximum principle for the optical  $R$ . By examining the identity (5.55), we can see that at a stationary point of  $R$ , so that  $\nabla_i R = 0$ , we have that  $\nabla^2 R \leq 0$ . This means that the stationary point cannot be a minimum. This in turn means that  $R$  must attain its minimum value on the boundary of the domain, the conformal boundary  $\partial M$ . By looking at a boundary expansion of the equations of motion, we can find that in fact the boundary value of  $R$  is given by

$$R|_{\partial M} = \frac{d}{d-2} \bar{R} \quad (5.64)$$

where  $\bar{R}$  is the Ricci scalar of the boundary geometry (in the ultrastatic frame). We therefore have that

$$\min R = \frac{d}{d-2} \min \bar{R} \quad (5.65)$$

which, when substituted into (5.63) yields

$$\omega^2 \geq \frac{\Delta^2 \min \bar{R}}{(d-1)(d-2)} = \frac{\Delta^2}{\mathcal{R}^2 (\min \bar{R})}. \quad (5.66)$$

By comparing with (5.21), we see we have derived the same lower bound as for the free scalar, but now for a general scaling dimension  $\Delta$  in these holographic strongly coupled CFTs.

### 5.4.5 An Upper Bound

Having bounded the gap from below, an interesting question is whether the energy gap can be arbitrarily large. As with the free scalar, we can write an upper bound on this gap, but unfortunately this bound is not in terms of CFT data. We do this by recasting (5.60) in terms of a functional

$$I_\Delta[\psi] = \frac{\int_M \sqrt{h} Z^{2\Delta+1-d} \left( \partial_a \psi \partial^a \psi + \frac{\Delta^2}{d(d-1)} R \psi^2 \right)}{\int_M \sqrt{h} Z^{2\Delta+1-d} \psi^2}. \quad (5.67)$$

where  $\psi$  is now any smooth bounded function on the optical geometry. The condition  $\frac{\delta I_\Delta}{\delta \psi(x)} = 0$  is precisely (5.60) where  $\omega^2 = I_\Delta[\psi]$ . The stationary points of this functional therefore correspond to the spectrum of the scalar operator.

The argument follows the same pattern as the free scalar. The smallest stationary point of this functional is given by the energy gap. So long as this functional is bounded from below, which is true so long as  $R$  is bounded from below, this means that this energy gap is the minimum value of the functional. From (5.65) it is sufficient for the boundary  $\bar{R}$  to be bounded from below. If this holds,  $I_\Delta[\psi] > \omega_{\min}^2$  for any trial function  $\psi$ .

Taking  $\psi(x) = 1$  we find an upper bound on the gap

$$\omega_{\min}^2 \leq I_{\Delta} [1] = \frac{\int_M \sqrt{h} Z^{2\Delta+1-d} \frac{\Delta^2}{d(d-1)} R}{\int_M \sqrt{h} Z^{2\Delta+1-d}} \leq \frac{\Delta^2 \max R}{d(d-1)}. \quad (5.68)$$

Unfortunately, this maximum value of  $R$  in the bulk cannot be related back to a boundary value of  $\bar{R}$  without knowing the explicit solution.

Taken together with the lower bound, we get the neat result

$$\frac{\Delta^2 \min R}{d(d-1)} \leq \omega_{\min}^2 \leq \frac{\Delta^2 \max R}{d(d-1)}. \quad (5.69)$$

As mentioned above, the lower bound can only be saturated if  $R$  is constant, when constant  $\psi$  is the solution. The same condition holds here. If  $R$  is not constant, for instance if  $\bar{R}$  is not constant on the boundary, then neither bound can be saturated, and we get the strict inequalities

$$\frac{\Delta^2 \min R}{d(d-1)} < \omega_{\min}^2 < \frac{\Delta^2 \max R}{d(d-1)}. \quad (5.70)$$

#### 5.4.6 Range of Applicability of the Bounds

In the example of global AdS considered above, the optical Ricci scalar is constant, and the bounds are saturated. An example where this is not true is the AdS Soliton (5.58). The optical Ricci scalar is no longer constant, it's zero on the boundary, but increases to a maximum of  $\max R = \frac{4(d-1)}{d\mathcal{R}^2}$ . Correspondingly, there is a non-zero energy gap [8], and this must satisfy  $0 < \omega_{\min}^2 < \frac{4\Delta^2}{d^2\mathcal{R}^2}$ . The lower bound is trivial, since stability implies that  $\omega^2 > 0$ , while for the upper bound we don't just need to know the boundary geometry, it depends on details of the AdS Soliton bulk.

What this example shows us is that there cannot be a simple upper bound on the energy gap of the form we presented for the free scalar in (5.21) in general. This example explicitly violates it. In addition, this also illustrates that the lower bound on the gap is only non-trivial when  $\bar{R} > 0$  on the boundary, and hence the optical  $R > 0$  everywhere.

An example where this bound is non-trivial is when the boundary is a deformed sphere. Since the sphere has constant  $\bar{R} > 0$ , we can consider deformations of this space where  $\bar{R} > 0$  everywhere. There is then presumably some bulk vacuum similar to global AdS, but where the optical Ricci scalar has some non-trivial profile. So long as our bulk satisfies our assumptions of no horizons or other asymptotic regions, which we would expect to be the case so long as the deformation is small enough, our bound on the gap will apply. The size of the gap may vary as we deform the boundary, but if we normalize it by the minimum value of the Ricci scalar, it will always be larger than the value on the sphere. If we instead normalize the energy gap by the another scale like the volume of the boundary, then it can of course decrease, and may vanish altogether. This bound also tells us that the gap can only vanish when we make the deformation big enough such that  $\bar{R} < 0$  somewhere on the boundary, or the bulk solution changes discontinuously to develop an extremal horizon or other asymptotic region.

In [32] they use this energy gap on global AdS as one of the signals of confinement. As we discussed in Sections 1.7.2 and 1.7.3, global AdS and the AdS soliton are examples of spacetimes that can be used to describe confining phases holographically. These are both examples where a compact factor in the boundary geometry shrinks to a point somewhere in the bulk, and it has been asserted[8] that the same behaviour should occur when other compact factors shrink in the bulk. Indeed, such an example is provided by [75] where they numerically construct spacetimes with  $3 + 1$  dimensional boundary whose spatial sections are  $S^2 \times S^1$ , where either the  $S^2$  factor or the  $S^1$  factor shrinks in the bulk. In either case, the boundary has positive Ricci scalar, so we can use our lower bound on the energy gap for all the bulks they discuss. Interestingly, our lower bound is completely oblivious to  $S_1$  factors like this on the boundary, since they don't effect  $\bar{R}$ .

## 5.5 Discussion

What we have found is that there is a lower bound for the energy gap of scalar fluctuations. The same bound can be derived for a free scalar on an arbitrary compact space and a scalar fluctuation about the universal sector in a holographic CFT, and it can also be confirmed for a scalar in an arbitrary CFT on a linear perturbation of a sphere. This is a wide class of CFTs, and in particular the fact that the same geometric quantity determined the lower bound in both the free and holographic case is non-trivial. This motivates the open question of whether there is a more general statement that holds for generic CFTs.

Perhaps the most straight forward step in generalizing this would be to go beyond the universal sector. Unfortunately, once you add other fields to the bulk, you then have more freedom for deciding how the scalar couples. In addition, the optical Ricci scalar no longer obviously satisfies the same minimum principle (5.65), so it's unclear that you would be able to make arguments along the same lines that we took here. Another way to generalize would be to consider fluctuations of non-scalar operators about the universal sector.

## Chapter 6

# Vacuum Energy

We are now going to use similar types of arguments to those in Chapter 5 to derive a bound for the Vacuum energy in holographic CFTs. Under AdS/CFT, the vacuum energy, or Casimir energy, is relatively straightforward to extract. Given a solution to Einstein's equation, it can be read off from the time-time component of the holographic stress-energy tensor which we discussed in Section 1.6. On highly symmetric spaces, this Casimir energy can be compared to the corresponding weakly coupled field theory calculation. For instance [33, 76] make such a comparison for a CFT on a torus with anti-periodic fermions, described in the bulk by the AdS-Soliton (1.49).

However, once we put the CFT on a generic curved spacetime, comparing results derived from the gravitational bulk to field theory calculations is more difficult. This is because the problem of finding the vacuum energy, even for a free scalar, is very complicated once the space-time is made arbitrary. For an example of a calculation of a Casimir energy see [77], where a scalar field between parallel 'plates'<sup>1</sup> is considered. The important point there is that all the energy states are relevant in the calculation, and it can only be solved because the full spectrum of the theory in this setup can be found. For the case of the free scalar, this means that we would have to solve for the full spectrum of the Laplacian on an arbitrary space. In contrast, when we were considering the energy gap for fluctuations, all we cared about was the lowest eigenvalue of this Laplacian. Because of this, unlike in Chapter 5, we will not be able to compare our holographic results to corresponding results for free CFTs. It is interesting that in this case we are able to derive a result in this strongly coupled context which we don't have the tools to approach for free theories.

We are going to specialize to  $d = 3$  CFTs dual to 4d static bulks. In this case we don't have to worry about any ambiguity in the stress tensor due to the conformal anomaly. The arguments we present here were published in [78, 79], with the work done in collaboration with Toby Wiseman and Sebastian Fischetti.

### 6.1 The Bound on the Free Energy

We will begin by presenting a derivation of a finite temperature bound on the free energy, as presented in [78]. This result is a generalization of a result in [80], where they derive

---

<sup>1</sup>The 'plates' are two parallel planes on which Dirichlet boundary conditions are applied forcing the field to vanish.

this bound in the case where the boundary is a round sphere, a flat torus, or constant curvature hyperbolic space. In fact, there is an elegant relation of this result to a geometric result in [81] which we will discuss in 6.1.1. We will present our more straightforward proof here, because it will allow a generalization to the inclusion of a massless scalar field, and to the local bounds that follow.

We are going to consider 3 + 1 dimensional static bulks describing finite temperature 2 + 1 dimensional holographic CFTs in the universal sector, so satisfying the vacuum Einstein's equation with negative cosmological constant. We will again make use of the optical geometry from (5.4.1). Compared with Chapter 5, we are going to relax our assumptions on the bulk geometry. We will still assume that the conformal boundary is compact, but we will now allow the bulk geometry to end not only on the conformal boundary, but also potentially on finite temperature horizons. We will consider the Riemannian 3-manifold  $(h_{ab}, \mathcal{M})$ , where  $\mathcal{M}$  is a spatial slice of the bulk, and  $h_{ab}$  is the optical geometry. As discussed in 5.4.1, the conformal boundary of the bulk spacetime is a regular boundary of the bulk geometry, and we will denote this 2 dimensional surface  $(\bar{h}_{ij}, \mathcal{B})$ , where the optical geometry induces a metric on this surface  $\bar{h}_{ij}$  which is the spatial section of the conformal boundary in the ultrastatic frame. In addition, the bulk may end on some number of finite temperature horizons, whose Hawking temperature corresponds to the CFT's temperature. We will denote these horizons as  $({}^I\bar{H}_{ij}, \mathcal{H}_I)$ , where the index  $I$  labels the horizons, and the metric  ${}^I\bar{H}_{ij}$  is the two dimensional spatial metric induced on the horizon by the physical bulk metric  $G_{\mu\nu}$ . We will see below that from the point of view of the optical geometry, these horizons are conformal boundaries.

The basic bound follows again from (5.55). In  $d = 3$  this identity implies that<sup>2</sup>

$$\nabla^2 R \leq 0 \tag{6.1}$$

everywhere. We can integrate this over the optical geometry  $\mathcal{M}$ , and use the divergence theorem to turn this into a sum of boundary integrals

$$\int_{\mathcal{M}} \nabla^2 R = \int_{\mathcal{B}} \star dR + \sum_I \int_{\mathcal{H}_I} \star dR \leq 0 \tag{6.2}$$

where the surfaces are orientated with outward facing normals. To calculate the two contributions from the conformal boundary and the horizons we need to look at expansions of the bulk equations about these regions.

Near the conformal boundary, we can write down a FG expansion of the physical bulk metric  $G_{\mu\nu}$ . Choosing an FG coordinate  $z$  such that the conformal boundary is in

---

<sup>2</sup>Once again, we drop the  $h$  superscript, but all equations are understood to be in the optical geometry unless otherwise stated.

the ultrastatic frame (5.52),

$$\begin{aligned} \frac{G}{\ell^2} &= \frac{dz^2 - dt^2 + \bar{h}_{ij} dx^i dx^j}{z^2} \\ &\quad - \frac{1}{4} \bar{R} dt^2 - \left( \bar{R}_{ij} - \frac{1}{4} \bar{R} \bar{h}_{ij} \right) dx^i dx^j \\ &\quad + \frac{z}{3c} (\langle T_{tt} \rangle dt^2 + \langle T_{ij} \rangle dx^i dx^j) + O(z^2), \end{aligned} \quad (6.3)$$

where  $\bar{h}_{ij}$  and  $\bar{R}_{ij}$  are the spatial metric and Ricci tensor of the boundary in this ultrastatic frame, and  $\langle T_{tt} \rangle$  and  $\langle T_{ij} \rangle$  are the expectation values of components of the CFT stress tensor in this frame.

From this, we could read off an expansion of the optical metric  $h$  near the conformal boundary in terms of this FG coordinate. However, it is more straight forward to calculate  $\int_{\mathcal{B}} \star dR$  if we take normal coordinates in the optical geometry. In these coordinates, the optical geometry near the conformal boundary is

$$h = d\bar{z}^2 + \gamma_{ij}(\bar{z}, x^i) dx^i dx^j, \quad (6.4)$$

with the boundary at  $\bar{z} = 0$  and  $\gamma_{ij}(0, x^i) = \bar{h}_{ij}(x)$ . The relation between this normal coordinate  $\bar{z}$  and the FG coordinate  $z$  can be found in an expansion  $\bar{z} = z(1 - \frac{1}{24} \bar{R} z^2 + \frac{1}{24c} \langle T_{tt} \rangle z^3 + O(z^4))$ . From this it follows that the optical geometry near the conformal boundary takes the form

$$\begin{aligned} Z(\bar{z}, x) &= \bar{z} \left( 1 - \frac{1}{12} \bar{R} \bar{z}^2 + \bar{z}^3 \frac{\langle T_{tt} \rangle}{8c} \right) + O(\bar{z}^4) \\ \gamma_{ij}(\bar{z}, x) &= \bar{h}_{ij} - \bar{R}_{ij} \bar{z}^2 + \left( \frac{\langle T_{tt} \rangle \bar{h}_{ij} + \langle T_{ij} \rangle}{3c} \right) \bar{z}^3 + O(\bar{z}^4) \end{aligned} \quad (6.5)$$

In these coordinates, we find that the optical Ricci scalar has an expansion in  $\bar{z}$

$$R = 3\bar{R} - 6\frac{\rho}{c} \bar{z} + O(\bar{z}^2). \quad (6.6)$$

where we have introduced the energy density  $\rho = \langle T_{tt} \rangle$ . The boundary integral is therefore

$$\int_{\mathcal{B}} \star dR = \frac{6}{c} \int_{\mathcal{B}} \rho = \frac{6E}{c}. \quad (6.7)$$

The other (potential) contribution to this integral comes from any horizons in the bulk. Since these are static Killing horizons, the physical bulk metric in a region around the horizon can be written in the form

$$G = -\kappa^2 r^2 f(r, x^i) dt^2 + dr^2 + H_{ij}(r, x^i) dx^i dx^j \quad (6.8)$$

where the  $x^i$  coordinates cover the horizon at  $r = 0$ ,  $f(0, x^i) = 1$ , and  $\kappa$  is the horizon's surface gravity.  ${}^I \bar{H}_{ij}(x^i) = H_{ij}(0, x^i)$  is the induced metric on the horizon  $\mathcal{H}_I$ . Moving

to the optical metric, we see that the horizon becomes a conformal boundary

$$h = \frac{dr^2 + H_{ij}(x, r)dx^i dx^j}{\kappa^2 r^2 f(r, x^i)}. \quad (6.9)$$

We can solve Einstein's equation in a series near the horizon to find

$$\begin{aligned} f(r, x^i) &= 1 - \frac{1}{6} {}^I \bar{R} r^2 + O(r^3) \\ H_{ij}(r, x^i) &= {}^I \bar{H}_{ij}(x^i) + \left( \frac{3}{2\ell^2} + \frac{1}{4} {}^I \bar{R} \right) {}^I \bar{H}_{ij}(x^i) r^2 + O(r^3), \end{aligned} \quad (6.10)$$

where  ${}^I \bar{R}$  is the Ricci scalar of  ${}^I \bar{H}_{ij}$  on the horizon. This allows us to find an expansion for the optical Ricci scalar

$$R = -6\kappa^2 + 3\kappa^2 \left( \frac{2}{\ell^2} + {}^I \bar{R} \right) r^2 + O(r^4), \quad (6.11)$$

From this, the horizon integral is

$$\int_{\mathcal{H}_I} \star dR = -12\kappa \frac{A_I}{\ell^2} - 6\kappa \int_{\mathcal{H}_I} {}^I \bar{R} \quad (6.12)$$

where  $A_I$  is the horizon area. Then, using the Hawking temperature,  $\kappa = 2\pi T$ , the Bekenstein-Hawking entropy  $S = \frac{Ac}{4\pi\ell^2}$  and the Gauss-Bonnet theorem  $\int R = 4\pi\chi$ , where  $\chi$  is the Euler character of the 2d surface, we find

$$\int_{\mathcal{H}_i} \star dR = -6 \frac{TS_I}{c} - 48\pi^2 T \chi_I. \quad (6.13)$$

Summing up the horizon integrals, and combining this with the boundary integrals yields

$$E - TS = F \leq 8\pi^2 cT \sum_I \chi_I. \quad (6.14)$$

Thus we find that the free energy is bounded from above by the temperature and Euler character of any horizons.

### 6.1.1 An Alternative Derivation of this Bound

At this stage we should point out that the bound (6.14) can actually be derived from a result in [81]. This result is a bound on the renormalized volume,  $V_{\text{ren}}$ , of a 4-d asymptotically locally hyperbolic space, in terms of its Euler characteristic  $\chi(\mathcal{M}_4)$ <sup>3</sup>

$$\chi(\mathcal{M}_4) \geq \frac{3}{4\pi^2} \frac{V_{\text{ren}}}{\ell^4}. \quad (6.15)$$

<sup>3</sup>This inequality comes from a relation involving the Euclidean action, which was used in [82] to relate gravity in euclidean AdS to conformal gravity

We can analytically continue the bulks we are considering here so that they become Euclidean asymptotically hyperbolic spacetimes. This renormalized volume is proportional to the renormalized Euclidean on-shell action<sup>4</sup>, renormalized using the techniques we discussed in Section 1.6. This on-shell action can be related to  $\frac{F}{T}$

$$F \leq 8\pi^2 c_\chi(\mathcal{M}_4) T. \quad (6.16)$$

After we had come up with the previous proof, it was pointed out to us by Juan Maldacena that the result (6.16) implies that  $F < 0$  whenever there are no horizons in the bulk. This is because the Euclidean time coordinate then corresponds to an overall  $S^1$  factor in the bulk topology, which implies that  $\chi(\mathcal{M}_4) = 0$ . In fact, when there are horizons we can use a relation from [83] which relies only on the existence of our Killing vector  $\frac{\partial}{\partial t}$ , and the fact that it is tangent to the conformal boundary. Under these conditions, we can use

$$\chi(\mathcal{M}_4) = \sum_A \chi(\mathcal{H}_A) + N \quad (6.17)$$

where  $\mathcal{H}_A$  are the two dimensional fixed point sets of the Killing vector field, the ‘bolts’, and  $N$  is the number of one-dimensional fixed points, or ‘nuts’. In this Euclidean picture, the horizons have been analytically continued to two-dimensional fixed point sets of  $\frac{\partial}{\partial t}$ , so these are the  $\mathcal{H}_A$ , and we have no nuts so  $N = 0$ . Substituting (6.17) into (6.16) yields (6.14).

### 6.1.2 A Vacuum Bound

Now let’s consider a zero temperature limit of the above bound. As  $T \rightarrow 0$ , so long as the entropy doesn’t diverge and any horizons remain smooth we find

$$E \leq 0. \quad (6.18)$$

So we find that the Casimir energy is non-positive in these holographic CFTs.

In taking this zero temperature limit, we have allowed ourselves to consider a wider class of vacuum states than we considered in 5. Our bulks may have zero temperature horizons, and in addition, we haven’t confined ourselves to non-singular zero temperature spacetimes. So long as the bulk is smooth at arbitrarily small finite temperatures, then we can take this zero temperature limit. In other words, at zero temperature we can have a singularity so long as, when we move to finite temperature, it is ‘masked’ by a smooth black hole horizon. This is precisely the criterion for a good singularity according to [71].

An important example of this is periodically identified Poincaré AdS. At zero temperature there is a singularity in the infrared, but at any finite temperature we can take the planar AdS black brane and periodically identify it and this provides a completely

---

<sup>4</sup>Since on-shell  ${}^G R$  is constant.

smooth bulk. We can get Poincaré AdS back as the  $T \rightarrow 0$  limit of these smooth bulks, and in this sense the singularity in the infrared is masked at finite temperature.

### 6.1.3 Addition of a Massless Scalar

In fact, we can quite easily generalize this result away from the universal sector for the particular case of a massless scalar in the bulk. This corresponds to a deformation by a marginal  $\Delta = d$  operator on the boundary. The bulk equations of motion written in the optical frame are

$$\begin{aligned}\mathcal{L}_{ab} \equiv R_{ab} - \partial_a \phi \partial_b \phi &= -\frac{2\nabla_a \partial_b Z}{Z} \\ \mathcal{L} &= 6 \left( \frac{1 - (\partial Z)^2}{Z^2} \right) \\ \nabla^2 \phi &= 2 \frac{\partial Z}{Z} \cdot \partial \phi.\end{aligned}$$

where we have introduced the tensor  $\mathcal{L}_{ab}$  which plays the same role in the first two equations as the optical Ricci tensor  $R_{ab}$  does in the vacuum equations.

Indeed, from these equations we can derive that

$$\nabla^2 \mathcal{L} = -3 \left( \tilde{\mathcal{L}}_{ab} \tilde{\mathcal{L}}^{ab} + (\nabla^2 \phi)^2 \right) \leq 0, \quad (6.19)$$

where  $\tilde{\mathcal{L}}_{ab}$  is the traceless part of  $\mathcal{L}_{ab}$ . From this it follows that  $\mathcal{L}$  satisfies the same minimum principle that the optical Ricci scalar satisfies in the absence of  $\phi$ .

We can carry through exactly the same integral argument as above. The expansion of the optical geometry near the conformal boundary (6.5) becomes

$$\begin{aligned}Z(\bar{z}, x) &= \bar{z} \left( 1 - \frac{1}{12} \bar{\mathcal{L}} \bar{z}^2 + \bar{z}^3 \frac{\langle T_{tt} \rangle}{8c} \right) + O(\bar{z}^4) \\ \gamma_{ij}(\bar{z}, x) &= \bar{h}_{ij} - \bar{\mathcal{L}}_{ij} \bar{z}^2 + \left( \frac{\langle T_{tt} \rangle \bar{h}_{ij} + \langle T_{ij} \rangle}{3c} \right) \bar{z}^3 + O(\bar{z}^4),\end{aligned} \quad (6.20)$$

where  $\bar{\mathcal{L}}_{ij} \equiv \bar{R}_{ij} - \partial_i \phi \partial_j \phi$  is defined in the ultrastatic frame conformal boundary geometry. This gives the expansion

$$\mathcal{L} = 3\bar{\mathcal{L}} - 6\frac{\rho}{c}\bar{z} + O(\bar{z}^2). \quad (6.21)$$

The horizon expansions (6.10) get replaced with

$$\begin{aligned}f(r, x^i) &= 1 - \frac{1}{6} {}^I \bar{\mathcal{L}} r^2 + O(r^3) \\ \tilde{h}_{ij}(r, x^i) &= {}^I \bar{H}_{ij}(x^i) + \left( \frac{3}{2\ell^2} + \frac{1}{4} {}^I \bar{\mathcal{L}} \right) {}^I \bar{H}_{ij}(x^i) r^2 + O(r^3),\end{aligned} \quad (6.22)$$

where  ${}^I\bar{\mathcal{L}} = {}^I\bar{R} - \partial_i\phi\partial_j\phi {}^I\bar{H}^{ij}$  is defined in the horizon geometry. This gives an expansion

$$\mathcal{L} = -6\kappa^2 + 3\kappa^2 \left( \frac{2}{\ell^2} + {}^I\bar{\mathcal{L}} \right) r^2 + O(r^4). \quad (6.23)$$

We see that these expansion are exactly the same as those in the absence of the scalar field, except for the substitution  $R \rightarrow \mathcal{L}$ . The finite temperature bound in this case becomes

$$E - TS \leq 8\pi^2 cT \sum_I \chi_I - 2\pi cT \sum_I \int_{\mathcal{H}_I} (\nabla\phi)^2 \quad (6.24)$$

and then, as  $T \rightarrow 0$  we get again that  $E < 0$ .

#### 6.1.4 Saturation of the bound

For this bound to be saturated, we require that  $\nabla^2\mathcal{L} = 0$  everywhere. From (6.19) this implies that

$$\begin{aligned} \tilde{\mathcal{L}}_{ij} &= 0 \\ \nabla^2\phi &= 0. \end{aligned} \quad (6.25)$$

These two equations, and the Bianchi identity, imply that  $\mathcal{L}$  is constant everywhere, and in particular, since on the boundary  $\mathcal{L} = 3\bar{\mathcal{L}}$ , the boundary  $\bar{\mathcal{L}}$  is constant. In addition, the near boundary expansion of  $\phi$  in the normal coordinates (6.5) is

$$\phi = \bar{\phi}(x) + \frac{1}{2}\bar{z}^2\bar{\nabla}^2\bar{\phi}(x) + O(\bar{z}^3) \quad (6.26)$$

so we find that on the boundary  $\nabla^2\phi = 2\bar{\nabla}^2\bar{\phi} = 0$ . Since the boundary is compact, this implies that the boundary  $\bar{\phi}$ , and so  $\bar{R}$ , is also constant. The energy is therefore strictly negative unless these conditions are met. In  $d = 3$  dimensions, constant  $\bar{R}$  means the conformal boundary is a sphere, a torus, or compact hyperbolic space.

At finite temperature, this bound basically cannot be saturated. This is because, from (6.23), on the horizon  $\mathcal{L} = -6\kappa^2$ , so unless it takes this value on the conformal boundary as well,  $\mathcal{L}$  must vary in the bulk.

## 6.2 A local statement

With a little bit more work, we can turn this global energy bound into a local statement.

Again working at finite temperature, with the same assumptions as above, let's consider a boundary geometry with non-constant  $\bar{\mathcal{L}}$ . For a smooth boundary and scalar field, there will be some minimum value  $\min\bar{\mathcal{L}}$ . For any  $\bar{\mathcal{L}}_* \geq \min\bar{\mathcal{L}}$ , we can consider a region of the spatial boundary geometry

$$\mathcal{B}(\bar{\mathcal{L}}_*) = \{x \mid \bar{\mathcal{L}}(x) \leq \bar{\mathcal{L}}_*(x)\}. \quad (6.27)$$

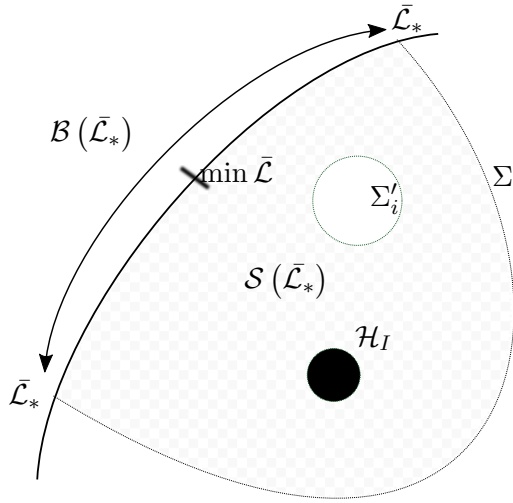


FIGURE 6.1: The region of integration  $\mathcal{S}$  defined by the condition  $R < R_*$ , it intersects the boundary in some region  $\mathcal{B}$  which includes the minimum value of  $R$  on the boundary, and it ends in the bulk either on surfaces where  $R = R_*$  or on black hole horizons.

If we choose  $\bar{\mathcal{L}}_*$  small enough, and there is one unique minimum  $\min \bar{\mathcal{L}}$  on the boundary,  $\mathcal{B}(\bar{\mathcal{L}}_*)$  will be a single connected region containing  $\min \bar{\mathcal{L}}$  as shown in Figure 6.1, but this isn't necessary for the argument.

Now we can consider an extension of this region into the bulk optical geometry  $\mathcal{S}(\bar{\mathcal{L}}_*)$ . This extension will meet the boundary at  $\mathcal{B}(\bar{\mathcal{L}}_*)$ , and is defined by the condition that the optical  $\mathcal{L} \leq 3\bar{\mathcal{L}}_*$ <sup>5</sup>. The bulk region  $\mathcal{S}(\bar{\mathcal{L}}_*)$  may also have a number of other boundaries. One of these will be the surface  $\Sigma$  defined by  $\mathcal{L} = 3\bar{\mathcal{L}}_*$ . One component of the surface  $\Sigma$  will end on the conformal boundary, but there may also be other disconnected components, which we denote by  $\Sigma'_i$  in Figure 6.1. In addition, if  $\bar{\mathcal{L}}_* > -2\kappa^2$ , the region may be bounded by black hole horizons  $\mathcal{H}_I$ , and in the special case where  $\bar{\mathcal{L}}_* = -2\kappa^2$ , the surface  $\Sigma$  may intersect these horizons.

If we integrate (6.19) over  $\mathcal{S}$  we can bound the boundary integral

$$\int_{\mathcal{S}} \nabla^2 \mathcal{L} = \int_{\partial \mathcal{S}} \star d\mathcal{L} = \int_{\mathcal{B}} \star d\mathcal{L} + \int_{\Sigma} \star d\mathcal{L} + \sum_I \int_{\mathcal{H}_I} \star d\mathcal{L} < 0. \quad (6.28)$$

The bound is strict because by assumption  $\mathcal{L}$  is not constant.

We know what the contributions from  $\mathcal{B}$  and  $\mathcal{H}_i$  are from the global arguments above, but the contribution from  $\Sigma$  isn't useful. To get rid of it, we introduce a weight function

<sup>5</sup>As we have defined it, the region  $\mathcal{S}(\bar{\mathcal{L}}_*)$  may have disconnected components that don't meet the conformal boundary. In that case, we could throw out those regions, and focus only on that part of  $\mathcal{S}(\bar{\mathcal{L}}_*)$  consisting of regions connected to the conformal boundary. However, this has no effect on the result, so it is an unnecessary complication.

which is positive inside  $\mathcal{S}$ , but vanishes on  $\Sigma$ . We insert a function  $f(x)$  such that for  $x < \bar{\mathcal{L}}_*$ ,  $f(x) > 0$ ,  $f(\bar{\mathcal{L}}_*) = 0$  and we also require  $f'(x) \leq 0$ . We then find that we can take

$$\begin{aligned} \nabla_a \left( f \left( \frac{\mathcal{L}}{3} \right) \nabla^a \mathcal{L} \right) &= f \left( \frac{\mathcal{L}}{3} \right) \nabla^2 \mathcal{L} + \nabla_a f \left( \frac{\mathcal{L}}{3} \right) \nabla^a \mathcal{L} \\ &= f \left( \frac{\mathcal{L}}{3} \right) \nabla^2 \mathcal{L} + \frac{1}{3} f' \left( \frac{\mathcal{L}}{3} \right) (\nabla \mathcal{L})^2 < 0, \end{aligned} \quad (6.29)$$

where the inequality holds inside the domain  $\mathcal{S}$ . This time, when we integrate we get

$$\begin{aligned} \int_{\mathcal{S}} \nabla_a \left( f \left( \frac{\mathcal{L}}{3} \right) \nabla^a \mathcal{L} \right) &= \int_{\partial \mathcal{S}} f \left( \frac{\mathcal{L}}{3} \right) \star d\mathcal{L} \\ &= \int_{\mathcal{B}} f \left( \frac{\mathcal{L}}{3} \right) \star d\mathcal{L} + \sum_I \int_{\mathcal{H}_I} f(-2\kappa^2) \star d\mathcal{L} < 0 \end{aligned} \quad (6.30)$$

since the terms on the other boundaries have a factor of  $f(\bar{\mathcal{L}}_*) = 0$ , so they vanish. The contribution on a horizon component is

$$\int_{\mathcal{H}_I} f(-2\kappa^2) \star d\mathcal{L} = -\kappa \frac{6f(-2\kappa^2)}{\ell^2} \int_{\mathcal{H}_I} (2 + \ell^2 I \bar{\mathcal{L}}) \quad (6.31)$$

As long as the integral over the horizon doesn't diverge, this vanishes when we take the  $T \rightarrow 0$  limit. Taking this limit, we are therefore just left with the boundary term, which we can write as

$$\int_{\mathcal{B}} f(\bar{\mathcal{L}}) \rho < 0. \quad (6.32)$$

In particular, the function  $f(\bar{\mathcal{L}}) = \theta(\bar{\mathcal{L}}_* - \bar{\mathcal{L}})$  obeys our conditions, so we can bound the total energy in this region

$$\int_{\mathcal{B}} \rho < 0. \quad (6.33)$$

We have therefore found that there are certain regions on the boundary where the energy must be negative. This bound holds independent of what happens in other regions on the conformal boundary, so long as  $\bar{\mathcal{L}}$  is everywhere greater than the values it takes in this region.

### 6.3 Spacelike Symmetries and Stress

Let's consider the case where, in addition to the timelike Killing vector, we have a spacelike one  $K = \frac{\partial}{\partial y}$  as well, and let's assume that  $K$  is hypersurface orthogonal. We can make the same arguments as for a timelike Killing vector to establish a bound on the stress. We can consider an equivalent of the optical geometry adapted to this Killing vector. We write the bulk metric as

$$G = \frac{\ell^2 (dy^2 - \omega(x^i) dt^2 + \alpha_{ij}(x) dx^i dx^j)}{W^2(x)}. \quad (6.34)$$

The  $x^i$  span a two dimensional space bounded by a one-dimensional slice of the boundary. We will use  $x$  as the coordinate on this slice of the boundary. Using  $W$  as the defining function, the representative of the boundary geometry is then of the form

$$\bar{h} = dy^2 - \bar{\omega}(x)dt^2 + \bar{\alpha}(x)dx^2, \quad (6.35)$$

and in fact we will choose the coordinate  $x$  such that  $\bar{\alpha}(x) = 1$ . We will take  $y$  to be a compact coordinate with period  $2\pi\mathcal{R}_y$ , and the  $x$  coordinate is also compact. We can now apply the same arguments as before where we replace our ‘optical’ metric with<sup>6</sup>

$$h = -\omega(x^i)dt^2 + \alpha_{ij}(x^i)dx^i dx^j. \quad (6.36)$$

The Ricci scalar of this geometry satisfies the same identity (5.55), which we can integrate. This integral picks up a boundary term

$$\int_{\partial M} \star dR = 6 \frac{\int dx dt \sqrt{\bar{\omega}} \langle T_{yy} \rangle}{c}. \quad (6.37)$$

We can make this integral finite by compactifying the time coordinate. If the  $y$  circle shrinks somewhere in the bulk, then there is a boundary term on this timelike surface  $\Sigma$ . This is the analogue of the horizon in the previous argument. If we write the bulk metric near this point as

$$G = \gamma^2 \rho^2 f(\rho, x) dy^2 + d\rho^2 - a(\rho, z) dt^2 + b(\rho, z) dz^2 \quad (6.38)$$

where  $f(0, x) = 1$ , and we require  $\gamma = \frac{1}{\mathcal{R}_y}$  by smoothness, then the corresponding contribution to the integral is

$$\int_{\Sigma} \star dR = -\gamma \int_{\Sigma} \sqrt{a(0, z)b(0, z)} dt dz \left( \frac{12}{\ell^2} + 6\bar{R} \right) \quad (6.39)$$

Because the metric is static, this surface has toroidal topology<sup>7</sup>, so the  $\bar{R}$  integral vanishes. Putting this together

$$\begin{aligned} \int_{\partial M} \star dR + \int_{\Sigma} \star dR &= 6 \frac{\int dx dt \sqrt{\bar{\omega}} \langle T_{yy} \rangle}{c} - \gamma \int_{\Sigma} \sqrt{a(0, z)b(0, z)} dt dz \left( \frac{12}{\ell^2} \right) \\ &= \frac{6}{2\pi\mathcal{R}_y} \int dt \left( \frac{\Pi_y}{c} - \frac{4\pi\mathcal{R}_{\Sigma}}{\ell^2} \right) \end{aligned} \quad (6.40)$$

where we have defined the the total stress  $\Pi_y = \int dx dy \sqrt{\bar{h}} \sqrt{\bar{\omega}} T_{yy}$ , and the size of the surface  $\Sigma$ ,  $\mathcal{R}_{\Sigma} = \frac{\int_{\Sigma} \sqrt{\bar{h}} dt dz}{\int dt}$ . We therefore have a bound on the total stress, in terms of the area of this surface  $\Sigma$

$$\Pi_y \leq \frac{4\pi c \mathcal{R}_{\Sigma}}{\ell^2}, \quad (6.41)$$

<sup>6</sup>Because it's static, the arguments follow through just like for the Riemannian optical metric corresponding to  $\frac{\partial}{\partial t}$ , because we can simply analytically continue to Euclidean signature.

<sup>7</sup>Since we can compactify the time coordinate.

with saturation only for a constant  $R$  boundary. In particular, this stress being positive would be a signal that the  $S^1$  associated with the  $y$  coordinate shrinks on a surface  $\Sigma$  in the bulk. Unfortunately, in the simplest example where this bound could be used, the AdS Soliton, this stress is negative, and so the bound is satisfied trivially.

## 6.4 A positivity constraint

We have therefore shown that, for a boundary of non-constant curvature, the total energy is negative, and there are certain regions on the boundary over which the integrated energy density is negative. This makes it tempting to postulate that the energy is negative everywhere, but this is, in fact, not the case. Furthermore, we can prove for a wide class of states that the energy must be positive somewhere. This discussion applies to the universal sector, and in particular we are not including a massless scalar field.

The tool needed is inverse mean curvature flow (IMCF) which was introduced in [84] as a tool to prove positivity of the Arnowitt-Deser-Misner (ADM) mass in asymptotically flat initial data<sup>8</sup> for the four dimensional Einstein's equation without cosmological constant. IMCF is a flow of two dimensional surfaces in a three dimensional Riemannian manifold. So we consider some set of two dimensional surfaces  $\Sigma_\lambda$ , labelled by a real parameter, the 'flow time'  $\lambda$ , which form a foliation of this space. We can think of this parameter  $\lambda$  as a function on the space whose level sets determine the surfaces  $\Sigma_\lambda$ .

The three dimensional metric in which we consider this flow is a time slice of the full spacetime, rather than the optical metric. We will write  $\sigma_{ij}(\lambda)$  for the induced metric on these surfaces. The condition that defines the flow is that<sup>9</sup>

$$n^a \partial_a \lambda = K \quad (6.42)$$

where  $n^a$  is the unit normal to the surfaces, and  $K$  is the trace of the extrinsic curvature, the mean curvature, of the surfaces. These flows have the neat feature that the area of these flow surfaces  $A(\lambda)$  satisfies

$$\frac{dA}{d\lambda} = \frac{d}{d\lambda} \int \sqrt{\sigma} = \frac{1}{2} \int \sqrt{\sigma} \frac{d\sigma_{ij}}{dn} = A \quad (6.43)$$

where  $\frac{d}{dn}$  is the normal derivative, and we have used the fact that

$$\frac{d\sigma_{ij}}{dn} = 2K_{ij}. \quad (6.44)$$

The key is then that the Hawking mass of these surfaces, defined by

$$m_H(\Sigma_t) = \sqrt{A} \left( \int_{\Sigma_t} 2^{\Sigma_t} R - \Sigma_t K^2 \right) \quad (6.45)$$

<sup>8</sup>Three dimensional metric and extrinsic curvature for an initial spacelike surface that satisfy the appropriate constraints.

<sup>9</sup>This means that if you take the surface normal to be pointing in the direction of flow,  $K > 0$ .

increases monotonically. It vanishes for very small spheres, and it's proportional to the ADM mass for very large surfaces, so if there exists an IMCF connecting these two regimes this proves that the ADM mass is positive. It was pointed out by [85], that if there is a spherical horizon in the bulk, and an IMCF exists starting at this horizon and expanding to infinity, then the monotonicity of  $m_H$  implies the Penrose inequality [86]

$$16\pi E^2 \geq A \quad (6.46)$$

where  $A$  is the area of the horizon, and  $E$  is the ADM mass. This is because  $K = 0$  on the horizon, so at the start of the flow  $m_H = 16\pi\sqrt{A}$ .

In fact, in many cases the flow doesn't exist, but this problem was surmounted in [87], where 'weak solutions' to the flow are defined which are shown to preserve this monotonicity property, where the flow is replaced by an elliptic differential equation for the function  $\lambda$ . This then leads to a proof of the Penrose inequality for asymptotically flat 3d spatial slices with non-negative curvature <sup>10</sup>.

With negative cosmological constant, the spatial slices are hyperbolic with negative curvature, so the above results don't apply. The generalization to this case is discussed in [88], and then made rigorous in [89] where the weak solutions of [87] are generalized to this setting. The Hawking mass now takes the form

$$m_H = \sqrt{A} \int 2R + \frac{4}{\ell^2} - K^2 = \sqrt{A} \left( 8\pi\chi + \frac{4}{\ell^2}A - \int K^2 \right) \quad (6.47)$$

and it still increases monotonically along the flow. They consider the case where the two dimensional spatial sections of the boundary are constant curvature spaces, and they show that 'weak' flows exist that reach the conformal boundary.

We can start the flow either at a small ball around a point, or on a horizon. The Hawking mass on a horizon  $K = 0$  is, using  $S = \frac{4\pi c A}{\ell^2}$ ,

$$m_H = \sqrt{A} \left( 8\pi\chi + \frac{4}{\ell^2}A \right) = \sqrt{\frac{\ell^2}{4\pi c} S} \left( 8\pi\chi + \frac{1}{\pi c} S \right) \quad (6.48)$$

while for a small ball, the Hawking mass vanishes. An important property is that the topology doesn't change along the flow, so if you want to start the flow at a point the boundary must have spherical topology, and if you want to start the flow on a horizon, the horizon must have the same topology as the boundary.

At the conformal boundary,  $m_H$  approaches a quantity related to the energy as we will discuss below, so in [89] a lower bound on this quantity is derived. We want to consider more general conformal boundaries where the curvature is non-constant, so we will demonstrate that the existence proof of [89] can be generalized to this case. We will then discuss the value of the Hawking mass at the conformal boundary, and how the resulting bound constrains the energy density.

<sup>10</sup>In these spatial slices, a static black hole horizon becomes a minimal surface where  $K = 0$ , so they proved a bound on the ADM mass in terms of the area of such a minimal surface.

### 6.4.1 Existence of Weak Solutions to IMCF flow

In [79] it was shown that the arguments in [89] can be generalized to boundaries of non-constant curvature. This proof is due to Toby Wiseman and Sebastian Fischetti, and I provide it here for completeness. Consider the Fefferman-Graham expansion of the bulk metric,

$$\frac{G}{\ell^2} = \frac{dz^2 + \bar{g}_{\alpha\beta}(x)dx^\alpha dx^\beta + O(z^2)}{z^2}, \quad (6.49)$$

where the  $x^\alpha = (t, x^i)$  are the boundary spacetime coordinates, and where for generality  $\bar{g}_{\alpha\beta}(x)$  is a static, but not necessarily ultrastatic, representative of the boundary geometry. The following pair of flows  $\Sigma_\lambda^\pm$ , where the surfaces  $\Sigma_\lambda^\pm$  are constant  $z$  surfaces with

$$z^\pm(\lambda) = \frac{1}{\left(\frac{1}{\xi} \pm c\right) e^{\frac{\lambda}{2}} \mp c}, \quad (6.50)$$

start at  $\lambda = 0$  with  $z^\pm(0) = \xi$ , and reach the conformal boundary as  $\lambda \rightarrow \infty$ . The point is then that these are sub(super)-solutions of IMCF, the existence of which is sufficient for an existence theorem in [87] to apply, and guarantee that their weak flows will reach the conformal boundary. Sub- and supersolutions to IMCF have flow velocities that are faster or slower than  $\frac{1}{K}$  respectively. The flow velocity can be calculated to be

$$\frac{dz^\pm}{d\lambda} \left| \frac{\partial}{\partial z} \right| = \frac{\ell}{2} (1 \pm cz + O(z^2)), \quad (6.51)$$

while the mean curvature of a constant  $z$  surface is

$$K = \frac{2}{\ell} + O(z^2). \quad (6.52)$$

For any  $c$ , we can choose  $\xi$  small enough, such that these flow velocities are always greater than or less than  $1/K$  respectively, so these are sub- and super-solutions to IMCF, and their existence tells us that we can construct weak flows starting at a point, or starting at a horizon, that reach the conformal boundary (subject to the above caveat that the topology of the initial surface must match the topology of the boundary).

### 6.4.2 Hawking Mass at Conformal Boundary

We now know that the flows will reach the conformal boundary, so we can discuss what the asymptotic value of  $m_H$  is for these flows in this limit. Taking the  $c = 0$  case in (6.51), we see that to lowest order in  $z$ , a solution to IMCF is provided by constant  $z$  surfaces flowing according to

$$z(\lambda) = z_0 e^{-\frac{\lambda}{2}} + O(z^2). \quad (6.53)$$

This means that in Fefferman-Graham coordinates, to leading order, constant  $z$  surfaces flow to constant  $z$  surfaces. Now consider a general IMCF that is approaching the conformal boundary. In the coordinates (6.49), a surface in the flow at any given  $\lambda$  will have

some profile

$$z = f(\lambda, x^i). \quad (6.54)$$

However, if we redefine our  $z$  coordinate  $z \rightarrow z \frac{z_0}{f(\lambda, x^i)} + O(z^2)$ , then this becomes a constant  $z$  surface to leading order. In fact we can construct our entire Fefferman-Graham coordinates adapted to the surface. Using the  $z$  coordinate as the defining function in our extraction of the conformal boundary metric, the flow in this way picks out a particular conformal frame on the boundary. Without loss of generality, let us therefore assume that we have chosen our coordinates in (6.49) adapted to the flow in this way. To higher order we can write

$$\begin{aligned} \frac{G}{\ell^2} = & \frac{dz^2 + \bar{g}_{\alpha\beta}(x) dx^\alpha dx^\beta}{z^2} \\ & - \left( \bar{g} \bar{R}_{\alpha\beta}(x) - \frac{1}{4} \bar{g} \bar{R}(x) \bar{g}_{\alpha\beta}(x) \right) dx^\alpha dx^\beta \\ & + \frac{z}{3c} \bar{g} \langle T_{\alpha\beta} \rangle dx^\alpha dx^\beta + O(z^2), \end{aligned} \quad (6.55)$$

which is (6.3) generalized away from the ultrastatic frame. In particular,  $\bar{g} \bar{R}_{\alpha\beta}$  is now the Ricci tensor of the full conformal boundary spacetime, and  $\bar{g} \langle T_{\alpha\beta} \rangle$  is the vev of the stress-energy tensor in this frame.

In this adapted frame, the Hawking mass is calculated on a constant  $t$ , constant  $z$  surface. For this we need the mean curvature

$$\begin{aligned} K &= \frac{1}{2} \sigma^{ij} \frac{d}{dn} \sigma_{ij} = -\frac{1}{2} \frac{z}{\ell} G^{ij} \frac{d}{dz} (G_{ij}) \\ &= \frac{2}{\ell} + \frac{z^2}{2\ell} (\bar{g} \bar{R} - 2 \bar{g} \bar{R}_t^t) - \frac{1}{2c} \frac{z^3}{\ell} \bar{g} \langle T_{ij} \rangle \bar{g}^{ij} \end{aligned} \quad (6.56)$$

where  $\sigma_{ij}$  is the induced metric on the constant  $z$  surfaces and we have used the outwards normal derivative  $\frac{d}{dn} = -\frac{z}{\ell} \frac{d}{dz}$ . If we write the boundary metric as

$$\bar{g} = -\omega(x^i)^2 dt^2 + \tilde{h}_{ij}(x^i) dx^i dx^j, \quad (6.57)$$

then we can replace the spacetime Ricci scalar with the Ricci scalar of its  $d-1$  dimensional spatial slices  $\tilde{h} \tilde{R}$  using the Gauss Equation

$$\bar{g} \bar{R} - 2 \bar{g} \bar{R}_t^t = \tilde{h} \tilde{R}. \quad (6.58)$$

The induced metric on the constant  $z$  flow surfaces  $\Sigma$ , is to leading order  $\sigma_{ij} = \frac{\ell^2}{z^2} \tilde{h}_{ij}$ , so we can write its Ricci scalar as

$$\Sigma R = \frac{z^2}{\ell^2} \tilde{h} \tilde{R}. \quad (6.59)$$

Using the tracelessness of the stress tensor we therefore get

$$K = \frac{2}{\ell} + \frac{\ell}{2} \Sigma R + \frac{1}{2c} \frac{z^3}{\ell} \frac{\bar{g} \langle T_{tt} \rangle}{\omega^2} \quad (6.60)$$

so that the Hawking mass of this surface can be written as an integral on the spatial slice of the conformal boundary in the frame specified by  $h_{ab}$

$$m_H = \frac{2\ell}{c} \sqrt{\int \sqrt{\tilde{h}} \int \sqrt{\tilde{h}} \frac{\bar{g} \langle T_{tt} \rangle}{\omega^2}}. \quad (6.61)$$

This equation is written in the frame adapted to this particular IMCF. We can recast this in terms of the optical frame by Weyl scaling the metric by a factor of  $\omega^{-2}$ . Written in this frame, the Hawking mass becomes

$$m_H = \frac{2\ell}{c} \sqrt{\int \sqrt{\tilde{h}} \omega^2 \int \sqrt{\tilde{h}} \frac{\rho}{\omega}}, \quad (6.62)$$

where  $\rho$  is now the energy density in the ultrastatic frame. We see that asymptotically,  $m_H$  does not tend to a universal value, but depends on a positive function  $\omega(x)$ . We do not know this function a priori, it depends on the details of the flow.

### IMCF on Global AdS

We might suppose that maybe IMCF always picks out some preferred conformal frame, and so we would be able to determine what the function  $\omega$  should be in general. We can demonstrate that this isn't the case by solving IMCF on global AdS. IMCF only cares about the geometry on the spatial sections. For global AdS, these take the form

$$\frac{g_{AdS}}{\ell^2} = \frac{dr^2}{1+r^2} + r^2 (d\theta^2 + \sin^2 \theta d\phi^2). \quad (6.63)$$

This is hyperbolic space, which is homogeneous and isotropic. This means that the space looks the same if we move our centre  $r = 0$  to any point. Also, it means that spheres centred around any point are going to evolve into larger spheres centred around the same point under IMCF. However, this does not mean that all IMCF that start as small balls around a point have the same asymptotics. The symmetry is broken by the redshift in the full space-time metric

$$\frac{G}{\ell^2} = -(1+r^2)dt^2 + \frac{dr^2}{1+r^2} + r^2 (d\theta^2 + \sin^2 \theta d\phi^2). \quad (6.64)$$

The red-shift picks out a natural centre where it is maximized, so only small balls that start at the origin in these coordinates asymptote to spheres over which the red-shift is constant. To figure out what happens when we start the flow at a more general point, we write AdS in coordinates centred around a point a distance  $z$  away from the point of maximum redshift. As we have discussed, the spatial sections still look the same, but the redshift changes

$$\frac{G}{\ell^2} = -\left(\sqrt{1+z^2}\sqrt{r^2+1} - zr \cos(\theta)\right)^2 dt^2 + \frac{dr^2}{1+r^2} + r^2 (d\theta^2 + \sin^2 \theta d\phi^2). \quad (6.65)$$

We have chosen the polar axis to run through the point of maximum redshift.

Now, we can look at what conformal frame is picked out by a flow of surfaces starting from a small ball near  $r = 0$ . Since the flow will consist of spheres centred around this point, we see that the frame that is going to be picked out is

$$\bar{g} = - \left( \sqrt{z^2 + 1} - z \cos(\theta) \right)^2 dt^2 + d\theta^2 + \sin^2 \theta d\phi^2, \quad (6.66)$$

and we see we get the boundary geometry in a frame which isn't ultra-static. The function  $\omega$  in (6.62) is therefore

$$\omega = \sqrt{z^2 + 1} - z \cos(\theta). \quad (6.67)$$

By choosing different points at different  $z$  at which to start our flow, there is a whole class of different functions  $\omega$  that we could find. We would expect that in less symmetric spacetimes than AdS, the dependence of  $\omega$  on where you start the flow would be even more complicated, and there is no reason in general to expect any special frame to be picked out.

### 6.4.3 What IMCF can tell us

Even though there is this unresolved ambiguity in the asymptotic value of  $m_H$ , we can still use the flow to derive some interesting constraints on the energy density. As we've discussed above, a crucial feature of even the weak solutions of flows in [89] is that the topology of the surfaces is unchanged along the flow. Where we can start a flow and have it reach the conformal boundary therefore depends on the topology of the boundary.

If the boundary has spherical topology, then we can start the flow on a small sphere centred around a point. For a vanishingly small sphere,  $m_H \rightarrow 0$ , so we have in this case

$$\frac{2\ell}{c} \sqrt{\int \sqrt{\bar{h}} \omega^2} \int \sqrt{\bar{h}} \frac{\rho}{\omega} \geq 0, \quad (6.68)$$

for some undetermined function  $\omega$ . For this to be true for some  $\omega > 0$ , we must have that the energy density  $\rho \geq 0$  somewhere. This result holds regardless of whether or not we are at finite temperature, and regardless of whether there are any horizons in the bulk.

For other topologies we can't start the flow on a small sphere, so we instead start it on a horizon. Since the topology doesn't change, this relies on their being a horizon component in the bulk  $\mathcal{H}$  whose topology is the same as the boundary  $\mathcal{B}$ . This gives

$$\text{If } \mathfrak{g}_{\mathcal{B}} = \mathfrak{g}_{\mathcal{H}} = \mathfrak{g}, \exists \omega \text{ s.t. } \frac{2\ell}{c} \sqrt{\int \omega^2} \int \frac{\bar{\rho}}{\omega} \geq \sqrt{\frac{\ell^2}{4\pi c}} S (16\pi (1 - \mathfrak{g}) + \frac{1}{\pi c} S)$$

where  $\mathfrak{g}$  is the genus and  $S$  is the entropy of the horizon. For a torus  $\mathfrak{g} = 1$ , this immediately shows again that  $\rho \geq 0$  somewhere, however for  $\mathfrak{g} > 1$  this is only true if  $S > 16\pi^2 c (\mathfrak{g} - 1)$ .

We can take the zero temperature limit of these results to derive constraints on the vacuum energy density. For a spheres, the result carries forward straightforwardly and we find

If  $g = 0$  then  $\rho \geq 0$  somewhere.

For a torus, we need to start the flow at a horizon, so we need to add the condition that the spacetime is the zero temperature limit of a finite temperature spacetime with a horizon of toroidal topology

If  $g = 1$  and at small finite temperature the bulk has a horizon with  $g_{\mathcal{H}} = 1$  then  $\rho \geq 0$  somewhere.

This condition holds, for instance, for periodically identified Poincare AdS, but not for the AdS soliton, where, indeed, the energy density is negative definite. A bound at zero temperature for  $g > 1$  is in principle possible by adding an additional requirement.

If  $g > 1$ , at small finite temperature the bulk has a horizon with  $g_{\mathcal{H}} = g$  and as  $T \rightarrow 0$ ,  $S \rightarrow 0$ , then  $\rho \geq 0$  somewhere.

Unfortunately, the example we know about, which is AdS-Schwarzschild with hyperbolic slices, doesn't satisfy this condition.

## 6.5 Discussion

In summary, we have been able to derive several bounds on the Casimir energies of 2 + 1 dimensional holographic CFTs in the universal sector. Firstly, we found that the Casimir energy is non-positive, and unless the space has constant curvature it is strictly negative  $E < 0$ . We were then able to show that there are certain regions on the boundary where the total energy contained therein must be negative. In particular, at the point where the Ricci scalar in ultrastatic frame is minimized, the energy density must be non-positive. Finally, for the case where the boundary has spherical topology, and under certain conditions for higher genus, we showed using IMCF that the energy density couldn't be negative everywhere.

Given the form of the regions in which the total energy had to be negative, it is tempting to guess that the region where the energy density is positive will be centred somehow around the point where the Ricci scalar in ultrastatic frame is maximized. Indeed, it can be shown quite simply that if the bulk solution is such that the optical Ricci scalar is maximized on the boundary, then at this point  $\rho > 0$ . However, there is no reason for this to be true generically, and in general we don't have much to constrain the region in which  $\rho > 0$ .

We were able to generalize the upper bounds on the energy density to the case where there was in addition a massless scalar in the bulk. This generalization was possible because we found that there was a quantity  $\mathcal{L} = R - (\nabla\phi)^2$  that satisfies a minimum principle like the optical Ricci scalar  $R$  does in the universal sector, and where  $\int \nabla^2 \mathcal{L}$  is related to the free energy. It would be interesting to figure out whether there is a generalization of this quantity to other types of matter, as this would allow us to generalize the bound to holographic CFTs deformed by other types of sources. We have been unable to find one so far.

In higher dimensions, there is still a minimum principle, which comes from the inequality

$$\nabla_a \left( \frac{\nabla^a R}{Z^{d-3}} \right) \leq 0. \quad (6.69)$$

This can be integrated as before to give a sum of an integral at the conformal boundary, and horizon integrals. The horizon integrals again give terms that vanish as  $T \rightarrow 0$ , but now the boundary integral has divergences. For a general boundary, we cannot therefore write down a bound using these same methods, but there may still be energy bounds when you choose specific boundary geometries where the divergences vanish.

This upper bound on the Casimir energy can be contrasted with a lower bound like the positive energy theorem for asymptotically global AdS spaces in [90]. In that case, they fix the conformal boundary to be a round sphere and prove that the energy is bounded from below by the global AdS solution. Whether it is possible to put a lower bound on the energy for generic boundary spacetimes remains an open question, but, for example, in [33] it is conjectured that the AdS-Soliton is the minimum energy solution when the conformal boundary is a flat torus.

## Chapter 7

# Temperature Gaps

In Chapters 5 and 6 we explored how the bulk geometry can tell us about properties of vacuum states in holographic CFTs. We now want to explore finite temperature states. In 1.7.2 we discussed black hole bulk states with round spheres on the boundary, and in 1.7.3 we discussed black hole states on a torus. In both cases there is a one parameter family of black holes, which can be labelled by the horizon area, and there is also a bulk solution with no-horizon that can be taken at any temperature. There can be a phase transition between these finite temperature bulks with and without horizons, and this can be interpreted in terms of a confinement/deconfinement transition in the CFT [3, 32].

There is an interesting difference between the stories on the torus and the sphere. While on the torus, the temperature of the horizon can be made arbitrarily small, on the sphere there is a minimum temperature that you can reach, below which there is no black hole solution. This minimum temperature is simply a function of the radius of the boundary sphere. In this chapter we want to explore how the existence of this minimum temperature, and the size of the resulting ‘temperature gap’, depends on the geometry of the boundary more generally. We will therefore be exploring what we can say about AdS static black hole solutions to Einstein’s equation with general conformal boundary geometries.

We won’t be able to derive a bound, but we will be able to provide some evidence that one exists. We will conjecture that, for universal sector solutions, the minimum temperature is bounded by the value it takes when the boundary is an Einstein space. Since temperature is a dimensionfull quantity, we need to normalize it by some length scale in the boundary geometry. The simplest quantity to take would be the volume, but we can see from the example of the torus, where we can have finite volume but no minimum temperature, that a bound in terms of volume doesn’t hold in general. We will argue instead that the correct length scale to use is, like for the energy gaps in Chapter 5, the minimum value of the Ricci scalar. The conjecture is that

$$\min T^2 \geq \frac{d \min \bar{R}}{4\pi^2 (d-1)} \quad (7.1)$$

where  $\min \bar{R}$  is the minimum value of the Ricci scalar on the boundary in the ultrastatic frame. This bound is only non-trivial when  $\min \bar{R} > 0$ . Also, we will add a massless

scalar and conjecture that a generalized version of the same bound holds,

$$\min T^2 \geq \frac{d \min \bar{\mathcal{L}}}{4\pi^2 (d-1)} \quad (7.2)$$

where we have replace  $\min \bar{R} \rightarrow \min \bar{\mathcal{L}}$ , with  $\bar{\mathcal{L}} = \bar{R} - \partial_i \bar{\phi} \partial^i \bar{\phi}$  defined again in the ultra-static frame, as in (6.19).

We will start in Section 7.1 with the known solutions when the boundary is Einstein, which generalizes the specific cases from 1.7.2 and 1.7.3. In Section 7.2 we will then derive a bound for small black holes when the boundary is more general, which will provide our main motivation for (7.1). In Section 7.3, we will examine the behaviour of large black holes as further evidence of the conjecture. We will then test a couple of different cases. Firstly, in 7.4 when the boundary is a product of spheres we can construct the bulk black hole solutions by numerically solving a system of ODEs, and then in 7.6 when the boundary is a deformed sphere, we can solve the PDEs to construct bulk solutions using the numerical techniques from Chapter 2. The work presented in this chapter was done in collaboration with Toby Wiseman.

## 7.1 Einstein Boundary Metric

We discussed in 1.7.2 black holes where the horizon and the spatial section of the conformal boundary were both round spheres, and in 1.7.3 the case where they were both tori. More generally, we can take any  $d-1$  dimensional Einstein space  $\Sigma_{d-1}$ , and write a set of black hole solutions which take the form[91]

$$ds^2 = -f(r)dt^2 + \frac{\ell^2 dr^2}{f(r)} + r^2 \Sigma \bar{h}_{ij} dx^i dx^j \quad (7.3)$$

where  $\Sigma \bar{h}_{ij}$  and  $x^i$  are the Einstein metric and  $d-1$  coordinates on  $\Sigma_{d-1}$ . The function  $f(r)$  depends on the  $\Sigma \bar{R}$ , the constant Ricci scalar of  $\Sigma_{d-1}$

$$f(r) = \frac{\Sigma \bar{R} \ell^2}{(d-1)(d-2)} + r^2 - \frac{r_0^{d-2} \left( \frac{\Sigma \bar{R} \ell^2}{(d-1)(d-2)} + r_0^2 \right)}{r^{d-2}}. \quad (7.4)$$

So there is a one a parameter family of black holes, labelled by  $r_0$  which is the size of the horizon. The temperature for these solutions is

$$T = \frac{1}{4\pi} \frac{r_0}{\ell} \left( d + \frac{\ell^2 \Sigma \bar{R}}{r_0^2 (d-1)} \right). \quad (7.5)$$

If  $\Sigma \bar{R} \leq 0$  this temperature can be brought all the way down to zero, but if  $\Sigma \bar{R}$  is positive, then there is a minimum temperature

$$\min T^2 = \frac{d \Sigma \bar{R}}{4\pi^2 (d-1)}. \quad (7.6)$$

This tells us that the minimum temperature normalized by the Ricci scalar,  $\frac{\min T^2}{\Sigma \bar{R}}$ , is the same for all Einstein conformal boundary metrics. If instead, for instance, we normalize by the volume, then

$$\min T^{\Sigma} V^{\frac{1}{d-1}} = \frac{\sqrt{\Sigma V^{\frac{2}{d-1}} \Sigma \bar{R}}}{2\pi} \sqrt{\frac{d}{d-1}}. \quad (7.7)$$

The quantity  $\Sigma V^{\frac{2}{d-1}} \Sigma \bar{R}$  is the Yamabe invariant[92] of  $\Sigma$ , and will depend on the precise Einstein manifold<sup>1</sup>.

## 7.2 Small Black Holes

Let's consider a particular conformal boundary geometry, taken in the ultrastatic frame. We assume that for this conformal boundary there is a bulk vacuum solution with no black hole horizons which satisfies the same assumptions we made when we were considering energy gaps in 5.4; namely that there are no asymptotic regions other than the conformal boundary. In particular, this means that the redshift  $Z$ , as defined in (5.53) is bounded. The prototypical example of such a bulk is global AdS.

Now, let's consider a small spherical black hole in this geometry. In the zero mass limit a small black hole behaves like a massive particle on the background of the vacuum solution[93, 94, 95]. This means that it will follow timelike geodesics in the spacetime. Potential points where you can insert a small static black holes can be therefore be found by finding static geodesics in the vacuum spacetime. Using the optical geometry, the geodesic equation takes the form

$$\frac{d^2 x^i}{d\tau^2} + \Gamma^i_{jk} \frac{dx^j}{d\tau} \frac{dx^k}{d\tau} = \frac{1}{2\ell^2} \partial^i (Z^2) + \frac{2}{Z} \partial_j Z \frac{dx^i}{d\tau} \frac{dx^j}{d\tau}. \quad (7.8)$$

A static geodesic therefore sits at a stationary point of  $Z$ . The small black hole will be dynamically unstable if this geodesic is unstable, and these geodesics are stable only if the stationary point of  $Z$  is a maximum. We will therefore consider black holes inserted at local maxima of the redshift, which we will denote  $Z_*$ .

In [93], a technique for constructing these small black holes in a series called matched asymptotic expansion is discussed. There are two regions, a near field and a far field. The far field is the vacuum solution plus linear corrections due to the massive particle, and the near field is the vacuum Schwarzschild black hole plus corrections due to the curvature scales in the vacuum geometry. The near field is then matched on to the far field.

To lowest order, this means that near a small black hole the metric is Schwarzschild. We can therefore write down the relationship between the temperature and entropy. However, the temperature we write down in this way is the temperature measured with

<sup>1</sup>For instance, in 4 dimensions we can compare  $S^4$ , where  $\sqrt{V}R = 8\sqrt{6}\pi$ , and  $S^2 \times S^2$  where  $\sqrt{V}R = 16\pi$ , both of which are Einstein spaces.

respect to the local proper time. With respect to the CFT time coordinate this is red-shifted by  $Z_\star$ . For small black holes we therefore have that

$$T_{\text{CFT}}^2(S) = \frac{\ell^2}{Z_\star^2} T_{\text{Sch}}^2(S) = \frac{\ell^2 R_\star}{d(d-1)} T_{\text{Sch}}^2(S), \quad (7.9)$$

where we have used Einstein's equation written in optical frame (5.54) to replace  $Z_\star$  with the optical Ricci scalar at this point  $R_\star$ . Then, recalling that  $R$  is minimized on the conformal boundary, and that on the conformal boundary it is proportional to the boundary Ricci scalar, we can bound the temperature of a small black hole as a function of the entropy

$$T_{\text{CFT}}^2(S) \geq \frac{\ell^2 \min \bar{R}}{(d-1)(d-2)} T_{\text{Sch}}^2(S). \quad (7.10)$$

This discussion of the temperature of small black holes is based on a discussion of their energy we published in [72].

The main thing we would like to observe here is that it's the minimum value of the boundary Ricci scalar that bounds the leading order behaviour of these small black holes. What's more, this bound can only be saturated if the optical Ricci scalar is constant everywhere, and hence the boundary has constant Ricci scalar. The behaviour in (7.10) is precisely the leading order behaviour, for instance, for AdS-Schwarzschild black holes. This bound tells us is that if we start from AdS-Schwarzschild and deform the conformal boundary away from a round sphere, the temperature at fixed entropy for the small black holes is pushed up, so long as we normalize by the minimum value of the boundary Ricci scalar. While there is no sign of the minimum temperature in this leading behaviour, this is the first indication that some sort of bound is plausible, and that  $\min \bar{R}$  enters naturally.

### 7.2.1 Addition of a massless Scalar

As further evidence that any bound should be in terms of the minimum Ricci scalar, we note that this generalizes quite naturally with the addition of a massless scalar. The argument for a small black hole on a background with a non-trivial scalar field carries through unchanged. The black hole now needs in addition to be small enough that the stress tensor for the scalar field is negligible on those scales. The optical form of Einstein's equation then imply

$$T_{\text{CFT}}^2(S) = \frac{\ell^2}{Z_\star^2} T_{\text{Sch}}^2(S) = \frac{\ell^2 \mathcal{L}_\star}{d(d-1)} T_{\text{Sch}}^2(S), \quad (7.11)$$

where  $\mathcal{L} = R - (\nabla\phi)^2$  as introduced in Chapter 6. Again, this can be bounded by it's minimum value on the boundary, and we have

$$T_{\text{CFT}}^2(S) \geq \frac{\ell^2 \min \bar{\mathcal{L}}}{(d-1)(d-2)} T_{\text{Sch}}^2(S) \quad (7.12)$$

so that the temperature normalized by the minimum value of the boundary  $\bar{\mathcal{L}} = \bar{R} - (\bar{\nabla}\bar{\phi})^2$  is bounded.

### 7.3 Large Black Holes

At the other end of the spectrum, very large black holes can be treated using Fluid-Gravity[39, 38, 40]. To leading order, the black holes look locally like planar-AdS-Schwarzschild black holes. To be more precise, consider the metric and scalar field

$$\begin{aligned} g^0 &= \left(\frac{\ell^2}{z^2}\right) \left(\frac{dz^2}{f(z)} - f(z)dt^2 + \bar{h}_{ij}(\theta)d\theta^i d\theta^j\right) \\ \phi^0 &= \bar{\phi}(\theta^i) \end{aligned} \quad (7.13)$$

with  $f(z) = 1 - z^d/z_0^d$ , and where  $\bar{h}_{ij}$  is an arbitrary  $d - 1$  dimensional spatial metric with coordinates  $\theta^i$  which describes a spatial slice of the conformal boundary. These spacetimes have a horizon at  $z = z_0$  with temperature  $T = \frac{d}{4\pi z_0}$ . If  $d\Sigma_{d-1}^2$  is flat space, and  $\phi$  is constant, this is planar AdS-Schwarzschild (1.40) and satisfies Einstein's equation. Otherwise, we find that

$$\begin{aligned} \mathcal{L}_{\tau\tau} + \frac{d}{\ell^2}g_{\tau\tau}^0 &= 0 \\ \mathcal{L}_{rr} + \frac{d}{\ell^2}g_{rr}^0 &= 0 \\ \mathcal{L}_{ij} + \frac{d}{\ell^2}g_{ij}^0 &= \bar{R}_{ij} - \partial_i\bar{\phi}\partial_j\bar{\phi} \equiv \bar{\mathcal{L}}_{ij}. \end{aligned} \quad (7.14)$$

where  $\bar{R}_{ij}$  is the Ricci tensor of  $\bar{h}_{ij}$ . If  $|\bar{\mathcal{L}}_{ij}| \ll \left|\frac{d}{\ell^2}g_{ij}^0\right|$ , then this is approximately a solution to Einstein's equation. Since  $\frac{d}{\ell^2}g_{ij}^0 = \frac{d}{z^2}\bar{h}_{ij}$ , this means that  $|z^2\bar{\mathcal{L}}_{ij}| \ll 1$  everywhere. For this it is sufficient that  $|z_0^2\bar{\mathcal{L}}_{ij}| \ll 1$  or equivalently  $|\bar{\mathcal{L}}_{ij}| \ll T^2$ . So this approximation holds whenever the temperature is large compared to the curvature of the boundary and the gradients of the scalar source.

This metric is the zeroth order term in a series, with higher order corrections suppressed by inverse powers of the temperature, and positive powers of the curvatures. This is the fluid-gravity gradient expansion. The structure of the gradient expansion means that at each order we only need to solve ODEs in  $z$ , sourced by the  $\theta$  derivatives of the lower order terms. Boundary conditions can be applied to these corrections so that they don't change the temperature, or the geometry on the conformal boundary. They will however affect the horizon metric. The metric on the horizon in the full solution will therefore be given in an expansion as

$$\frac{H}{\ell^2}g_{ij} = \left(\frac{4\pi T}{d}\right)^2 \left(\bar{h}_{ij} + O\left(\frac{\Sigma R}{T^2}\right)\right). \quad (7.15)$$

This universal behaviour exists for large black holes independent of the choice of boundary metric.

We can find the next to leading order corrections to this behaviour. Motivated by the Einstein space solutions (7.3), we write down an ansatz<sup>2</sup>

$$\begin{aligned} ds^2 &= -f(r)dt^2 + \frac{\ell^2 dr^2}{f(r)} + r^2 \bar{h}_{ij} d\theta^i d\theta^j - \lambda(r) \tilde{\mathcal{L}}_{ij} d\theta^i d\theta^j + O(\partial^3) \\ \phi &= \bar{\theta}(\theta^i) + \gamma(r) \bar{\nabla}^2 \bar{\theta}(\theta^i) + O(\partial^3) \\ f(r) &= \frac{\bar{\mathcal{L}} \ell^2}{(d-1)(d-2)} + r^2 - \frac{r_0^{d-2} \left( \frac{\bar{\mathcal{L}} \ell^2}{(d-1)(d-2)} + r_0^2 \right)}{r^{d-2}}. \end{aligned} \quad (7.16)$$

where  $\tilde{\mathcal{L}}_{ij}$  is the traceless part of  $\bar{\mathcal{L}}_{ij}$ . This ansatz solves Einstein's equation to second order in gradients on the boundary, where the functions  $\lambda(r)$  and  $\gamma(r)$  satisfy ODEs

$$\begin{aligned} -\ell^2 &= \frac{1}{2} \frac{d}{dr} (\lambda'(r) f_0(r)) + \frac{d-5}{2} \lambda'(r) \frac{f_0(r)}{r} + 2\lambda(r) \frac{f_0(r)}{r^2} - d\lambda(r) \\ -1 &= \frac{d}{dr} (r^2 f_0(r) \gamma'(r)), \end{aligned} \quad (7.17)$$

where  $f_0(r) = r^2 - \frac{r_0^d}{r^{d-2}}$ . The horizon radius  $r_0$  is related to the temperature through  $r_0^2 = \left( \frac{4\pi T \ell}{d} \right)^2 - \frac{2\ell^2 \bar{\mathcal{L}}}{d(d-1)} + O(\bar{\mathcal{L}}^2)$ , and so the metric on the horizon is given by

$$\frac{H g_{ij}}{\ell^2} = \left( \left( \frac{4\pi T}{d} \right)^2 - \frac{2}{d(d-1)} \bar{\mathcal{L}} \right) \bar{h}_{ij} - \frac{\lambda(r_0)}{\ell^2} \tilde{\mathcal{L}}_{ij} + O(\partial^3). \quad (7.18)$$

Taking the determinant of both sides of this equation, we can find an expansion for the temperature

$$T = \frac{d}{4\pi} \sigma^{\frac{1}{d-1}} \left( 1 + \frac{1}{d(d-1)} \sigma^{-\frac{2}{d-1}} \bar{\mathcal{L}} + O(\sigma^{\frac{-4}{d-1}} \partial^4) \right), \quad (7.19)$$

where  $\sigma = \frac{H \sqrt{g}}{\ell^{d-1} \sqrt{h}}$  is proportional to the entropy density. Unfortunately, this expansion doesn't give us access to the minimum temperature, since this will occur in a regime where the expansion parameter is  $O(1)$ . However, it is interesting to note that if we take this formula at face value, and throw away all the potential corrections, it would imply

$$T \geq \frac{\sqrt{\min \bar{\mathcal{L}}}}{2\pi} \sqrt{\frac{d}{d-1}}, \quad (7.20)$$

which is precisely the bound we are proposing. This happened because, by comparing with (7.5), we can see that (7.19) is actually exact when the boundary is Einstein, so all the higher order corrections in this case must vanish.

What is perhaps more interesting to note is that it is again this quantity  $\bar{\mathcal{L}}$  which is controlling the leading order behaviour. In particular, we can use it to bound the leading

<sup>2</sup>The Einstein space solutions with the replacement  $R \rightarrow \mathcal{L}$ , to first order in curvatures satisfy the tt, and the trace of the  $ij$  components of the equation. That's why this ansatz is possible.

order behaviour of the temperature as a function of entropy density

$$T \geq \frac{d}{4\pi} \sigma^{\frac{1}{d-1}} \left( 1 + \frac{1}{d(d-1)} \sigma^{-\frac{2}{d-1}} \min \bar{\mathcal{L}} + O\left(\sigma^{-\frac{4}{d-1}} \partial^4\right) \right). \quad (7.21)$$

There is also an integrated version of this relationship

$$T \geq \frac{d}{4\pi} \left( \frac{{}^H\mathcal{A}}{\bar{\mathcal{A}}} \right)^{\frac{1}{d-1}} \left( 1 + \frac{1}{d(d-1)} \left( \frac{{}^H\mathcal{A}}{\bar{\mathcal{A}}} \right)^{-\frac{2}{d-1}} \min \bar{\mathcal{L}} + O\left( \left( \frac{{}^H\mathcal{A}}{\bar{\mathcal{A}}} \right)^{-\frac{4}{d-1}} \partial^4 \right) \right), \quad (7.22)$$

where  ${}^H\mathcal{A}$  and  $\bar{\mathcal{A}}$  are areas of the horizon and the conformal boundary.

## 7.4 The Product of Spheres

In [75], the case where the conformal boundary is  $\text{time} \times S^1 \times S^2$  is considered, and black hole solutions with horizons that share this topology are constructed. This boundary metric has constant positive Ricci scalar, but it is not Einstein, so you can't immediately write down analytic solutions. They found solutions numerically by solving the system of ODEs corresponding to Einstein's equation for static spacetimes that respect the  $SO(2) \times SO(3)$  symmetry of the boundary. They found that there is, like for the positive Ricci scalar Einstein metrics, a minimum temperature black hole.

We have reproduced these results, as well as repeated the same calculation for a boundary  $S^1 \times S^3$ , and the results are shown in Figure 7.1. We have compared the Ricci normalized temperature to the corresponding Einstein space solutions for  $S^3$  and  $S^4$ . We find that the minimum Ricci normalized temperature goes up compared to these spaces, which is consistent with our conjecture. These examples also illustrate why we can't use volume normalization. Taking any given one of these black hole solutions, we can freely scale the  $S^1$  factor. This scales the boundary volume and horizon area, but does not effect the surface gravity of the horizon. By scaling the  $S^1$  in this way, we can make the volume normalized temperature arbitrarily small, while the Ricci scalar normalized temperature is unaffected.

For  $d = 5$ , we can also consider the case where the boundary is  $S^2 \times S^2$ . This case is perhaps more interesting, as we have a whole one parameter family of conformal boundaries, labelled by the ratio of the sizes of the two  $S^2$  factors. As a result, there is a two parameter family of horizons labelled by the radii of the two  $S^2$  factors in the horizon metric. The temperature as a function of the two radii of the horizons is shown in Figure 7.2. When the two radii are equal, the boundary is Einstein, and there is a one parameter family of analytic solutions. We find that the maximum temperature occurs along this one parameter family. In this case it is true regardless of whether we use volume or Ricci scalar normalization.

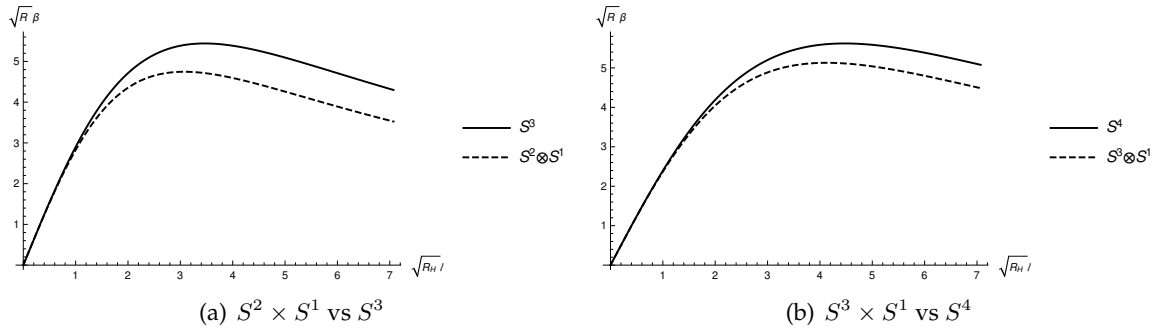


FIGURE 7.1: The  $R$  normalized inverse temperature as a function of horizon Ricci scalar, compared between  $S^{n-1} \times S^1$  and  $S^n$ . Each line is drawn through 500 points that have been found numerically. We see in each case that the dashed line non-Einstein space solution has a larger minimum temperature than the solid line Einstein space solution. We can also see the universal behaviour of large black holes towards  $\bar{R} \rightarrow 0$ .

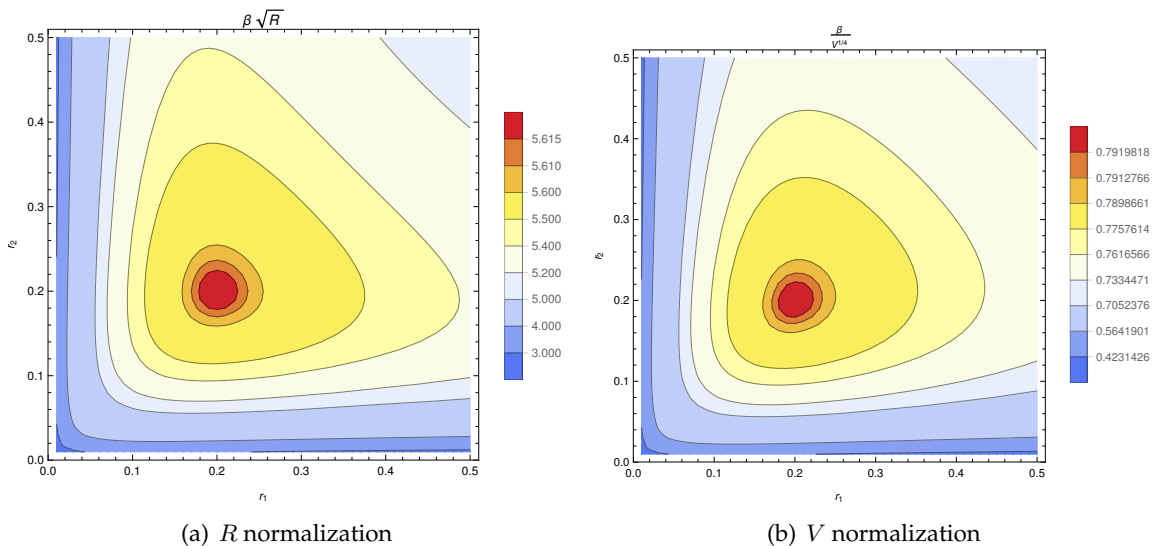


FIGURE 7.2: The inverse temperature for  $S^2 \times S^2$ , as a function of the two radii of the horizons.

### 7.4.1 Numerical Solution of the ODEs

The ODEs which are solved to find the black hole solutions when the conformal boundaries are products of spheres are solved with the aid of Mathematica[57]. We write the metric in normal coordinates which take the form

$$ds^2 = dr^2 - \phi_0(r)dt^2 + \sum_j \phi_j(r)d\Omega_{n_j}^2, \quad (7.23)$$

where the choices of values of  $n_j$  determine which conformal boundary we are solving for. The equations of motion consist of one second order equation for each  $\phi_j$  and an additional first order constraint equation, whose derivative is implied by the other equations.

We take  $r = 0$  to be the horizon where  $\phi_0(0) = 0$ . The other  $\phi_j(0)$  then control the size of the horizon,  $\phi_j(0) = \rho_j^2$ . The equations are singular here, so we need to step out to a small radius  $r = \epsilon$ . We series expand the equations and the constraint to order  $\epsilon^2$  to get initial values and first derivatives at  $r = \epsilon$  consistent with the constraint. In this expansion, the second derivative  $\phi_0''(0)$  is undetermined, and corresponds to the surface gravity of the horizon. Because of the scaling symmetry, we can without loss of generality fix  $\phi_0''(0) = 2$ .

We then integrate outwards using the second order equations to large  $r$ . The  $\phi_j(r)$  eventually start growing exponentially, but their ratios go to constants, and these ratios tell us the boundary geometry. The numerical integration is terminated when we detect that these ratios have become effectively constant.

## 7.5 Linearised Perturbations of a Sphere

In this section and the next, we are going to look at the specific case where the spatial section of the boundary is a  $d - 1$  sphere, but with a deformed metric. In addition, we will add a massless scalar field, which will be non-homogeneous over the sphere. When the scalar field is turned off, and the boundary metric is a round sphere, we have the AdS-Schwarzschild solutions. In this section we will consider linear perturbations to these bulks.

To begin with, we will deform the boundary metric without turning on the scalar field. We will consider deformations to the metric in Lorentz gauge. So, if we write our boundary metric as

$$\bar{g} = -dt^2 + \Omega_{ij}d\theta^i d\theta^j - \epsilon\delta\bar{h}_{ij}d\theta^i d\theta^j \quad (7.24)$$

where  $\Omega_{ij}$  is the  $d - 1$  dimensional sphere, then we require

$$\bar{\nabla}_\mu \delta\bar{h}_\nu^\mu = \frac{1}{2}\bar{\nabla}_\nu \delta\bar{h}, \quad (7.25)$$

with covariant derivatives taken with respect to the unperturbed boundary metric. The boundary Ricci scalar picks up a shift from this perturbation

$$\delta\bar{R} = \epsilon \left( \frac{\delta\bar{h}\bar{R}}{d-1} + \frac{1}{2}\bar{\nabla}^2\delta\bar{h} \right). \quad (7.26)$$

So, traceless perturbations where  $\bar{h} = 0$  don't shift the Ricci scalar.

When we solve the bulk Einstein's equation with this perturbed metric on the conformal boundary, there will be a family of black hole bulks with a Hawking temperature which varies with their entropy. For any choice of  $\delta\bar{h}$ , we can therefore consider the function  $T(\epsilon, S)$ . When  $\epsilon = 0$  this will be the AdS-Schwarzschild black holes, but as epsilon is varied the temperature as a function of entropy will be deformed in some way. Because of the rotational symmetry, we can expand  $\delta\bar{h}$  in modes on the sphere. This leads to separation of variables in the bulk equations, and for each mode, we can solve a separate ODE to find the perturbation to the bulk. In particular, there is a homogeneous perturbation where  $\delta\bar{h}_{ij} = \lambda\Omega_{ij}$ , which simply scales the boundary spatial sections. This change in boundary volume is simply equivalent to a change in temperature, and this is the deformation that moves us along the one-parameter family of AdS-Schwarzschild black holes.

All other modes have  $\int\delta\bar{h} = 0$ , so they will not affect the boundary volume or the black-hole entropy. In particular, it also follows from (7.26), that they will satisfy

$$\int\delta\bar{R} = 0. \quad (7.27)$$

This means that either  $\delta\bar{R} = 0$  everywhere, or  $\min\delta\bar{R} < 0$ . Since the perturbation isn't affecting the Hawking temperature of the horizons, if  $\min\delta R < 0$ , then for the minimum Ricci scalar normalized temperature

$$\delta\frac{T(S)}{\sqrt{\min R}} = -\frac{1}{2}\frac{T(S)}{\min R^{3/2}}\delta\min R \geq 0 \quad (7.28)$$

at any fixed entropy. In particular, this would mean that the minimum temperature normalized in this way would go up, so we see that these linear perturbations are consistent with our conjecture.

In the other situation, where to linear order  $\delta\bar{R} = 0$  everywhere, there is no linear shift in the minimum temperature normalized in this way to first order. We have to go to second order in  $\epsilon$  to figure out whether it goes up or down. This gets complicated, and we haven't been able to prove anything in general about this special case.

However, another scenario we can consider is perturbing the massless scalar. To first order, a scalar field simply satisfies

$$\nabla^2\phi = 0 \quad (7.29)$$

on the background. The coupling to gravity through the stress the tensor is only  $O(\phi^2)$ , specifically

$$\tilde{T}_{\mu\nu} = \partial_\mu\phi\partial_\nu\phi, \quad (7.30)$$

where  $\tilde{T}_{\mu\nu}$  enters into the equations of motion as

$$R_{\mu\nu} + \frac{d}{\ell^2}g_{\mu\nu} = \tilde{T}_{\mu\nu}. \quad (7.31)$$

If we consider a perturbation to a black hole space time in the form of such a scalar field, the first order solution to (7.29) obviously doesn't affect it at all. However, this then feeds back at second order through (7.31) to source a backreaction on the metric. This backreaction can be expanded in modes just like the original gravitational perturbations above, but this time the modes are sourced by the corresponding modes in  $\tilde{T}_{\mu\nu}$ . In particular, the homogeneous mode that can shift the temperature and entropy of the horizon will no longer simply move us along the AdS-Schwarzschild family of solutions. These equations will be sourced by the homogeneous part of  $\tilde{T}_{\mu\nu}$ .

The source term for the backreaction is

$$\tilde{T} = (\partial_r\phi)^2 dr^2 + \partial_i\phi\partial_j\phi d\theta^i d\theta^j \quad (7.32)$$

and the homogeneous part of this is

$$\tilde{T}_H = \frac{\int (\partial_r\phi)^2 d\Omega_{d-1}}{\Omega_{d-1}} dr^2 + \frac{\int \Omega^{ij}\partial_i\phi\partial_j\phi d\Omega_{d-1}}{(d-1)\Omega_{d-1}} d\Omega_{d-1}^2. \quad (7.33)$$

Note that unless the scalar field is a constant, this homogeneous component is always non-zero, and both  $\tilde{T}_{rr} > 0$  and  $\tilde{T}_\Omega > 0$ .

We can take an ansatz for the homogeneous backreaction on the metric

$$g = -f(r)dt^2 + (1 + \epsilon^2 a(r)) \frac{\ell^2 dr^2}{f(r)} + (1 + \epsilon^2 b(r)) r^2 d\Omega_{d-2}^2, \quad (7.34)$$

where  $\phi \sim O(\epsilon)$ . Using this ansatz, we can find an integral solution for the backreaction, without knowing the precise form of  $\phi$ . This involves solving a second order ODE for  $a(r)$ , with the function  $b(r)$  then determined. We solve the ODE subject to boundary conditions that fix the horizon and boundary areas. These boundary conditions are equivalent to  $b(r_0) = 0$  and  $\lim_{r \rightarrow \infty} b(r) = 0$ . The solution for the perturbation to the

minimum temperature bulk is

$$\begin{aligned}
a(r) = & \frac{2 \left( (d-1)^2 r^{2-2d} r_0^{2d} - (d-1)^2 (r^2 + r_0^2) \left( \frac{r_0}{r} \right)^d + r_0^2 \right) \left( \int_r^\infty x^3 \left( 1 - \left( \frac{r_0}{x} \right)^d \right) \tilde{T}_{rr}(x) dx \right)}{(d-2)r^2 r_0^2 \left( (d-1) \left( \frac{r_0}{r} \right)^d + 1 \right)^2} \\
& - \frac{d \left( (d-1)^2 r^{2-2d} r_0^{2d} - (d-1)^2 (r^2 + r_0^2) \left( \frac{r_0}{r} \right)^d + r_0^2 \right) \tilde{T}_\Omega(\infty)}{(d-2)^2 r^2 \left( (d-1) \left( \frac{r_0}{r} \right)^d + 1 \right)^2} \\
& + \frac{(d-1)d \left( \frac{r_0}{r} \right)^d \left( \left( \frac{r_0}{r} \right)^d - 1 \right) \tilde{T}_\Omega(r_0)}{(d-2) \left( (d-1) \left( \frac{r_0}{r} \right)^d + 1 \right)^2},
\end{aligned} \tag{7.35}$$

where  $r_0 = \ell \sqrt{\frac{d-2}{d}}$ . Note that from the expansion of the scalar field near the conformal boundary (6.26),  $\tilde{T}_{rr} \sim O(r^{-6})$  so  $\int_r^\infty x^3 \left( 1 - \left( \frac{r_0}{x} \right)^d \right) \tilde{T}_{rr}(x) dx$  is finite. From this we can extract the shift in temperature

$$\frac{\delta T^2}{T^2} = \frac{2 \int_{r_0}^\infty r^3 \left( 1 - \left( \frac{r_0}{r} \right)^d \right) \tilde{T}_{rr}(r) dr}{dr_0^2} - \frac{\tilde{T}_\Omega(\infty)}{d-2}. \tag{7.36}$$

Now we note two things. Firstly, the integral is positive, and secondly the boundary quantity  $\tilde{T}_\Omega(\infty)$  is related to shift in  $\mathcal{L}$  through

$$\tilde{T}_\Omega(\infty) = \frac{\int (\nabla \bar{\phi})^2}{(d-1)V_\Omega} = -\frac{\delta \int \mathcal{L}}{(d-1)V} \tag{7.37}$$

Putting this together yields a bound on this temperature shift

$$\frac{\delta T^2}{T^2} \geq \frac{\delta \int \mathcal{L}}{\int \mathcal{L}} \geq \frac{\delta \min \mathcal{L}}{\min \mathcal{L}}. \tag{7.38}$$

This shows that the shift in minimum temperature normalized by the minimum value of  $\mathcal{L}$  increases to linear order for all scalar perturbations, which is consistent with our bound.

## 7.6 Deformations of Spheres

So far we have only been able to consider explicit examples when the boundary metric is either highly symmetric, or an Einstein space, as well as certain linear perturbations to some of these cases. As further tests of this conjecture, we use the numerical methods introduced in Chapter 2 to examine the spectrum of black holes when the conformal boundary is a deformed sphere. We take the cases where  $d = 3$  and  $d = 4$  and the conformal boundary is, in ultrastatic frame<sup>3</sup>,

$$ds^2 = -dt^2 + s(\theta)^{\frac{2}{d-1}} \left( d\theta^2 + \sin^2 \theta d\Omega_{d-2}^2 \right), \tag{7.39}$$

<sup>3</sup>The power to which  $s(\theta)$  is taken is chosen for convenience so that the measure,  $\sqrt{s}$ , is just proportional to  $s(\theta)$ .

so these are deformed spheres with an  $SO(d-1)$  symmetry group maintained. If  $s(\theta)$  is constant, then the boundary is a sphere, and the bulk black holes are the global AdS-Schwarzschild black holes. In addition, we will add a massless scalar field with a profile on the boundary

$$\phi = \bar{\phi}(\theta). \quad (7.40)$$

There are two functions worth of freedom in the choice of boundary conditions here, so we restrict ourselves to a four parameter family<sup>4</sup>

$$\begin{aligned} s(\theta) &= \frac{1}{1 - \left(1 - \frac{2}{d}\right)\epsilon} (1 + \lambda \cos \theta + \epsilon \cos 2\theta) \\ \bar{\phi}(\theta) &= \lambda_2 \cos \theta + \epsilon_2 \cos 2\theta. \end{aligned} \quad (7.41)$$

In Figure 7.3 we plot the minimum temperature for some choices of purely metric deformations, so  $\lambda_2 = \epsilon_2 = 0$ , and a range of values of  $\lambda$  and  $\epsilon$  are considered. Regardless of whether we normalize by the volume or the minimum value of the Ricci scalar<sup>5</sup>, the temperature is minimized when  $\lambda = \epsilon = 0$ .

In Figure 7.4 we plot the same for some choices of purely scalar deformations, so  $\lambda = \epsilon = 0$ , and a range of values of  $\lambda_2$  and  $\epsilon_2$  are considered. Now it makes a big difference whether we just normalize using the boundary geometry, or involve the boundary value of  $\phi$  by normalizing by the minimum value of  $\mathcal{L}$ . The volume normalized minimum temperature goes down if you move away from AdS-Schwarzschild, but the  $\mathcal{L}$  normalized temperature is minimized for  $\lambda_2 = \epsilon_2 = 0$ .

Finally, the distinction between the two normalizations is made clear by looking at the mixed deformations in Figure 7.5. In these plots  $\lambda = \epsilon_2 = 0$ , and the other two parameters are varied. The minimum  $\mathcal{L}$  normalized temperature always goes up away from global AdS, whereas the volume normalized temperature goes up or down depending on whether the metric deformation or scalar deformation is larger.

### 7.6.1 Numerical Solution of the PDEs on Deformed Spheres

We solved the bulk equations using the techniques of Chapter 2, which we used in Chapter 4. Again, initial solutions were found on a desktop, and then the full parameter scans were done using Imperial College's HPC[70]. The metric ansatz we take is

$$\begin{aligned} ds^2 &= \frac{4}{(1-r^2)^2} (r^4 dt^2 F(r, \theta) + (r^2 dt^2 + dr^2) H(r, \theta) + 2r dr d\theta \sin \theta L(r, \theta) \\ &\quad + M(r, \theta)(d\theta^2 + d\Omega_{d-2}^2 \sin^2 \theta) + S(r, \theta) \sin^2 \theta d\theta^2), \end{aligned} \quad (7.42)$$

so that the holographic coordinate  $r$  runs between  $0 \leq r \leq 1$ , with  $r = 0$  being the horizon, and  $r = 1$  being the conformal boundary. The two dimensional domain of our

<sup>4</sup>The prefactor in  $s(\theta)$  ensures that the total volume of the space is fixed. This is purely for convenience, since we are going to normalize all temperatures by length scales in this geometry anyway.

<sup>5</sup>For this normalization, we have to restrict ourselves to those deformations where  $R > 0$  everywhere.

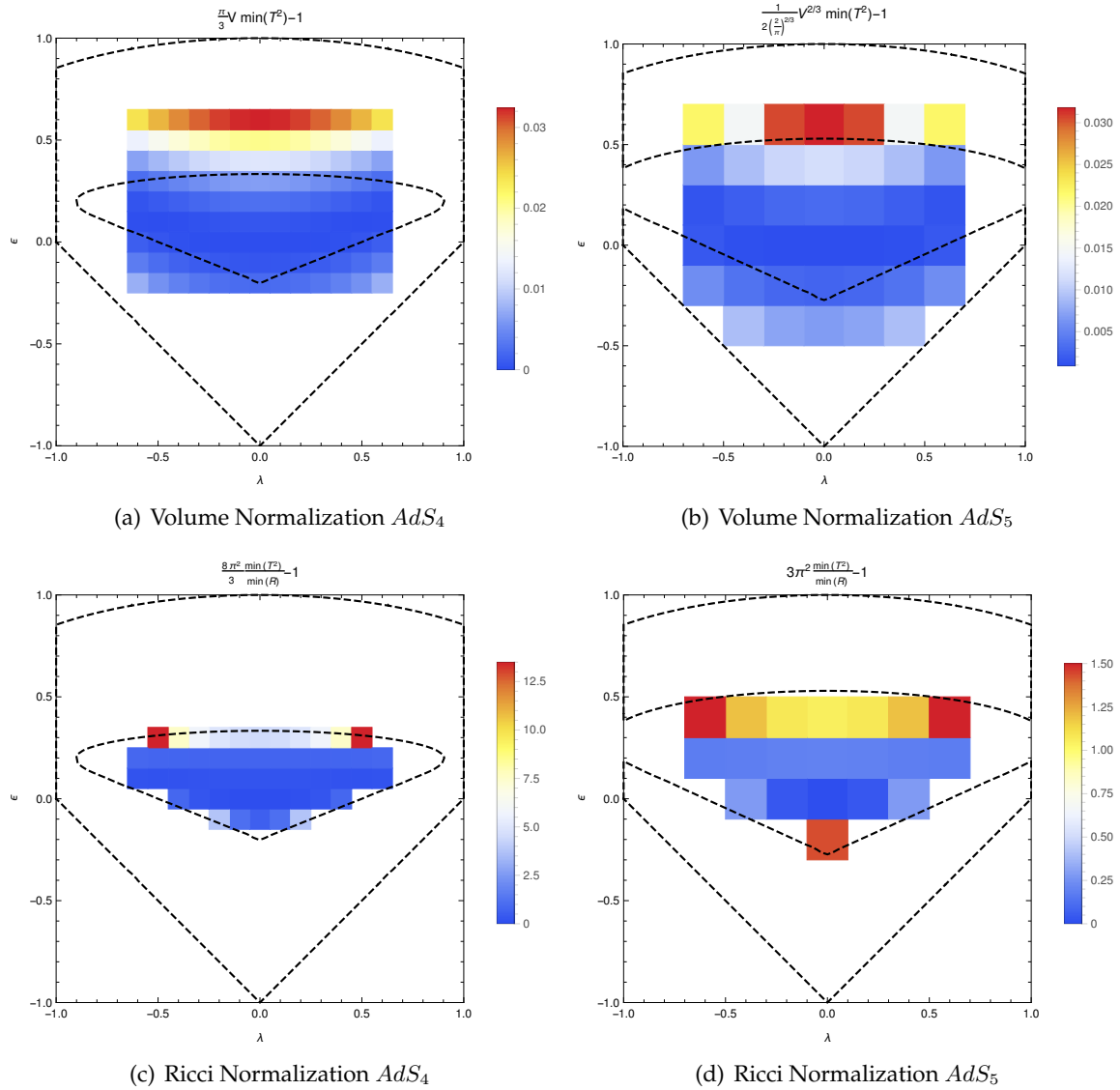


FIGURE 7.3: The change in minimum temperature as compared to an undeformed sphere for the metric deformations. The inner dotted line is the region where  $R > 0$ , and the outer one is the region where the deformation is non-singular ( $s(\theta) > 0$  everywhere).

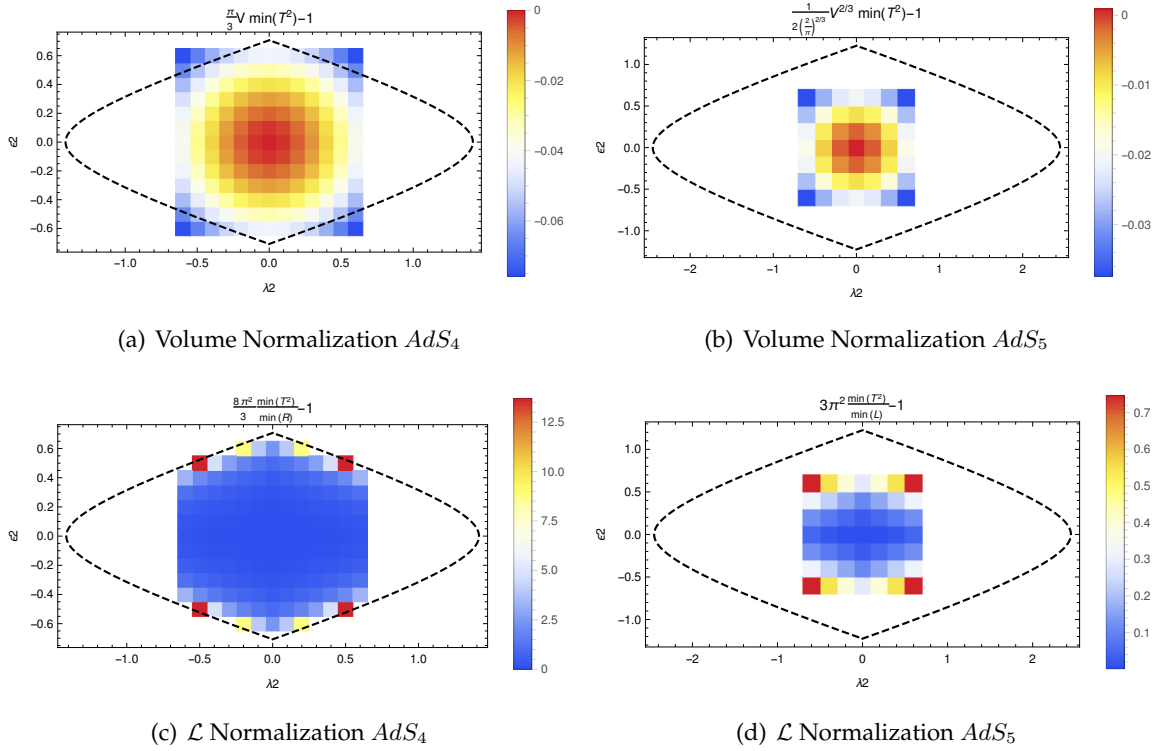


FIGURE 7.4: The change in minimum temperature as compared to an undeformed sphere for the scalar deformations. The dotted line is the boundary of the region where  $\mathcal{L} > 0$

PDEs is then characterized by

$$\begin{aligned} 0 \leq r \leq 1 \\ 0 \leq \theta \leq \pi \end{aligned} \tag{7.43}$$

There are three special points where this coordinate system breaks down, so we need to make sure we impose smoothness explicitly. These are the horizon  $r = 0$  and the two poles of the sphere  $\theta = 0, \pi$ . We will choose our coordinate lattice such that smoothness at these points is imposed automatically, and the only boundary condition we will need is the one that fixes the boundary metric at  $r = 1$ .

We use Chebyshev polynomial pseudospectral differencing in the  $r$  direction and Fourier spectral differencing in the  $\theta$  direction. For the  $r$  coordinate we build in the assumption that all our functions are even under  $r \rightarrow -r$ , which automatically imposes smoothness at the horizon  $r = 0$ . As described in Chapter 2, we take an even number of points in the total lattice (so in particular there is no point at  $r = 0$ ), project the derivative matrix on that lattice to even functions, which gives us an effective matrix for the points on that lattice for  $0 < r \leq 1$ .

For the  $\theta$  lattice, we note that the solutions we are looking for are both periodic with period  $2\pi$ , and also have a symmetry  $\theta \rightarrow -\theta$ . They therefore admit a cosine expansion

$$a_0 + \sum_{n=1}^{N-1} a_n \cos n\theta, \tag{7.44}$$

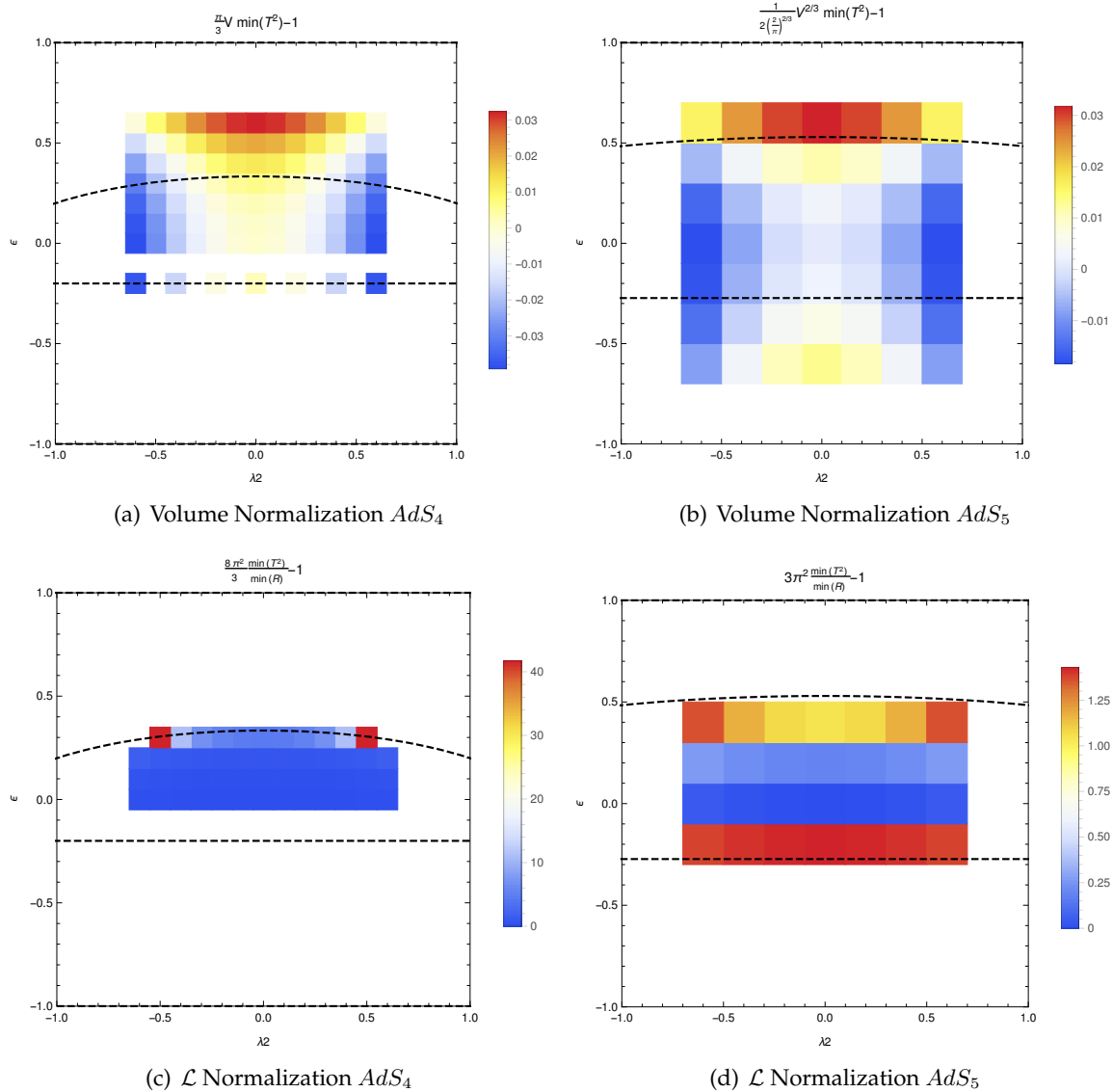


FIGURE 7.5: The change in minimum temperature as compared to an undeformed sphere for the mixed deformations. The dotted line is the boundary of the region where  $\mathcal{L} > 0$

which builds in smoothness at the poles. We use this expansion to construct the derivative matrices, using the lattice points

$$\theta_n = \frac{\pi}{2N} + n \frac{\pi}{N}. \quad (7.45)$$

For  $d = 3$  we use a reference metric where

$$\begin{aligned} F(r, \theta) &= \frac{2 (r^2 - 3) r_0^2 (r_0^2 + 1) (r^4 - r^2 + (r^4 + 3r^2 + 6) r_0^2 + 2)}{(r^2 + 1) (3r_0^2 + 1)^2 ((r^4 + 3) r_0^2 + (r^2 - 1)^2)} \\ H(r, \theta) &= \frac{2 (r^2 + 1) r_0^2}{(r^4 + 3) r_0^2 + (r^2 - 1)^2} \\ L(r, \theta) &= 0 \\ M(r, \theta) &= \frac{1}{4} (r^2 + 1)^2 r_0^2 (s(\theta)) \\ S(r, \theta) &= 0 \end{aligned} \quad (7.46)$$

and in  $d = 4$  we take

$$\begin{aligned} F(r, \theta) &= -\frac{8r_0^2 (r_0^2 + 1) (r^4 + 2 (r^4 + r^2 + 1) r_0^2 + 1)}{(r^2 + 1)^2 (2r_0^2 + 1)^2 (2 (r^4 + 1) r_0^2 + (r^2 - 1)^2)} \\ H(r, \theta) &= \frac{(r^2 + 1)^2 r_0^2}{2r^4 r_0^2 + r^4 - 2r^2 + 2r_0^2 + 1} \\ L(r, \theta) &= 0 \\ M(r, \theta) &= \frac{1}{4} (r^2 + 1)^2 r_0^2 (s(\theta)) \\ S(r, \theta) &= 0 \end{aligned} \quad (7.47)$$

These are chosen so that if  $\lambda = \epsilon = 0$  then these are the vacuum AdS-Schwarzschild solutions parametrized by  $r_0$ .

### 7.6.2 Convergence Tests for PDEs

We focus here on the 4 dimensional solutions. We look at the vacuum AdS solutions, along with 3 metric deformations, 3 scalar deformations, and 3 mixed deformations. We take the smallest, and the largest black hole we found in each of these deformations and find these solutions at a range of resolutions. To start off with, we stick to pseudospectral interpolation in the radial direction, and the Fourier differencing in the angular direction, where we run at resolutions from  $10 \times 10$  to  $40 \times 40$ , with the radial and angular resolution increasing together.

The first thing to check is that the equations of motion are satisfied on the solutions. We look at the trace of the offset of the Ricci scalar  $\Delta R$ , and the offset of the Ricci tensor squared  $\Delta R_{ij} \Delta R^{ij}$ , from the values implied by Einstein's equation. These are shown in Figure 7.6.

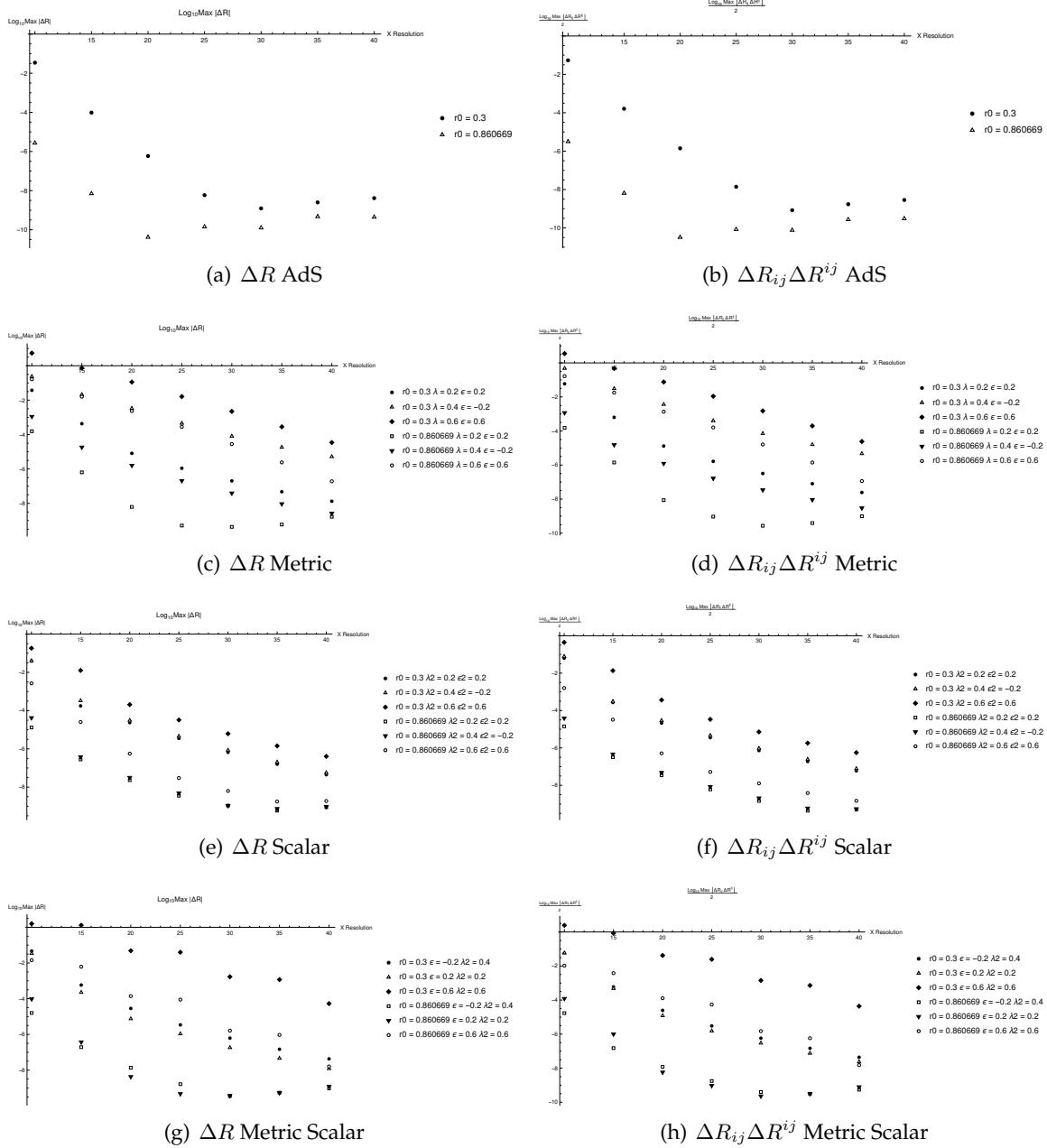


FIGURE 7.6: Agreement with Einstein's equation at various resolutions. We see that as the resolution is increased, the agreement improves.

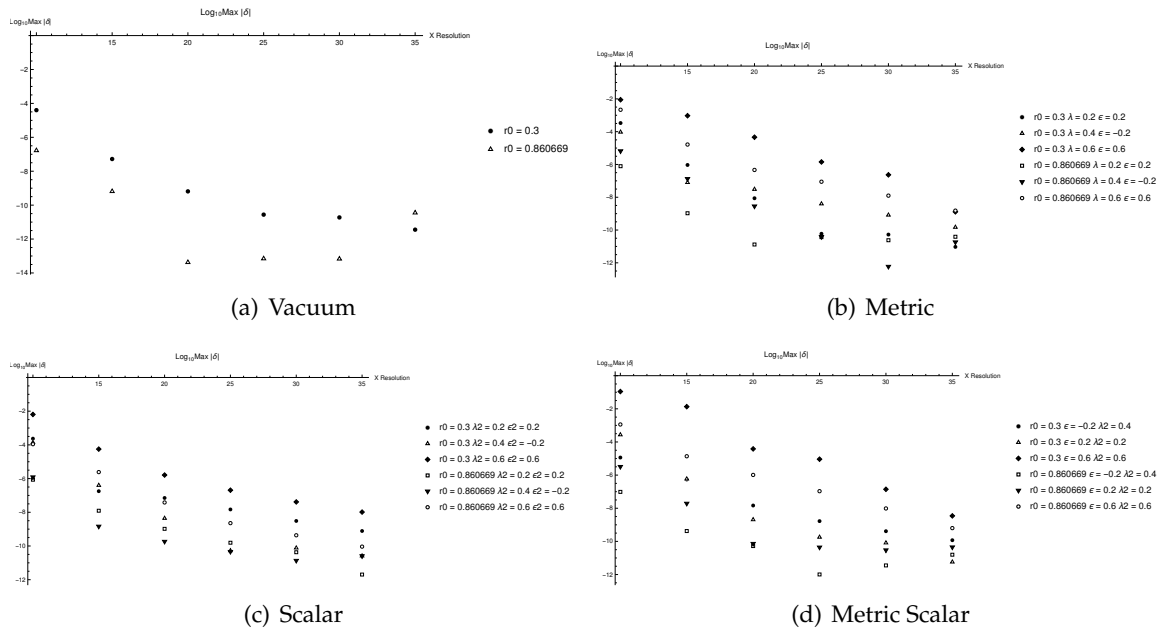


FIGURE 7.7: Shift in solution from resolution to resolution using pseudospectral interpolation. The decreasing size of the shift at increasing resolution demonstrates convergence.

The next thing we check is whether the shift in solutions from resolution to resolution converges for high resolutions. What we do is interpolate all the solutions, and evaluate them at all the points on the largest lattice. We then compare the solutions at successive resolutions, and plot the largest shift at any of these points from resolution to resolution. These are shown in Figure 7.7 and show convergence.

Finally, we focus on the expansion of our solutions near the conformal boundary. We extract the energy via a FG expansion. This energy depends on the third derivatives of our functions at the conformal boundary. The shift in energy from solution to solution is shown in 7.8. Here we see an issue, as these do not converge. This suggests a lack of smoothness at the conformal boundary, which would come from logarithmic behaviour in our boundary expansion much as in Chapter 4.

Pseudospectral interpolation is very sensitive to this lack of smoothness, so we instead move to finite difference interpolation. We use sixth order finite difference in the radial direction, and we repeated these tests at fixed angular resolution (40 points) and with  $x$  resolutions varying from 150 to 450 points. A few examples of this are shown in Figure 7.9. With finite difference interpolation, we expect a power law interpolation, so we fit lines through log-log plots of the shifts versus the resolution. The slope tells us the order of convergence, as discussed in Chapter 4. We see that the bulk quantities converge much faster than the boundary energy, which is consistent with a lack of smoothness at the boundary. At the resolutions we have considered here, the error on the  $R$  and  $R_{ij}$  is limited by  $\phi$  resolution. We demonstrate that these are still fine using finite difference by increasing the  $\phi$  and  $X$  resolution together. Figure 7.10 illustrates this using fourth order finite difference at  $X$  resolutions ranging from 30 to 180 points in steps of 30, where the

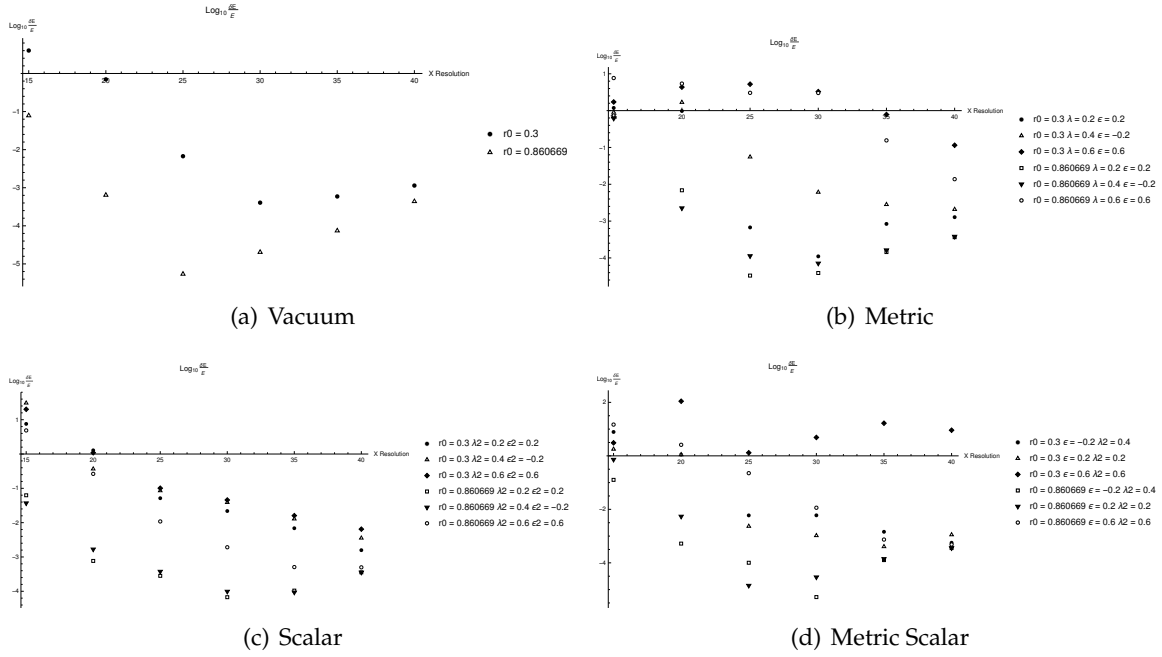


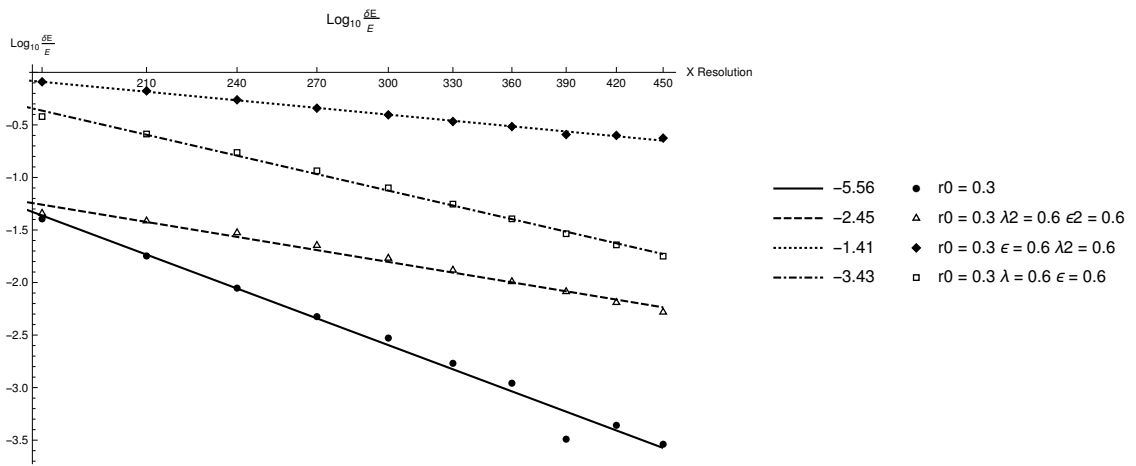
FIGURE 7.8: Energy Shift for pseudospectral interpolation. Here we see a potential issue with convergence. This is due to a lack of smoothness at the boundary, and is resolved by moving to finite difference.

$\phi$  resolution increases from 10 to 60 points in steps of 10.

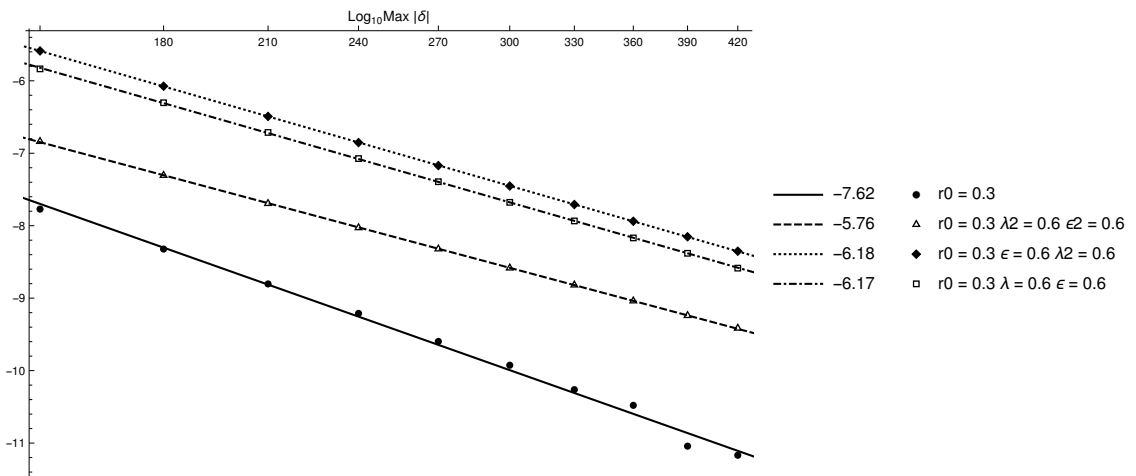
## 7.7 Discussion

We have presented evidence for a bound on the minimum temperature of AdS black holes as a function of their conformal boundary geometry. We conjectured the bound (7.1), relating this ‘temperature gap’ to the minimum value of the Ricci scalar on the boundary geometry (in the ultrastatic frame). Below this temperature, one would expect there to be some finite temperature bulk solution with no horizons, like global AdS, which would correspond to a confined state in the CFT. As with the transition from AdS-Schwarzschild to global AdS, this transition could generically occur at some temperature above the minimum temperature black hole, but this ‘temperature gap’ acts as a lower bound on the transition temperature, and so a lower bound on the former translates into a lower bound on the latter. We also conjectured that this bound generalizes with the addition of a massless scalar in the bulk. The minimum temperature would then be bounded by the minimum value of  $\bar{\mathcal{L}}$  as in (7.2).

This bound is very non-trivial from the point of view of the CFT. We can consider the CFT in a finite temperature canonical ensemble, and think of varying the boundary geometry and the classical source for the marginal scalar  $\bar{\phi}$ . The conjectured bound (7.2) would tell you, for instance, that for all geometries and sources where  $\bar{\mathcal{L}} > 0$  everywhere, there is a phase transition between a confined and a deconfined phase at some finite temperature.

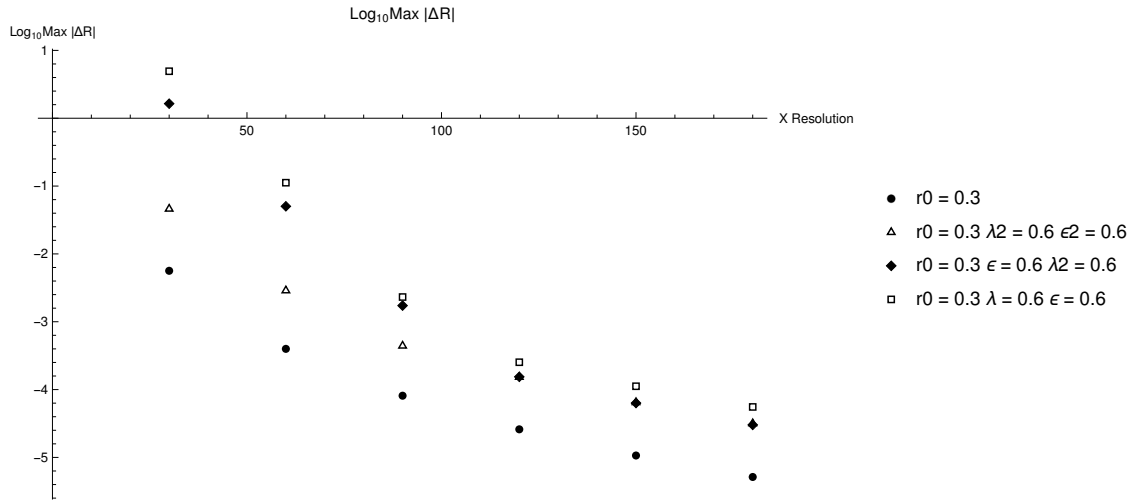


(a) Energies

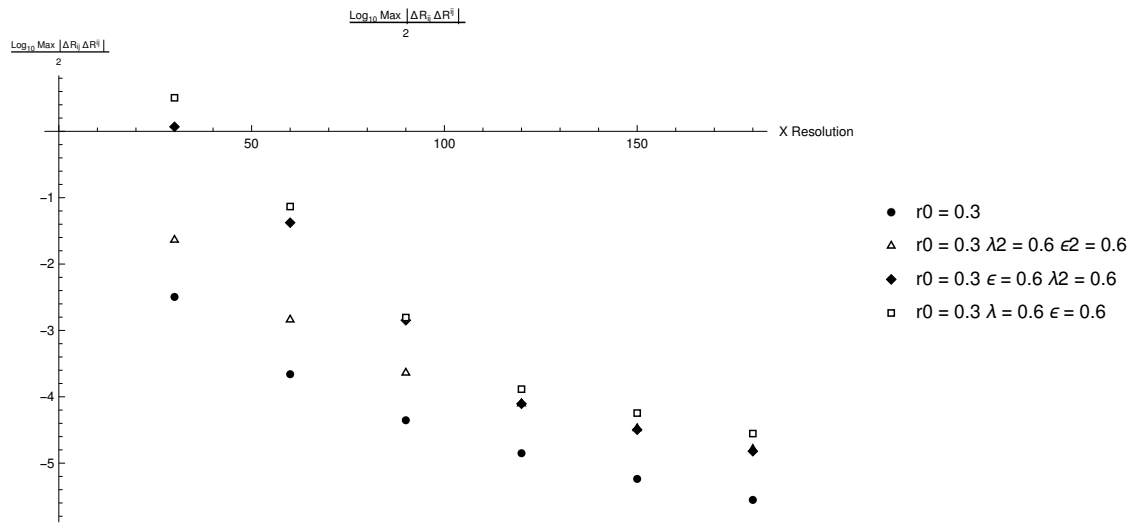


(b) Function Shifts

FIGURE 7.9: Energy Shift and Bulk Function Shift for Finite Difference Interpolation. The  $X$  resolution is increased on it's own, with the  $\phi$  resolution fixed at 50 points.



(a)  $\Delta R$



(b)  $\Delta R_{ij} \Delta R^{ij}$

FIGURE 7.10: Agreement with Einstein's equation for Finite Difference Interpolation. Here the  $\phi$  resolution is increased with the  $X$  resolution. (The number of points in the  $\phi$  direction is everywhere  $1/3$  the number of points in the  $X$  direction).

---

Unlike the bounds in previous chapters, we have no proof. The behaviour of small and large black holes in Sections 7.2 and 7.3 illustrate how  $\bar{\mathcal{L}}$  enters naturally into  $T(S)$ , and how  $\min \bar{\mathcal{L}}$  bounds the behaviour in both of these extremes. The examples of space-times where the boundary is a product of spheres, and the linear perturbations of AdS-Schwarzschild are then consistent with this bound. Finally, the numerical solutions we constructed in 7.6.1, illustrated that this bound is comfortably satisfied on the full solutions to the unlinearized equations for certain deformations of AdS.



## Chapter 8

### Summary

We have explored various ways that features of the bulk geometry in AdS/CFT can reflect and constrain physical properties of the dual CFT. In Chapters 3 and 4 we found that a certain large scale limit in a holographic CFT could be related to a throat-like infrared region in the bulk. The source terms and boundary geometry in this limit were the boundary conditions for equations that determined the geometry which in turn described the large scale limit of the CFT state. Holographic CFTs are therefore constrained to have a certain relationship between the large scale limit of inserted sources, and the corresponding limit of one-point functions, determined by the solutions to these equations.

The extremal horizons which describe a particular class of these large scale limits are well understood, with many examples of near horizon geometries known analytically. However, this is not the case for the scale invariant singularities we discussed in Chapter 4, and it would be useful to study these in more detail. In particular, to demonstrate explicitly that these are ‘good’ singularities, we could take these bulks to finite temperature and find the corresponding black hole solutions. Also, it would be interesting to add other matter fields to the bulk, so that we can explore these singularities when the large scale limit of the CFT source terms is something other than a metric deformation or a chemical potential.

In Chapters 5, 6 and 7 we then considered the bulk descriptions of holographic CFTs on spacetimes with compact spatial sections. We found that the existence of the bulk geometry could be used to bound the energy gap of scalar fluctuations, and we gave evidence to suggest that it could also bound a temperature gap, below which the CFT would have to be in a confined state. This bound was given in terms of the minimum value of the Ricci scalar on the boundary. We also found that we could prove that for certain types of bulk geometry, the vacuum energy must be negative. What’s more, the energy density at the point corresponding to this minimum value of the Ricci scalar in the CFT had to be non-positive as well. In addition, we used IMCF to show that in many cases the energy density had to be positive somewhere.

The results we derived applied in the universal sector of any holographic CFT. The fact that we could generalize most of our results with the addition of a massless scalar suggests that there could be similar types of bounds outside of the universal sector for particular combinations of bulk matter fields. Also, there are most likely many more

holographic results to be found in the universal sector using techniques similar to the ones we have used here.

For a particular class of CFTs, AdS/CFT rephrases the complicated problem of curved space QFT in terms of a classical geometric problem in a bulk geometry, the Einstein's equation. This allows us to use simple geometric tools to derive surprisingly powerful results. Even forgetting the fact that these CFTs are strongly coupled, these results would have been very difficult to derive using only QFT tools, since they give constraints on the properties of these curved space QFTs as a function of the geometry they live on. For the energy gap bound in Chapter 5 there were hints that the result might be applicable to a wider class of CFTs, and in particular we were able to derive the bound for a free scalar. It would be interesting to understand more generally under what conditions the bounds we have explored here could be derived in non-holographic CFTs, and to what extent the results depend on the existence of the bulk geometric description.

# Bibliography

- [1] Juan Martin Maldacena. “The Large N limit of superconformal field theories and supergravity”. In: International Journal of Theoretical Physics 38 (1999), pp. 1113–1133. DOI: [10.1023/A:1026654312961](https://doi.org/10.1023/A:1026654312961). arXiv: [hep-th/9711200](https://arxiv.org/abs/hep-th/9711200) [hep-th].
- [2] Steven S. Gubser, Igor R. Klebanov, and Alexander M. Polyakov. “Gauge theory correlators from noncritical string theory”. In: Physics Letters B428 (1998), pp. 105–114. DOI: [10.1016/S0370-2693\(98\)00377-3](https://doi.org/10.1016/S0370-2693(98)00377-3). arXiv: [hep-th/9802109](https://arxiv.org/abs/hep-th/9802109) [hep-th].
- [3] Edward Witten. “Anti-de Sitter space and holography”. In: Advances in Theoretical and Mathematical Physics 2 (1998), pp. 253–291. arXiv: [hep-th/9802150](https://arxiv.org/abs/hep-th/9802150) [hep-th].
- [4] Stephen W. Hawking. “Black hole explosions?”. In: Nature 248.5443 (Mar. 1974). [10.1038/248030a0](https://doi.org/10.1038/248030a0), pp. 30–31. DOI: <http://dx.doi.org/10.1038/248030a0>.
- [5] Ofer Aharony et al. “Large N field theories, string theory and gravity”. In: Physics Reports 323.3-4 (Jan. 2000), pp. 183–386. ISSN: 03701573. DOI: [10.1016/S0370-1573\(99\)00083-6](https://doi.org/10.1016/S0370-1573(99)00083-6). arXiv: [hep-th/9905111](https://arxiv.org/abs/hep-th/9905111) [hep-th]. URL: <http://arxiv.org/abs/hep-th/9905111>.
- [6] Philip C Argyres. “Introduction to the AdS/CFT Correspondence”. In: From gravity to thermal gauged theories. Ed. by E Papantonopoulos. Berlin Heidelberg New York: Springer, 2011. ISBN: 9783642048630.
- [7] Joseph Polchinski. “Introduction to Gauge/Gravity Duality”. In: Proceedings, Theoretical Advances in String Theory 2010, pp. 3–46. DOI: [10.1142/9789814350525\\_0001](https://doi.org/10.1142/9789814350525_0001). arXiv: [1010.6134](https://arxiv.org/abs/1010.6134) [hep-th]. URL: <http://inspirehep.net/record/875017/files/arXiv:1010.6134.pdf>.
- [8] Donald Marolf, Mukund Rangamani, and Toby Wiseman. “Holographic thermal field theory on curved spacetimes”. In: Classical and Quantum Gravity 31 (2014), p. 063001. DOI: [10.1088/0264-9381/31/6/063001](https://doi.org/10.1088/0264-9381/31/6/063001). arXiv: [1312.0612](https://arxiv.org/abs/1312.0612) [hep-th].
- [9] Eric D’Hoker and Daniel Z. Freedman. “Supersymmetric gauge theories and the AdS / CFT correspondence”. In: Strings, Branes and Extra Dimensions: TASI 2001: Proceedings. 2002, pp. 3–158. arXiv: [hep-th/0201253](https://arxiv.org/abs/hep-th/0201253) [hep-th].
- [10] G. ’t Hooft. “A planar diagram theory for strong interactions”. In: Nuclear Physics B 72.3 (Apr. 1974), pp. 461–473. ISSN: 05503213. DOI: [10.1016/0550-3213\(74\)90154-0](https://doi.org/10.1016/0550-3213(74)90154-0). URL: <http://inspirehep.net/record/80491>.

- [11] Jerome P. Gauntlett, Julian Sonner, and Toby Wiseman. “Holographic superconductivity in M-Theory”. In: *Physical Review Letters* 103 (2009), p. 151601. DOI: [10.1103/PhysRevLett.103.151601](https://doi.org/10.1103/PhysRevLett.103.151601). arXiv: [0907.3796](https://arxiv.org/abs/0907.3796) [hep-th].
- [12] Jerome P. Gauntlett et al. “Consistent supersymmetric Kaluza-Klein truncations with massive modes”. In: *JHEP* 04 (2009), p. 102. DOI: [10.1088/1126-6708/2009/04/102](https://doi.org/10.1088/1126-6708/2009/04/102). arXiv: [0901.0676](https://arxiv.org/abs/0901.0676) [hep-th].
- [13] Sean A Hartnoll. “Lectures on holographic methods for condensed matter physics”. In: *Classical and Quantum Gravity* 26.22 (2009), p. 224002. URL: <http://stacks.iop.org/0264-9381/26/i=22/a=224002>.
- [14] Christos Charmousis. “Introduction to Anti de Sitter Black Holes”. In: *From gravity to thermal gauge theory*. Ed. by E Papantonopoulos. Berlin Heidelberg New York: Springer, 2011. ISBN: 9783642048630.
- [15] Stephen W. Hawking et al. *The Large Scale Structure of Space-Time* (Cambridge Monographs on Mathematical Physics). Cambridge University Press, 1975. ISBN: 0521099064.
- [16] A. Ashtekar and A. Magnon. “Asymptotically anti-de Sitter space-times”. In: *Classical and Quantum Gravity* 1 (1984), pp. L39–L44. DOI: [10.1088/0264-9381/1/4/002](https://doi.org/10.1088/0264-9381/1/4/002).
- [17] Kostas Skenderis. “Lecture notes on holographic renormalization”. In: *Classical and Quantum Gravity* 19 (2002), pp. 5849–5876. DOI: [10.1088/0264-9381/19/22/306](https://doi.org/10.1088/0264-9381/19/22/306). arXiv: [hep-th/0209067](https://arxiv.org/abs/hep-th/0209067) [hep-th].
- [18] Charles Fefferman and C. Robin Graham. “The ambient metric”. In: (2007). arXiv: [0710.0919](https://arxiv.org/abs/0710.0919) [math.DG].
- [19] Slava Rychkov. “EPFL Lectures on Conformal Field Theory in  $D \geq 3$  Dimensions”. In: (2016). arXiv: [1601.05000](https://arxiv.org/abs/1601.05000) [hep-th].
- [20] Philippe Francesco, Pierre Mathieu, and David Sénéchal. “Chapter 4: Global Conformal Invariance”. In: *Conformal Field Theory* (Graduate Texts in Contemporary Physics). Springer, 1999. ISBN: 038794785X.
- [21] N. D. Birrell and P. C. W. Davies. “Chapter 3: Quantum Field Theory in Curved Spacetime”. In: *Quantum Fields in Curved Space* (Cambridge Monographs on Mathematical Physics). Cambridge University Press, 1984. ISBN: 0521278589.
- [22] M. Henningson and K. Skenderis. “The Holographic Weyl anomaly”. In: *Journal of High Energy Physics* 07 (1998), p. 023. DOI: [10.1088/1126-6708/1998/07/023](https://doi.org/10.1088/1126-6708/1998/07/023). arXiv: [hep-th/9806087](https://arxiv.org/abs/hep-th/9806087) [hep-th].
- [23] Sebastian de Haro, Sergey N. Solodukhin, and Kostas Skenderis. “Holographic reconstruction of space-time and renormalization in the AdS / CFT correspondence”. In: *Communications in Mathematical Physics* 217 (2001), pp. 595–622. DOI: [10.1007/s002200100381](https://doi.org/10.1007/s002200100381). arXiv: [hep-th/0002230](https://arxiv.org/abs/hep-th/0002230) [hep-th].
- [24] Massimo Bianchi, Daniel Z. Freedman, and Kostas Skenderis. “Holographic renormalization”. In: *Nuclear Physics B* B631 (2002), pp. 159–194. DOI: [10.1016/S0550-3213\(02\)00179-7](https://doi.org/10.1016/S0550-3213(02)00179-7). arXiv: [hep-th/0112119](https://arxiv.org/abs/hep-th/0112119) [hep-th].

- [25] Shinsei Ryu and Tadashi Takayanagi. “Holographic derivation of entanglement entropy from AdS/CFT”. In: *Physical Review Letters* 96 (2006), p. 181602. DOI: [10.1103/PhysRevLett.96.181602](https://doi.org/10.1103/PhysRevLett.96.181602). arXiv: [hep-th/0603001](https://arxiv.org/abs/hep-th/0603001) [hep-th].
- [26] Juan Martin Maldacena. “Wilson loops in large N field theories”. In: *Physical Review Letters* 80 (1998), pp. 4859–4862. DOI: [10.1103/PhysRevLett.80.4859](https://doi.org/10.1103/PhysRevLett.80.4859). arXiv: [hep-th/9803002](https://arxiv.org/abs/hep-th/9803002) [hep-th].
- [27] Soo-Jong Rey and Jung-Tay Yee. “Macroscopic strings as heavy quarks in large N gauge theory and anti-de Sitter supergravity”. In: *European Physical Journal C* 22 (2001), pp. 379–394. DOI: [10.1007/s100520100799](https://doi.org/10.1007/s100520100799). arXiv: [hep-th/9803001](https://arxiv.org/abs/hep-th/9803001) [hep-th].
- [28] Vijay Balasubramanian and Per Kraus. “A Stress tensor for Anti-de Sitter gravity”. In: *Communications in Mathematical Physics* 208 (1999), pp. 413–428. DOI: [10.1007/s002200050764](https://doi.org/10.1007/s002200050764). arXiv: [hep-th/9902121](https://arxiv.org/abs/hep-th/9902121) [hep-th].
- [29] J. David Brown and Jr. James W. York. “Quasilocal energy and conserved charges derived from the gravitational action”. In: *Physical Review D* 47 (1993), pp. 1407–1419. DOI: [10.1103/PhysRevD.47.1407](https://doi.org/10.1103/PhysRevD.47.1407). arXiv: [gr-qc/9209012](https://arxiv.org/abs/gr-qc/9209012) [gr-qc].
- [30] Kostas Skenderis. “Asymptotically Anti-de Sitter space-times and their stress energy tensor”. In: *International Journal of Modern Physics A* 16 (2001), pp. 740–749. DOI: [10.1142/S0217751X0100386X](https://doi.org/10.1142/S0217751X0100386X). arXiv: [hep-th/0010138](https://arxiv.org/abs/hep-th/0010138) [hep-th].
- [31] Hari K. Kunduri and James Lucietti. “Classification of near-horizon geometries of extremal black holes”. In: *Living Reviews in Relativity* 16 (2013), p. 8. arXiv: [hep-th/1306.2517](https://arxiv.org/abs/hep-th/1306.2517) [hep-th].
- [32] Edward Witten. “Anti-de Sitter space, thermal phase transition, and confinement in gauge theories”. In: *Advances in Theoretical and Mathematical Physics* 2 (1998), pp. 505–532. arXiv: [hep-th/9803131](https://arxiv.org/abs/hep-th/9803131) [hep-th].
- [33] Gary T. Horowitz and Robert C. Myers. “The AdS / CFT correspondence and a new positive energy conjecture for general relativity”. In: *Physical Review D* 59 (1998), p. 026005. DOI: [10.1103/PhysRevD.59.026005](https://doi.org/10.1103/PhysRevD.59.026005). arXiv: [hep-th/9808079](https://arxiv.org/abs/hep-th/9808079) [hep-th].
- [34] Gary T. Horowitz. “Introduction to Holographic Superconductors”. In: *From Gravity to Thermal C* Ed. by Eleftherios Papantonopoulos. Berlin, Heidelberg: Springer Berlin Heidelberg, 2011, pp. 313–347. ISBN: 978-3-642-04864-7. DOI: [10.1007/978-3-642-04864-7\\_10](https://doi.org/10.1007/978-3-642-04864-7_10). URL: [http://dx.doi.org/10.1007/978-3-642-04864-7\\_10](http://dx.doi.org/10.1007/978-3-642-04864-7_10).
- [35] Rong-Gen Cai et al. “Introduction to Holographic Superconductor Models”. In: *Sci. China Phys. Mech. Astron.* 58.6 (2015), p. 060401. DOI: [10.1007/s11433-015-5676-5](https://doi.org/10.1007/s11433-015-5676-5). arXiv: [1502.00437](https://arxiv.org/abs/1502.00437) [hep-th].
- [36] Aristomenis Donos and Jerome P. Gauntlett. “The thermoelectric properties of inhomogeneous holographic lattices”. In: *JHEP* 01 (2015), p. 035. DOI: [10.1007/JHEP01\(2015\)035](https://doi.org/10.1007/JHEP01(2015)035). arXiv: [1409.6875](https://arxiv.org/abs/1409.6875) [hep-th].

- [37] Amos Yarom. "The Gauge-Gravity Duality and Heavy Ion Collisions". In: From Gravity to Thermal Gauge Theory. Ed. by Eleftherios Papantonopoulos. Berlin, Heidelberg: Springer Berlin Heidelberg, 2011, pp. 205–233. ISBN: 978-3-642-04864-7. DOI: [10.1007/978-3-642-04864-7\\_7](https://doi.org/10.1007/978-3-642-04864-7_7). URL: [http://dx.doi.org/10.1007/978-3-642-04864-7\\_7](http://dx.doi.org/10.1007/978-3-642-04864-7_7).
- [38] Mukund Rangamani. "Gravity and hydrodynamics: lectures on the fluid-gravity correspondence". In: Classical and Quantum Gravity 26.22 (2009), p. 224003. URL: <http://stacks.iop.org/0264-9381/26/i=22/a=224003>.
- [39] Sayantani Bhattacharyya et al. "Nonlinear Fluid Dynamics from Gravity". In: Journal of High Energy Physics 02 (2008), p. 045. DOI: [10.1088/1126-6708/2008/02/045](https://doi.org/10.1088/1126-6708/2008/02/045). arXiv: [0712.2456](https://arxiv.org/abs/0712.2456) [hep-th].
- [40] Veronika E. Hubeny, Shiraz Minwalla, and Mukund Rangamani. "The fluid/gravity correspondence". In: Black holes in higher dimensions. 2012, pp. 348–383. arXiv: [1107.5780](https://arxiv.org/abs/1107.5780) [hep-th]. URL: <http://inspirehep.net/record/920982/files/arXiv:1107.5780.pdf>.
- [41] Sayantani Bhattacharyya et al. "Local Fluid Dynamical Entropy from Gravity". In: Journal of High Energy Physics 06 (2008), p. 055. DOI: [10.1088/1126-6708/2008/06/055](https://doi.org/10.1088/1126-6708/2008/06/055). arXiv: [0803.2526](https://arxiv.org/abs/0803.2526) [hep-th].
- [42] P. Kovtun, Dan T. Son, and Andrei O. Starinets. "Viscosity in strongly interacting quantum field theories from black hole physics". In: Physical Review Letters 94 (2005), p. 111601. DOI: [10.1103/PhysRevLett.94.111601](https://doi.org/10.1103/PhysRevLett.94.111601). arXiv: [hep-th/0405231](https://arxiv.org/abs/hep-th/0405231) [hep-th].
- [43] Sergei Khlebnikov, Martin Kruczenski, and Georgios Michalogiorgakis. "Shock waves in strongly coupled plasmas II". In: Journal of High Energy Physics 07 (2011), p. 097. DOI: [10.1007/JournalofHighEnergyPhysics07\(2011\)097](https://doi.org/10.1007/JournalofHighEnergyPhysics07(2011)097). arXiv: [1105.1355](https://arxiv.org/abs/1105.1355) [hep-th].
- [44] Sergei Khlebnikov, Martin Kruczenski, and Georgios Michalogiorgakis. "Shock waves in strongly coupled plasmas". In: Physical Review D 82 (2010), p. 125003. DOI: [10.1103/PhysRevD.82.125003](https://doi.org/10.1103/PhysRevD.82.125003). arXiv: [1004.3803](https://arxiv.org/abs/1004.3803) [hep-th].
- [45] Johanna Erdmenger et al. "Fluid dynamics of R-charged black holes". In: Journal of High Energy Physics 01 (2009), p. 055. DOI: [10.1088/1126-6708/2009/01/055](https://doi.org/10.1088/1126-6708/2009/01/055). arXiv: [0809.2488](https://arxiv.org/abs/0809.2488) [hep-th].
- [46] Nabamita Banerjee et al. "Hydrodynamics from charged black branes". In: Journal of High Energy Physics 01 (2011), p. 094. DOI: [10.1007/JournalofHighEnergyPhysics01\(2011\)094](https://doi.org/10.1007/JournalofHighEnergyPhysics01(2011)094). arXiv: [0809.2596](https://arxiv.org/abs/0809.2596) [hep-th].
- [47] Michal P. Heller, Romuald A. Janik, and Przemyslaw Witaszczyk. "A numerical relativity approach to the initial value problem in asymptotically Anti-de Sitter space-time for plasma thermalization - an ADM formulation". In: Physical Review D 85 (2012), p. 126002. DOI: [10.1103/PhysRevD.85.126002](https://doi.org/10.1103/PhysRevD.85.126002). arXiv: [1203.0755](https://arxiv.org/abs/1203.0755) [hep-th].

- [48] Michal P. Heller, Romuald A. Janik, and Przemyslaw Witaszczyk. “The characteristics of thermalization of boost-invariant plasma from holography”. In: Physical Review Letters 108 (2012), p. 201602. DOI: [10.1103/PhysRevLett.108.201602](https://doi.org/10.1103/PhysRevLett.108.201602). arXiv: [1103.3452](https://arxiv.org/abs/1103.3452) [hep-th].
- [49] Daniel Farquet et al. “Gravity duals of supersymmetric gauge theories on three-manifolds”. In: Journal of High Energy Physics 08 (2016), p. 080. DOI: [10.1007/JournalofHighEnergyPhysics08\(2016\)080](https://doi.org/10.1007/JournalofHighEnergyPhysics08(2016)080). arXiv: [1404.0268](https://arxiv.org/abs/1404.0268) [hep-th].
- [50] Niklas Beisert et al. “Review of AdS/CFT Integrability: An Overview”. In: Letters in Mathematical Physics 99 (2012), pp. 3–32. DOI: [10.1007/s11005-011-0529-2](https://doi.org/10.1007/s11005-011-0529-2). arXiv: [1012.3982](https://arxiv.org/abs/1012.3982) [hep-th].
- [51] Matthew Headrick, Sam Kitchen, and Toby Wiseman. “A New approach to static numerical relativity, and its application to Kaluza-Klein black holes”. In: Classical and Quantum Gravity 27 (2010), p. 035002. DOI: [10.1088/0264-9381/27/3/035002](https://doi.org/10.1088/0264-9381/27/3/035002). arXiv: [0905.1822](https://arxiv.org/abs/0905.1822) [gr-qc].
- [52] Pau Figueras, James Lucietti, and Toby Wiseman. “Ricci solitons, Ricci flow, and strongly coupled CFT in the Schwarzschild Unruh or Boulware vacua”. In: Classical and Quantum Gravity 28 (2011), p. 215018. DOI: [10.1088/0264-9381/28/21/215018](https://doi.org/10.1088/0264-9381/28/21/215018). arXiv: [1104.4489](https://arxiv.org/abs/1104.4489) [hep-th].
- [53] Alexander Adam, Sam Kitchen, and Toby Wiseman. “A numerical approach to finding general stationary vacuum black holes”. In: Classical and Quantum Gravity 29 (2012), p. 165002. DOI: [10.1088/0264-9381/29/16/165002](https://doi.org/10.1088/0264-9381/29/16/165002). arXiv: [1105.6347](https://arxiv.org/abs/1105.6347) [gr-qc].
- [54] Toby Wiseman. “Numerical construction of static and stationary black holes”. In: Black Holes in Higher Dimensions. Ed. by Gary T. Horowitz. 1st ed. Cambridge University Press, May 2012. ISBN: 9781107013452. arXiv: [1107.5513](https://arxiv.org/abs/1107.5513) [gr-qc]. URL: <https://inspirehep.net/record/920553/files/arXiv:1107.5513.pdf>.
- [55] William H. Press et al. Numerical Recipes in C++: The Art of Scientific Computing. Cambridge University Press, 2002. ISBN: 0521750334.
- [56] Lloyd N. Trefethen. Spectral Methods in MATLAB (Software, Environments, Tools). SIAM: Society for Industrial and Applied Mathematics, 2001. ISBN: 0898714656.
- [57] Wolfram Research, Inc. Mathematica 10.3. Version 10.3. 2015. URL: <https://www.wolfram.com>.
- [58] Timothy A. Davis. SuiteSparse. URL: [faculty.cse.tamu.edu/davis/suitesparse.html](http://faculty.cse.tamu.edu/davis/suitesparse.html).
- [59] Andrew Hickling, James Lucietti, and Toby Wiseman. “Null infinity and extremal horizons in AdS-CFT”. In: Classical and Quantum Gravity 32.3 (2015), p. 035008. DOI: [10.1088/0264-9381/32/3/035008](https://doi.org/10.1088/0264-9381/32/3/035008). arXiv: [1408.3417](https://arxiv.org/abs/1408.3417) [hep-th].

- [60] Brian Hall. “Chapter 1: Matrix Lie Groups”. In: Lie Groups, Lie Algebras, and Representations: An Elementary Introduction. Springer, 2004. ISBN: 0387401229.
- [61] H. Osborn and A. C. Petkou. “Implications of conformal invariance in field theories for general dimensions”. In: Annals of Physics 231 (1994), pp. 311–362. DOI: [10.1006/aphy.1994.1045](https://doi.org/10.1006/aphy.1994.1045). arXiv: [hep-th/9307010](https://arxiv.org/abs/hep-th/9307010) [hep-th].
- [62] Eric Poisson. A Relativist’s Toolkit: The Mathematics of Black-Hole Mechanics. Cambridge University Press, 2007. ISBN: 0521537800.
- [63] Robert M. Wald. “Chapter 12: Black Holes and Thermodynamics”. In: General Relativity. University Of Chicago Press, 1984. ISBN: 0226870332.
- [64] Hari K. Kunduri, James Lucietti, and Harvey S. Reall. “Near-horizon symmetries of extremal black holes”. In: Classical and Quantum Gravity 24 (2007), pp. 4169–4190. DOI: [10.1088/0264-9381/24/16/012](https://doi.org/10.1088/0264-9381/24/16/012). arXiv: [0705.4214](https://arxiv.org/abs/0705.4214) [hep-th].
- [65] Piotr T Chruściel, Harvey S Reall, and Paul Tod. “On non-existence of static vacuum black holes with degenerate components of the event horizon”. In: Classical and Quantum Gravity 23.2 (Jan. 2006), pp. 549–554. ISSN: 0264-9381. DOI: [10.1088/0264-9381/23/2/018](https://doi.org/10.1088/0264-9381/23/2/018). arXiv: [gr-qc/0512041](https://arxiv.org/abs/gr-qc/0512041) [gr-qc]. URL: <http://arxiv.org/abs/gr-qc/0512041>.
- [66] Gary T. Horowitz et al. “Hovering Black Holes from Charged Defects”. In: Classical and Quantum Gravity 32 (2015), p. 105001. DOI: [10.1088/0264-9381/32/10/105001](https://doi.org/10.1088/0264-9381/32/10/105001). arXiv: [1412.1830](https://arxiv.org/abs/1412.1830) [hep-th].
- [67] Roberto Emparan, Gary T. Horowitz, and Robert C. Myers. “Exact description of black holes on branes”. In: Journal of High Energy Physics 01 (2000), p. 007. DOI: [10.1088/1126-6708/2000/01/007](https://doi.org/10.1088/1126-6708/2000/01/007). arXiv: [hep-th/9911043](https://arxiv.org/abs/hep-th/9911043) [hep-th].
- [68] Andrew Hickling. “Bulk Duals for Generic Static, Scale-Invariant Holographic CFT States”. In: Classical and Quantum Gravity 32.17 (2015), p. 175011. DOI: [10.1088/0264-9381/32/17/175011](https://doi.org/10.1088/0264-9381/32/17/175011). arXiv: [1504.03723](https://arxiv.org/abs/1504.03723) [hep-th].
- [69] R. Jackiw. “Topics in Planar Physics”. In: Physics, Geometry and Topology. Ed. by H. C. Lee. Boston, MA: Springer US, 1990, pp. 191–239. ISBN: 978-1-4615-3802-8. DOI: [10.1007/978-1-4615-3802-8\\_6](https://doi.org/10.1007/978-1-4615-3802-8_6). URL: [http://dx.doi.org/10.1007/978-1-4615-3802-8\\_6](http://dx.doi.org/10.1007/978-1-4615-3802-8_6).
- [70] Imperial College High Performance Computing Service. URL: <http://www.imperial.ac.uk/ict/services/teachingandresearchservices/highperformancecomputing>.
- [71] Steven S. Gubser. “Curvature singularities: The Good, the bad, and the naked”. In: Advances in Theoretical and Mathematical Physics 4 (2000), pp. 679–745. arXiv: [hep-th/0002160](https://arxiv.org/abs/hep-th/0002160) [hep-th].
- [72] Andrew Hickling and Toby Wiseman. “AdS/CFT and the geometry of an energy gap”. In: Classical and Quantum Gravity 33.3 (2016), p. 035007. DOI: [10.1088/0264-9381/33/3/035007](https://doi.org/10.1088/0264-9381/33/3/035007). arXiv: [1507.00015](https://arxiv.org/abs/1507.00015) [hep-th].

- [73] M.A. Abramowicz, B. Carter, and J.P. Lasota. "Optical reference geometry for stationary and static dynamics". In: General Relativity and Gravitation 20:11 (Nov. 1988).
- [74] Igor R. Klebanov and Edward Witten. "AdS / CFT correspondence and symmetry breaking". In: Nuclear Physics B556 (1999), pp. 89–114. DOI: [10.1016/S0550-3213\(99\)00387-9](https://doi.org/10.1016/S0550-3213(99)00387-9). arXiv: [hep-th/9905104](https://arxiv.org/abs/hep-th/9905104) [hep-th].
- [75] Keith Copsey and Gary T. Horowitz. "Gravity dual of gauge theory on  $S^{*2} \times S^{*1} \times R$ ". In: Journal of High Energy Physics 06 (2006), p. 021. DOI: [10.1088/1126-6708/2006/06/021](https://doi.org/10.1088/1126-6708/2006/06/021). arXiv: [hep-th/0602003](https://arxiv.org/abs/hep-th/0602003) [hep-th].
- [76] Robert C. Myers. "Stress tensors and Casimir energies in the AdS / CFT correspondence". In: Physical Review D60 (1999), p. 046002. DOI: [10.1103/PhysRevD.60.046002](https://doi.org/10.1103/PhysRevD.60.046002). arXiv: [hep-th/9903203](https://arxiv.org/abs/hep-th/9903203) [hep-th].
- [77] Stephen A. Fulling. Aspects of Quantum Field Theory in Curved Spacetime (London Mathematical Cambridge University Press, 1989, pp. 96–104. ISBN: 0521377684.
- [78] Andrew Hickling and Toby Wiseman. "Vacuum energy is non-positive for  $(2 + 1)$ -dimensional holographic CFTs". In: Classical and Quantum Gravity 33.4 (2016), p. 045009. DOI: [10.1088/0264-9381/33/4/045009](https://doi.org/10.1088/0264-9381/33/4/045009). arXiv: [1508.04460](https://arxiv.org/abs/1508.04460) [hep-th].
- [79] Sebastian Fischetti, Andrew Hickling, and Toby Wiseman. "Bounds on the local energy density of holographic CFTs from bulk geometry". In: (2016). arXiv: [1605.00007](https://arxiv.org/abs/1605.00007) [hep-th].
- [80] Gregory J. Galloway and Eric Woolgar. "On static Poincaré-Einstein metrics". In: Journal of High Energy Physics 06 (2015), p. 051. DOI: [10.1007/JournalofHighEnergyPhysics051](https://doi.org/10.1007/JournalofHighEnergyPhysics051). arXiv: [1502.04646](https://arxiv.org/abs/1502.04646) [gr-qc].
- [81] M. T. Anderson. " $L^2$  curvature and volume renormalization of AHE metrics on 4-manifolds". In: ArXiv Mathematics e-prints (Nov. 2000). eprint: [math/0011051](https://arxiv.org/abs/math/0011051).
- [82] Juan Maldacena. "Einstein Gravity from Conformal Gravity". In: (2011). arXiv: [1105.5632](https://arxiv.org/abs/1105.5632) [hep-th].
- [83] G. W. Gibbons and S. W. Hawking. "Classification of Gravitational Instanton symmetries". In: Communications in Mathematical Physics 66.3 (1979), pp. 291–310. ISSN: 1432-0916. DOI: [10.1007/BF01197189](https://doi.org/10.1007/BF01197189). URL: <http://dx.doi.org/10.1007/BF01197189>.
- [84] Robert Geroch. "Energy Extraction". In: Annals of the New York Academy of Sciences 224.1 (1973), pp. 108–117. ISSN: 1749-6632. DOI: [10.1111/j.1749-6632.1973.tb41445.x](https://doi.org/10.1111/j.1749-6632.1973.tb41445.x). URL: <http://dx.doi.org/10.1111/j.1749-6632.1973.tb41445.x>.

- [85] Pong Soo Jang and Robert M. Wald. “The positive energy conjecture and the cosmic censor hypothesis”. In: Journal of Mathematical Physics 18.1 (1977), pp. 41–44. DOI: [10.1063/1.523134](https://doi.org/10.1063/1.523134). URL: <http://scitation.aip.org/content/aip/journal/jmp/18/1/10.1063/1.523134>.
- [86] Roger Penrose. “Naked Singularities”. In: Annals of the New York Academy of Sciences 224.1 (1973), pp. 125–134. ISSN: 1749-6632. DOI: [10.1111/j.1749-6632.1973.tb41447.x](https://doi.org/10.1111/j.1749-6632.1973.tb41447.x). URL: <http://dx.doi.org/10.1111/j.1749-6632.1973.tb41447.x>.
- [87] Gerhard Huisken and Tom Ilmanen. “The Inverse Mean Curvature Flow and the Riemannian Penrose Inequality”. In: Journal of Differential Geometry 59.3 (Nov. 2001), pp. 353–437. URL: <http://projecteuclid.org/euclid.jdg/1090349447>.
- [88] G W Gibbons. “Some comments on gravitational entropy and the inverse mean curvature flow”. In: Classical and Quantum Gravity 16.6 (1999), p. 1677. URL: <http://stacks.iop.org/0264-9381/16/i=6/a=302>.
- [89] Dan A. Lee and André Neves. “The Penrose Inequality for Asymptotically Locally Hyperbolic Spaces with Nonpositive Mass”. In: Communications in Mathematical Physics 339.2 (2015), pp. 327–352. ISSN: 1432-0916. DOI: [10.1007/s00220-015-2421-x](https://doi.org/10.1007/s00220-015-2421-x). arXiv: [1310.3002](https://arxiv.org/abs/1310.3002) [math.DG]. URL: <http://dx.doi.org/10.1007/s00220-015-2421-x>.
- [90] G.W. Gibbons, C.M. Hull, and N.P. Warner. “The stability of gauged supergravity”. In: Nuclear Physics B 218.1 (1983), pp. 173–190. ISSN: 0550-3213. DOI: [10.1016/0550-3213\(83\)90480-7](https://doi.org/10.1016/0550-3213(83)90480-7). URL: <http://www.sciencedirect.com/science/article/pii/0550321383904807>.
- [91] Gary Gibbons and Sean A. Hartnoll. “A Gravitational instability in higher dimensions”. In: Physical Review D 66 (2002), p. 064024. DOI: [10.1103/PhysRevD.66.064024](https://doi.org/10.1103/PhysRevD.66.064024). arXiv: [hep-th/0206202](https://arxiv.org/abs/hep-th/0206202) [hep-th].
- [92] Hidehiko Yamabe. “On a deformation of Riemannian structures on compact manifolds”. In: Osaka Mathematical Journal 12.1 (1960), pp. 21–37. URL: <http://projecteuclid.org/euclid.ojm/1200689814>.
- [93] Yasushi Mino, Misao Sasaki, and Takahiro Tanaka. “Gravitational radiation reaction to a particle motion”. In: Physical Review D 55 (6 1997), pp. 3457–3476. DOI: [10.1103/PhysRevD.55.3457](https://doi.org/10.1103/PhysRevD.55.3457). URL: <http://link.aps.org/doi/10.1103/PhysRevD.55.3457>.
- [94] Samuel E. Gralla and Robert M. Wald. “Derivation of Gravitational Self-Force”. In: Fundamental Theories of Physics 162 (2011), pp. 263–270. arXiv: [0907.0414](https://arxiv.org/abs/0907.0414) [gr-qc].
- [95] Robert M. Wald. “Introduction to Gravitational Self-Force”. In: Fundamental Theories of Physics 162 (2011), pp. 253–262. arXiv: [0907.0412](https://arxiv.org/abs/0907.0412) [gr-qc].